AN INVESTIGATION OF AN ADSORPTION COGENERATION SYSTEM FOR POWER AND COOLING USING LOW GRADE HEAT

Thesis by

Constantinos Charalambous

Doctor of Philosophy

Newcastle Institute for Research on Sustainability
2nd Floor, Stephenson Building
Newcastle University
Newcastle Upon Tyne, NE1 7RU
United Kingdom

Abstract

Cogeneration is a hot topic in the efforts to reduce dependence on fossil fuel usage and to reduce greenhouse gas emissions by replacing the primary energy source with a low-grade heat source. Cogeneration simultaneously produces power and cooling using a low-grade heat source (e.g. solar energy, geothermal energy or waste heat), which ideally provides a renewable carbon-free solution for implementation in domestic, industrial as well as isolated areas.

This research thesis describes for the first time the development and construction of the Low Heat cogeneration chemisorption system, explores its potential and makes suggestions for its future development based on the experience gained during the experiments. The design uses two adsorption cycles operating out of phase and alternatively connected to a scroll expander in order to reach 3kW of cooling and 1kW of electricity. Each adsorption cycle consists of a reactor, a condenser and an evaporator. Each reactor contains a composite mixture of $CaCl_2$ and activated carbon at a ratio of 4:1 by mass. The system was experimentally investigated for its cooling as well as for its cogeneration performance.

Experimental investigations were performed for different heating and cooling temperatures, cycle times and the optimum overall ammonia for the system. The maximum refrigeration coefficient of the performance (COP_{ref}) of the machine was found to be 0.26 when the refrigeration power was 3.52kW. At the same time, the specific cooling power (SCP) per side was 201.14W/kg (402.28W/kg per cycle) and the cooling capacity 168.96kJ/kg (337.92kJ/kg per cycle). During the cogeneration experiments it was found that the expander affected the pressure and temperature; the refrigerant flow rate and the pressure across the expander were important for the system's power production. The maximum power recorded was 486W which provides a power coefficient of performance (COP_W) of 0.048.

A model to describe the desorption power generation as well as the evaporation refrigeration process was developed using the ECLIPSE software. The cooling model was validated from the experimental results and later the power model was used for

further investigation of the system power performance. The optimisation of the machine completes the study by using both experimental and simulation data.

Dedicated to the memory of my father, who passed away on May 26th 2013.

I am sure he is very proud and happy with a big honest smile on his face, seeing from heaven this work reach its end.

Wish you were here κουμπαρε μου to tell you how much I love.

Wish had told you this when you were alive.

Acknowledgements

I would like to express my deepest gratitude first and foremost to my supervisors, Professor Tony Roskilly and Dr Yaodong Wang, for their guidance and support throughout my PhD study.

Secondly, I would like to express my deep respect to Dr Huashan Vicky Bao for her support and kindness during this study, and especially when we were in China. Without her support, this study would never be completed.

Also, I want to express my heartfelt gratitude to the students of Shanghai Jiao Tong University, especially Pan and Dragon for their understanding and support, as well to Dr Liwei Wang and Dr Lu.

I also owe my sincere gratitude to colleagues and staff for their continuous help and support including: Mr Jonathan Heslop; Dr Barbara Sturm; Mr Thomas Zunderp; Mr Razali Hanipah; Mr Mohammad Royapoor; Mr YiJi Lu: Mr Eric Siqueiros Valencia; Mr Ian Milne; Mr Stephen Crosby; Dr Dawei Wu; Mr Paul Watson; Mr Leigh Ingle; and Mrs Jan Fairless. As wee my deep regards and appreciation to Mr Aidan Wightman for the time spent in proof reading my thesis.

I also owe my sincere gratitude to friends who were always available for support during this study. More specifically Mr Charalambos Karapatakis; Georgia Kastanou and their children Sotiris and Elena Karapataki; Dr Nicos Aggastiniotis; Dr Christopher Markides; Mr Dimitris Themistokleous; Mr Nicos Politis and family; Charalambos Charalambous; Elena Charalambous; George Papadopoulos and Grigoris Theodorou and Loizos (Ivan) H'Ioannou.

To my love, Alina-Elena Gaidea. Trough her I see the way forward to life. Thanks' God for bring her in my life and for the benefits I gain from her. Love you both. Wish I could tell you how much I love you when we were together. I will show you soon.

Last but not least, my gratitude to my mother who has been assisting as much as she could especially during hard periods. Love you mother a lot even I late to admit.

Table of Contents

Paper

Huashan Bao, Yaodong Wang, Constantinos Charalambous, Zisheng Lu, Liwei Wang, Ruzhu Wang, Anthony Paul Roskilly, *Chemisorption cooling and electric power cogeneration system driven by low grade heat*, Energy 72 (2014) 590-598

List of figures

List of tables

Nomenclatures

A	adsorption potential (J/kg)
ALT	atmospheric life time
COP	cycle coefficient of performance
COP_{cogen}	cogeneration COP
COP_W	power generation COP
COP_{ref}	refrigeration COP
cp	specific heat (kJ/kgK)
exp	scroll expander
F	flow rate (m^3/hr, kg/s)
G	reactive gas
GWP	global warming potential
h_{fg}	enthalpy of vaporisation (kJ/kg)
H	heater element
H_cT_c	enthalpy of refrigerant at condensation temperature (kJ/mol)
H_eT_e	enthalpy of refrigerant at evaporation temperature (kJ/mol)
HTS	high-temperature salt
ln_{equil}	equilibrium pressure drop (MPa)
L	litre
L/G	liquid gas
LR	low temperature reactor
LTS	low-temperature salt
$\dot{m}$	mass flow rate (kg/s)
m	mass (kg)
mm	millimetre
MTS	medium-temperature salt
M	molar mass (g mol^{-1})
MX	reactive solid salt
n,n_s, p	number of moles of reactive salt
N	rotational speed (rpm)
NH_3	ammonia refrigerant
ODP	ozone depletion potential
ORC	Organic Rankine Cycle
C-CHP	Combined cooling heat and power

P	pressure (MPa)
Pc	constraining pressure (MPa)
Q	energy related to a process (kJ/kg)
Q_{high}	heating desorption power (W, kW)
Q_{ref}	refrigeration power (W, KW)
R	reactor
R	ideal gas constant (kJ/kgK)
S/G	solid gas
t	time (sec or min)
T	temperature (^{O}C or ^{O}K)
s	entropy (kJ/kgK)
SOFC	solid oxide fuel cell
SCP	Specific Cooling Power (W/kg_{adso})
V	volume (m^3/kg)
W	power (W or kW)
Z	adsorption volume (m^3/kg)

Greek letters

α	linear expansion coefficient (m/K)
γ_s	ideal number of moles of refrigerant consumed per mole of reactance
ε	uncertainty (error)
ΔH	heat of chemical reaction (kJ mol^{-1},kJ/kg)
ΔT	temperature difference (^{0}C)
ΔP	pressure difference (MPa)
ΔP_{exp}	pressure difference across the expander
ΔS	Reaction entropy (kJ/kg)
$\Delta\chi(X,\chi)$	concentration, degree of conversion (kg_{NH3}/kg_{NH3}, kg_{NH3}/kg_{salt})
H	enthalpy (kJ/kg)
σ	standard deviation

Subscripts

a	adsorbent material
ac	activated carbon
ads, A	adsorption

ADD	Additive model error
avg	average
cond, C	condensation
des, D	desorption
ea	equilibrium at adsorption
ed	equilibrium at desorption
EG	expanded graphite
equ	equilibrium
eva, e, E	evaporator
exp	expander
H, high	high
HVAC	heating ventilation and air conditioning
is	isentropic
loss	loses
L	low
m	medium
me	evaporator metal construction
mr	metallic reactor construction
HR	high-temperature reactor
HTS	high-temperature salt
LTS	low-temperature salt
MTS	medium-temperature salt
n	efficiency
refr	refrigerant
th, rev	thermal, reversible
RSS	Root-sum-square
r	random error
s	standard error
v	manual valve
V	pneumatic valve

Chemistry

$Al_2(SO_4)_3$	aluminium sulphate
$BaCl_2$	barium chloride

$CaCl_2$	calcium chloride
CaO	calcium oxide
CO_2	carbon dioxide
H_4SiO_4	hydrated silicon oxygen
$LaNi_s$	lanthanum nickel
$MgCl_2$	magnesium chloride
MgO	magnesium oxide
$MgSO_4$	magnesium sulphate
$MnCl_2$	manganese chloride
N_2	nitrogen molecule
NaS	sodium sulphide
Ti	titanium
PbCl	lead chloride

Chapter 1. Introduction

1.1 Research Background

The harmful environmental issues of Global Warming as well as the oil crisis which results in fossil fuel price instability are two major concerns of environmental scientists. The worldwide increase in energy demand increases the CO_2 emissions released into the atmosphere from burning fossil fuels and that is considered the main reason for the planet's continual heating. Global warming has been linked to increased skin cancer incidence as well as an increase in respiratory problems, breathing issues, allergies and other diseases [1, 2]. Global warming has also been shown to contribute to ice melting in the polar regions and as a result the populations of animals like polar bears and penguins shrink every year. Ice melting increases the sea level continually and thus, small islands and cities that are not very much above the sea level are in severe danger of flooding. Climate change can lead to strange weather phenomena like extensive rainfall in traditionally dry areas or drought in areas that normally enjoyed extensive rainfall. Also, the increase of the humidity level in the atmosphere can lead to heavy storms [3, 4].

The increase in energy demand is the main reason for fossil fuel price instability for the oil companies' benefit, resulting in higher electricity prices, transportation prices with the result also that the goods prices go up [5, 6]. At the moment the world population is fossil-fuel dependent [7], and the oil companies look to take advantage of this, by increasing or decreasing fossil fuel prices according to their own agenda. Another issue related to the extent of fossil fuel use is related to the production and precautions to consider during oil extraction in order to avoid accidents. Accidents similar to the BP Deepwater Horizon rig in the Gulf of Mexico in 2010 when eleven people died and tons of oil spurted out in a massive sea area, unfortunately cannot be avoided from time to time. Accidents like that cause huge environmental disasters resulting in the long-term damage of the sea life and of the agricultural activities in the nearest bays as well [8, 9]. In order to decrease CO_2 emissions, the Kyoto protocol was established in 1997 in Japan. This is an international agreement linked to the United Nations Framework Convention on Climate Change, which set down internationally binding emissions reduction targets [10].

Also, many researchers have proposed new ideas, mainly by utilising renewable resources or any wasted heat by recovering energy from low heat sources (heat around 120^0C) and medium heat sources (around 220^0C) with the aim of saving fossil fuels [11]. Solar radiation is considered a renewable low-to-medium heat source and so is industrial waste. Attention is already given to cogeneration plants which provide combinations of power and heat or combinations of cooling and power as well as trigeneration plans for the simultaneous production of power, heat and cooling.

It is evident we cannot yet relax our dependence on fossil fuels, thus this proposal intends to examine the possibility of an alternative idea for the provision for the needs of domestic and industrial sectors, and for isolated areas. The necessity of utilising a low-energy source efficiently is the basis on which this proposal is built.

1.2 Aims and objectives

The idea proposed in this study is a low-heat-driven cogeneration adsorption chiller-rankine cycle which produce simultaneous cooling and power. This low-heat-driven system is a modified continuous chemisorption adsorption chiller at which a scroll expander is attached to produce power as well. The aims of the study are to examine the idea of the cogeneration of cooling and power, and provide useful feedback for future work.

The specific objectives of the study are to:

a) Attempt to understand fully the theory behind the refrigeration cycle used and the power media device under investigation;
b) Build the cogeneration system and prepare it for demonstration and data collection;
c) Prove the concept of the chemical adsorption cogeneration principle running the LH cogen system prototype and investigate the system cooling and cogeneration performance for different working conditions;
d) State the operational approach for similar systems that maximises system efficiency.
e) Compile a computational model for the proposed cogeneration system operating in only-cooling mode and in cogeneration mode and further investigate the parameters affect the system's power generation and to optimise system performance. The cooling simulation should be able predict the LH cogen system cooling performance for vary conditions.

f) Since is the first ever attempt on similar cycles, set out a series of suggestions for future reference in order to improve the system performance associated to the operating process, the sensible losses and the adsorbent;

1.3 Methodology

The methodology for this report includes a literature review to identify the problem and locate the gap in the literature and also to state the potential of the proposed system to cover that gap. A literature review for the chemical adsorption chiller and the selected power media device will be carried out as well. A full-scale test rig will be used to investigate the proposed system's potential and also to identify limitations. The computational analysis is required to understand the parameters that affect the system and investigate parameters that will not be carried out experimentally.

1.3.1 Literature survey

A literature survey for refrigeration solid-gas sorption type technologies will be carried out. It is necessary to identify the limitations of the solid-gas sorption technologies as well as suggestions to increase the system's efficiency in order to become suitable for commercialisation. The potential of a scroll expander as a power generation medium for low flow-rate refrigerant will also be investigated. Also cogeneration cycle for simultaneous cooling and power should be identified from the literature. Additionally, it must be ascertained whether the combination of an adsorption cycle using a scroll expander has been used in the past for a similar cogeneration system. This could help to identify the 'state of the art' of the proposed idea.

1.3.2 Computational modelling and simulation

The simulation will be used initially in order for to experimental results to be validated to create a model that can describe the LH cogen system cooling performance. This model can be used in the future to identify the system cooling performance. Later data from the cooling results is used to predict the system power performance before any power generation results are taken. The power simulation will help to investigate further the system power performance after the power experimental tests. Also, it will help identify the optimised design parameters of the cogeneration system for different working conditions.

1.3.3 Experimental test rig

Since the system is a new idea which has never been tested before as a cogeneration system, the aim is to build an experimental test rig while remaining faithful to the

original design in order to prove the principle. From the test rig, the potential of the system will be identified, as well as any drawbacks and suggestions and recommendations for future investigation. Also a test rig using nitrogen at high pressure and temperature to drive the scroll expander to identify the potential for power generation will be set up. This will provide important information about the device's parameters and the operation principle. At the same time the performance of the solid gas adsorption refrigerator will be examined under varied working conditions.

1.4 Contribution to existing thesis

Cogeneration can provide great benefits to reduce primary energy input especially to isolated and removable areas so reducing carbon emissions at the same time. Most of the research on cogeneration for cooling and power is based on the absorption chiller but no experimental research until now, based on the adsorption cycle, has appeared. This research presents an experimental investigation of the LH cogen system and will contribute to the existing research in the following fields:

a) To gain experience with the LH cogen system construction and design;
b) To improve the system by understanding and exploring its performance under different operating conditions;
c) To provide a computational modelling that describes the system accurately and explore its power and cooling performance further;
d) To explore the scroll expander's power generation potential.

Chapter 2. Literature Review

Cogeneration for cooling and power is a technology which was developed to utilise renewable or waste low-to-medium heat sources which have a variety of applications in a similar industry, such as the commercial, for isolated areas as well for household use. The term cogeneration is mainly related to CHP systems (combined heat and power) but recently cogeneration for cooling and power has also been getting some serious attention. The increasing demand of cooling makes cogeneration a hot and promising topic for a greener and more efficient cooling and power production. Benefits of the idea have been proven experimentally and some of them have been developed as well.

The aim of this chapter is to provide an overview of the topics covered in this study. More specifically, will explore the power and cogeneration cycles driven from low heat sources and the need for this study will be identified. A deep analysis of the chemical adsorption cycles will follow and details of the materials and refrigerant used will be provided as well. Furthermore, it will present the expanders found in the literature with the main focus on the scroll expander.

2.1 Low grade heat-driven power generation and cogeneration cycles

In this section will explore the basic power generation cycles and also will be presented power and cogeneration cycles driven by a low-heat source found in the literature. Advantages and disadvantages will be examined and the gaps in the literature and the need for this study will be identified in order to introduce the LH cogen system.

2.1.1 Carnot Cycle

The Carnot cycle is considered the ideal cycle for heat engines in thermodynamics since it is the most thermally efficient cycle operating between two specific operating temperature levels (high and low). It is considered to have no heat losses and consists of two isothermal and two adiabatic processes. Assuming that steam is a working fluid process 1-2 from Figure 2-1 [12] there is a reversible isothermal heating of the fluid to the boiler (from saturated liquid to saturated vapour), process 2-3 vapour is the isentropical expansion in the expansion device, process 3-4 is the isothermal cooling of the expanded fluid at the condenser and process 4-1 is the isentropical compression at the compressor [12, 13]. The efficiency of the Carnot cycle is given in Equation 2.1

which H denotes the high boiler temperature (process 1-2) and L the low cycle cooling temperature (process 3-4).

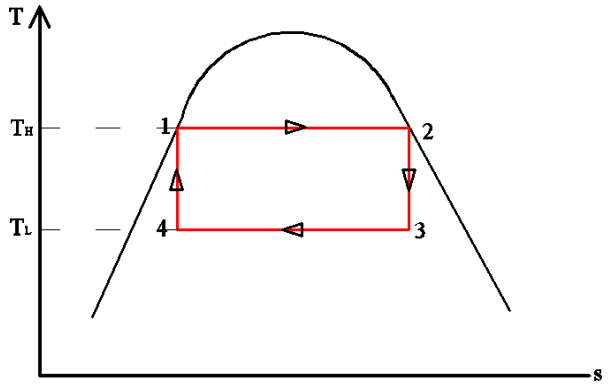

Figure 2-1: T-s diagram of Carnot cycle (a)

$$\eta_{th,rev} = 1 - \frac{T_L}{T_H} \qquad \textbf{2-1}$$

There are some irreversibilities related to the Carnot cycle and the first one is that the cycle's thermal efficiency is limited by the maximum temperature. The second issue is the low quality steam (steam with high moisture content) that the expansion device should deal with during the isentropic expansion process. The third issue is associated with the isentropic process 4-1 in which the liquid vapour mixture should be compressed to a saturated liquid. Two issues arise from this now and the first is that it is not practical to design such a pump for this application and the second is that, at the end of the condensation process (state 4), we cannot get a desirable quality of steam since the end of the process is not easy to design precisely [12].

Some of the issues of the Carnot cycle of Figure 2-1 can be eliminated using the Carnot cycle of Figure 2-2 [12] where the superheating process is above the critical point. This cycle faces other problems like the isentropic compression to extremely high pressure and isothermal heat transfer process to variable temperatures.

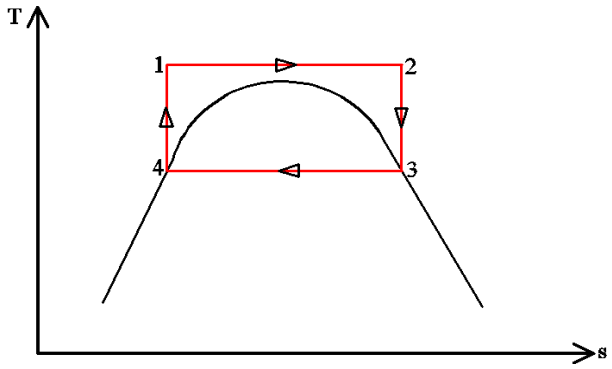

Figure 2-2: T-s diagram of Carnot cycle (b)

2.1.2 Rankine cycle

The Rankine cycle of Figure 2-3 [12] is designed to deal with most of the impracticalities of the Carnot cycle and is considered the closest to Carnot cycle vapour power plants which do not include any internal irreversibilities. The Rankine cycle is similar to the Carnot cycle by consisting of four processes.

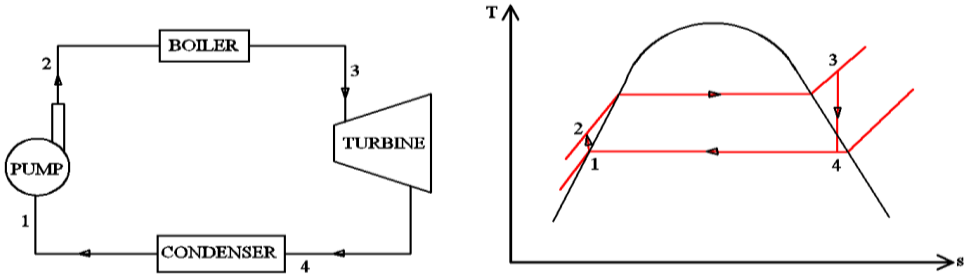

Figure 2-3: The ideal Rankine cycle

The 1-2 process is the pump isentropic compression process followed by the 2-3 process where the refrigerant's constant pressure adds heat to the boiler resulting in a superheating steam. The steam is then expanded isentropically to an expansion device in the 3-4 process, and is finally condensed at constant pressure in the condenser process 4-1 [12].

The actual Rankine vapour power cycle can result in some irreversibilities in various components (Figure 2-4). These irreversibilities are basically fluid friction and heat losses with the surroundings when the steam is travelling around the system. Fluid friction causes a pressure drop in the boiler, the condenser and the pipeline in between the various components. The pressure drop in the pipeline between the boiler exit and turbine inlet results in the turbine's inlet pressure to be lower than in the boiler's outlet.

The pressure drop in the condenser is considered to have a lower impact resulting in the use of a bigger pump size to increase the fluid pressure at the required level. The cycle heat losses require the boiler's heat input to be increased resulting in a decrease in the cycle's efficiency for the same power output. All these irreversibilities result in the increase of the pump's work input and the decrease of the turbine's power output [12].

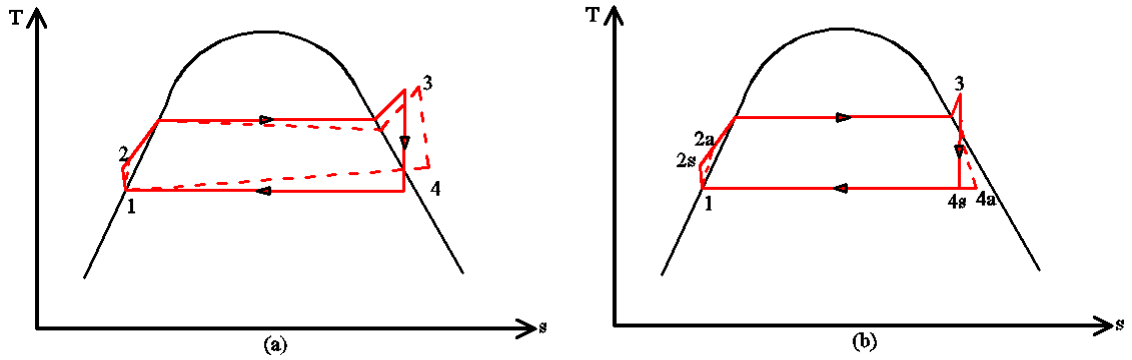

Figure 2-4: Deviation of the actual vapour power cycle from the Rankine cycle; (b) The effect of pump and turbine irreversibilities on the ideal Rankine cycle

In case an organic working fluid is used instead of steam, the cycle is called the Organic Rankine Cycle (ORC). The organic working fluid has a lower boiling point than water, therefore, ORC cycles are suitable to recover low-heat sources like solar and geothermal energy [13, 14]. Figure 2.5 [14] presents a configuration of an ORC and its T-s diagram.

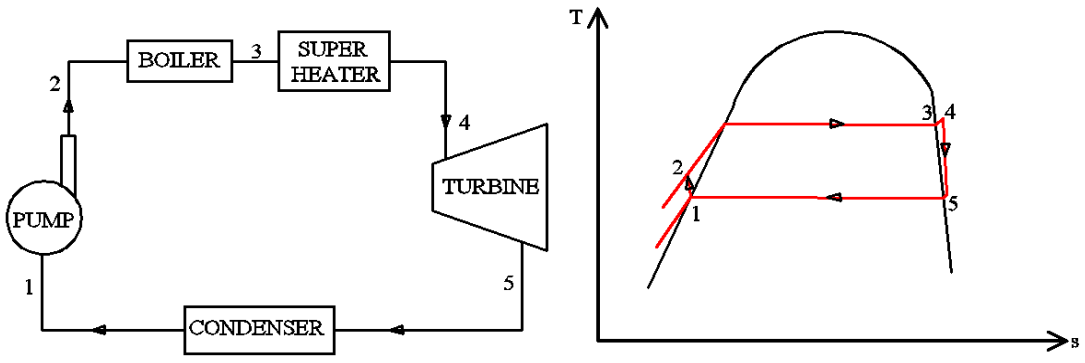

Figure 2-5: ORC configuration and T-s diagram

The organic working fluids can be classified as positive, negative and vertical based on the saturation line slope on the T-s diagram or as wet, dry and isentropical according to the current state of the refrigerant at the end of the expansion process. For a wet-positive slope fluid, at the end of the expansion process the refrigerant is a mixture of vapour

and liquid. For a dry-negative slope fluid, at the end of the expansion process the working fluid is still superheated. For an isentropic-vertical slope fluid, the expansion process is almost parallel to the superheating region of the T-s diagram. Wet fluid may need to be superheated compared to dry or isentropic fluid which may not [14]. Advantages and disadvantages of each fluid will not be discussed in this context.

Using ammonia as a refrigerant for 1MW power production, found that the heat input required is more compared to other refrigerants as well as, at the same time, the power production increases as the turbine's inlet pressure increases. That leads to a low COP as a result of the excessive heat input required because of the low molecular weight which results in excess sensible heat losses [15]. For a heat source of 200^{O}C and for 2MPa turbine inlet pressure the system's electricity COP is 0.095. Yamamoto, et al. [16] found that for a maximum 120^{O}C heat source, for various working fluids the turbine power output can be up to 400W.

2.1.3 Kalina cycle

In the direction of reducing heat transfer irreversibilities in similar cycles and converting to power the available heat source more efficiently, Dr. Alexander Kalina introduced a multi-component working fluid cycle, called the Kalina cycle [17]. The Kalina cycle is in principle a modified Rankine cycle which uses a binary ammonia water mixture as a working fluid, therefore it can utilise the available exergy better than can the Rankine cycle. The bottoming of the Kalina cycle is presented in Figure 2-6 [18, 20].

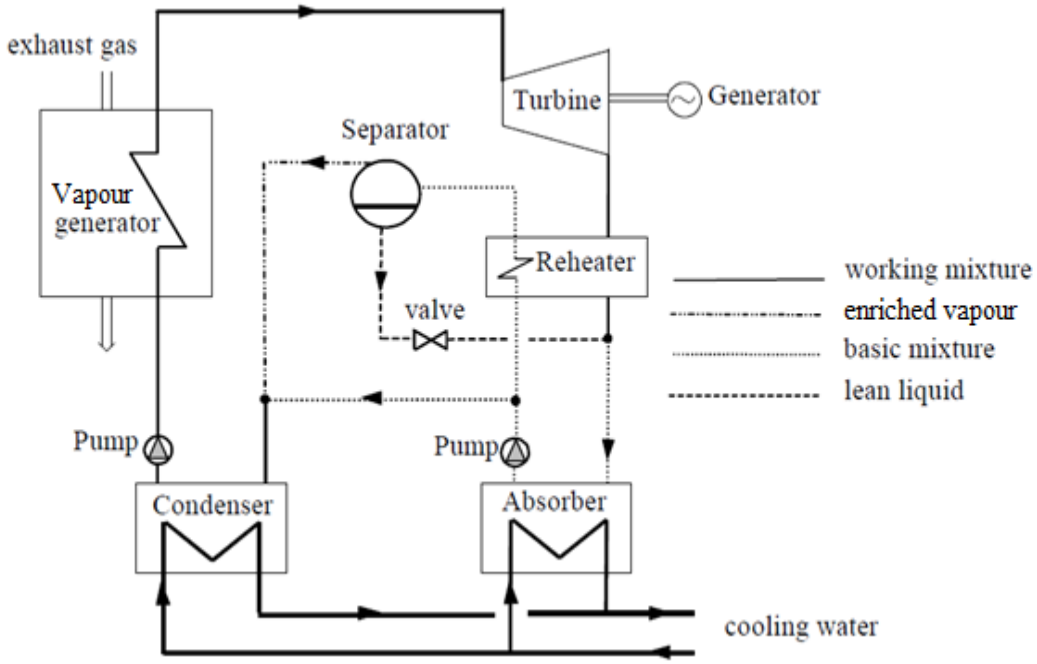

Figure 2-6: A simplified Kalina cycle

The composition of the mixture in the various components of the cycle depends on the application and the heat sources available. The Kalina cycle's binary working fluid results in ammonia evaporating initially during the heating process, followed by water vaporisation resulting in the cycle's heating process's taking place in a non-isothermal and non-isobaric process. Similarly, the system's cooling process does not take place in an isothermal and isobaric environment as it does in Rankine. The two non-isothermal processes result in an overall cycle's heat loss reduction so the working fluid can be very close to the heat source. This is the main reason why the Kalina cycle in theory is superior to the ORC cycle [13, 18, 19].

Figure 2-7 indicates the T-s diagram for a Rankine cycle [12] and a Kalina cycle [18]. Figure 2-7 also indicates the average high (heating process) and low (cooling) temperatures for each of them. This result offer higher Carnot efficiency compare to Rankine cycle. Kalina cycle offers a more practical and efficient way for the mixture's condensation back to liquid for a repeatable cycle.

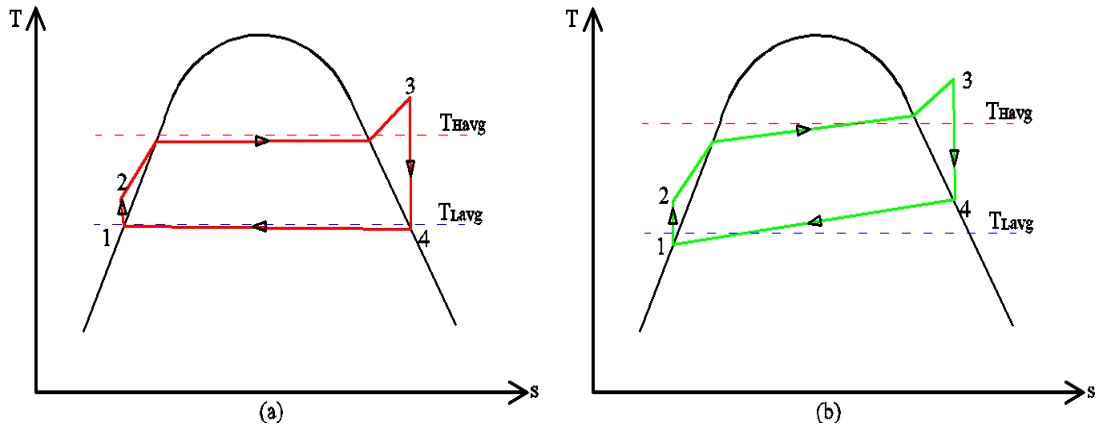

Figure 2-7: T-s diagram for Rankine and Kalina cycles

For the Kalina cycle the separator is a necessary component for the cycle to run efficiently. It is essential to reduce the mixture's concentration at the absorber's inlet since like that absorption temperature it is satisfied at a higher cooling temperature (ambient) which for higher concentrations could be very low therefore unrealistic to be used.

In theory, a cycle mixture of water and ammonia can produce 15-20% more power output than can the Rankine cycle and 10-20% more exergy [13, 19]. The Kalina cycle is considered beneficial to apply to geothermal applications compared to ORC power plants; in theory the performance can increase 30-50%. A Kalina geothermal plant offers advantages in terms of cost, safety and environmental advantages compared to ORC [13]. In reality, for low-heat sources (108^{O}C-122^{O}C) the Kalina cycle efficiency compared to the ORC cycle is no more than 3%. Kalina is more efficient to be used for low-to-medium temperature heat sources (no more than 400^{O}C). For low-temperature heat sources, the Kalina cycle requires a more complicated plant scheme and a larger heat exchanger surface area. For a 175^{O}C geothermal heat source, the ORC cycle has better thermal and exergy efficiencies than Kalina [13, 14, 20].

The parameters affecting the Kalina cycle's power performance are the turbine's inlet conditions' pressure and temperature and ammonia composition. Also, the turbine's outlet pressure should be kept as low as possible [18, 21]. Lolos and Rogdakis [22] examine a solar-driven Kalina cycle with a maximum superheated temperature of 130^{O}C and the maximum efficiency was found to be 0.083 with the minimum expander's outlet temperature under certain conditions being 15^{O}C which is good for

space cooling. Periklis A. Lolos [23] studied a modified version of the Kalina cycle installed in Husavic, Iceland, using a 120^{O}C heat source, the cycle's efficiency was found to be 0.24.

2.1.4 Goswami cycle

Another thermodynamic cogeneration cycle which used an ammonia-water mixture is the Goswami cycle which is a combination of a Rankine-absorption refrigeration cycle. This cycle is primarily designed to produce power similar to the Kalina cycle as well as refrigeration, taking advantage of the high ammonia concentration's low boiling point at the turbine's exit. Similar to the Kalina cycle, the Goswami cycle has the same advantages as a binary fluid cycle [24-27]. The schematic of the Goswami cycle is given in Figure 2-8 [24, 25, 28].

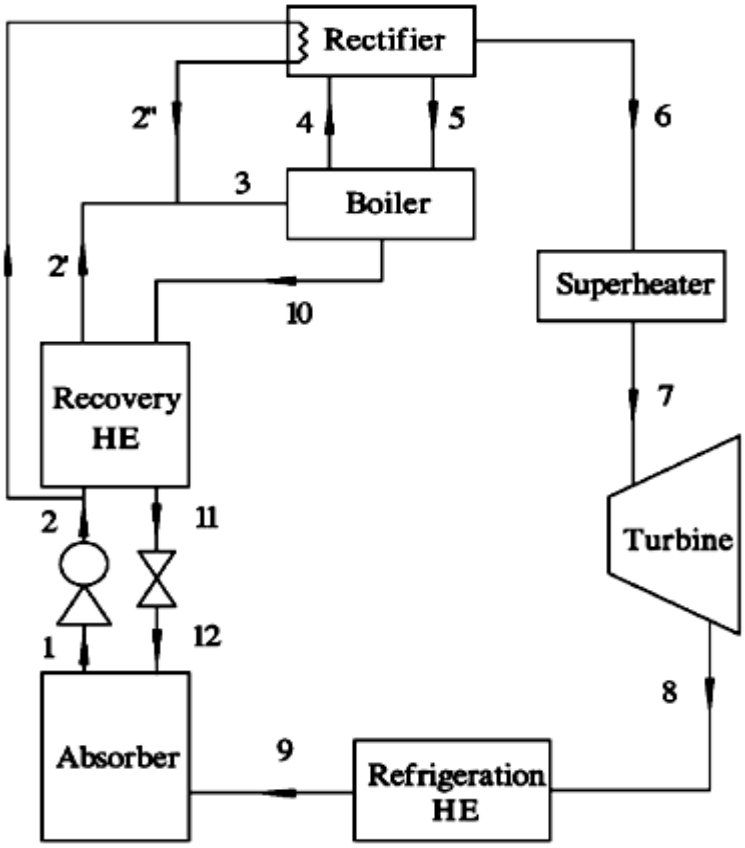

Figure 2-8: Goswami ammonia-based power/refrigeration cycle

Goswami cycle compared to the Kalina cycle does not have constraints on the lowest temperature of the working fluid exiting the turbine because it is not restricted by the condenser. This concern can be eliminated in the Goswami cycle by employing only an absorption-condensation process and eliminating condenser. Also, the rectifier is

necessary for a high concentration of ammonia enters the turbine therefore at the turbine's exit the low-boiling-point ammonia used for cooling [17]. The Goswami cycle mainly uses a turbine as a power generation medium [17, 27] or an expander [26].

The Goswami cycle suffers from low cooling performance because the cooling effect is a result only of the sensible heat transfer. Large cooling effects mean phase changes for the working fluid which is not the case for the Goswami cycle. Generally, a large cooling load for the Goswami cycle means a heat source around 450^{O}C should be used [29].

For low-temperature heat sources the Goswami cycle can reach a thermal theoretical efficiency of 0.18. From [30] the cycle efficiency was found to be 0.18 for a 2MPa maximum pressure and 137^{O}C maximum temperature. For a 110^{O}C heat source the cycle efficiency was found to be 0.17 and the lower temperature at the turbine's exit was 7^{O}C [31]. Obviously, the power generation is related to the flow rate as well.

2.1.5 Cogeneration cycles using an ejector

There are theoretical cogeneration studies using an ejector to maximise the refrigeration effect [32, 33]. Figure 2-9 [35] shows a modified Goswami cycle based on the absorption cycle which uses a binary working fluid where an ejector is used between the rectifier and the condenser to maximise the refrigeration effect. High pressure ammonia rich vapour mixture from the rectifier enters the ejector resulting in low pressure ammonia entering the evaporator for the cycle cooling production. At the same time another stream leaves the rectifier to eventually enter the turbine after it's superheated for the cycle power production. For this cycle, a superheated temperature of 300^{O}C is required to produce power from 250kW to 619kW and for -26^{O}C refrigerant temperature enters the evaporator. The refrigeration and the power production depend on the ammonia concentration at various components in the cycle.

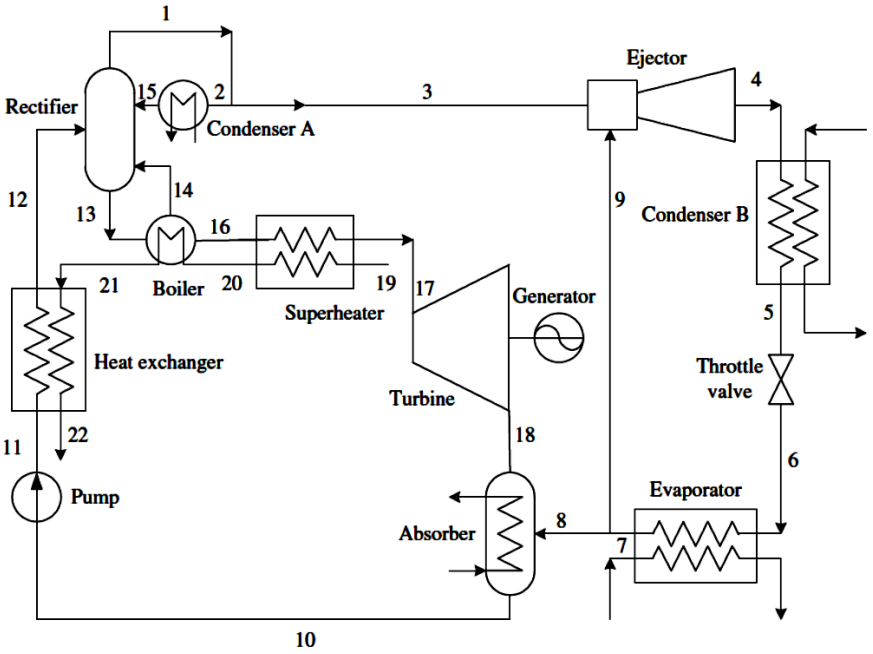

Figure 2-9: Combined power and ejector-absorption refrigeration cycle

Another cogeneration cycle which uses an ejector is, in principle an ORC ejector cycle similar to Figure 2-10 [36]. For this theoretical single fluid idea (R245fa), the refrigerant enters the ejector after it expands for further expansion and at the exit utilises the low temperature refrigerant. This cycle was examined for a maximum temperature of 125^{O}C and could achieve an ejector refrigerant temperature of 0^{O}C.

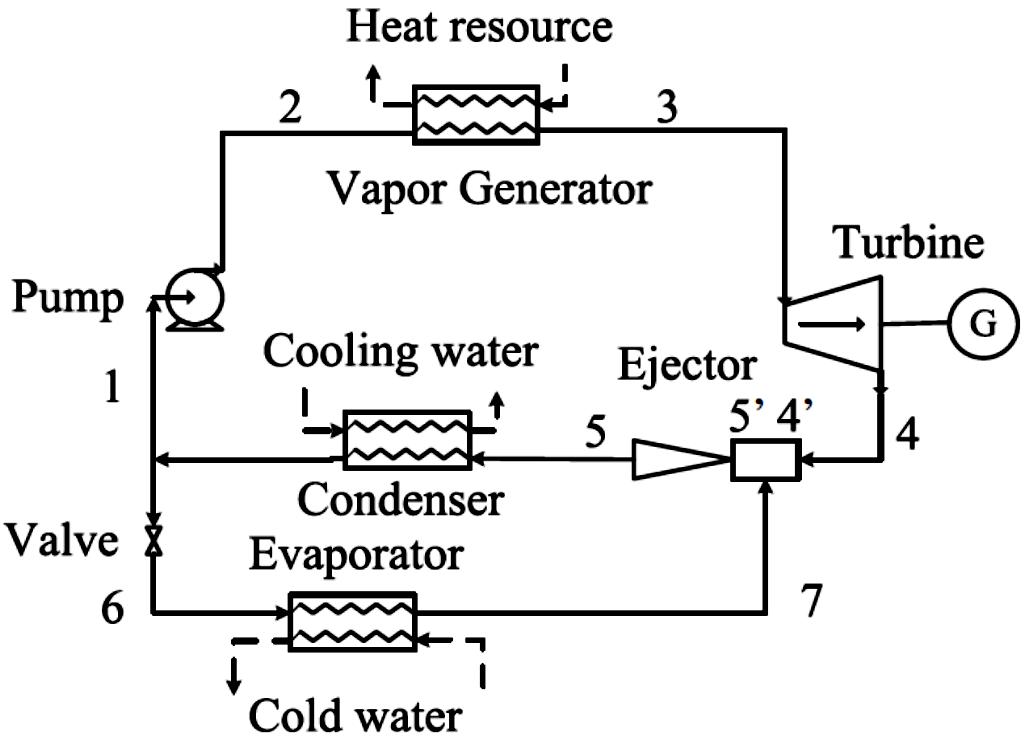

Figure 2-10: ORC-ejector refrigeration cycle

2.1.6 Resorption cogeneration cycle

L.W.Wang., et al. [34] proposed a theoretical new type of resorption-cogeneration system for power and refrigeration running with low-to-medium heat sources. According to the author this theoretical analysis, for similar working conditions, the new cycle has a slightly lower power COP_W than the Goswami cycle; however, it has 2.5 times higher cogeneration performance than the Rankine cycle and 4 times more than the Goswami cycle. For this study, a scroll expander is proposed as the power generation medium.

Figure 2-11 present the schematic of a resorption cogeneration cycle which consists of two set of resorption cycles to achieve continuous cooling and power. The power is achieved through the superheating of the desorbed refrigerant at temperatures higher than $300^{O}C$. The cycle cooling produced is mainly derived from the low pressure resorption (Q_{ref2}) process and to a lesser extent from the refrigerant expansion at the expander exit in case the temperature there is below ambient (Q_{ref1}, super cooler). This idea remain a theoretical approach of a chemical desorption cogeneration cycle and there are no an experimental results so far to support the theoretical analysis.

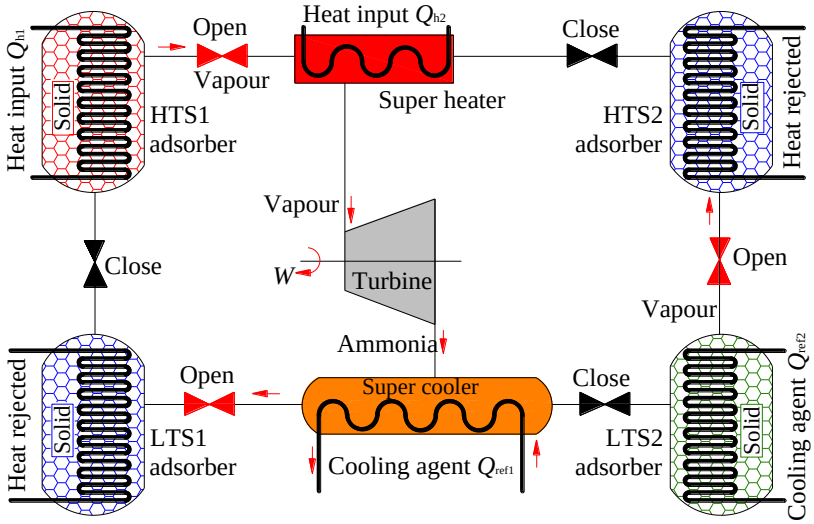

Figure 2-11: The resorption cogeneration cycle

2.1.7 Diesel-Absorption cogeneration cycle

B.Agnew., et al. [35] proposed a combined diesel-absorption cogeneration cycle for power and cooling. This theoretical study is considered ideal for isolated areas where a diesel generator is available and the generator exhaust gasses used heat input for the absorption chiller generator using a water curcuir. This cycle can also be considered environmentally friendly in the case where the engine runs on biofuel.

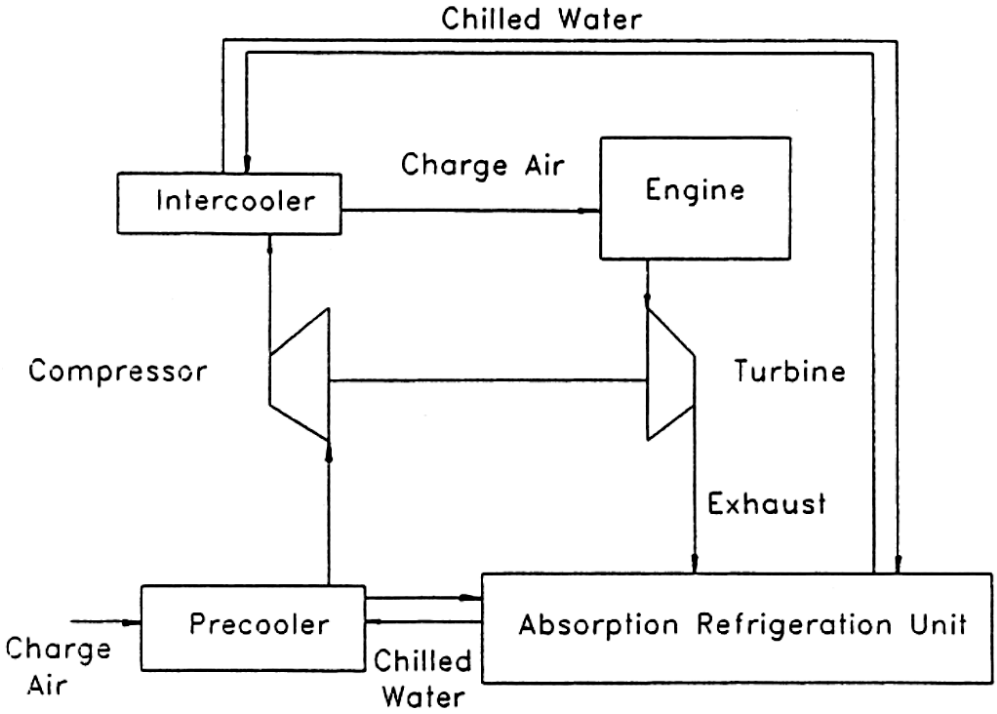

Figure 2-12: Schematic of a Diesel-absorption cogeneration

G.Paloso., et al. [36] proposed a cascading vapour absorption cycle with the Organic Rankine Cycle. Takezawa et al. examine a solid oxide fuel cell (SOFC) and gas turbine combined with an adsorption chiller [37].

A trigeneration system (C-CHP-combined cooling power and heat) using an adsorption chiller has been investigated [38, 39], as well as a trigeneration cycle using an adsorption chiller and a screw expander [40]. Most of the above studies can also be driven by low-temperature or higher heat sources. An injector-type trigeneration solar system was examined as well [32, 41]. Porteiro, et al. [41] examine a trigeneration system in which a reciprocating internal combustion engine is moving an electric generator and a heat recovery system. At the same time, the engine drives a heat pump compressor which can operate in reverse as well to meet summer cooling requirements.

2.2 Adsorption Process

The adsorption process can be classified in two categories associated with the constrained forces which appear during the process. Either can be physical adsorption (physisorption) or chemical adsorption (chemisorption) which is the type this report will focus on [42]. Adsorption is defined as the process by which a substance molecule (which can be gas or a liquid) which is called adsorbate, collected on the surface of

another substance such as a solid, and is called adsorbent. The molecules are attracted to the surface but do not enter the solid's minute spaces [43-45].

2.2.1 The adsorption principle

The basic adsorption refrigerator in principle is consisted from two linked vessels and presented in its simplest form in Figure 2-13 [46]. The left vessel is called the generator and contains the solid adsorbent material. The other vessel is called the receiver and either functions as a condenser or evaporator. The arrangement operates in the absence of air (in vacuum) and only the refrigerant is contained in the vessel. Two processes are repeated and the first process is the evaporation-adsorption process which takes place in low-temperature/ low-pressure conditions and the second one is the desorption-condensation process which takes place in high-pressure/ high-temperature conditions.

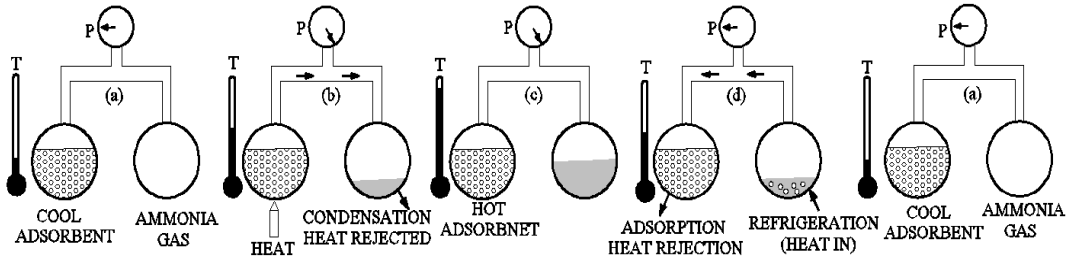

Figure 2-13: Principle of adsorption refrigeration technology

Initially, the system is at low temperature and pressure (Figure 2-13a). The adsorbent contains a high concentration of refrigerant, whilst the receiver contains only a small quantity of refrigerant gas. The first step (Figure 2-13b) consists of the generator's heating resulting in the system's pressure and temperature increase. These conditions lead to the refrigerant's desorption from the adsorbent. The desorption process causes a further increase in the system's pressure and temperature as well. The desorbed vapour refrigerant leaves the adsorbent and moves to the second vessel (receiver) which is now undercooling (by the ambient) and functions as a condenser at this stage resulting in the desorbed gas's condensation rejecting heat to the ambient. At the end of the desorption-condensation process, the left vessel (adsorbent) contains a very low concentration of refrigerant and the right vessel contains a high concentration of "warm" liquid refrigerant. The system's pressure at this stage is at a high level (Figure 2-13c). The next stage consists of the generator's cooling back to its initial temperature resulting in the re-adsorption of the refrigerant from the right vessel (Figure 2-13d). The adsorption

process causes the pressure system's drop. The system's low pressure (as a result of the adsorbent's cooling) causes the evaporation of the liquid refrigerant at the right vessel which is operated as an evaporator at this stage, absorbing the required latent heat from the surroundings and from an external chilling water circuit for that. The refrigerant's enthalpy of vaporisation is produced for the required cooling effect (refrigeration heat in). The chilling water utilises the cooling effect generated in the evaporator during its way out from there.

Since the quantity of the refrigerant contained in the two vessels is constant, the continual adsorption process reduces the quantity of the remaining refrigerant in the evaporator, so its density and pressure decrease as well. The evaporator's pressure reduction results in the boiling point's increase for the same temperature. The adsorption rate depends on the refrigerant's quantity availiable in the system, i.e. at the evaporator, and the refrigerant is possessed by the adsorbent before adsorption-evaporation starts.

Adsorption is an exothermic process and heat is released (heat of adsorption) during the process. In order to enhance the adsorption process, thus the evaporation rate, the generator is cooled down by a cooling medium, usually air or water, to remove the heat of adsorption. On the other hand desorption is an endothermic process which means energy coming from a heat source should be provided to the adsorbent in order to take place. Adsorption in the left vessel stops when the adsorbent cannot absorb any more gas refrigerant, i.e. the solid material is saturated. At this point the high-gas-concentrated generator is ready to warm up again in order for a new refrigeration cycle to begin (Figure 2-13a) [46-48].

The solid-gas chemical sorption machines based their operation on the thermal effect of reversible physicochemical processes between the salt (adsorbent) and the refrigerant (adsorbate). For a chemical adsorption (thermochemical sorption) cycle, a chemical bond is created in between the adsorbate molecule and the adsorbent surface as a result of the chemical reaction. The forces involving chemisorption are similar to those during the chemical compound formation which are higher than the condensation heat of the refrigerant [42, 43, 49, 50]. During the reaction, electrons are transferred and atoms are rearranged resulting in that the adsorbate and adsorbent molecules never keep their

original state [43, 51]. The reversible physicochemical process is given in Equation 2-2 [52].

$$MX.nG + pG \; 2 \leftrightarrow 1 \; MX.(n+p)G + p\Delta H \qquad 2\text{-}2$$

MX from Equation 2-2 is the reactive solid salt (usually a metal chloride), G is the reactive gas (usually ammonia). ΔH is the heat of the chemical reaction (reaction's enthalpy difference) of the refrigerant at the end and at the start of each process. During the refrigerant's adsorption (synthesis) process, the MX.nG compound becomes a new solid substance [53], the MX.(n+p)G with different properties from the reactive salt and the refrigerant. During desorption, the MX.(n+p)G breaks back to the salt and releases ammonia vapour as well. ΔH is positive during the endothermic desorption process and negative during the exothermic adsorption process. ΔH depends on the stoichiometry of the equation (how many moles of refrigerant (p) are involved in Equation 2-2 and the state of the reactants involved. n and p are the number of moles of the refrigerant [52].

The equilibrium in the chemisorption is monovariant which means that pressure and temperature is a functional equation of one variable (Equation 2-3) [51]. That is translated as if the operating temperature is known, then automatically the working pressure is known as well and vice versa, no matter what the concentration is (amount of refrigerant). The working region between the adsorbent and the refrigerant is the solid-gas equilibrium line. As is indicated in Figure 2-13, for chemisorption there is only one line the S/G (Solid/Gas) equilibrium line to describe the reaction's concentration [42, 43, 51].

$$P = f(T)_{adsorbent} \qquad 2\text{-}3$$

For adsorption or desorption to take place, the adsorbent should be moved from its equilibrium S/G line. More specifically, for the adsorption-evaporation process to take place, the constraining temperature/ pressure should be at least just lower than the equilibrium temperature/ pressure of the adsorbent at the evaporation pressure of the refrigerant (L/G). In other words, for adsorption to take place, the adsorbent should be cooled down lower than the system's adsorption equilibrium, point A in Figure 2-14 [42]. The T_{ea} point indicates the equilibrium point at the S/G line where adsorption

starts for the selected working conditions. For the desorption-condensation process to take place, the constraining temperature/ pressure should be higher than the equilibrium's temperature/ pressure of the adsorbent at the condensation pressure of the refrigerant. In other words, for desorption to take place, the adsorbent should be heated at least to the desorption equilibrium point and more, as indicated in Figure 2-14. The T_{da} point indicates the equilibrium point at the S/G line where desorption starts for the selected working conditions. The equilibrium drop's increase (ΔT_{ads}, ΔP_{ads}, ΔT_{des}, ΔP_{des}) will result in the faster chemical reaction rate, adsorption or desorption. Points A and D are points away from T_{ea} and T_{da} which satisfy adsorption and desorption since ΔP and ΔT are established away from T_{ea} and T_{da} and the equilibrium S/G line as shown in Figure 2-14. At the S/G line, the refrigerant, the reactive salt and the new compound created appear all together, and adsorption and desorption take place in a way that cancels out each other since the reaction rates are similar. Away from the S/G line, both processes still take place at the same time but sometimes one is stronger than the other according to the working conditions [42, 43, 51].

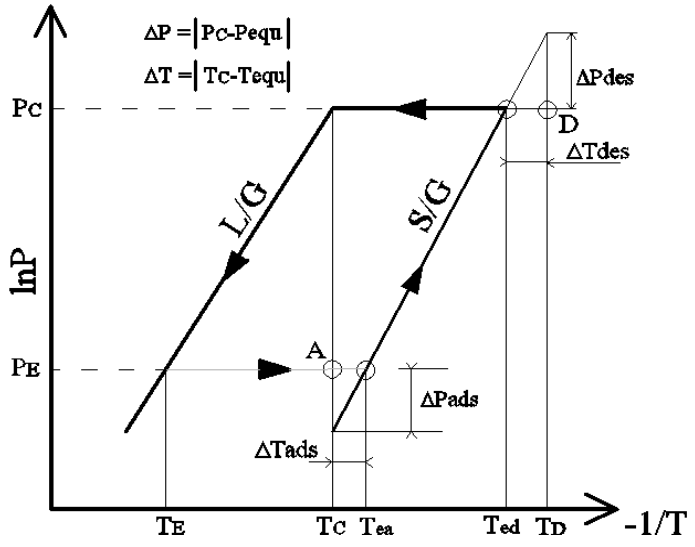

Figure 2-14: Monovariant characteristic of the chemical adsorption refrigeration cycle

The chemical sorption working pairs suffer from low heat transfer performance and poor gas permeability [51]. Phenomena like salt expansion (also called swelling [54]) appear which reduced the system's heat transfer [55]. Expansion is the excess volume possessed by the new compound created (MX.(n+p)G) during the chemical adsorption compared to the pure reactive salt (MX.nG). The other phenomenon is called agglomeration and affects the system's mass transfer. This appears as a result of the

new properties of the new compound formation compared to purifying the reactive salt. What is happening with the new compound is that its porosity is less compared to $CaCl_2$ which means the heat transfer increases (a smaller area to be conducted by heat) but at the same time the mass transfer decreases. Both expansion and agglomeration reduced the reaction's efficiency and are considered the most critical issue for chemisorption systems [51]. A design of a chemisorption system should be a compromise of these two phenomena.

The chemical working pairs appear to provide a greater adsorption quantity (quantity of the adsorbate adsorbed from the adsorbent) and higher volume cooling density per size of sorbent (cooling load per adsorbent volume) over the physical adsorbent. Therefore, the size of a chemisorption system can be theoretically reduced compared to a physiosorption one and therefore the cost for similar systems [49, 51].

Adsorption refrigeration in comparison to the conventional mechanical vapour compression systems has the benefits of saving energy in case wasted heat or solar energy is used. Also it has simpler control, offers no vibration and the operating cost is lower [56].

In comparison to the absorption refrigeration, the temperature range of adsorption refrigeration is wider. It can start from $50^{O}C$ and can be up to $600^{O}C$. Also, it does not require any pump or rectifier to run and that makes it simpler and more reliable. Normally, it does not have any corrosion issues and is sensitive to shocks and vibration which makes it ideal for a variety of applications. Furthermore, no crystallisation issues arise [56-58]

2.3 Chemical and composite adsorbents

The most common chemical adsorbents according to Wang, et al. [51] are the metal chlorides, the salt and metal hydrides, and the metal oxides. The selection of the adsorbent and the adsorbate is a matter of the system's utility, i.e. it operates as a heat pump or as a refrigerator and the heating and cooling power output. Composite adsorbents are those that are a mixture of a physical with a chemical adsorbent or a mixture of inner material with a chemical adsorbent.

2.3.1 Metal chlorides

There are many metal chlorides of which some can be found on the P-T Clausius-Clapeyron diagram which presents the equilibrium lines of metal chlorides with ammonia [59]. Ammonia is the most common refrigerant used with the metal chlorides. Salt expansion and agglomeration phenomena can appear during the chemical adsorption which affect the refrigerant heat and mass transfer to the adsorbent [51]. Some frequently used metal chlorides are $BaCl_2$, $MnCl_2$, $MgCl_2$ and $CaCl_2$ [60].

2.3.2 Salt hydrates and metal hydrates

There are four types of hydrates created when hydrogen reacts with most of the elements. These are the salt hydrates, metal hydrates, the covalent high-polymerized hydrates and the non-metal molecular hydrides. Only the first two can be used for adsorption refrigeration. The density of the metal hydrides is smaller than the density of a simple metal compared to the density of salt hydrides which are larger. The reason is the volume and the mass of the salt hydrides do not increase proportionally in the adsorption process [51]. Some commonly used salt hydrates are $MgSO_4$, $CaCl_2$, NaS and $Al_2(SO_4)_3$. Some metal hydrates used are $LaNi_5$, $Ti_{0.98}$ and ZrMnFe [60, 61].

2.3.3 Metal oxides

Metal oxides are mainly used for heat pump applications. There are four elements which influence the adsorption performance on the metal oxides' surfaces. These are the co-ordination number of the metal ion, the unsaturated degree of co-ordination, the direction of the chemical bond on the surface of the chemical material, the symmetrical characteristic of the transition metal's ligand field, the number of d electrons of the transition metal's ligand field, and the arrangement of the active centres. Metal oxides also suffer from expansion and agglomeration problems [51]. Some metal oxides are MgO and CaO [60, 61].

2.3.4 Composite adsorbents

The composite adsorbents are used to improve the performance of the physical and the chemical adsorbents. In the case of an original system including only a chemical adsorbent, they are mixed with a porous high-thermal-conductivity material (which can either be a physical adsorbent or an inner material) to reduce the expansion and agglomeration phenomena. Like that the low gas permeability and the refrigerant heat transfer to the adsorbent have been improved. The proportion of the composite adsorbent is a compromise between the adsorption capacity and the mass and heat transfer performance since the reactive salts have a higher adsorption capacity but lower

mass and heat transfer compared to a physical adsorbent [51]. The literature so far has mentioned the activated carbon, activated carbon with fibre, expanded graphite silica gel or zeolite frequently used as a materials mix with a chemical adsorbent. All of them have high thermal conductivity therefore ensuring good heat transfer while their large porosity increases the gas permeability and enhances the mass transfer as well [51, 62-64]. Also, materials like activated carbon have a high bulk density which helps to improve the system's volumetric capacity [65].

In a composite adsorbent, when a physical adsorbent or an inner material is mixed with a chemical adsorbent, the porous material starts to react with the refrigerant at the very early stage of the cooling or heating process and completes its action after the chemical reaction is finished. The pressure change in the reactor is fast and it starts before the salt begins to react with the refrigerant. A good porous material is responsible for the uniform pressure distribution in the reactor since it helps to distribute the microcrystal salt through the whole volume of the adsorbent bed during the adsorption and desorption periods. Like that, it allows the complete reaction to occur during the adsorption and desorption processes. The porous adsorption material is acting as a fast-reacting material which decreases the pressure drop between the cold production and desorption phase, thus increasing the system's performance, especially in the resorption system rather than adsorption [62-64, 66, 67]. The ideal active carbon sorbent bed according to L. L. Vasiliev et al., needs to have a micropore volume near 50%, solid carbon near 40% and a meso/ macropore volume near 10% [63].

The adsorbent's porous size (microporous) affects also the temperature lift during the adsorption-evaporation and desorption-condensation processes of a chemical adsorption cycle as well as during the adsorption (synthesis) and desorption (decomposition) processes of a resorption cycle. In general the smaller the micropores the higher the temperature lift. There is a limitation of how small the adsorbent's micropores can be because if they are too small they cannot receive the refrigerant molecules. The point at which desorption begins is only a temperature lift matter (chemisorption monovariant behaviour) [62]. In the case of the physical adsorbents, chemical adsorbents are mixed with them, in order to increase the adsorption's capacity. The $CaCl_2$ is a very common chemical adsorbent used to increase the adsorption capacity of the physiosorption adsorbent [61-63].

2.4 Chemical adsorption systems and current application

In this section will briefly discussed the chemical adsorption cycles found in the literature. The basic principle of an adsorption refrigerator (physical or chemical adsorption) is presented in Figure 2-15 which in principle consists of a reactor, an evaporator and a condenser. For the adsorption system, the processes take place between the liquid gas (L/G line Figure 2-14) refrigerant and the solid adsorption material (S/G line Figure 2-14) in the reactor in which the refrigerant is adsorbed or desorbed from there in gas form. This arrangement is called a *simple effect adsorption unit* [68] and presented in Figure 2-15 [51].

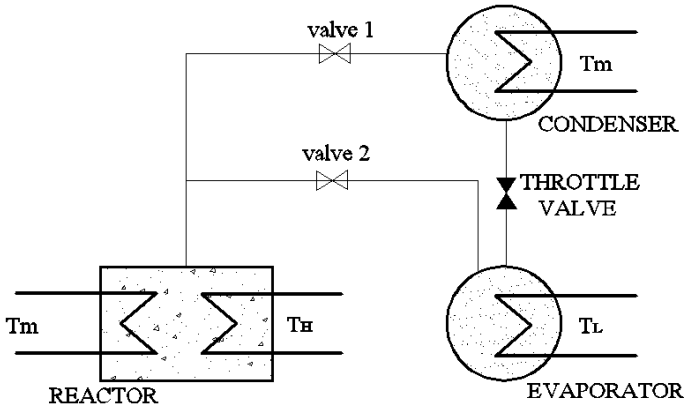

Figure 2-15: Basic simple-effect adsorption refrigeration system

In order to eliminate the liquid phase of the refrigerant in similar systems and for only a gas refrigerant to be transferred between each system component, the condenser and the evaporator have been replaced by a second reactor containing a material of different thermodynamic properties from the reactor [69]. That means at least two reactors are required which possess reactive salts of different thermodynamic properties [67]. The salt with the higher thermodynamic properties is called the High-Temperature Salt (HTS) and the other is called the Low-Temperature salt (LTS). This arrangement is called the *basic single effect resorption system* as shown in Figure 2-16 [70]. The cooling effect of a single effect resorption system is a result of the decomposition energy of the LTS. The resorption system in theory has a higher refrigeration power and COP than the adsorption system because the low-temperature salt decomposition reaction energy is higher than the latent heat of vaporisation of the adsorption system [70].

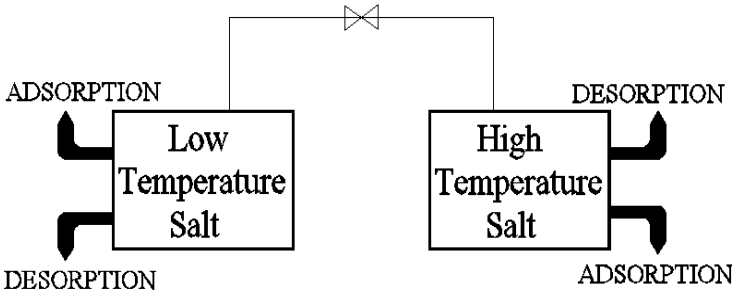

Figure 2-16: Single effect resorption system

According to Wang, et al. [70] if we compare an adsorption and a resorption system for similar working conditions and ammonia as the refrigerant, it is concluded that the mass transfer performance for a resorption during the LTS adsorption process (resorption) system is much lower than at the adsorption system resulting in a lower refrigeration performance. The reason is the lower reaction pressure develops at the resorption system for the same refrigeration temperature affecting the system's performance. The resorption system is also suffering from refrigeration power loss because of high sensible heat requirements of the low-temperature reactor (adsorbent and reactor material). Li, et al. [71] compared a resorption with an adsorption unit experimentally and found that the desorption rate of the resorption cycle is higher than the adsorption rate but, at the same time, the adsorption rate is lower for the same constraining temperatures. The results of Li, et al. [71] agree with the results of Wang, et al. [70] which are expressed as mass transfer performance rather than reaction rate.

Neveu and Castaing [72] introduced an *internal heat recovery adsorption system* where the adsorption heat of one reactor is used for the desorption of the other rector. V.Goetz., et al. [68] proposed an *internal heat recovery for a resorption system* by using three reactive salts: i.e. a high-temperature salt (HTS); medium-temperature salt (MTS); and low-temperature salt (LTS), and four reactors. The low-temperature salt reactors are connected once with the HTS and the other with the LTS. Therefore when the HTS is in adsorption mode, the energy released during the process is used for heating of the MTS which is under desorption mode at the same time.

Li, et al. [49] proposed a *two-stage desorption thermodynamic cycle* to reduce the regeneration temperature to the solid-gas thermochemical systems. This idea adds another secondary reactive salt of lower thermodynamic (LTS) properties to reduce the

desorption temperature, therefore the maximum constraining pressure during that phase. The results are that the refrigerant follows a desorption-condensation process, it desorbs at a lower temperature from the primary salt (HTS) and absorbs from the secondary salt at a lower pressure. For the desorption process to take place the equilibrium pressure of the primary should be higher than the secondary salt. Thus, by cooling the secondary salt to the same cooling temperature, the salt is prepared for adsorption, and by heating the primary salt the necessary pressure drop is prepared for desorption. The second stage is to desorb the refrigerant from the secondary salt for condensation to the same cooling temperature. Similarly in principle, *multi-stage desorption cycles* can appear using many salts of different thermodynamic properties.

Similar to the two-stage desorption machine, Li, et al. [55] examined a *two-stage sorption refrigeration system* using a *multifunction pipes* enhanced as well by a *heat recovery process*. The multifunction heat pipes in the reactive beds are used to improve further the mass transfer there, and the heat recovery process between the two reactors is performed by them. The pipes which provide the reactive bed with the hot and the cold streams are not the same (heat pipe). The one providing the hot stream is inserted from the bottom and afterwards the cool leaves from the bottom. The cold stream is provided from the top of the reactor and afterwards is warmed up as a result of the exothermic adsorption process, the stream is leaving from the top of the bed. Heat pipe technology also means that the hot and the cold streams in the system are provided from an internal circuit through heat exchangers instead of the heat source or the cooling circuit directly. That means the heat sources, hot or cold, are never directly fed into the system, but they are just its external circuit.

There are two heat recovery processes in this design. The first one is during the switch period of the HTS desorption to the LTS and the other one when the LTS is desorbed to the evaporator and the HTS absorbs refrigerant from there. During the switch period, the heat recovery valves connect the two reactive beds open resulting in the returning hot stream from the HTS to heat the LTS, like a pre-heating process.

The second heat recovery is during the second stage of the system where the LTS desorbs to the condenser and the liquid refrigerant is then moved to the evaporator and the HTS absorbs refrigerant from there. When desorption and adsorption finish, the

HTS which contains the refrigerant should be heated up for the next cycle, while the LTS should be cooled down. Therefore the second heat recovery in the system takes place to recover heat from the LTS to the HTS which is currently at a lower temperature and pressure than the LTS.

Li, et al. [59] also proposed a *double way chemisorption refrigeration cycle* based on adsorption and resorption processes. In this cycle, two different thermodynamic reactive salts are used, a condenser and an evaporator to obtain useful latent heat cooling during the resorption process so resulting in a large cooling capacity per unit heat input compared to a conventional adsorption and a resorption system. The working principle for this system takes place in between three working pressures. The first stage of the cycle includes the HTS to heat from an external high-temperature source so resulting in desorbing the refrigerant at high pressure to the condenser for condensation. The liquid refrigerant then moves to the evaporator while at the same time the LTS is undercooling to adsorb the refrigerant from the evaporator at a middle temperature resulting in the evaporator's cooling by the refrigerant's latent heat. The second stage takes place at low pressure and includes the resorption process between the two salts. The HTS is undercooling to adsorb the refrigerant from the LTS, so resulting in another cooling effect within the cycle, this time from the decomposition energy of the LTS.

Xu, et al. [73] proposed a *double*-way double-effect thermochemical sorption system which used three reactive salts, a high-, a medium- and a low-temperature salt resulting in four cooling effects in a single cycle. The cycle is enhanced by an internal heat recovery process as well. Except for the three reactive salts, the cycle contains another low-temperature salt, an evaporator and a condenser. The cycle is divided into two phases. The first phase consists of a desorption process from the HTS to the condenser, an adsorption process from the evaporator to the LTS2 (cooling effect 1), and a resorption process from the LTS1 to the MTS (cooling effect 2). The second phase consists of a resorption process between the LTS2 and the HTS (cooling effect 3), an adsorption process between the evaporator and the HTS1 (cooling effect 4) and a heat recovery process between the adsorption heat of the HTS which is used as a desorption heat of the MTS to desorb ammonia to the condenser.

Li, et al. [74] examined a novel $CaCl_2$ expanded graphite adsorption refrigerator. In that system, only three valves were used (two at the water and one at the ammonia circuit), so increasing the system's reliability. Also, the system is enhanced by the mass recovery process before the switch period from the high-pressure side to the low one.

2.5 $CaCl_2$ reaction with NH_3

For the complete reaction of $CaCl_2$ and ammonia (NH_3), 8 moles of NH_3 are required to react with 1 mole of $CaCl_2$. The adsorption and desorption processes of ammonia with $CaCl_2$ is actually completed in three phases based on the energy level each process requires. These processes can be explained using Figure 2-17 [55, 71] which is the P-T diagram of $CaCl_2$ with NH_3 for 2, 4 and 8 moles of NH_3 reacting with $CaCl_2$.

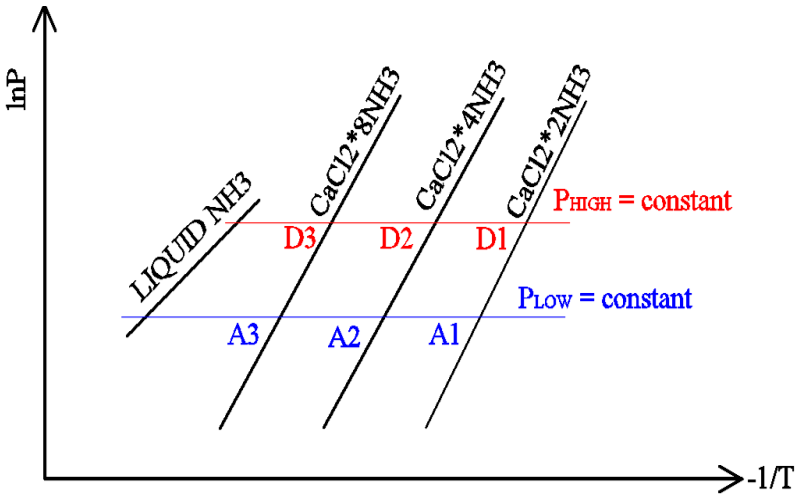

Figure 2-17: P-t diagram for $CaCl_2$ and NH_3

The three phases are the reactions between 0 and 2 moles of ammonia (phase 1) Equation 2-4, the second stage from 2-4 moles (phase 2) Equation 2-5 and the final stage from 4-8 (phase 3) Equation 2-6 [71].

$$CaCl_2 + 2NH_3 \leftrightarrow CaCl_2 \bullet 2NH3 \qquad 2\text{-}4$$

$$CaCl_2 \bullet 2NH_3 + 2NH_3 \leftrightarrow CaCl_2 \bullet 4NH_3 \qquad 2\text{-}5$$

$$CaCl_2 \bullet 4NH_3 + 4NH_3 \leftrightarrow CaCl_2 \bullet 8NH_3 \qquad 2\text{-}6$$

Figure 2-17 indicates the conditions for adsorption and desorption to take place for each of the three reactions related to the working conditions (pressure and temperature). The

reactions shown in Equations 2.4, 2.5 and 2.6, and can take place if the adsorption (A1, A2 and A3) and desorption (D1, D2 and D3) temperatures from Figure 2-17 are satisfied by the heat sources available. This means for adsorption to take place the cooling heat source temperature should not be greater than A1, A2 and A3 and for desorption to take place, the heat source temperature should have as minima the D1, D2 and D3 values.

In order to achieve 8 NH_3 moles in a compound of $CaCl_2.8NH_3$, a $CaCl_2$ compound with 2 moles of NH_3, initially $CaCl_2.2NH_3$ will be formed (phase 1), and then 4 moles of $CaCl_2.4NH_3$ (phase 2) and finally 8 moles (phase 3). The conditions for these three reactions have to be satisfied by the adsorption temperature level as described in Figure 2-17, i.e. A1, A2 and A3 respectively. The rates of the adsorption and desorption processes are strongly dependent on the cooling water and heating temperatures. The reaction enthalpy for phase 2 is 40.9 kJ/mol and for phase 3 it is 39.6 kJ/mol [50].

For a chemisorption system using $CaCl_2$ salt, the rate of adsorption for phases 1 and 2 is faster compared to phase 3 assuming the same cooling temperature. The reason is that it is easier for the molecular structure of $CaCl_2$ to attempt to bond to ammonia when initially it is free (single molecule) and as a result the bonds created for the first 4 moles of ammonia with the $CaCl_2$ are very strong compared to the bonds created later on in phase 3. The stronger bonds created in phases 1 and 2 can be confirmed by the reaction's enthalpy from 0-4 moles of NH_3, which is more than the reaction's enthalpy in phase 3. This means that more energy is required to split the molecule during desorption [50]. As more ammonia is attached to the $CaCl_2$, the bonding forces become weaker because ammonia molecules are attached at a bigger distance from the $CaCl_2$ nucleus.

Adsorption is an exothermic process and as its rate is decreased, the heat of adsorption decreases as well. As more ammonia is compounded with the $CaCl_2$, the heat of adsorption is decreased and the ammonia bonds with $CaCl_2$ become weaker so resulting in a lower adsorption temperature to ensure the continuation of the process. The temperatures A1, A2 and A3 in Figure 2-17 are according to the heat of adsorption required for each of the three processes to be completed and depend on the bonds between the $CaCl_2$ and NH_3 in each phase. The adsorption capacity is higher for 0-4

moles of NH_3 compared to 4-8 moles for the same cooling temperature. The stronger the bonds are, the higher the adsorption capacity and the more the heat of adsorption [50].

For the desorption process the opposite from adsorption is true. Since the bonds of the $CaCl_2$ with NH_3 for 0-4 moles of NH_3 are stronger than 4-8 moles of NH_3, higher desorption temperatures are required for the 4-0 compound moles for desorption to take place, compared to the 8 moles. Therefore, for a fixed heating temperature, the desorption process is more efficient when considered from 8-4 moles of ammonia.

2.6 Existing expansion machines

The selection for any expansion machine is determined by the size of the system and the working conditions. For the LH cogen case low flow rates, high pressure and low heat are the system's characteristics. Expanders can be categorized as a dynamic velocity type like an axial turbine expander or displacement volume type like a screw expander and a scroll expander. The volume-type expanders are considered more suitable for ORC applications because they can deal with lower flow rates, offer higher pressure ratings and much lower rotational speeds compared to the velocity type [75]. For this analysis I will mainly focus on the scroll expander but also briefly talk about turbine expanders; a screw expander and air motor operate as an expander.

2.6.1 Turbine expander

The turbine expanders usually called micro high speed turbines are a velocity type and are actually a scaling-down of the turbines used for big power plants similar to Figure 2-18. Their operation principle is simple and includes the high-pressure working fluid which drives the turbine blades which turn the turbine. They offer a compact and simple lightweight design, good manufacturability, high efficiency and a single stage rate which indicate a big expansion enthalpy drop. On the other hand, they are generally applied at 50kWe and more and for smaller applications like 10kWe the efficiency is low. Also, the smaller the size the more expensive it becomes. At the same time, their rotational speed is high which might result in reliability issues and also will require a gearbox to match the generator's rotational speed. Smaller scale turbines are under investigation but for now are not considered an option since they are still in the R&D stage. Turbine expanders are generally used on occasions where low flow rates are available and small power outputs are required [75-78].

Figure 2-18: Typical microturbine

2.6.2 Screw expander

Screw machines are positive displacement machines which usually operate at high speeds. They mainly operate, designed as lubricating compressors, but reversing their operation can make them operate as expanders also. Their simple configuration consists of a pair of male and female helical rotors which have a clearance of 50μm and are contained in a casing. The clearance of the rotors and the casing determine the flow rate and the efficiency is determined by manufacturing limitations (Figure 2-19). As the rotor rotates, the fluid is trapped in between them and the casing and, according to the rotor's direction, it can operate as either a compressor or expander. Screw machines offer long lifetimes, a high volumetric efficiency, low noise and low vibration. Even though experimental units of 20-50kWe have been developed, at the current stage they are hard to obtain in the current market therefore are more suitable for high power production. Their installation cost is low (around $1500 to $2000kWe) because they are easily installable [75, 79, 80].

Figure 2-19: Screw set operation principles

2.6.3 Air motor as expander

Air motor vane rotary machines were initially used to compress air in order to drive a rotor. When operating in reverse they can operate as expanders. This is the working principle of the air motor shown in Figure 2-20. The expansion process happens between the cylinder wall and the sliding vanes. The high-pressure working fluid enters the inlet port, feeding chamber A, and the space between them increases with the rotor movements due to pressure differences with the other chambers. The working fluid expands in the other chambers and leaves the expander from the outlet port. The rotor consists of 4 longitudinal slots in which the vanes are free to move (slightly) outwards by centrifugal force against the cylinder wall and the rotor. Operating an air motor as an expander results in losses which without the necessary modifications make the machine inefficient. Precautions should be taken to make sure the contact between the vanes and the cylinder wall is tight, also to feel the gap between the suction and the discharge port. These seals will maintain a pressure difference in the machine and will ensure the flow rate. This kind of machine has a simpler structure, is easy to manufacture and the cost is low. It mainly needs lubrication to run but some free oil with very good performance can be found as well [75, 81, 82]. For a modified air motor, the volumetric efficiency was 30% and at the same time the isentropic efficiency was 23% at 800rpm speed [82].

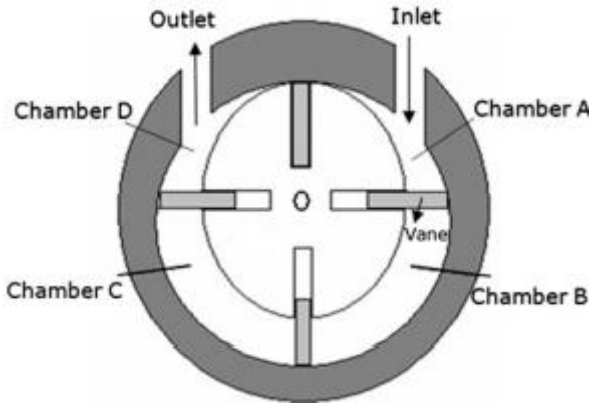

Figure 2-20: Vane type expander

2.6.4 Scroll device

A scroll device is made of two identical involutes (two scrolls) assembled together with a phase difference. One scroll is inverted, rotated and inserted into the gaps of the second scroll as presented in Figure 2-21 [83]. The design consists of the “fixed scroll” and the “orbiting scroll”. During the scroll operation, the fixed scroll always remains stationary and the orbiting scroll is eccentrically attached to a motor shaft, allowing an

orbiting rotation motion within the fixed scroll. The phase difference between the two scrolls is maintained by using an anti-rotation device [83-86].

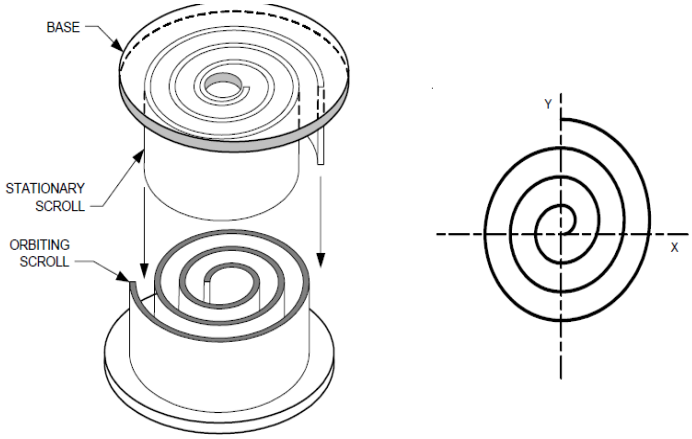

Figure 2-21: **A scroll set and a simple spiral**

Scroll devices have been widely adapted in the HVAC industry to operate as compressors. Scroll compressors have a simple design (fewer moving parts without including any valves), low friction, low torque pulsation and compliance, reliability and low cost due to high volume production. The continual compression results in a smoother power output and consequently less noise and vibration than a piston type device [85-87]. A scroll compressor that is converted into an expander has nearly the same advantages as a scroll compressor i.e. no valves, no self-starting and fewer moving parts [86].

When a scroll device operates in a compressor mode (Figure 2-22) [88], the low-pressure working fluid enters at the periphery of the two scrolls and moves towards the centre. As the moving spiral orbits, the volume between the two spirals is reduced. That results in the fluid's being trapped there and moving toward the centre. The pressure of the fluid is increased as it moves and it is then eventually discharged through the discharge port [85, 88].

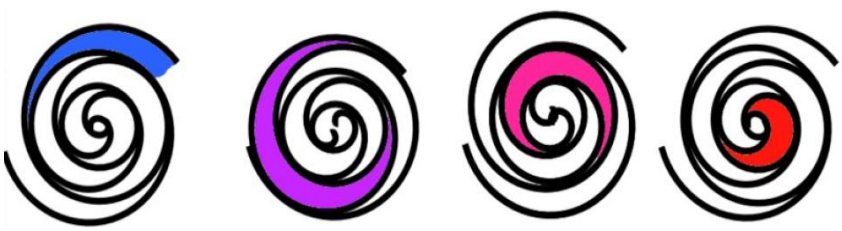

Figure 2-22: Scroll compressor working principle

When a scroll compressor is converted into an expander (Figure 2-23) [84], the device is simply operated in reverse. That means the high-pressure working fluid is inserted into the scroll from the smaller-diameter port located at the centre (originally the discharge port of the scroll compressor). The fluid is then expanded steadily so increasing its volume (points 2-5). At point 6, a low-pressure low-temperature high-volume working fluid exits the device through the biggest-diameter port (intake port of the scroll compressor) at the periphery of the two wraps [84, 86].

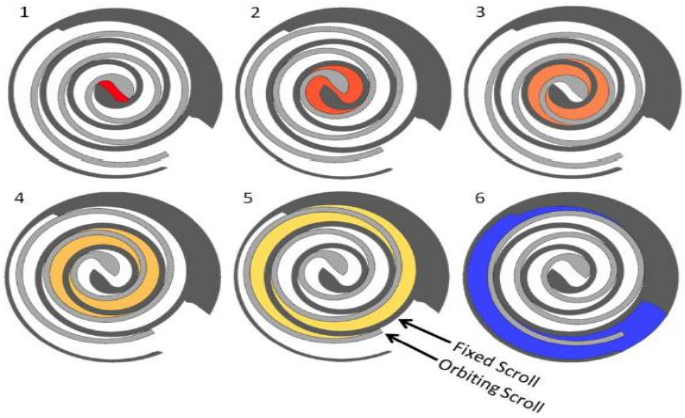

Figure 2-23: Scroll expander working principle

2.6.4.1 Scroll device classification

Scroll devices can be classified as kinematically constrained (also called non-compliant or controlled orbit design) [83]. In a *kinematically constrained* device, the orbiting scroll follows a fixed path where the orbiting and fixed scrolls are never in contact. There is no compliance in the relative positions of two scroll wraps and manufacturing tolerances are critical to minimise the gap at the point of near-contact between the two scrolls. This means a small clearance gap is always maintained between them which remains the same for any operating conditions. A tip seal is used to prevent air leaks though the clearance gap and resist axial leakages. Usually a three crank arm (set 120^0 apart) and a linkage mechanism are used to allow the orbiting scroll to move relative to the stationary one. The amount of radial (flank) leakage is minimised only from the low tolerance of the wraps. For this kind of device, an oil film is not always required to provide a gap-filler between the scrolls. If it does, this is the device's sealing

mechanism. Kinematically constrained scrolls do not employ a centrifugal effect [83-86, 89].

Compliant technology design uses a sliding surface contact which always uses lubricating oil at the interface. The radial compliance appears from the centrifugal effect on the orbiting scroll which pushes its wrap into contact with the fixed scroll. The axial compliance can be achieved by applying an axial force on top of the fixed scroll which is pressing it onto the orbiting scroll. This allows minimal leakages when lubrication is used so promoting sealing reduction. Compliant design uses less lubricant because the rolling contact provides a seal so large that volumes of oil are not required. Therefore, leakage is reduced so promoting axial and radial sealing and so minimising friction and wear to reasonable levels [83-86, 89].

The term compliance is used to define the interaction (contact mechanism) of the two scroll wraps during operation. An axial compliance compressor has the ability to separate axially the orbiting and stationary scrolls. A radially compliant compressor allows the orbiting scroll to follow a flexible path so resulting in the contact with the orbiting scroll. In a non-complaint compressor, the scrolls follow a flexible path and are never in touch axially or radially [83].

Compliant scrolls can provide better radial and axial sealing than the kinematically constrained because the scrolls are only separated by a lubrication film. Also compliant scrolls are tolerant of liquids and allow them to increase the gap size if excessive pressure builds up inside the device. Most high-efficiency scroll compressors for residual heat pumps are compliant in design and they require an initial spinning motion to engage the scrolls [83-86, 88, 89].

2.6.4.2 Converting a scroll compressor to expander

There are several decisions to be taken before a scroll compressor can be converted into an expander. In general, the power output of the scroll expander depends on irreversibilities (losses) related to leakages between the interfaces of the two wraps (axial losses) and between the scroll vase tip (the free involute scroll edge) with the opposite scroll base plate (radial losses) and also from heat transfer interactions between the working fluid and scroll material (Figure 2-24) [83]. From all the losses, the most crucial are considered to be the axial leakages. The leakage point can be at the same

time friction contact points. The need for radial and axial sealing is important to ensure device performance and keep wear at the points of contact in acceptable levels [83, 84, 88]. If those losses are reduced, lower exhaust working fluid pressure and temperature can be achieved which are translated as more work done by the expander [84, 85, 88]. The leakage increases power consumption, leads to capacity reduction and results in lower efficiency [83]. Some studies used the term internal leakages to describe the radial and flank leakages [87].

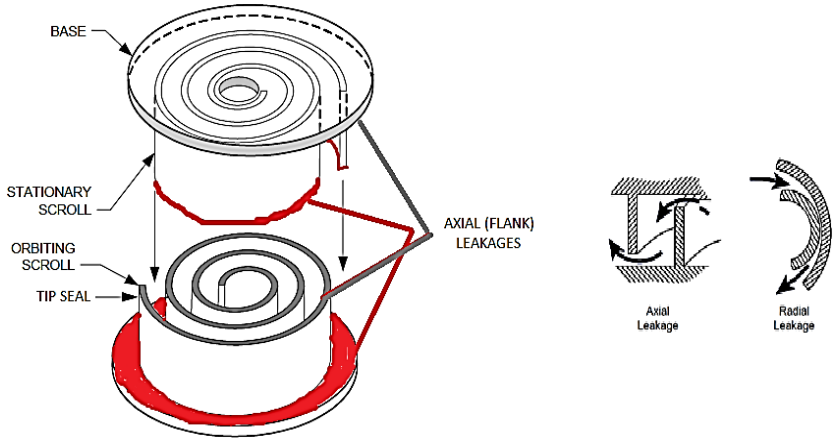

Figure 2-24: Main leakage mode of a scroll expander

Radial sealing for a kinematically constrained device can be achieved from a precise scroll profile which ensures scroll flank tightening. The use of CNC machines can provide this precise profile where the geometry maintaining tolerances are measured in microns. The tolerances are so precise that a thin lubricant film seals the gap and provides a lubricating surface for the orbiting scroll to pass over with minimum friction and wear. As mentioned above, the compliant design uses the contact between the scrolls as a sealing mechanism. This design requires a 'wear-in' period, when it is new, so all the surfaces and all the contacts can to be uniformly in contact [83, 85].

Axial sealing for a kinematically constrained device is provided by maintaining dynamic contact between the orbiting vane tips and the stationary base plate with floating seals. Grooves machined into the vane tips hold the seal elements that float between the vane and the opposite base plate can be used as an axial sealing mechanism. Compliant design uses gas pressure to load the stationary scroll against the orbiting scroll. This results in dynamic contact between the orbiting vane tips and the

stationary base plate to provide allowances for thermal growth and wear. The use of a lubricant at the point of contact results in very small contact forces because of a combined reduction in contact surface area. Thus friction is reduced and the device's efficiency is increased [83].

To deal with these irreversibilities, a lubricant scroll device is preferable rather than the oil-free one. Another solution is to replace the lubricant oil by axially and radially sealing the affected contact areas according to the suggestion of Thomas C. B. Smith [90].

When a scroll compressor is operating (mainly the kinematically constrained), the oil is swept 'up'. That means the oil can deal with the low pressure of the intake so the lubricant can be carried into the scroll wraps along with the intake flow. When a scroll compressor operates as an expander, during the expansion operation of the device, the oil is swept 'down'. That means that the lubricant cannot deal with the high pressure conditions at the expander's intake thus the lubricant itself does not have the necessary potential to be carried along with the intake flow. Therefore operating a scroll compressor in reverse will lead to excessive leakage (a bigger gap between scrolls) of the working fluid through the gaps since lubrication cannot be ensured. To solve this, the oils should pump the refrigerant at the intake and be carried to the device along the intake flow [85, 86, 90]. The oil should be collected at the exit of the device and pumped again to the intake. Working in expander mode, the pressure and the temperature of the working fluid are possibly higher than those in compressor mode. Therefore, lubrication and oil management is essential. Proper oil management will also provide the required sealing [85, 86].

Another thing to be considered is the check valve (one-way valve) located on the scroll compressor to prevent back flow, usually located at the exit of the compressor. It is a safety precaution to prevent high-pressure fluid entering the low-pressure chamber for the scroll compressor. In case the device reverses its operation as an expander, this check valve should be removed [84].

The expander selection must be sized correctly for the ratio of the flow rate and the operating pressure to lead to the maximum power output [85]. A scroll compressor in

reverse achieves up to 84% maximum isentropic efficiency for certain working conditions [91]. We have in mind that a scroll expander (originally a scroll compressor) has been designed to compress and not to expand the working fluid.

So far a scroll expander has been tested as a power generation medium mainly in an Organic Rankine Cycle to investigate the potential of an alternative to turbine power generation using low- to medium-heat sources [86, 89, 92, 93]. Also a hermetic arrangement (expander and generator sealed together in a box) was tested in the same direction [94, 95].

2.6.5 Expansion device selection

From the above analysis regarding the expansion devices, the turbine is not considered an option since for low power production the turbines are still in the research stage and offer low efficiency. A screw expander and air motor can be an option but since at the moment the market do not offer an expander itself but compressor running in reverse, that means modifications are required to run it as an expander.

The selected expansion device is the scroll expander which researchers focus more than the screw or vane expander because has a very simple design, it is small and compact and that make it convenience to be easily attached to the adsorption chiller. Carry minimum rotational part so increases its reliability level and by design there is an oil free type which is ideal for our case. The one used for the experiments is 1kW oil-free scroll expander provided from the Air Squared company [96] carries an AC/DC generator and is ammonia compatible also. Requires no modification since is design as an expander and is not a compressor running in reverse and the overall cost including the generator was around $3000.

2.7 Refrigerants

There are four main refrigerants tested so far for the adsorption technology and their selection is based on the application – cooling or heating. According to Wang, et al. [51], the properties of a suitable refrigerant to use for solid gas systems are the high latent heat (enthalpy) of vaporisation (h_{fg}), which provides the cooling effect, should be thermally stable which means the molecules stay stable at the system's high temperature, not be restricted by having high ODP, being non-flammable, innoxious and having the saturation pressure to be from 0.1 to 0.5MPa for machine-safety reasons in case of a leak. For a chemical adsorption refrigerator, the most common refrigerant is

ammonia mainly paired with a chloride-based reactive salt. Also hydrogen or water uses metal hydrides as an adsorbent, as well as water or oxygen using metal oxides as an adsorbent [51, 60, 61, 97].

For a power Organic Rankine Cycle the parameters that should be considered to select a suitable refrigerant include the curve of saturation where isentropic (vertical) or dry (negative) fluids are considered more suitable rather than wet (positive) fluids since at the end of the expansion process no liquid appears at the expansion device's exit. Also the critical point (pressure and temperature) that should be associated with the heat source so the refrigerant is not above its critical point is a lower freezing point that lowers the cycle's temperature, high latent heat and molecular weight which means more energy can be absorbed from the heat source and that reduces the required flow rate, environmental (ODP-related), stability and safety (non-toxic, non-flammable, not auto-igniting and not a chemical reaction). Also it should be easily available, be as cheap as possible and also be compatible with the system's components [14, 98].

In general, a working fluid should offer high cycle efficiency, high density, low specific liquid heat, high latent heat, and high density which will maximise the turbine's (or any other rotary power medium's) efficiency. Also it should have good thermal stability, a small environmental impact and not be flammable. We have in mind that the critical point is another important parameter which affects the condensation process as does the power production. Assuming ambient conditions for the system's condensation temperature, for refrigerants with a boiling point below that temperature, the condensation process is an issue. The freezing point of the selected refrigerant should be much lower than the system's lower temperature. Auto-igniting refrigerants are good to be avoided. We have in mind that the molecular weight suggests the density of the fluid and the critical point suggests the operating conditions, i.e. pressure and temperature [14, 99]

Based on Jorge Facao [99] water is the best working fluid in terms of efficiency but it is a wet fluid and we suggest tuluene, cyclohexane and n-pentane. Based on the work of Chacartegui, et al. [100], tuluene and cyclohexane present the highest efficiency but require specially designed turbines to deal with the fluid properties. Yamamoto, et al. [16] suggest that HCFC-123 improves the low-heat ORC cycle's performance. Pei

Gang [101] suggests that the best fluid for ORC performance between R123, R113, R245fa, pentane and butane, R113 offers the maximum ORC performance. Madhawa Hettiarachchi, et al. [11] suggest that ammonia has a minimum objective function (measure of a power plant's cost) and maximum geothermal water utilisation, but not necessarily a maximum cycle efficiency. Exergy analysis shows that the efficiency of the ammonia cycle has been more compromised in the optimisation process than that of other working fluids. HCFC 123 and n-Pentane have a better performance than PF 5050, although the latter has the most preferable physical and chemical characteristics compared to the other fluids considered.

For the purpose of this study, even ammonia might not be the best refrigerant for an ORC system since it is toxic and has a low molecular weight and that increases the heat input required but on the other hand it is preferable for a chemical adsorption cycle. It is a wet fluid so some liquid might appear at the expander exit therefore the scroll expander should be able to deal with it. On the other hand it is cheap, has a high critical pressure and temperature, high specific heat, high latent heat and produces more power compared to other refrigerants. Most important it has a very good match with the reactive salt [14, 102]

2.8 LH cogen system fundamental theory

This section will identify the basic equations to describe the LH cogen system. The equations provided mainly describe the adsorption chiller and the expander. The equations which describe the adsorption chiller include the equilibrium equation for the $CaCl_2$ and NH_3 reaction, the adsorption physics the conversion rate during adsorption and desorption, the ammonia quantity adsorbed and the equation to estimate the heating and the cooling power. Equations to describe the scroll expander include the mass flow rate and the power.

The basic reversible thermochemical equation for any reactive salt with ammonia is given from Equation 2.2. Equation 2.7 [103] desribes the equilibrium pressure drop for the $CaCl_2$-NH_3 reaction. It provides the equilibrium pressure at each the equilibrium line from 0-8 moles of ammonia by fixing the temperature (Figure 2-17). At the equilibrium line no adsorption or desorption takes place since both processes occur at the same rate so they cancel each other. This equation uses the reaction enthalpy (ΔH), the reaction entropy (ΔS), the ideal gas constant (R) and the reaction temperature (T). The

adsorption and desorption takes place away from the equilibrium line plotted from this equation as explained previously.

$$\mathbf{lnP_{eguil} = \frac{\Delta H}{RT} + \frac{\Delta S}{R}} \qquad \textbf{2-7}$$

Equation 2.8 [104] is useful to estimate the adsorption enthalpy which is roughly similar to the desorption enthalpy. The h_{fg} is the ammonia enthalpy of vaporization, A is termed the adsorption potential which describes the adsorption conditions (pressure and temperature), α is the linear thermal expansion coefficient of the refrigerant in the adsorbent state and Z is the adsorption volume which describes how much vapour can be adsorbed.

$$\mathbf{h_{ads} = h_{fg} + A - T*\alpha\left(\frac{\theta A}{\theta \ln Z}\right)_T} \qquad 2\text{-}8$$

The adsorption and desorption rate is not the same. Even though, it may be assumed that that for repeated cycles the ammonia quantity adsorbed and desorbed is the same for a fixed cycle time, the rate of these reactions are not similar. Equation 2.9 and Equation 2.10 [105] describes the kinetics of the adsorption and desorption processes calculating the conversion rate (χ). Ideally during adsorption, the conversion rate can take values from 0-1 and during desorption from 1-0.

$$\mathbf{\frac{d\chi}{d_t} = A_r * (1-\chi)^{Mr} \frac{Pc - Pegui(T)}{Pc}} \qquad \textbf{2-9}$$

$$\mathbf{\frac{d\chi}{d_t} = _{Ar} * \chi^{Mr} \frac{Pc - Pegui(T)}{Pc}} \qquad \textbf{2-10}$$

In Equations 2.9 and 2.10, the A_r is called the Affhenius factor which describes the correlations between the reaction velocity and the working temperature, M_r indicates the influence of the vacant sites on the reaction progress and P_c is the constraining pressure.

Equation 2.11 calculates the cycle adsorption quantity (Δx_{NH3}), which is similar to the desorbed ammonia for infinity cycle tome.

$$\Delta\chi_{NH3} = \frac{Q_{ref}+Q_{NH3}+Q_{me}}{m_a \Delta H + Q_a} \quad \textbf{2-11}$$

Equation 2.11 considers the adsorbent heat transfer in the reactor ($Q_{adsorbent}$), the ammonia heat transfer at the evaporator (Q_{NH3}), the evaporator metal material heat transfer (Q_{me}) and the refrigeration cooling (Q_{ref}). The heat transfer equation (Q) is given from Equation 2.12 [12, 106].

$$Q=mcp\Delta T \quad \textbf{2-12}$$

The last two equations to describe the system response are the useful cooling production (Q_{ref}) and the heating power (Q_{high}).

$$Q_{ref}= n_s\gamma_s\Delta H(T_e) – (H_cT_c-H_eT_e) \quad \textbf{2-13}$$

In Equation 2.13, n_s is the number of moles of the reactive salt, γ_s is the ideal number of moles of refrigerant consumed per mole of reactive salt, ΔH is the vaporization enthalpy of refrigerant, T_e is the evaporator temperature, H_cT_c is the refrigerant enthalpy at condensation temperature and H_eT_e is the refrigerant enthalpy at evaporation temperature.

$$Q_{high}=n\gamma\chi_{deso}\Delta H_{deso}+nMrcp_a(Td_{-h}-T_{a-h})+cp_{ac}m_{ac}(Td_{-h}-T_{a-h})+cp_{mr}m_{mr}(Td_{-h}-T_{a-h}) \quad \textbf{2-14}$$

In Equation 2.14 the first part provides the reaction heat during desorption, the second part provides the sensible heat during desorption, the third part denote the sensible heat of the activated carbon (inner material used) and the last component provide the sensible heat of the reactor metallic part. The last two equations consider everything that the evaporator and the reactor is constructed which means the losses at the various components for the evaporator and the reactor can be estimated.

During cogeneration, the expander inlet pressure is the main parameter affects the system power generation. This is direct related to the maximum pressure limit of the suction chamber which might not exceed the desorbed ammonia pressure.

The theoretical expander mass flow rate which includes no leaks can be estimated from Equation 2.15 [107] where ρ_s is the refrigerant density at the inlet of the expander, N is the expander rotational speed and the V_{in} is the is the inlet chamber volume.

$$\dot{m}=\rho_{in}NV_{in} \quad \textbf{2-15}$$

The isentropic expander power can be calculated using Equation 2.16, in which $\dot{m}_{in}$ is the refrigerant mass flow rate at the expander suction, h_{in} is the refrigerant enthalpy at the expander suction and h_{out} the refrigerant enthalpy at the expander outlet.

$$W_{is}=\dot{m}_{exp,in}(h_{exp,in}-h_{exp,out}) \quad \textbf{2-16}$$

2.9 Summary

From the literature, no similar chemical adsorption cogeneration system's experimental study was found. The proposed system has a simpler design and is more compact than the Kalina and Goswami cycles since no pump is used for the refrigerant, no separator or rectifier or any expansion valve is required. Compared to the ejector based cogeneration cycles, it has a simpler design and less components are required by the absorption-ejector cycle. The LH cogen system has been designed to examine the potential to produce power in the range of 1-3kW for lower flow rates and using a lower heat source around 100^{O}C instead of 300^{O}C. Compared to the Diesel-absorption cycle, the LH cogen system has a more compact design and no need to burn diesel fuel so a greener primary energy input can be used since the main heat input can be from renewable, waste heat or geothermal. The resorption cogeneration system heat input operates at 250^{O}C or higher, which is beyond range of the LH cogen system heat source since no super heater is present.

Most of the cogeneration ideas found in the literature for power and cooling are theoretical or simulation studies and only some Kalina and Goswami cycles are actually in operation but no actual data is shared. All of the ideas produce cooling and power from a single cycle but the LH cogen system produced from power and cooling from two adsorption cycles operate parallel without interact to each other. That expects to increase the overall cogeneration system performance.

A scroll expander was selected to be attached to the machine for power production. Among other expanders, the selected one was originally designed as an expander and is not a compressor running in reverse. Also, it is compatible with ammonia and therefore no modification is required to run. Scroll expander is small and compact with a minimal rotational parts and that increases its reliability.

For the proposed LH cogen system, the selected adsorbent bed is a composite mixture of calcium chloride ($CaCl_2$), and activated carbon and ammonia are the selected refrigerants. The $CaCl_2$ is a common material widely used for similar machines to utilise low- to medium-heat sources to be regenerated (desorbed) easily compared to other reactive salts for similar temperatures. It is also readily available and is inexpensive. The $CaCl_2$-NH_3 pair can provide a high adsorption capacity compared to other salts. Furthermore, active carbon is a cheap physical adsorption material which is used extensively to improve chemisorption systems' performance. It can increase the system's mass and heat transfer resulting in a more stable cycle operation. The activated carbon also offers no corrosion of metals compared to other chloride chemical adsorbents [65]. Furthermore, the adsorbent lifetime is increased since the composite mixture can reduce significantly the phenomena of salt expansion and agglomeration [108]. Ammonia (NH_3) is the selected cycle's refrigerant because of its good thermodynamic properties (high enthalpy of vaporisation) and because at the cycle's low working conditions, ammonia's pressure is higher than the atmospheric. An oil-free scroll expander is the system's selected power medium to satisfy the expected low flow rates during the desorption process.

Chapter 3. Experimental Apparatus and Test Plan

3.1 Introduction

This chapter will provide all the necessary information regarding the system's experimental set-up used for this project. The analysis will include figures and photos for each test rig and detail explanations of their purpose. More specifically, the LH cogen system was initially tested for its cooling and later for its cogeneration performance. Also, the scroll expander itself was tested by using nitrogen under different conditions. The components and the sensors installed will identify the machine components as well.

For the purpose of this project, a low heat-driven cogeneration chemical adsorption machine was designed and manufactured in order to evaluate the cooling and the cogeneration system's performance. The LH cogen is designed to produce 3kW of cooling and 1kW of power by utilising low-heat sources. It is a continuous refrigeration production chemical adsorption chiller which used its condensers and the adsorption process on the low-pressure side to produce power as well, thus expanding the ammonia refrigerant in a scroll expander. Water is used a medium fluid to provide heating and cooling to the system.

The main test conditions include heating and cooling temperatures and cycle time in order to identify the refrigeration and the cogeneration system's performance. The inlet pressure and temperature were the parameters for investigating the scroll expander's performance tests. Data from all the experimental results will be used for the cogeneration simulation program.

3.1.1 Cogeneration experimental set-up

The LH cogen system concept is to utilise the refrigeration's performance of an existing chemisorption adsorption chiller consisting of two sets of adsorption cycles operating at an offset at which during the high pressure period the refrigerant expanded in a scroll expander while the other side produces cooling. To secure the power production, the refrigerant will condensate using the chiller condenser or will be adsorbed from the current low-pressure reactor. The design is kept as compact and simple as possible, with minimal electronic parts. In that direction, a new design was created by using pipes and

manual valves to connect the reactors to the expander. The machine performance is enhanced from a mass recovery process between the system's high- and low-pressure evaporators, either during the only-cooling or cogeneration modes. The adsorption unit was built in China with the collaboration and the expertise of the Shanghai Jiao Tong University and carries all the necessary instruments at various positions to provide useful data.

A set of plans was scheduled to investigate the system's cooling and cogeneration system performances as well as the scroll expander's performance individually. The tests listed below are in the order presented in this study:

1) LH cogen cooling performance;
2) LH cogen cogeneration performance;
3) Scroll expander's power generation performance.

When performing test a) Was examining the system refrigeration performance for different reactor high temperatures, cycle times, the ammonia mass the machine carries and the required evaporator refrigeration. The data include the system's heating power (Q_{high}), refrigeration power (Q_{ref}) and pressure and temperatures at various points. There were also calculated the refrigeration coefficient of its performance (COP_{ref}) and specific cooling power (SCP).

When performing test b) the power (COP_W) and the cogeneration (COP_{cogen}) performance of the system were investigated since now the scroll expander is connected to the system. The data now also include the expander's inlet and outlet refrigerant pressure and temperature and the expander's power output given from the power meter connected to it.

When performing test c) the expander was tested for its power performance when running with nitrogen for various inlet pressures and temperatures for the same outlet expander's pressure. The collected data include the expander's power generation from using a power meter, the nitrogen's inlet pressure and temperature in the expander as well the outlet temperature.

The LH cogen system schematic is presented in Figure 3-1. In this figure are shown all the system's components, the working fluids and the instrument positions. The black line represents the heat exchange fluid route (water). The blue dotted line represents the refrigerant route (ammonia) during the only-cooling mode and the green dotted line the ammonia path during cogeneration. The modifications required for power production as well are shown on the green dotted line. All the data were recorded using data acquisition and additionally a power meter was used to record the power during cogeneration.

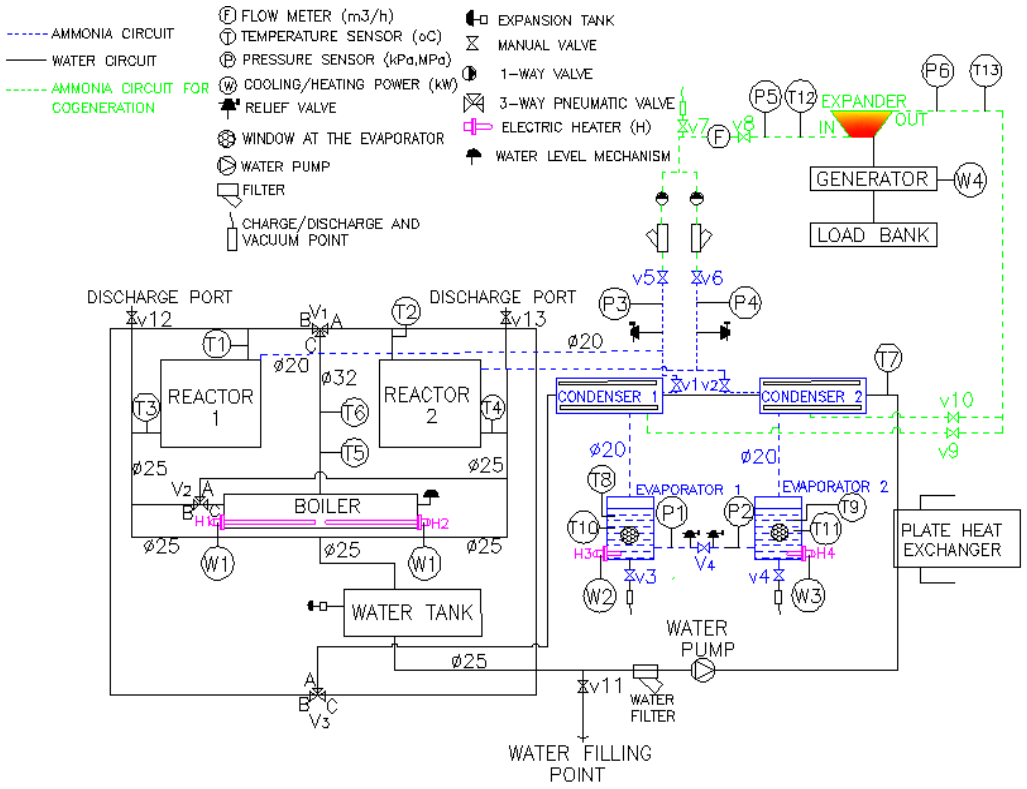

Figure 3-1: LH cogen system schematic

The system possesses a number of manual valves in order to function efficiently. All the manual valves are indicated with the small letter v and the pneumatic valves with the capital V. Table 3-1 identifies the position of the v1-v10 manual valves and the V4 pneumatic valve installed on the ammonia circuit Table 3-2identifies the v11-v13 manual valves and V1-V3 pneumatic valves for the water circuit.

Name	From	To
v1	Reactor 1	Condenser 1
v2	Reactor 2	Condenser 2
v3	Evaporator 1	To environment for system vacuum and NH_3 charging
v4	Evaporator 2	To environment for system vacuum and NH_3 charging

v5	Reactor 1	Expander inlet
v6	Reactor 2	Expander inlet
v7	For vacuum and NH_3 charging at the power side	
v8	At expander inlet to support power generation	
v9	Expander outlet	Condenser 1
v10	Expander outlet	Condenser 2
V4	Evaporator 2	Evaporator 1

Table 3-1: List of regulating valves for the ammonia circuit

Name	From	To
v11	External Water tank (water source)	System's pump
v12	Return water from reactor 1	Environment
v13	Return water from reactor 2	Environment
V1	Boiler	Reactor 1 or 2
V2	Reactor returns hot and cold water	Boiler and cold water tank
V3	Pump (cold water)	Reactor 1 or 2

Table 3-2: List of regulating valves for the water circuit

Each adsorption cycle (which is call side 1 and side 2 in this report) possesses a reactor (in two pieces), a condenser and an evaporator and produce alternative cooling and power. For the power generation (cogeneration mode), one expander is attached to the other reactor under high pressure. The expanded refrigerant returns to the machine through the condenser at the same side.

Furthermore, four pressure-relief valves are also installed for safety reasons to keep the system pressure within certain limits, two 1-way valves at the reactors' exit to make sure only the refrigerant from the P_{high} reactor enters the expander, a flow meter and two refrigerant ammonia filters before the expander. A generator and a load bank are also used, connected to the scroll expander in order to identify the system's electricity generation through a power meter.

The heat exchange water fluid circuit (hot and cold) is in reality a single circuit split into two. The hot part includes a water boiler to provide the high temperature steam for desorption to which a water-level mechanism is attached in order to identify when the water level in the boiler is low. The cooling circuit (called the temperature heat sink) includes a water tank which provides cooling water to the reactors and the condensers to which an expansion tank is attached to keep the circuit pressure within certain limits. A water pump is used to distribute the cool water from the water tank to the system and a water filter is used to prevent and distribute debris around the water circuit. A plate heat

exchanger which is connected to a cooling tower was installed after the water pump to cool down the water before entering the reactor and the condenser.

The operating principle of the machine to sustain continuous refrigeration and power production is for half the cycle, one side of the machine (reactor 1) is underheating, using steam from the boiler and cooling water from the water tank, and the other side (reactor 2) is undercooling by using cool water from the water tank. At the same time, both condensers are fed with cool water from the water tank. For the other half-cycle hot and cool sources feed the other reactors for a complete cycle to take place. That procedure continues so resulting in continuous cooling and power production.

The system's pneumatic valves V1, V2 and V3 are 3-way valves which mean two ports are open and one is closed during the operation in order to drive the working fluid in the required direction. The ports are indicated with capital letters A, B and C around each valve (Figure 3-1) indicating the water's direction. The V1 is used to deliver hot water (steam) from the boiler either to reactor 1 or reactor 2. Therefore, port C is always open (direction of the steam leaving the boiler) and ports B and A are alternatively open in case reactor 1 or reactor 2 is underheating. The V2 valve is the one for the returning hot water from the underheating reactor to the boiler. In that case, port C is always open (direction of the water returning to the boiler) and ports B and A are open when reactor 1 or reactor 2 is underheating. The V3 valve is the one used to provide cold water to the reactors from the water tank. Port A is always open (water out from the water tank) and ports B and C are alternatively open for reactor 1 and reactor 2 to feed with cool water. The V4 mass recovery valve is a 2-way type (open/closed) and is used as advised. The four pneumatic valves need to be charged with air or nitrogen at a constant pressure of 0.020-0.030MPa in order to function (change direction) when directed.

Thirteen temperature and six pressure sensors are installed. The eleven temperature and the four pressure sensors are distributed all around the chiller and the other two temperature and pressure sensors are used at the power generation part, at the inlet and outlet of the expander. At the boiler can be identified the heaters H1 and H2, and H3 and H4 at evaporator 1 and evaporator 2. H1 and H2 are used to provide steam to the reactors at the required temperature and H3 and H4 are used to replace the fluid circuit at the evaporators to provide the system's refrigeration effect (power). The letter W

indicates the power consumed from those heaters. W1 provides the heating power (i.e. energy) required for desorption to take place (Q_{high}) at the set-up boiler temperature from the two 8kW heaters (H1 and H2) at the boiler and W2 and W3 are 5kW each and are used to provide the refrigeration power (Q_{ref}) to the evaporator (from H3 and H4). All the heaters are automatically ON when the temperature is below the set-up temperature and turn OFF when the temperature reaches the set-up temperature. Table 3-3 lists the temperature and pressure sensors and the heaters as indicated in Table 3-1. Figure 3-2 to Figure 3-11 present all the above components carrying the LH cogen system.

	Quantity	**Location**
T1	Temperature	Reactor 1 inlet
T2	Temperature	Reactor 2 inlet
T3	Temperature	Reactor 1 outlet
T4	Temperature	Reactor 2 outlet
T5	Temperature	Boiler
T6	Temperature	Boiler
T7	Temperature	Condenser 2 inlet
T8	Temperature	Evaporator 1 (Liquid)
T9	Temperature	Evaporator 2 (Liquid)
T10	Temperature	Evaporator 1 (Liquid)
T11	Temperature	Evaporator 2 (Liquid)
T12	Temperature	Expander inlet
T13	Temperature	Expander outlet
W1	Power	Boiler
W2	Power	Evaporator 1
W3	Power	Evaporator 2
P1	Pressure	Evaporator 1
P2	Pressure	Evaporator 2
P3	Pressure	Reactor 1
P4	Pressure	Reactor 2
P5	Pressure	Expander inlet
P6	Pressure	Expander outlet

Table 3-3: List of all the instruments and heaters

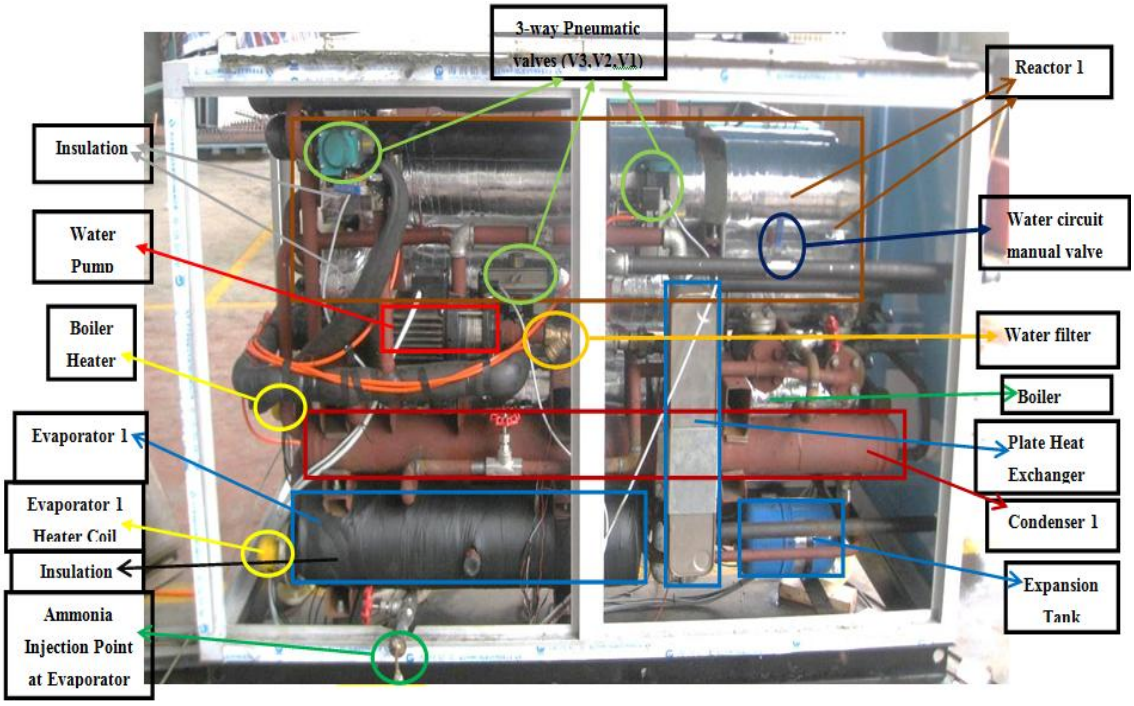

Figure 3-2: LH cogen system: side 1 view

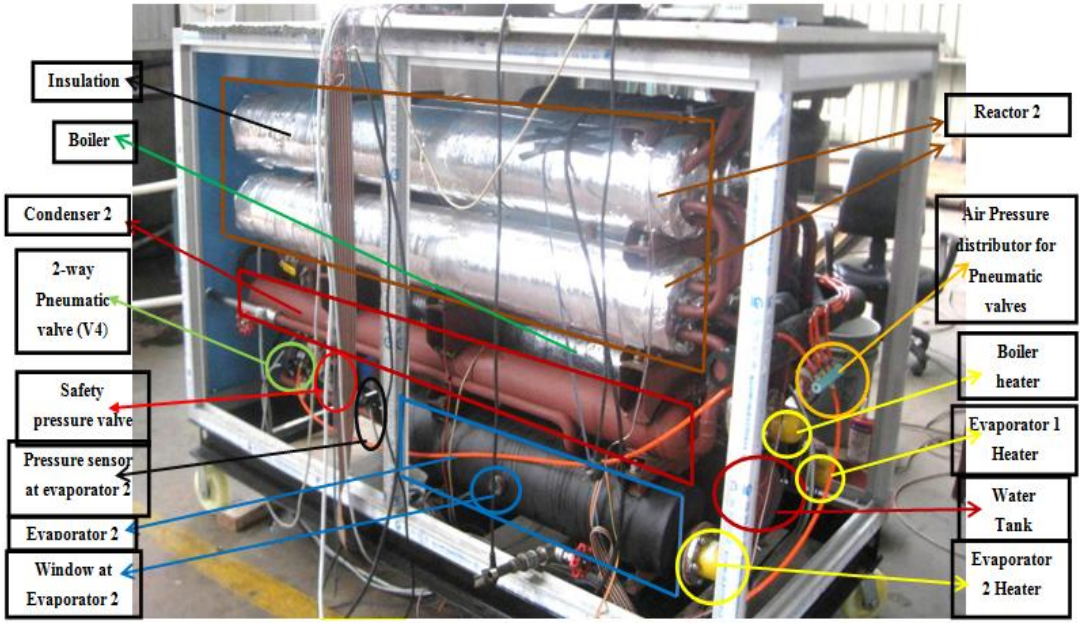

Figure 3-3: LH cogen system: side 2 view

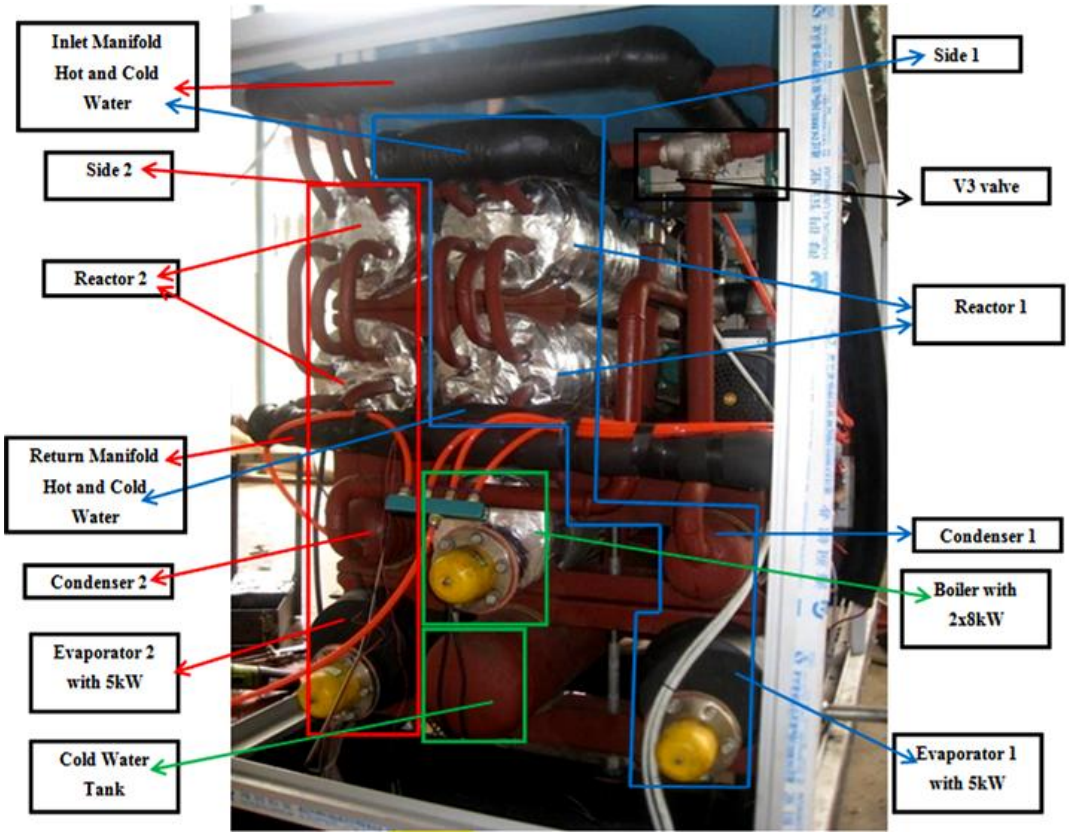

Figure 3-4: Side view of the LH cogen system

Looking at the system side view (Figure 3-4) the arrangement of each component in the machine becomes clearer. It also indicated the inlet and the return water manifolds to the reactors. The colours chosen for the inlet and outlet manifold are for explanatory reasons assuming that that side 1 is undercooling (blue line) and side 2 underheating (red line). Three of the four heaters (H) of the system are clearly indicated and the other one is on the other side of the boiler. The water tank is clearly indicated.

Figure 3-5 shows the V4 pneumatic valve (with the electronic valve of the valve, and the connection to the air distributor supply of the valve) which connects the two evaporators which are used for the mass recovery process, the pressure sensor and a relief valve at evaporator 2.

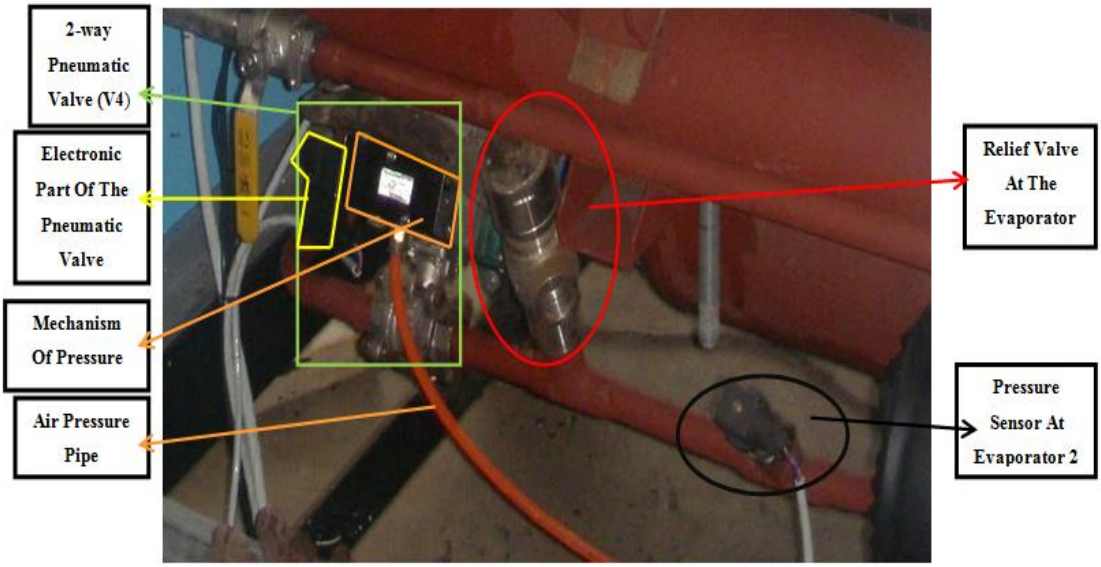

Figure 3-5: V4, relief valve and pressure sensor

Figure 3-6: LH cogen system: side view 1

Figure 3-7: LH cogen system: side view 2

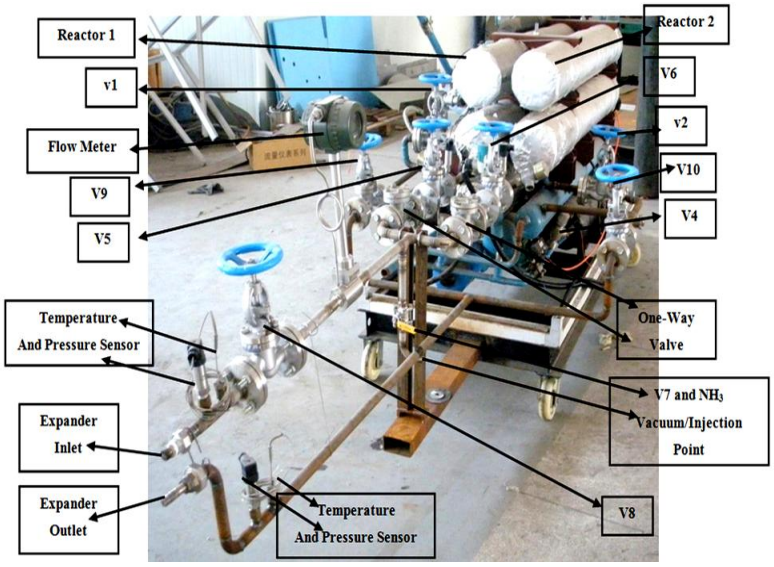

Figure 3-8: Cogeneration set-up 1

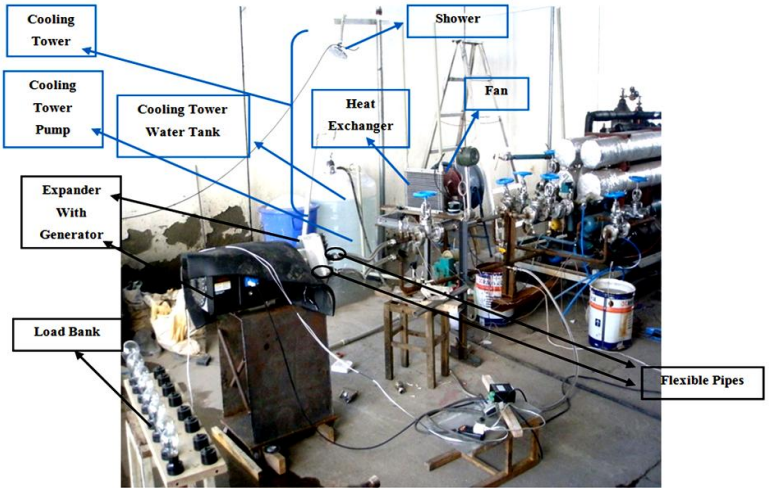

Figure 3-9: Cogeneration set-up 2

Figure 3-6Figure 3-6 indicates the machine's control panel while Figure 3.7 shows an overall side view of the cogeneration system and Figure 3.8 points out the extra components and sensors added to the chiller in order to produce power as well (power production side) except for the expander. Figure 3-9 and Figure 3-10 provides further details of the modifications and the components placed to extract power from the adsorption chiller and Figure 3.11 shows a successful power trial (bulbs on the load bank are ON), the power meter used to collect the power and the PC to back up the results.

The cooling tower used during the cogeneration test is shown in Figure 3-9 with blue arrows. This includes an external cooling tower pump, a heat exchanger, a fan, a shower and a cooling tower water tank.

Figure 3-10: Cogeneration set-up 3

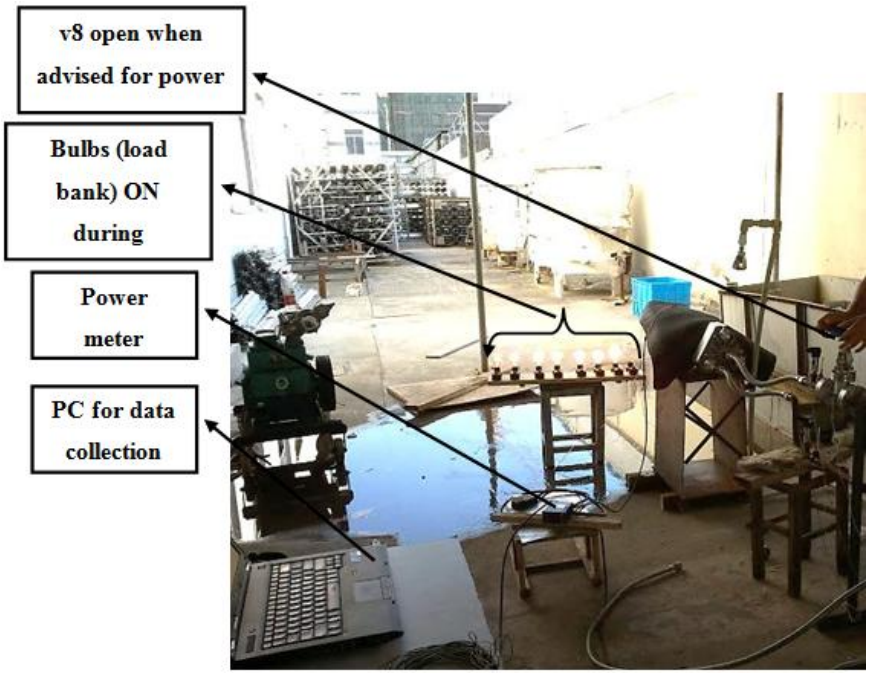

Figure 3-11: Power production during cogeneration

3.2 Main system components

A more detailed explanation regarding the machine's main components like the reactors (adsorbent bed), condenser, evaporator, boiler, water tank and the oil-free scroll expander will follow. The analysis will include figures and detailed information about the machine's construction. The adsorption chiller is constructed of steel because it is easily available, cheap and easy to be modified (cutting and welding) and is also ammonia-compatible.

3.2.1 Reactor (adsorbent bed)

The reactor is a cylindrical tube consisting of a number of heat exchangers (adsorbent bed) which is used to adsorb and to desorb ammonia using cool or hot water. Its size is 1370mm long and 159mm high. For safety reasons, the reactor is in two parts and not in a single bigger one. Each reactor consists of two cylinders per side (Figure 3.12), each enclosed by 6 aluminium-finned-type heat exchangers, which are filled with the $CaCl_2$ – activated carbon composite mixture. A copper pipe of 20mm in diameter is used to carry the aluminium fins which the water passes through in order to exchange heat with the adsorbents resulting in refrigerant adsorption or desorption. The copper pipe is part of the water circuit and never comes in contact with the ammonia, and is just used to cool or heat the reactor.

The size of the reactor is based on the 17.5kg of CaCl2 and the 4.4kg of activated carbon that are on each side to achieve 3kW of cooling during the adsorption-evaporation process. Having in mind that the aluminium-finned-type heat exchangers are standard size, the reactor size should be big enough to carry the composite mixture.

Figure 3-12 also shows the water in and water out circuit designs which includes an inlet and an outlet manifold per side. The water enters the upper reactor from the inlet manifold using the top three fins heat exchangers, and exits from the same side using the other three heat exchangers fins, with the water flowing the opposite direction. The water then leaves the upper reactor and, enters and leaves the lower reactor in the same way. At the exit of the lower reactor it collects in the outlet manifold before returning either to the boiler or the water tank as shown in Figure 3-4 through the bottom three fins heat exchangers.

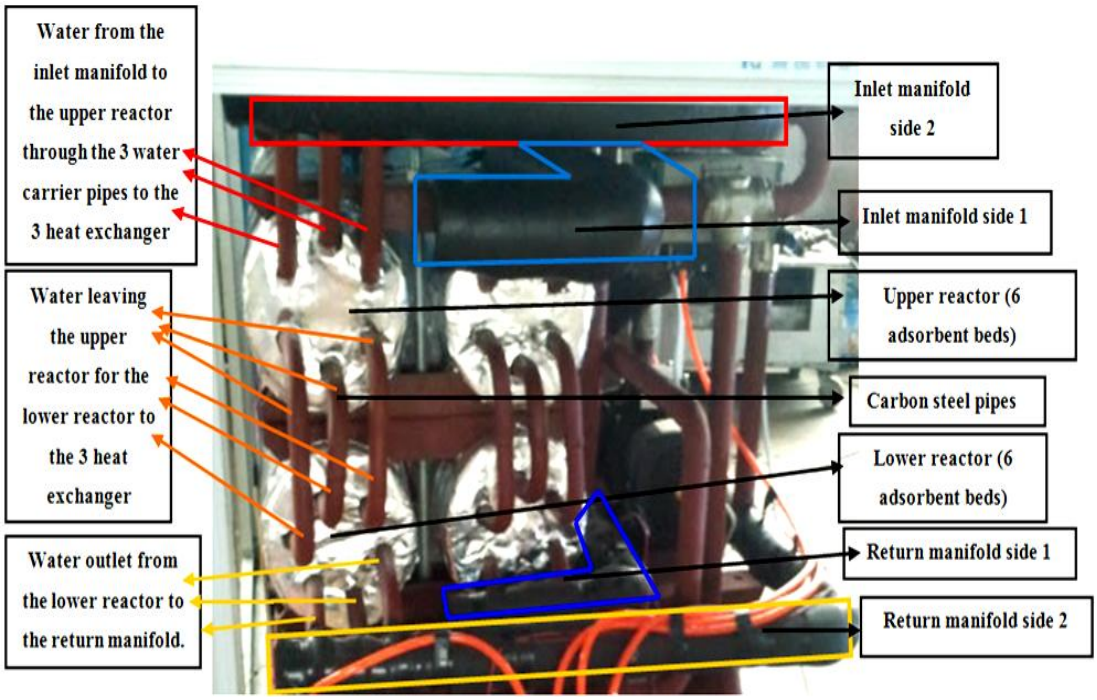

Figure 3-12: Reactor design

Figure 3-13 shows the components included in the reactor in more detail. The six adsorbent beds heat exchanger in each reactor is placed in position using flanges (one at each end of each cylinder) of diameter similar to the adsorbent bed inner diameter and 21mm width. The flanges carry 6 holes drilled at 60 degree angles. The copper pipe placed the finned heat exchanger, has an overall length of 1280mm. The aluminium fins

are 1240mm long and the distance between the fins is around 2mm. Their height is around 42mm and the gap between them is about 3.5mm at the point where the adsorbent is placed.

After the drying procedure, the 6 heat exchanger copper pipes and the aluminium fins with the adsorbent material, are placed into the two flanges and welded at the inner cylinder surface in order to avoid the contact of ammonia with the bronze water pipes, which are also welded on the outside. This set up is placed into the steal reactor and the flanges also are welded to the reactor to fill the gap in between. The heat exchanger is covered with a mesh grid and a mesh pipe to eliminate any adsorbent material escaping the reactor. In order for the reactor to be closed at the ends, two covers are welded. Finally, six holes for the water circuit pipe to be combined with the heat exchangers should be drilled in the covers, and the gap between the pipes and the cover is filled by welding.

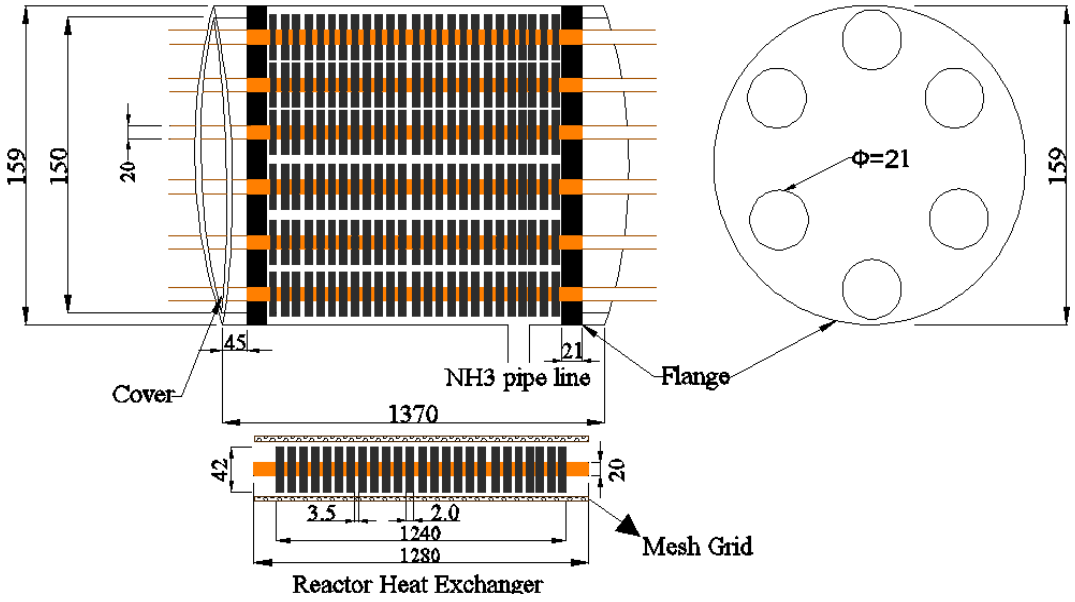

Figure 3-13: Reactor schematic diagram

Figure 3-14 shows how it looks in reality when all the components are included in a reactor before being welded together. That includes the reactor's main cylindrical body, the aluminium fins carried by the copper pipe, the flanges to support the aluminium fins and how a reactor looks externally with the insulation on.

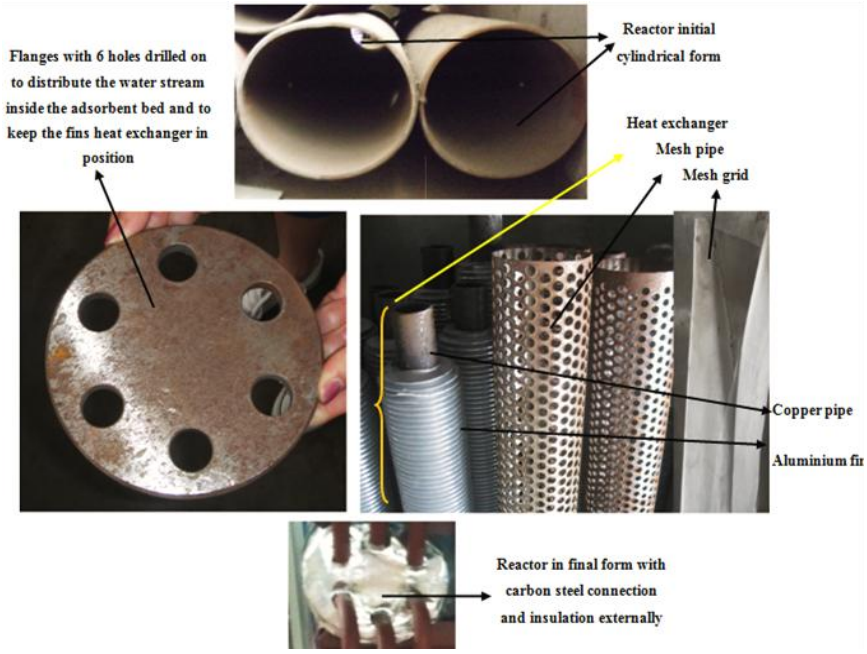

Figure 3-14: Random selection of all the components included in the reactor

The efficiency of the reactor can be estimated if it is examined as a heat exchanger. The one fluid circuit is the water in and out and the other is the ammonia at the beginning and the end of each process. Therefore, the efficiency of the reactor which may be estimated according to Fakheri [109] using Equation 3.1 where a measure of the actual heat transfer rate (Q_{actual}) is divided by the maximum optimum heat transfer rate.

$$n_{reactor} = \frac{Q_{actual}}{UA\Delta T_{ave}} \qquad 3\text{-}1$$

In Equation 3.1, U is the reactor overall heat transfer coefficient, A its surface area, and the ΔT_{ave} is the temperature difference between the average hot and the average cold stream.

3.2.2 Condenser heat exchanger

The condenser is also a cylindrical heat exchanger in which the high pressure desorbed gas is liquefied (cooled down) at the high constant operating pressure. The size is approximately 1330mm long and 110mm high. The condensation is achieved as a result of the cool water carried from 14 pipes crossing each condenser which are acting as 14 independent heat exchangers. Similar to the reactors, each condenser carries two flanges. The gap between the flanges' 14 holes and the heat exchanger pipe is welded. These 14 pipes which carry cool water never come in contact with the ammonia and are

just used to cool down the condenser so resulting in the high pressure gas condensation (liquefied desorbed gas at high pressure by lower condenser temperature). Figure 3-15 shows the pipes inside the condenser which carry cool water and the flanges used to keep them in place. The size of the condenser is chosen bear in mind that the entire desorbed refrigerant should condensate efficiently in a way that will keep the system high pressure at an acceptable limit (2MPa) under ambient conditions. Also, the amount of water leaving the condenser should be kept as small as possible since this will later be used to cool the reactor. Figure 3-16 shows an inside view of the condenser and how it is constructed. The condenser efficiency can estimated using an equation similar to Equation 3.1.

Figure 3-15: The condenser's heat exchanger

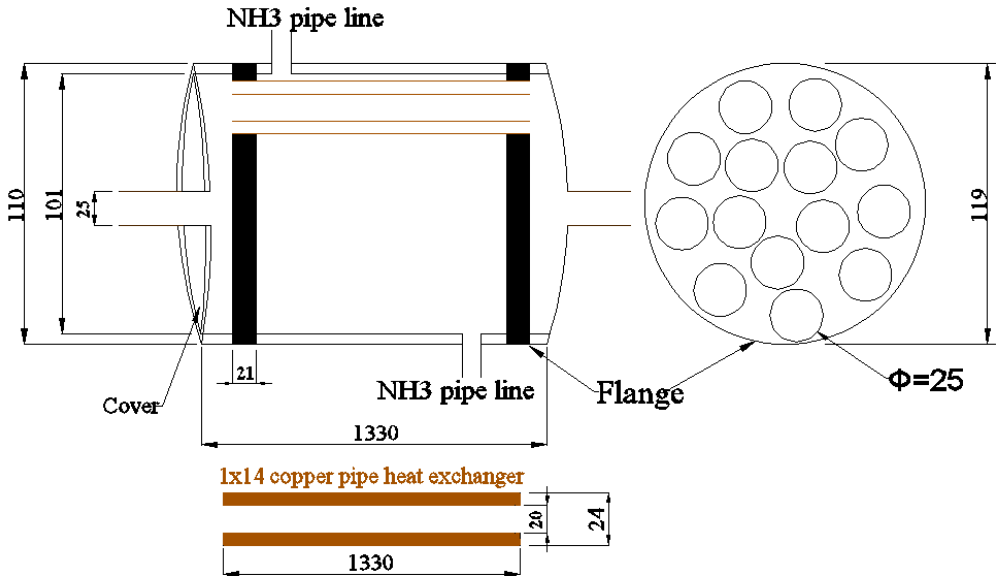

Figure 3-16: Condenser schematic diagram

3.2.3 Evaporator

The evaporator is a crucial component in which the system refrigeration is produced and measured and also in between the two evaporators the mass recovery process is achieved. It is also used to store all the available system's excess liquid ammonia. As was mentioned previously, there is no cooling circuit to utilise the chilling effect at the evaporator. Instead, a heater coil of 5kW was installed in each evaporator to estimate the cooling load according to the thermal balance theory. The heaters are installed in a closed shell in which they are placed inside in order never to come in contact with the refrigerant. In between the heater and the heater's shell there is a tolerance to avoid any contact during the heater's deformation (expansion) when it is ON. The heater can easily be removed for maintenance reasons.

The evaporator also carries a glass window to inspect the amount of liquid ammonia visually. Figure 3-17 presents both an inside and an outside view of the heater shell. It also indicates how the ammonia circuit is connected to the condenser, the evaporator window, the cavity in the evaporator where the temperature sensor is placed and the heater's connection to the heater shell. Figure 3-18 present an inside view of the evaporator and provide more details about the evaporators construction.

The size of the evaporator is similar in diameter to the reactor but shorter. Its purpose is to be able to carry the entire available liquid refrigerant to any point. Having in mind that the maximum charge of the machine is 5.2 moles per side of ammonia (14kg) and that 4 moles is always in the reactor in the form of CaCl2*4NH3 compound, therefore the maximum ammonia that each evaporator should be carry is around 3.52kg.

The evaporator efficiency for the LH cogen system cannot be estimated from Equation 3.1 because there is no chilling circuit to utilise the refrigeration power but instead a heater coil is used to estimate the refrigeration power. This kind of heater can convert all the electricity to heat therefore assume to have 100% efficiency [110, 111].

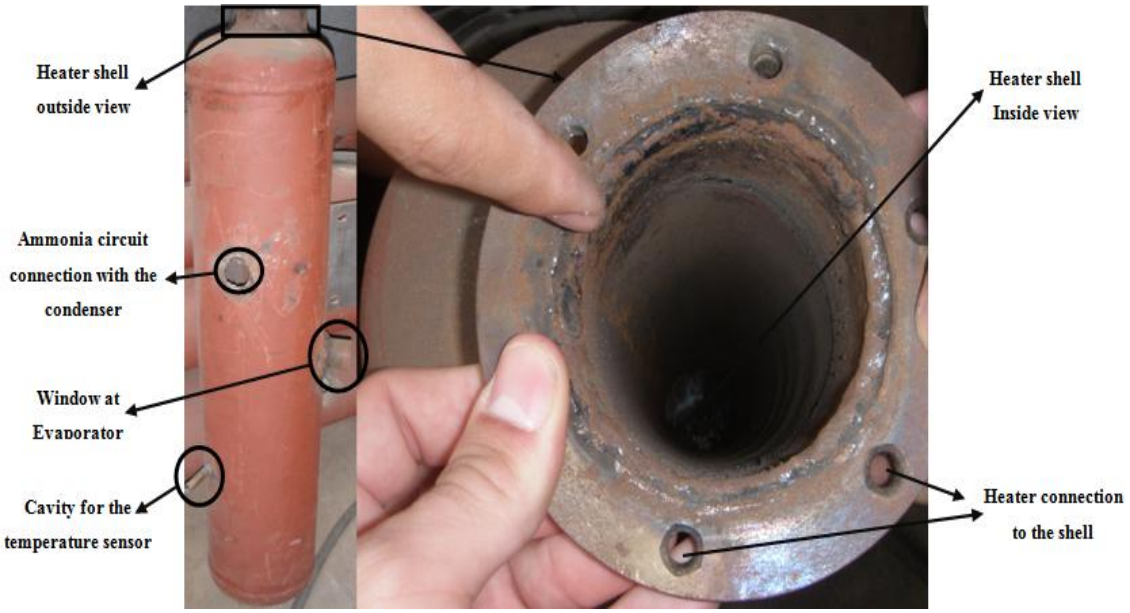

Figure 3-17: Evaporator details

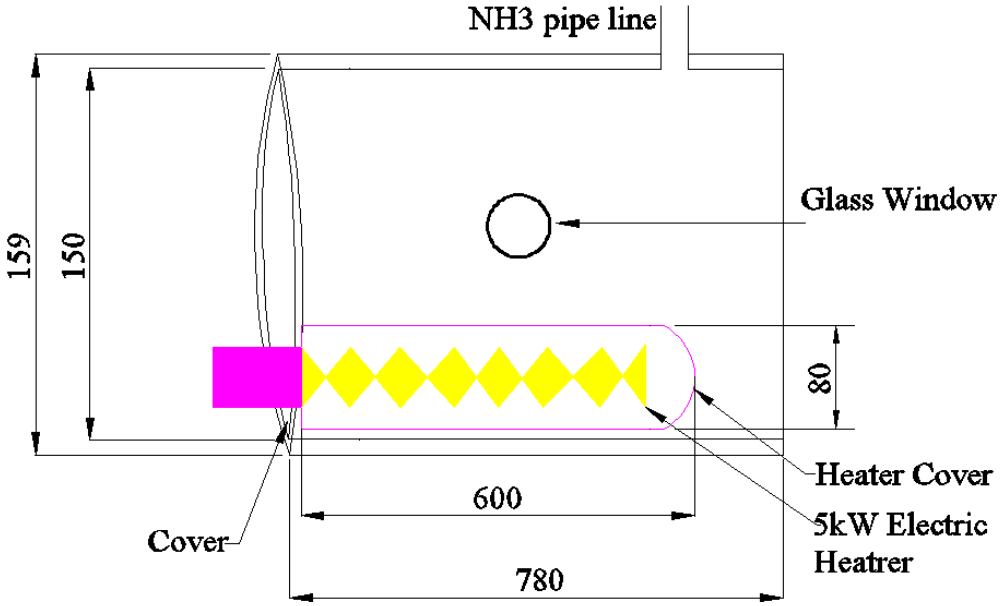

Figure 3-18: Evaporator schematic diagram

3.2.4 Boiler

The primary purpose of the boiler is to carry as much water and produce steam to feed the reactor during. The boiler diameter is similar to the evaporator but longer. The difference from the evaporator design is that two electric heaters coil is used instead of one. Also, the electric heaters coil at the boiler is exposed to the working fluid (water) since there are no compatibility issues as with ammonia. A boiler-water-level check mechanism is installed to alert when the water in the boiler (so for the water circuit) is

low. Figure 3-19 presents the boiler schematic including the boiler-water-level check mechanism. The net boiler capacity is estimated to be around 0.025m^3 (25L).

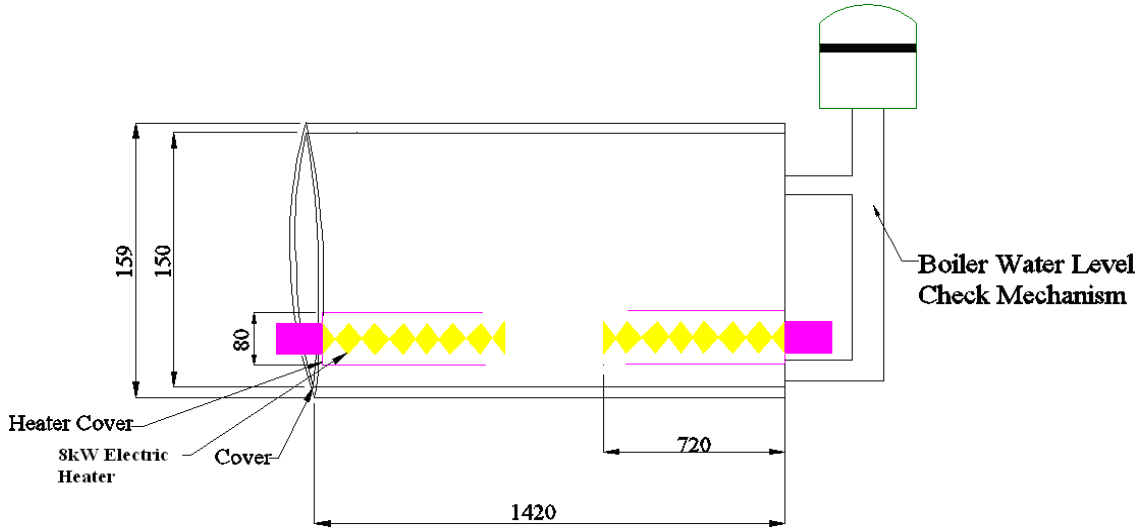

Figure 3-19: Schematic diagram of the boiler

3.2.5 Water tank

The water tank is used to provide cold water to the reactors and the condenser and also to collect the water leaving the undercooling reactor. The water from the tank is pumped to the heat exchanger which is connected to a cooling tower in order to be cooled down before it is distributed to the system. The water tank is connected to an expansion tank to prevent the extensive system pressure from increasing during the switch period when hot water from the high-pressure side ends there after the switch period. Figure 3-20 presents a schematic of the water tank and the expansion tank. The net volume of the water tank is estimated to be around 0.02m^3 (20L). Assuming that approximately 50L of water is used for the water circuit, and the boiler and the water tank accounts for 45L (25L and 20L respectively), then around 5L of water is carried by the system's water pipes.

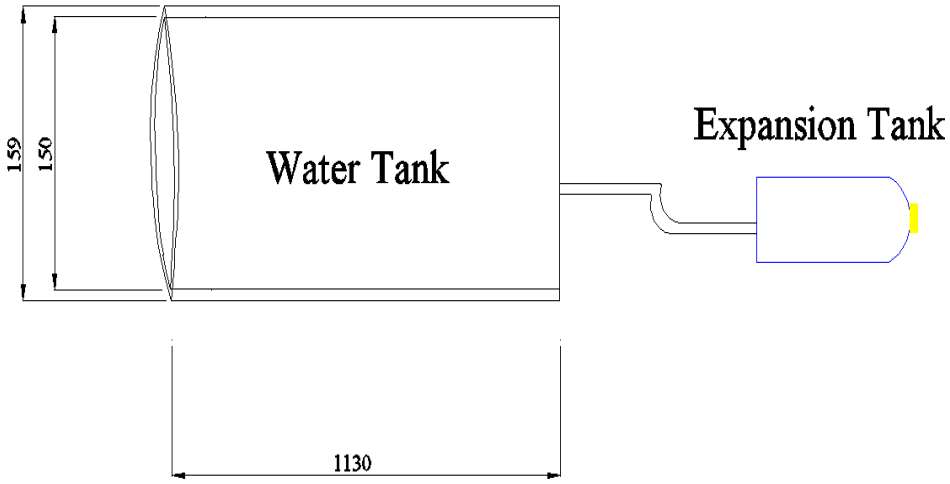

Figure 3-20: Schematic diagram of the water tank

3.2.6 Scroll expander

The power media device selected for this study is the 1kW oil-free scroll expander (Figure 3-21), the E15H22N4.25 model design from Air Squared. The machine specifications are presented in Table 3-4 as found from the Air Squared web site. The machine is originally a scroll expander and not a compressor running in reverse. The selected expander had a specification closer to the specifications we were looking for at the time even though it does not completely cover our needs. Also it is oil-free and compatible with ammonia. The expander can be directly attached to a rotary DC/AC Generator. Figure 3-21 [96] does not include the generator but just the scroll expander which Figure 3-9 has.

Figure 3-21: 1kW scroll Air Squared scroll expander E15H22N4.25 model

Nominal output	1 kW
Max. Working Pressure	13.8MPa
Max. Working Flow	12 cm^3/Rev
Max. Working Speed	3600 RPM
Maximum Inlet Temperature	175^{O}C
Average Sound Level	55dB(A)
Net Weight	9.07KG

Expansion Rate	3.5

Table 3-4: 1kW Air Squared scroll expander E15H22N4.25 model specifications

3.3 Adsorbent material

The adsorbent bed of the LH cogen system is a composite mixture of the $CaCl_2$ as a reactive salt and activated carbon as the inner material. The mass of $CaCl_2$ is 17.5kg mixed with 4.4kg of activated carbon having a mass ratio of 4:1 per reactor. The composite mixture is a combination of anhydrous $CaCl_2$ with water initially and then the solution is enhanced by the activated carbon (Figure 3-22). In the end, the mixture is formed at the adsorbent bed in the cylindrical aluminium-finned-tube heat exchanger. The heat exchangers with the mixture are dry in the oven at $200^{O}C$ to dry the water. The exact drying procedure is described by Li, et al. [74]. To prevent any big part of the mixture collapsing during the reaction with ammonia, a mesh grid is placed around the heat exchanger and on the top a stainless steel mesh pipe (Figure 3-23).

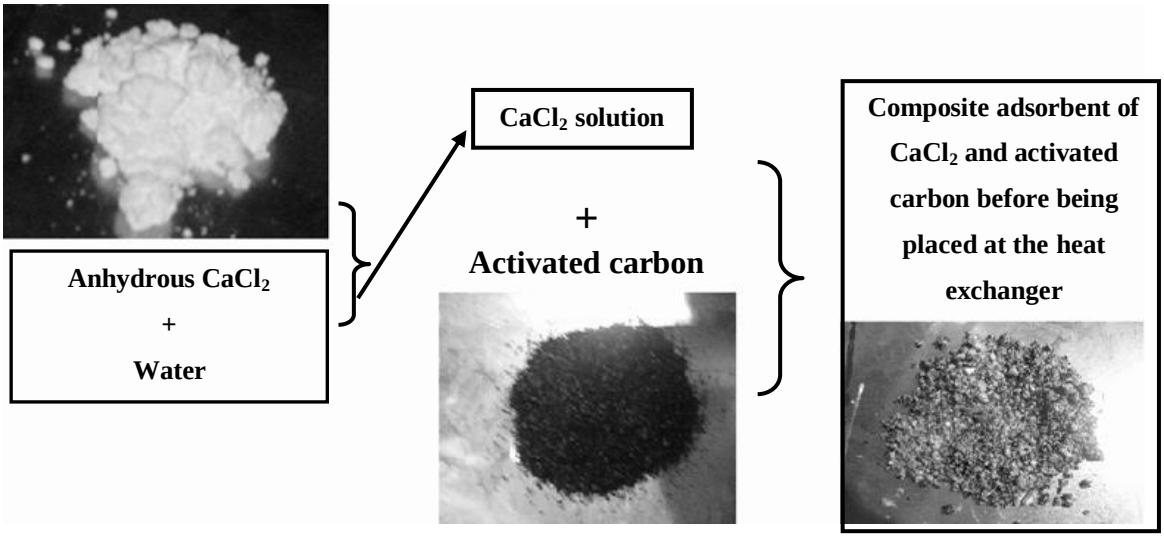

Figure 3-22: Adsorbent preparation

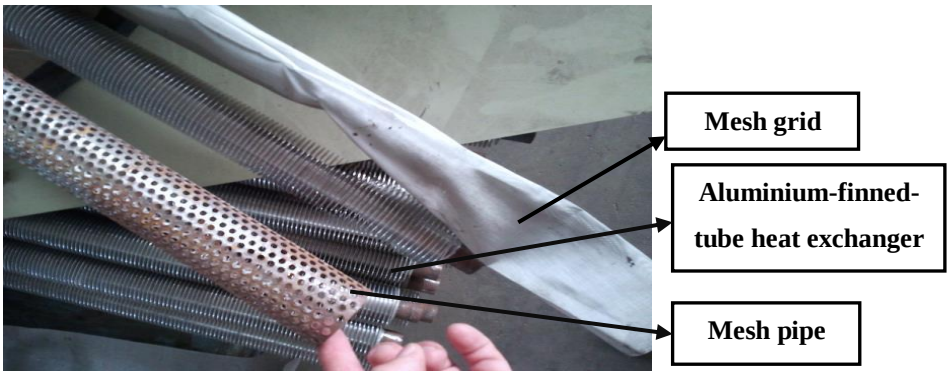

Figure 3-23: Adsorbent bed heat exchanger, mesh grid and mesh pipe

3.4 Control system controllers and measurements

In this section a detailed explanation of the controls and the system's measurements will be given. An introduction to the machine's control panel will be given, and will also be mentioned all the measurements the machine can provide and also discuss the machine's operation mode.

3.4.1 Control panel

The control panel of the system is presented in Figure 3-24 which shows all the controllers and the switches on the control panel. Figure 3-25 shows the inside view of the control panel. The colours used in Figure 3-25 are similar to those in Figure 3-24 to describe the connection of the controllers and the switches.

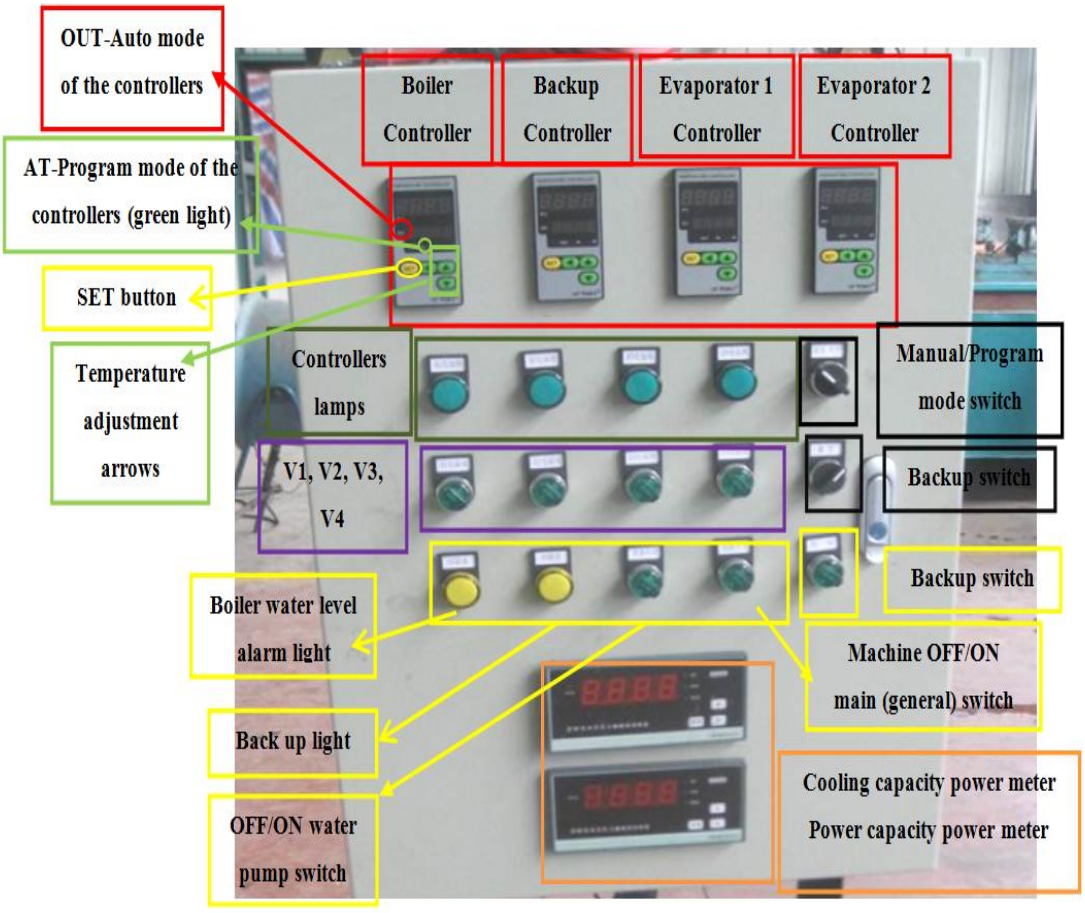

Figure 3-24: The control panel for the cogeneration machine

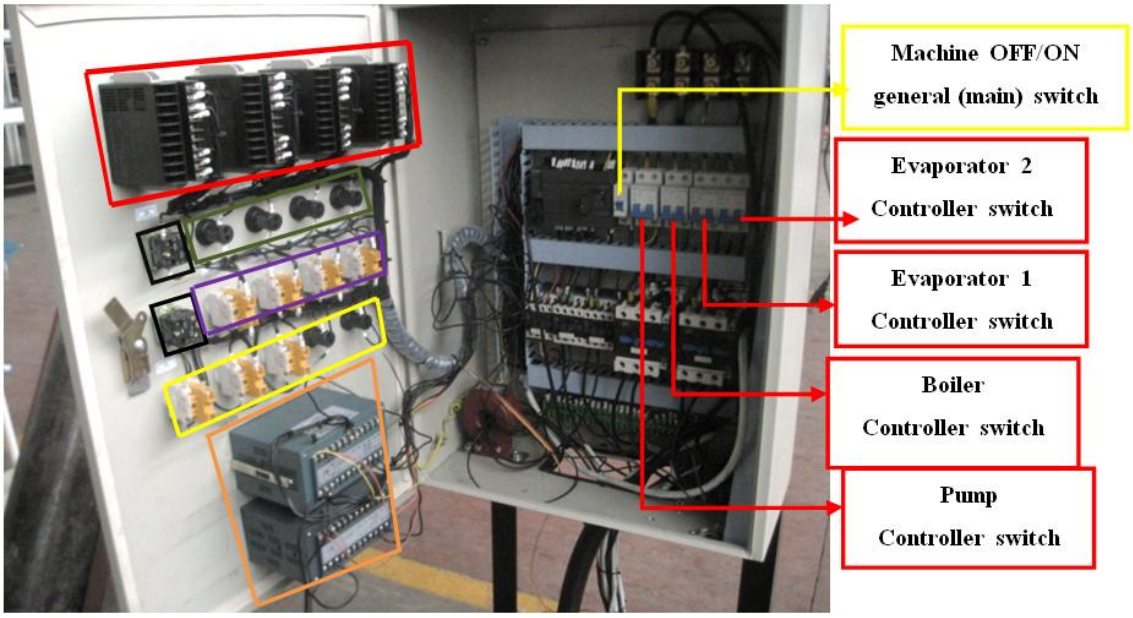

Figure 3-25: The inside view of the control panel

The control panel provides the general system's ON/OFF switch. It can also be used to set the steam boiler's temperature from the boiler controller and the cooling temperature at the evaporator from the evaporator's controller. The machine can also be selected to run in manual or program mode. In case it is run in manual mode, the V1, V2, V3 and V4 valves can be operated manually from the control panel as well the pump. There is also an emergency indicator for whenever the water level at the boiler is low. Two power meters are also installed to measure the heating power recorder from the heaters at the boiler and the refrigeration power from the evaporators.

3.4.2 Sensors and data collection

All around the LH cogen machine for both the ammonia and water circuits are distributed thirteen temperature sensors and six pressure sensors. From those, two temperature sensors and two pressure sensors are specially used when the machine runs in cogeneration mode. Ten of the temperature sensors as well as the six pressure sensors are connected to a PC through data acquisition equipment. The remaining three temperature sensors are those to provide feedback to the control panel related to the heaters at the evaporator and the boiler to go ON and OFF.

Eight of the temperature sensors can identify the water temperature in and out of the two reactors: the cooling water at condenser 2's inlet; and the boiler's water temperature and the liquid ammonia temperature at each evaporator. Two pressure sensors are

placed at each of the evaporators, and the other two at each reactor. All these are installed at the adsorption chiller and mainly used when the machine is running only as a chiller. Furthermore, the machine carries two more temperature and pressure sensors: each one at the inlet and the outlet of the expander, used to record data when the machine runs in cogeneration mode. Data for the cooling power and the heating power can be collected from the power meter at the control panel and collected by data acquisition equipment. All the data are provided from the data acquisition device except for the generated power during cogeneration (W4) which are provided by another, second power meter. Table 3-5 presents all the data the machine can provide and where each senor is located. Table 3-6 presents the specifications (accuracy) for all the instrument and equipment carrying the LH cogen system.

Name	Quantity	Location	Fluid	Unit	Collected to
T1	Temperature	Reactor 1 inlet	Water	^{O}C	Data acquisition
T2	Temperature	Reactor 2 inlet	Water	^{O}C	Data acquisition
T3	Temperature	Reactor 1 outlet	Water	^{O}C	Data acquisition
T4	Temperature	Reactor 2 outlet	Water	^{O}C	Data acquisition
T5	Temperature	Boiler	Water	^{O}C	Data acquisition
T6	Temperature	Boiler	Water	^{O}C	Control Panel
T7	Temperature	Condenser 2 inlet	Water	^{O}C	Data acquisition
T8	Temperature	Evaporator 1 (Liquid)	Refrigerant	^{O}C	Data acquisition
T9	Temperature	Evaporator 2 (Liquid)	Refrigerant	^{O}C	Data acquisition
T10	Temperature	Evaporator 1 (Liquid)	Refrigerant	^{O}C	Control Panel
T11	Temperature	Evaporator 2 (Liquid)	Refrigerant	^{O}C	Control Panel
T12	Temperature	Expander inlet	Refrigerant	^{O}C	Data acquisition
T13	Temperature	Expander inlet	Refrigerant	^{O}C	Data acquisition
W1	Power	Boiler heating power		kW	Data acquisition and Control panel
W2	Power	Evaporator 1 cooling power		kW	Data acquisition and Control panel
W3	Power	Evaporator 2 cooling power		kW	Data acquisition and Control panel
W4	Power	Generator		W	Power meter
P1	Pressure	Evaporator 1	Refrigerant	MPa	Data acquisition
P2	Pressure	Evaporator 2	Refrigerant	MPa	Data acquisition
P3	Pressure	Reactor 1 exit	Refrigerant	MPa	Data acquisition
P4	Pressure	Reactor 2 exit	Refrigerant	MPa	Data acquisition
P5	Pressure	Expander inlet	Refrigerant	MPa	Data acquisition
P6	Pressure	Expander outlet	Refrigerant	MPa	Data acquisition
F	Flow Rate	Expander inlet	Refrigerant	kg/s	Data acquisition

Table 3-5: All the measurements the system can provide

AC Generator (Voltmaster©, AB30L)	
Vortex Flow Meter	±1% Tolerance
Qingzhi©, ZW2613 Power meter	0.5% accuracy
Data Logger from DataTaker© DT85	
Pressure sensor	0-2.5MPa, ±1% Tolerance
Pt 100 Thermal Resistance Temperature Sensors	0.5% accuracy

Table 3-6: Concentrated instrument specifications

Each temperature sensor is placed in a cavity made at a required depth mainly attached to the bottom of the vessel or to the installed pipe so are never in contact with the working fluid. The cavity should be full of high-thermal-conductivity oil or any another substance to remove the air from the cavity. The freezing point of the thermal-conductivity oil at the evaporators should be less than the expected lower temperature of the evaporator. For the evaporator, a cryogenic conductivity oil can be used or a mixture of water with $CaCl_2$ or activated carbon to eliminate any freezing of the liquid. At the top of each cavity, a play dough can be used to prevent the conductivity fluid from escaping (Figure 3-26). The pressure sensors installed are in direct contact with the refrigerant as Figure 3-27 shows.

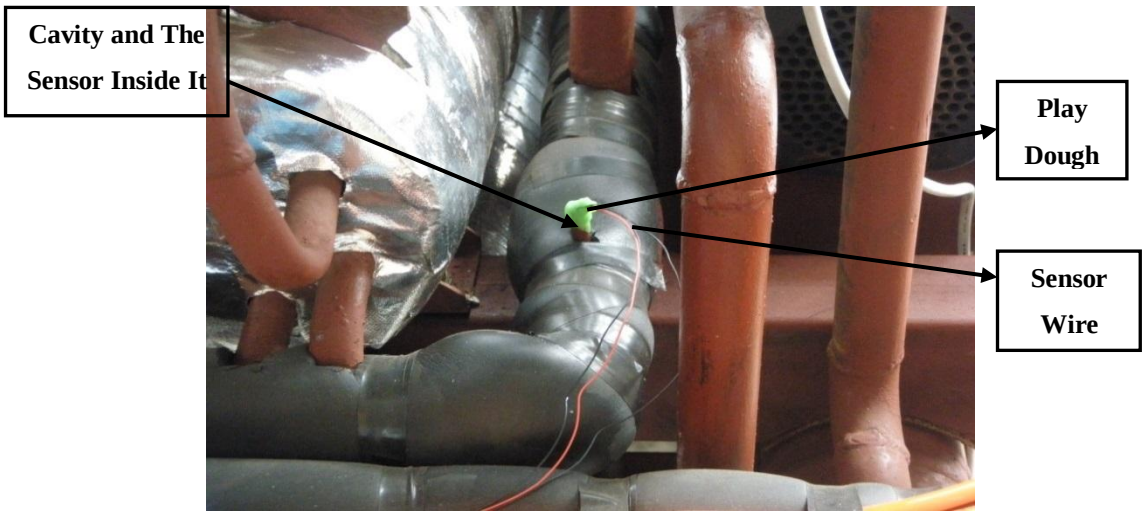

Figure 3-26: Temperature sensor preparation

Figure 3-27: Pressure sensor at Evaporator 2

3.5 Cooling and cogeneration operations

The system can either run in only-cooling mode or in cogeneration mode according to the route the ammonia takes. No matter what the operation mode, the water circuit (hot and cold) follows a specific route.

3.5.1 Cooling mode

Figure 3-28 shows a simplified schematic when the system runs in only-cooling mode. During that mode, the machine operates as an adsorption chiller so the refrigerant is moved from the reactors to the evaporators through the condensers on the high pressure side and from the evaporator to the reactor on the low pressure side. The ammonia manual valves v1 and v2 which connect the reactors to the condenser are always open and mass recovery valve V4 which connects the two evaporators is open when is required.

The machine for the only-cooling mode is running in program mode because it is more accurate and easier to compare to the manual operation because the whole operation is programmed and requires no other work. Only adjustments to the boiler and evaporator temperature are needed; the rest is according to the program. Before explaining how the machine operates during the only-cooling mode should be identified the mechanism that operates the chiller and, more specifically, how V1, V2, V3, V4 and the pump function during the cycle.

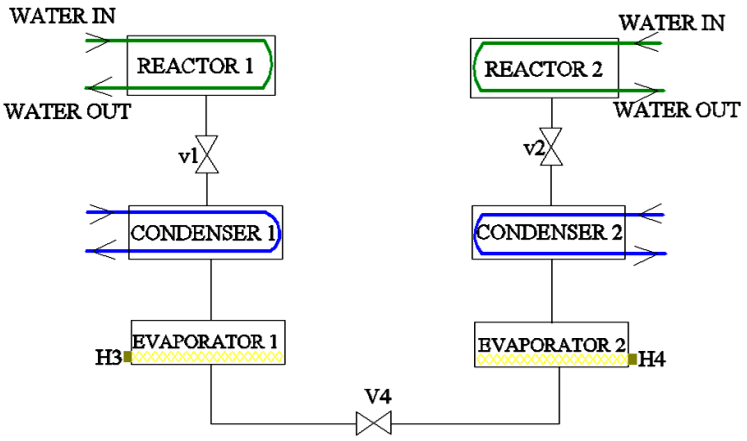

Figure 3-28: Schematic for only-cooling operation

A complete cycle is completed when both sides each complete a single cycle of underheating and cooling. The cycle during the cooling mode (programming or manual mode) includes the basic cycle time which is the majority of the cycle, followed by a mass recovery time before the switch period. Assuming a 14min-cycle time per side and the last 1min for the mass recovery, Table 3-7 indicates how the machine is programmed to operate for a typical only-cooling mode operation.

	Process Duration	**Time Each Process Takes Place**
One complete cycle	28 min	From 0-28 min
Half cycle duration	14 min	From 0-14 and 14-28 min
Mass recovery duration	1 min	From 13.00-14.00 and 27-28 min
Switch period takes place at		14 and 28 min
Time the pump remains OFF	1min	From 13.30-14.30 and 27.30-28.30 min

Table 3-7: Cycle time for only-cooling mode for 14 minutes' cycle time

The above operation includes a 13min basic cycle when one side is undercooling and the other underheating. At exactly 13min cycle time the mass recovery valve (V4) opens. At 13.30min, the pump is stopped, and starts again after 1min (14.30min). The mass recovery process stops after 1min in the 14min cycle time so the mass recovery valve is now closed. The switch period takes place at the same time as the mass recovery process ends. A new cycle now starts at 14min cycle time. The water circuits now change to switch the working fluid to the reactors through the V1 and V3 valves. At 27min cycle time, the mass recovery process takes place again and at 27.30min the pump is turned OFF. At 28min cycle time, the V1, V2, V3 and V4 valves change directions and the water streams feed the reactors as initially (0min cycle time) and at

the same time the mass recovery process ends. At 28.30min cycle time the pump is ON again.

The pump turns OFF for security reasons before the switch period (before water fluids change direction) to avoid the direct contact of the cold and hot water which remains in the high-pressure reactor just after V1 and V3 change direction. That might lead to vibration and possibly cracks on the water circuit pipeline since steam and liquid cannot mix. Therefore, if the cold water is pumped when the pump is ON again, it would violently enter the reactor which was previously used for heating and come in direct contact with the steam. To make sure that that will not happen, the pump stops for 30sec before the switch period and is ON 30 sec afterwards (the pump stays OFF for a minute), hot and cold streams exchange heat within the pipelines for a minute. This period was found experimentally before tests of 25sec and 45sec and resulted in the minimum vibration in the water circuit's piping system.

During the only-cooling mode operation, the boiler water temperature is managed from the set-up temperature at the controllers and is independent from the system's operation. The system's cooling capacity is recorded as long as the set-up temperature at the low-pressure evaporator is below the set-up temperature and the heater is ON. Similarly, the heating capacity is recorded as long the water temperature at the boiler is below the set-up temperature and the heaters there are ON to recover the temperature to the set-up value. In case the manual mode was used for the cooling experiments, the V1, V2 V3 V4 valves and the pump's ON/OFF would be performed from the control panel manually at the right time and in order. That makes the whole procedure in cooling mode more complicated and less accurate.

3.5.2 Cogeneration mode

During cogeneration mode, the machine does not run any more in program mode but on manual because of the complexity of the procedure. Before discussing the cogeneration mode, It will discussed about how the machine can run in manual mode. Figure 3-29 indicates at the control panel the pneumatic valves V1, V2, V3 and V4 and how the pump's ON/OFF mode should function for the machine to run in cogeneration mode.

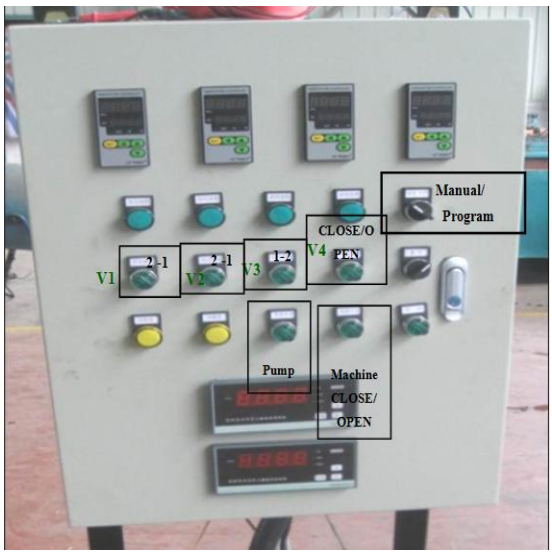

Figure 3-29: Manual control panel operation for cogeneration mode

The main difference between the only-cooling and cogeneration modes is the mass recovery valve used during the cycle and not once at the end. For the manual operation, a stopwatch should be used to remember when V1, V2 and V3 should be turned in the other direction, also when it is time for the pump to turn OFF and ON. The mass recovery valve is used whenever it is required before the power trials. From Figure 3-29, when side 1 is undercooling and side 2 underheating, V1, V2 and V3 should be turned to the left and after the switch period to the right for side 1's underheating and side 2's undercooling.

In cogeneration mode, the route of the refrigerant and the approach to using the mass recovery valve differs from the cooling mode.

Figure 3-30 is a simplified schematic of all the system's necessary manual valves of the ammonia circuit. The main difference from the cooling mode is that the scroll expander is now involved in producing power during the desorption process and that the condensation process takes place after the refrigerant expansion. Therefore, the high pressure refrigerant is expanded in the expander and produces power and then returns to the chiller using the v9 or v10 manual valves according to which side is underheating (side 1 and side 2). At the same time, the low-pressure side produces cooling similar to the only-cooling mode adsorbing the reactor's refrigerant from the connected evaporator. V4 valve is used to ensure the expander's exit pressure before each power-generation trial by utilising the pressure difference between the two sides.

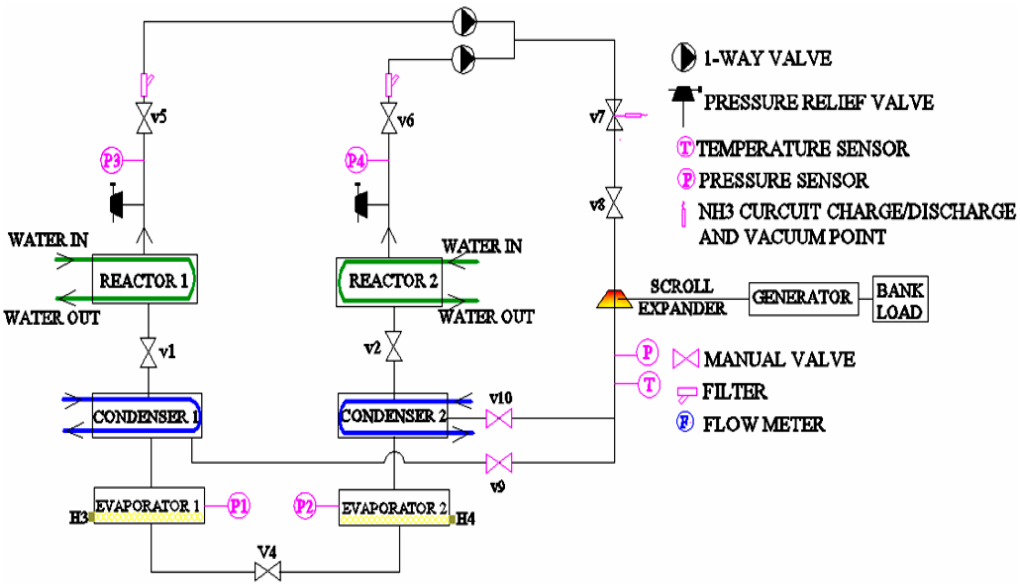

Figure 3-30: Schematic for cogeneration operation

In Figure 3-30, the v1 and v2 valves each connect the reactors with the condenser on their side. The v5 and v6 manual valves connect the outlet of reactors 1 and 2 to the expander and v9 and v10 connect the expander's outlet to the condensers 1 and 2. The v8 valve is the one before the expander's inlet and is used to discharge the ammonia to the expander when the pressure is high enough. The v7 valve is used to isolate that cogeneration part of the system by using v5 and v6 also, in case the filters need to be cleaned. The v7 valve also includes a vacuum valve to remove any air if required.

The machine is more beneficial to run in cooling mode before it switches to the cogeneration mode. Just before turning to the first cogeneration cycle, no mass recovery should take place in the previous cooling of the side currently undercooling which will later be used for power generation so possessing a low pressure at the evaporator before the switch period. If mass recovery takes place, that will increase the cooling side's pressure and this is unwanted for power generation since it will decrease the expander's pressure difference (ΔP_{exp}) at the expander's inlet and the expander's outlet which is the connected evaporator pressure.

3.6 System fluid circuit

The system includes two fluid circuits, the refrigerant (ammonia) and the heat exchange fluid circuit (water). The water is a single circuit and is a design based on a heat pipe theory which increases the transport's thermal efficiency [55, 112, 113]. The two fluids

are never in contact and just exchange heat in various system components as described in the main system component (section 3.2).

3.6.1 Ammonia circuit

The ammonia circuit is recirculated at the reactors, the condenser and the evaporator during the cooling mode and through the expander during cogeneration mode and returns to the chiller via the condensers. The V4 mass recovery valve is installed in between the two evaporators. For the ammonia circuit, the system's operating pressure at the reactor, condenser and evaporator per side are almost the same during adsorption or desorption when the mass recovery valve is closed.

3.6.2 Water circuit

The water circuit (cold and hot streams) is actually one circuit which is distributed by the three 3-way valves V1, V2 and V3. Its purpose is to prepare the reactors for adsorption or desorption and also condensates the desorbed refrigerant. This design aims to keep the system compact and simple. The hot and the cold water streams return from the reactors to meet together but are not mixed before the V2 valve, and through this, they return either to the boiler (returning water from the high-pressure reactor) or to the water tank (returning water from the low-pressure reactor).

The cold water distributing from the water tank follows a constant route before returning there. The cold-water pump is used to pump water from the water tank to the heat exchanger to cool it down from an external source, before it is distributed to the machine. After the cold water leaves the heat exchanger, it enters into condenser 2, then to condenser 1 and then through the V3 valve it enters the reactor currently undercooling. After the cooling water leaves the low-pressure reactor it returns to the water tank. At the same time the hot steam feeds into the reactor currently underheating, leaving the boiler and going through V1 and through V2 it returns to the boiler after it leaves the reactor.

When the water circuit initially fills with water, the V1, V2 and V3 valves are normally open so approximately 50L of water is fed into the system, including at the boiler and the water tank. During the machine's operation, any air in the water circuit should be removed for safety reasons. Any noise or vibration in the water circuit is a sign of air in the system or an indication of excess or not enough water. Therefore, manual valves v12 and v13 are located at the discharge port with one at each reactor exit (Figure 3-1)

which is used to remove any air (bubbles) in the system when that side is underheating. In case more water is needed, that will come through the v11 manual valve and the charge point there.

3.7 Mass recovery process

One of the most important things needed for the LH cogen system to improve system efficiency is the mass recovery process which takes place between the high- and the low-pressure sides through the V4 valve with the two evaporators connected. The process starts just after V4 opens and finishes when it is closed. The mass recovery process takes place for a small period of time late in the cooling cycle and when it is required during the cogeneration cycle.

With the process the whole system instantly reaches pressure equilibrium but not temperature equilibrium. During the process, ammonia is transferred from the high-pressure to the low-pressure side. This transfer stops (or takes place at very low rates) seconds after V4 opens, when pressures between the two sides become equal. That means, in case one of the two evaporators possesses more refrigerant, when the pressures become equal, no further refrigerant (liquid and/ or vapour) is transferred. The more refrigerant at the evaporator, the more there is sensible heat during the adsorption-evaporation process and that affects the refrigeration.

3.7.1 Mass recovery process during only-cooling mode

During cooling mode, one evaporator is at high pressure and the other is at low pressure and when the V4 valve is open, the pressure differences between the two sides are equalised a few seconds later. With that result, just after the mass recovery process, the pressure difference between the reactors and the evaporators increases suddenly. For the reactor under heating, this pressure difference increases the desorption rate so extra ammonia leaves the high pressure reactor. Therefore, that reactor which will later be used for adsorption will have a higher adsorption capacity since there will be more ammonia free.

The literature states that the adsorption and desorption process rates are different but related processes. In case the pressure difference between equilibrium and the operating conditions increases, then the desorption and adsorption rates are also increased. This is true for desorption, in case sufficient ammonia appears in the high-pressure reactor. It is also true for adsorption in the low-pressure reactor in case the adsorbent can still adsorb

refrigerant at efficient rates. The mass recovery process simply uses this principle to improve the system's efficiency by desorbing as much refrigerant as possible before the switch period. The desorption process at the later stages of the desorption process before V4 opens is poor and the mass recovery process gives a boost to the process, so improving the system's cooling performance.

3.7.2 Mass recovery during cogeneration mode

For the cogeneration mode, the mass recovery is used to improve the system's power performance but at the same time that reduces the cooling efficiency. The mass recovery valve is now used every time before the next power production during the cycle when it is required in case the condenser at the desorption side after the power production cannot create low pressure and there is a significant pressure difference with the expander's inlet.

That use of the mass recovery valve will directly affect the cycle's cooling production since the cooling procedure will interrupt whenever V4 is used. A high-pressure and high-temperature refrigerant will transfer at the low-pressure side and that will stop the cooling procedure. Also ammonia is adsorbed from the low pressure reactor so reducing its adsorption capacity. At the same time more liquid ammonia will be transferred to the evaporator to increase the sensible heat.

3.8 Programming-Step 7

In order for the machine to run in programming mode, software should be used to specify the operation of the pneumatic manual valves (V1, V2, V3 and V4) and heaters. Step 7 is the selected software for programming the machine's operation in only-cooling mode. How the machine typically runs was explained previously using Table 3-7. The time set for Step-7 for the machine to run in program mode for only-cooling mode is explained below:

- Set the basic cycle time;
- Set the mass recovery time which starts just after the cycle time expires;
- Set when the time pump is switched off just after the mass recovery process;
- Set the time pump to remain OFF;
- The switch period is programmed to take place just after the mass recovery process finishes.

Obviously, the cycle time and the mass recovery duration should be found out experimentally as well as the duration for the pump to remain OFF.

3.9 Scroll expander test rig

The scroll expander itself was under a performance test using nitrogen (N_2) under various pressures and temperatures. The schematic test rig used is shown in Figure 3-31 and Figure 3-32 shows the real experimental test rig. Numbers in both figures are used to identify each component.

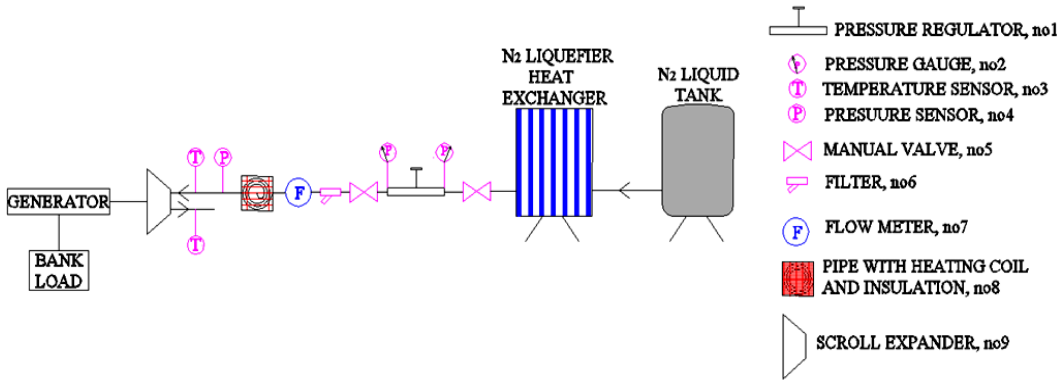

Figure 3-31: Schematic of expander test rig using Nitrogen

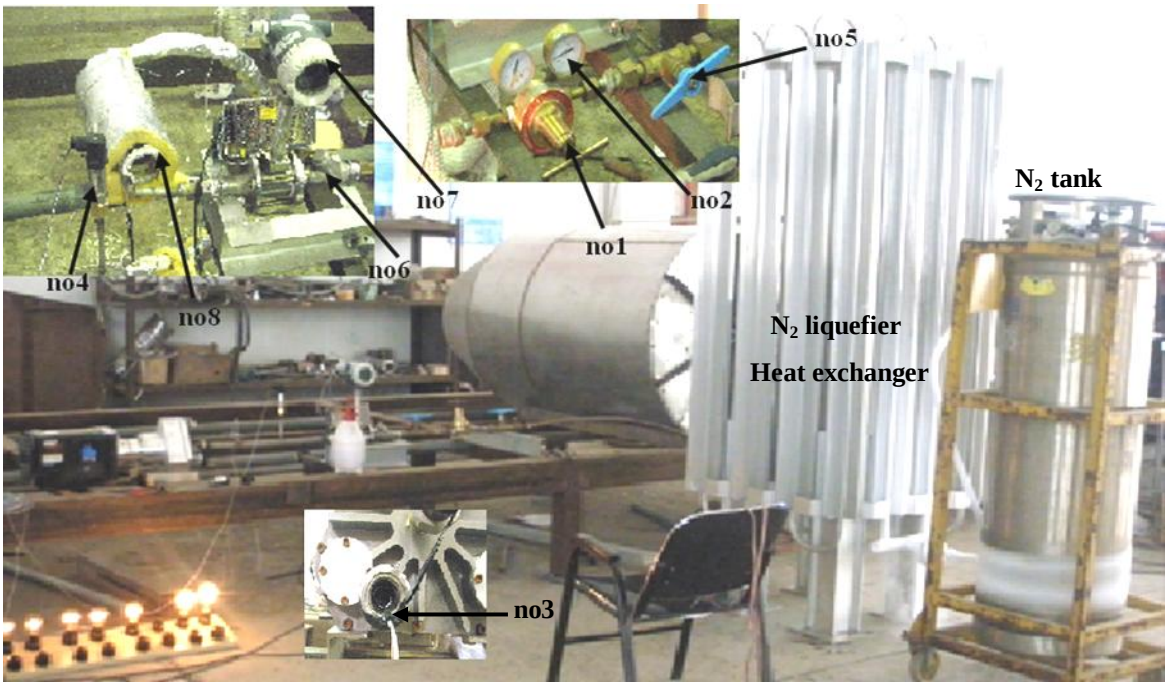

Figure 3-32: Expander test rig using Nitrogen: real set-up

Figure 3-31 includes a liquid nitrogen (N_2) tank followed by a heat exchanger to liquefy the refrigerant, and a pressure regulator with two manual valves in between. Before and after the pressure regulator, a pressure gauge is installed. An air filter is installed before the flow meter, also pressure and temperature sensors are installed before the expander's inlet. The connection pipe after the flow meter is wrapped with heaters. A temperature sensor was also installed at the expander's exit. There is no need for pressure sensors at the expander's exit since it is exposed to the ambient pressure (i.e. the pressure there is always the atmospheric).

The experimental procedure to test the expander's performance initially was under different inlet pressures, assuming more or less the same inlet temperature. Later heater coils were attached to the inlet pipeline and the experiments repeated for a similar inlet pressure and higher temperatures. From the recorded results the expander's tendency in performance can be extracted since the pressure for heating and non-heating trials was closed. Also the expander's efficiency can be found. The expander was also tested for any leak at its main joints where gaskets were attached, running for a few minutes at around 1.4Mpa. For this analysis, graphs will be plotted to support results. Average values for pressure, temperature and power will be used to make the analysis easier.

The performance of the expander is necessary in order to identify its behaviours under different conditions (pressure and temperature) and for different flow rates. After that it will be easier to find power production using the same equipment for ammonia and design the cogeneration system again. Also, it will be helpful to identify the correct scroll expander's size in case it is not under the LH cogen system's specification to maximise the power output.

3.10 LH cogen system preparation

Before the LH cogen system is charged with ammonia and the water circuit is filled with water, should be confirmed experimentally that the system (ammonia and water circuit), is leak free. Therefore the two circuits are tested using nitrogen or compressesed air at a pressure around 2MPa. Pressure gauges are installed temporarily one at the evaporator (ammonia circuit) and one at the reactor water return (water circuit). The machine should remain under high pressure for few days and in case after that period, if the pressure remains the same, then it is safe to assume that the system contains no leak. Figure 3-33 shows a pressure gauge at the evaporator when the

ammonia circuit is tested for leaks. If any leaks should appear, the exact point should be identified, the nitrogen discharged, the leak managed, and the system tested again

Figure 3-33: Pressure gage at the evaporator

Before the data collection, it should be ensured that the temperature sensors are properly calibrated for the results to be considered reliable. Therefore, a calibration bath is used similar to the one shown in Figure 3-34, which can provide accurate temperature and the machine temperature sensors can calibrated. The temperature sensors that were attached to the LH cogen system, are put into the calibration bath and the temperature indicated is compared to the one at the calibration bath. If the sensors temperature is not the same as the calibration bath, then correlations to the data locker are made in order for temperature sensors to show the same value. The system is now ready to be filled with water (water circuit) and with ammonia (ammonia circuit).

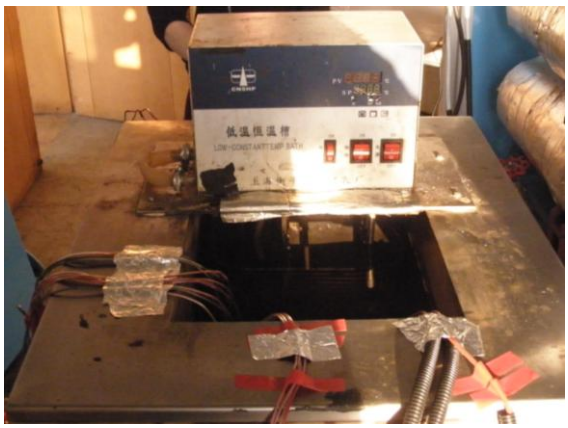

Figure 3-34: Calibration bath

3.11 Power generation scroll expander test

The selected scroll expander's performance will be investigated below using nitrogen gas and not ammonia. There are several reasons for this. The first one has to do with the simplicity of the test rig using nitrogen compared to the ammonia one. If ammonia was used, the circuit has to be in a closed loop. After expansion, the refrigerant must be collected and condensated since it cannot be rejected to the atmosphere. This makes the test ring more complicated, more time consuming to prepare and more expensive.

The other important reason is that in case nitrogen is released to the atmosphere after expansion, the expander outlet pressure will be more or less always constant, the atmospheric pressure, and this is a very useful experimental tool to fix one of the parameters. Using ammonia, the ammonia conditions after expansion will be identified from the heat source running at the condenser. In case tap water from the mains is used as the cooling medium, that means the temperature will not be constant and neither will the expander outlet conditions.

3.11.1 Inlet pressure investigation

The expander's response as a power generation device will be presented and analysed in this section. Figure 3-35 and Figure 3-36 will be used to investigate the expander system's performance for different inlet pressures and similar inlet temperatures. The collected results for these tests can be found in Appendix 1 and show the expander inlet's temperature (^{O}C) and average power production (W) by assuming a similar inlet temperature (^{O}C) for various inlet pressures (MPa). The nitrogen's inlet temperature was dependent on the atmospheric conditions which the heat exchanger was exposed to when it vaporised the liquid nitrogen.

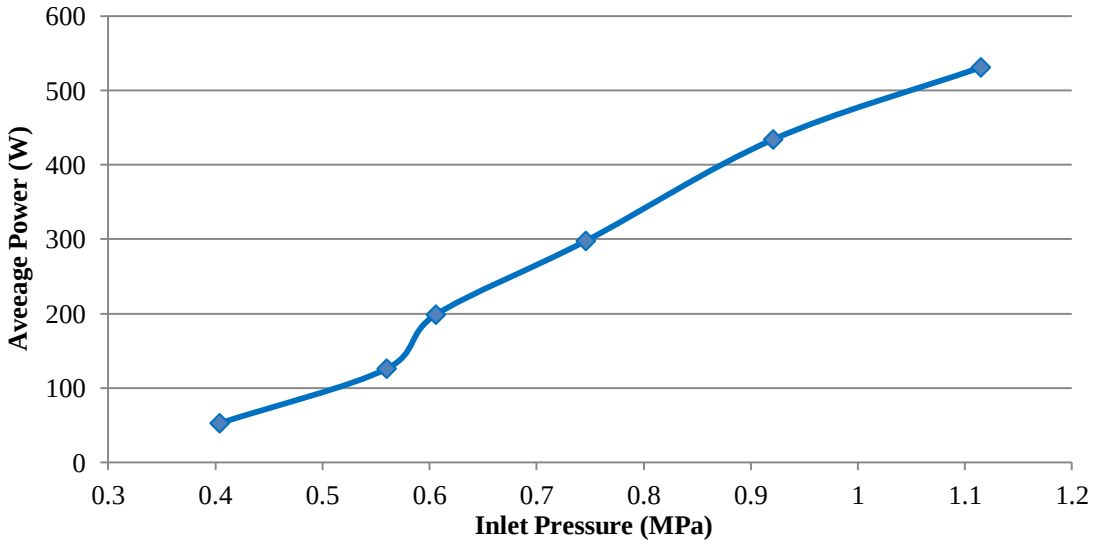

Figure 3-35: Average power variation for different inlet pressures (non-heating)

Figure 3-35 indicates that the expander's power output increases linearly as the inlet pressure increases for similar inlet temperatures. This behaviour was expected, based on the expander's specification where the maximum power output can be achieved at 1.38MPa pressure. The tests were performed for five different inlet average pressures for a sufficient period of time. The pressure variation was from 0.4 to 1.1MPa with a power production range of 52-531W when the average inlet temperature was 25.8^{O}C. The expander's outlet temperature was measured from 10.9 to -23^{O}C.

Figure 3-36 shows the expander's average outlet temperature for different average inlet pressures. The results show that the outlet temperature decreases linearly as the inlet pressure increases. That means the expansion's efficiency increases with the pressure, resulting in more power output. Assuming nitrogen as the ideal gas, when increasing the inlet pressure, the mass flow rate increases for the same gas volume, so the temperature should be decreased.

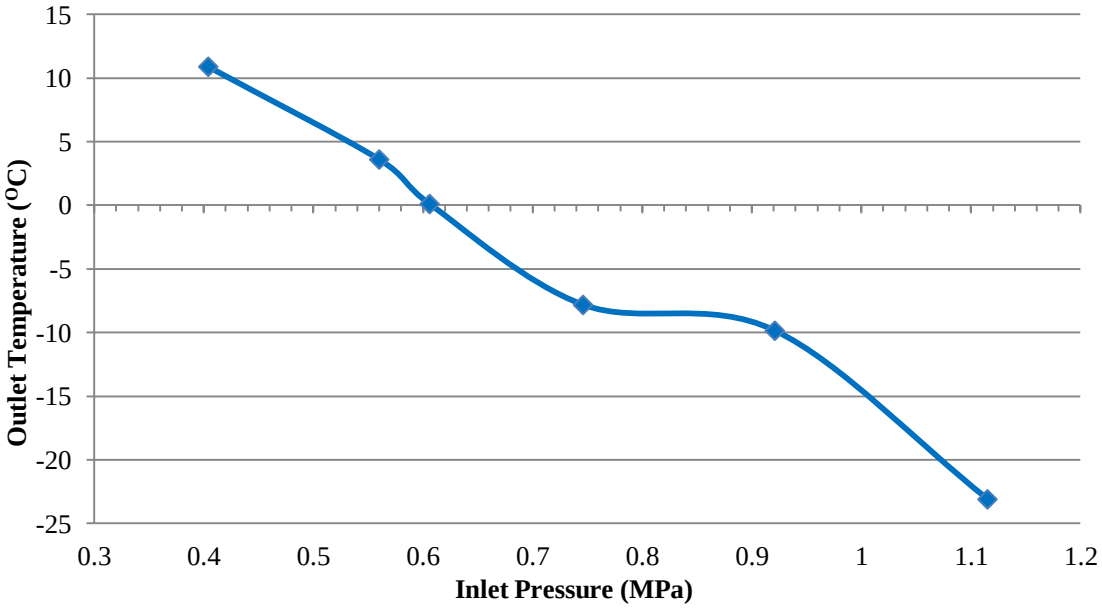

Figure 3-36: Outlet temperature for different inlet pressures (non-heating)

3.11.2 Inlet temperature investigation

Figure 3-37and Figure 3-38 were plotted from the recorded results when the expander was tested for various inlet temperatures assuming more-or-less similar inlet pressures like the one used previously during the inlet pressure investigation. Appendix 2 shows the collected results for varying inlet temperatures.

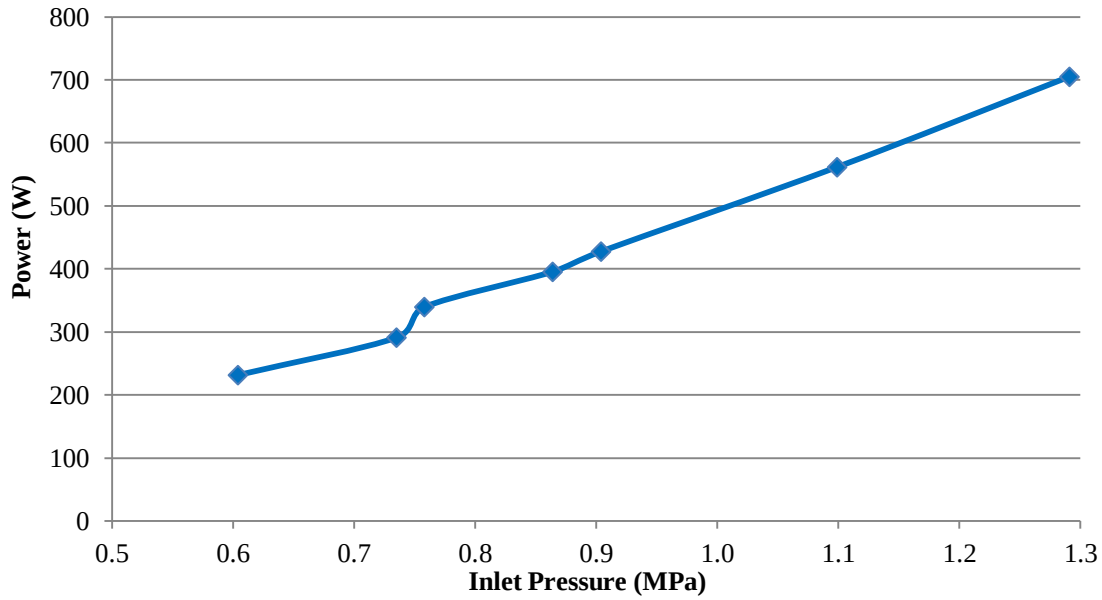

Figure 3-37: Average power for different inlet pressures (heating)

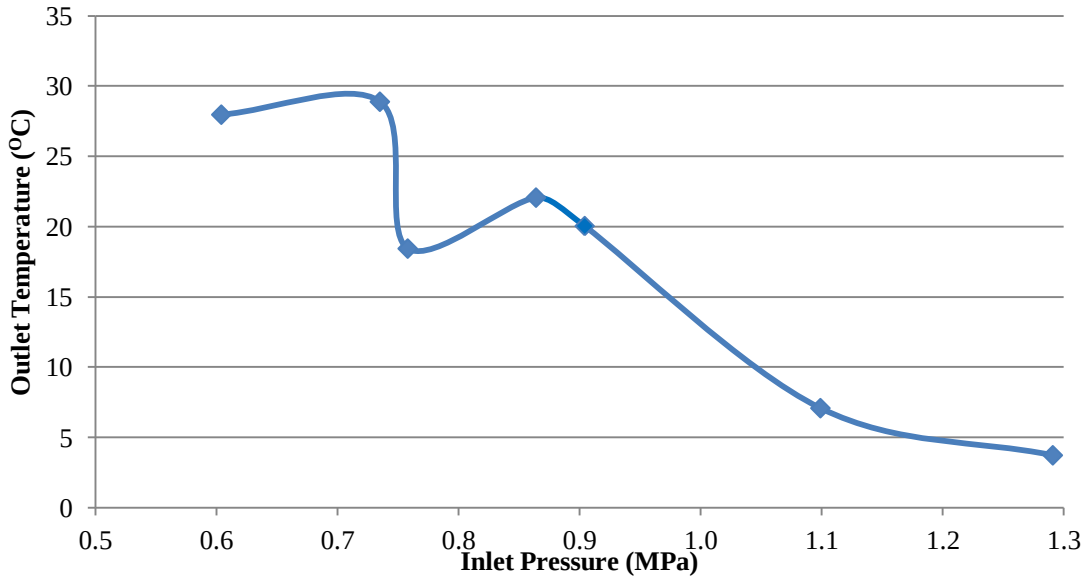

Figure 3-38: Outlet temperature for different inlet pressures (heating)

The response of Figure 3-37 and Figure 3-38 is similar to the non-heating Figure 3-35 and Figure 3-36. That means the power production increases linearly when the inlet pressure and inlet temperature increase and at the same time, the outlet temperature decreases almost linearly.

For the heating trials of Figure 3-37 the operating pressure range was from 0.6 to 1.29MPa when the average inlet temperature was 67.6^{O}C. Under those conditions, the power output was 231-705W on average. The expander's outlet temperature was measured from 28 to 3.7^{O}C.

3.3.2.1 Comparison of heating and non-heating trials

A comparison between the non-heating and the heating trials will follow. Using selected data from Appendix 1 and Appendix 2 for similar inlet pressures, Figure 3-39 was plotted from them. Figure 3-39 shows a comparison of the power production between non-heating and heating power trials.

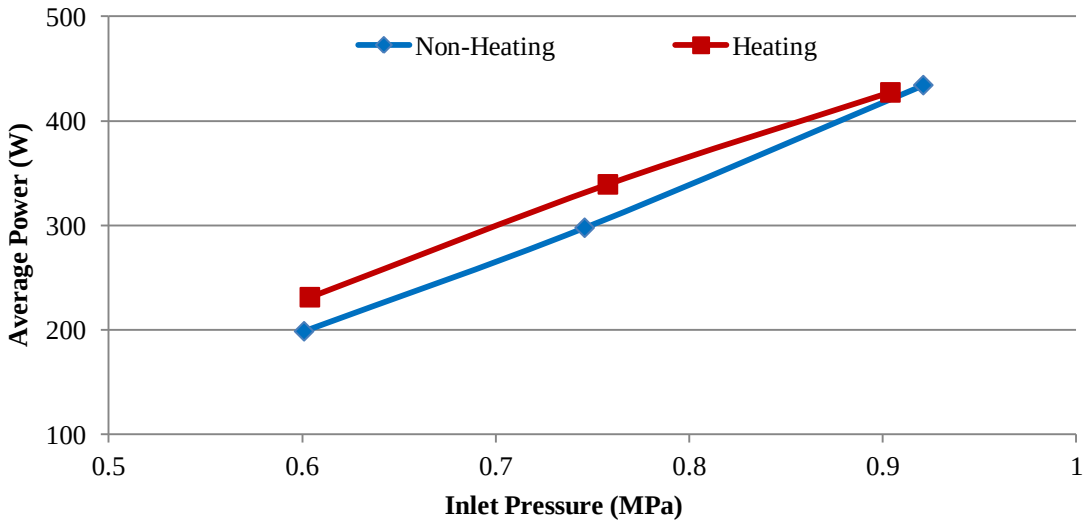

Figure 3-39: Power variation for different inlet pressures (heating and non-heating)

Figure 3-39 shows that as the pressure increases, the power output is increased for both trials and also for the same pressure inlet, the power increases for the heating trials. The importance of that figure is that the average power for the heating trials is greater compared to the non-heating trials. The increase might not be big – around 33W – but the expander's behaviour can be examined. This 33W difference is a result of an approximate temperature increase of 42^{O}C.

According to Appendix 2, the maximum design pressure and temperature were not reached during these experiments, therefore in case even more energy is carried in the expander (higher pressure and temperature), more power will be produced. Another parameter which is important as pressure and temperature increase, is the expander's internal leaks which cannot be eliminated since it is a design factor and related to the refrigerant's flow rate.

3.11.3 Flow-rate investigation

To investigate the flow rate effect on the expander's performance three Pressure-Time (P-t) diagrams will be used. These are: Figure 3-40 which assumes 434W average power production for an inlet pressure of 0.922MPa and 28.8^{O}C inlet temperature; Figure 3-41 which assumes 261W average power production for an inlet pressure of 0.968kPa and 29.1^{O}C inlet temperature; and Figure 3-42 which assumes 431.5W average power production for an inlet pressure of 0.908kPa and 76^{O}C inlet temperature.

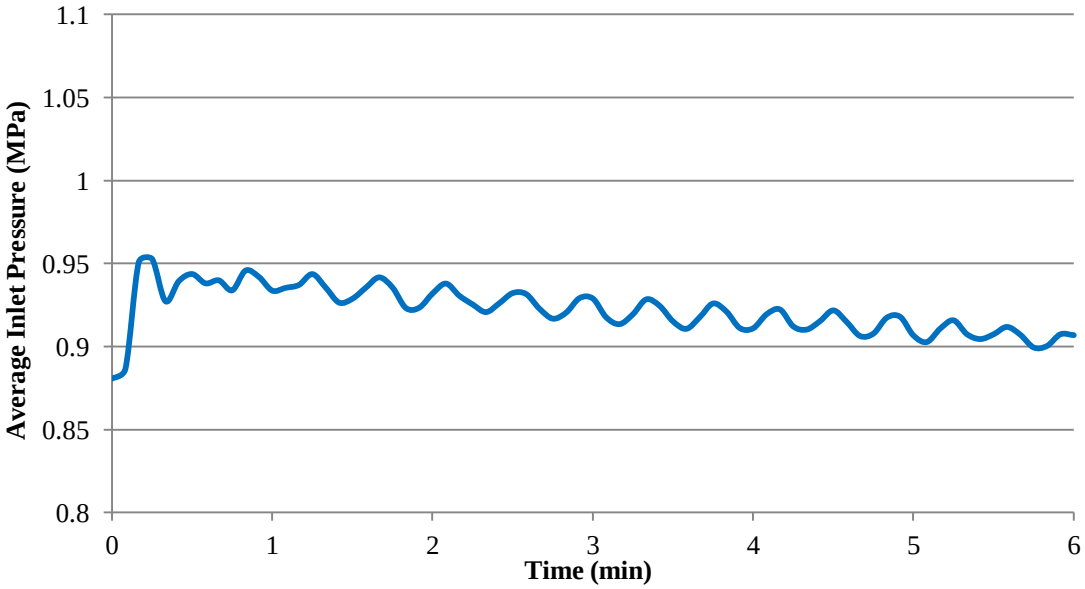

Figure 3-40: P-t diagram for 0.922MPa average inlet pressure

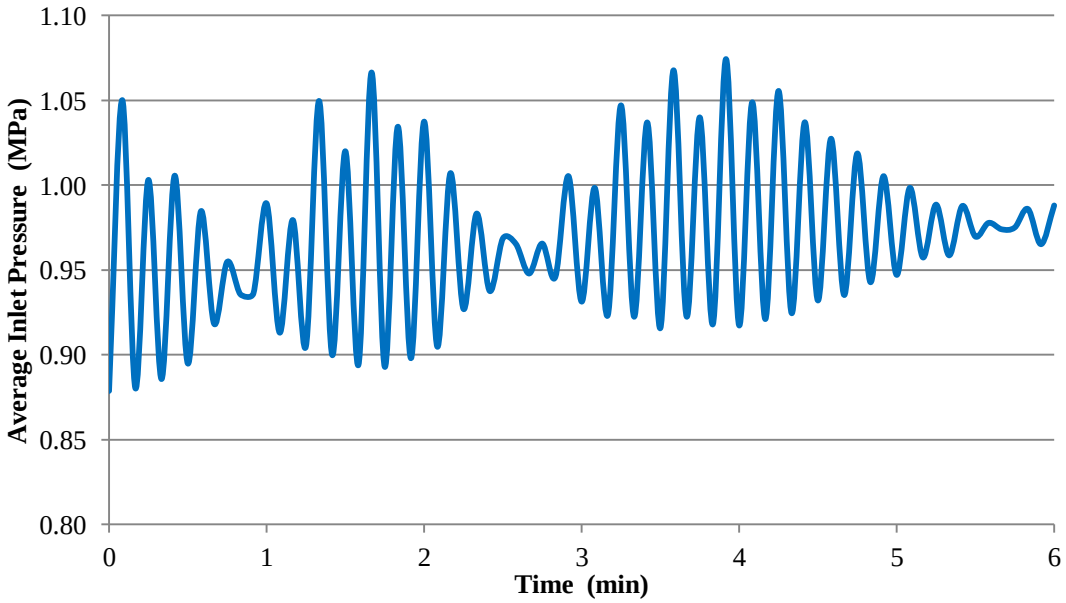

Figure 3-41: P-t diagram for 0.968MPa average inlet pressure

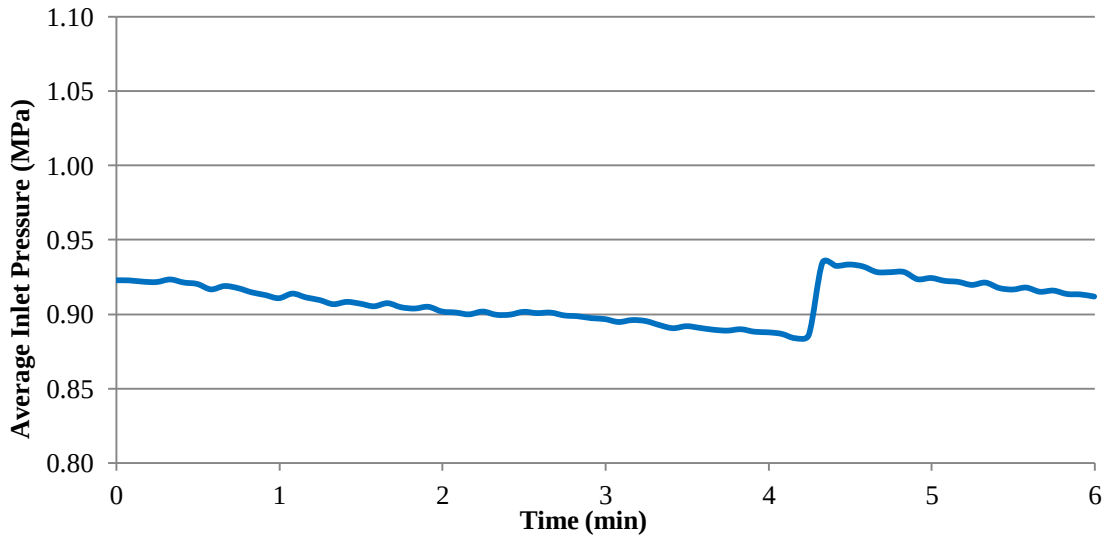

Figure 3-42: P-t diagram for 0.908MPa average inlet pressure

The pressure variation of Figure 3-40 shows a small continual reduction with time which denotes that the refrigerant's flow rate is almost constant. The path is not a straight line but slightly decreases with time, without affecting the power production significantly. For this analysis, this response considers the ideal, i.e. almost constant inlet pressure compared with the rest of the results. The pressure variation was from 0.946MPa to 0.906MPa which is only a narrow 0.040MPa difference.

Figure 3-41 (0.968MPa case-261W on average) shows a different response from Figure 3-40 where the pressure inlet of the expander is fluctuating a lot through the cycle with maximum and minimum values repeated through the cycle. The maximum pressure recorded was 1.075MPa and the minimum 0.880MPa which means around 0.195MPa difference compared to 0.040MPa in Figure 3-40. The explanation is the lower flow rate and even the average inlet pressure are similar because the nitrogen tank runs out of gas. During the experimental procedure, as the nitrogen quantity runs out, the regulator valve was further opened to maintain a high pressure resulting in the pressure fluctuation similar to Figure 3-41. The power output of Figure 3-41 is 261W on average compared to 434W on average in Figure 3-40 which indicates that gas travel in the expander is less for the same inlet conditions.

Figure 3-42 plotted for 0.908MPa and 76^{O}C inlet temperature has high results for 431.5W average power. Even though the inlet temperature is high, the average power output was 431.5W which is almost the same (slightly lower) compared to 434W for the

0.922MPa case (Figure 3-42) and higher than 261W for the 0.968MPa case (Figure 3-41). By examining the pressure variation of Figure 3-42, we can see that it is different from both Figure 3-40 and Figure 3-41. Initially, the pressure decreases slowly and then suddenly peaks and then starts dropping again. This response is repeated until the end of the trial. The maximum inlet pressure recorded was around 0.935MPa and the minimum 883kPa which means around 0.052MPa difference. This is closer to Figure 3-40 response but the sudden pressure increase through the cycle denotes that the nitrogen tank is staring to run out.

3.12 Error analyses

Any value measured in any experiment, is the results of the true value plus or minus the experimental error. Precision and accuracy are two terms used to describe error. Precision indicates the difference between the mean values of many separates measurements and the actual true value and is related to the random error distribution. Accuracy indicates how close the measurement value is believed to be the actual one and depends on both magnitude of both systematic and random error. This kind of error can be a result of incorrect calibration. Precision and accuracy should be improved in every experiment to reduce error.

Systematic errors are cause by to improper instrument calibration or due to limitations of the measuring equipment and cannot be analysed using statistics only estimated by the person making the measurement. After it is discovered it can be corrected by instrument recalibration.

Random error is caused due to measurement equipment limitations, operator experimental approach or accidental change of the experimental conditions. This kind of error cannot be eliminated or corrected by improving the test method or test equipment and it follows a statistical law for repeatable measurements to be described. It can be estimated by calculating the mean value for repeatable measurements and the standard deviation. Error analysis is discussed in the British Standard ISO TR 5168:1998 and BS ISO TR 7066-1:1997.

3.12.1 Uncertainly of the experimental results

For this analysis, the greeκ letter ‘ε’ will be used to denote the uncertainty. The systematic error which is the one provided for the selected instrument on Table 3-6 is denoted as ε_s. The random error ‘ε_r’ is found using the standard deviation ‘σ’ approach

and for the thermal resistance, for a water mean temperature in the reactor of 129.8^{O}C, σ is 1.28 therefore the ε_r is:

ε_r=1.28/(129.8+273)=0.032%

The total system uncertainties can then be estimated using the additive model (ε_{ADD}) and the root-sum-square model (ε_{RSS}).

$$\boldsymbol{\varepsilon_{ADD} = \varepsilon_s + 2\varepsilon_r} \quad \textbf{3-2}$$

$$\boldsymbol{\varepsilon_{RSS} = \sqrt{\varepsilon_s^2 + 2\varepsilon_r^2}} \quad \textbf{3-3}$$

For the above example, ε_{ADD} is (0.5)+2(0.32)=1.14%. At the same time, ε_{RSS} is $\sqrt{(0.005)^2+(2*0.0032)^2}$= 0.81%

The results of the total uncertainties following similar approach like before presented to Table 3-8.

Position	Measurement	Systematic Uncertainty ε_s %	Random Uncertainty ε_r %	Total Uncertainty ε_{ADD} %	Total Uncertainty ε_{RSS} %
Water in the condenser	Temperature	0.5	0.2	0.5	0.50
Water in at reactor 2	Temperature	0.5	0.25	0.99	0.64
Water out at reactor 2	Temperature	0.5	0.22	0.95	0.70
Water in at reactor 1	Temperature	0.5	0.32	1.14	0.81
Water out at reactor 1	Temperature	0.5	0.04	0.58	0.50
Expander ammonia out	Temperature	0.5	0.2	0.5	0.5
Evaporator 1	Temperature	0.5	0.10	0.69	0.54
Evaporator 2	Temperature	0.5	0.25	0.99	0.70
Evaporator 1	Pressure	1	0.01	1.02	1.00
Evaporator 2	Pressure	1	0.00	1.00	1.00
Expander in	Pressure	1	0.02	1.02	1.00
Expander out	Pressure	1	0.02	1.02	1.00

Table 3-8: Uncertainties of measurements at the LH cogen system

Table 3-8 shows that the total uncertainties for the temperature and pressure sensors are low and in some cases negligible. The temperature sensors were calibrated before the experiments took place and as a result their uncertainties are very low.

3.13 Conclusions and discussions

This chapter analyses the construction approach for the LH cogen system. An overall system schematic is provided as is one for its cooling the cogeneration operation with the necessary explanations of the machine's operation modes. Similarly, a schematic of the expander nitrogen test is provided.

In terms of the LH cogen system construction, this chapter provide in detail all the information (size, method of construction and material used) for the reactor, condenser, evaporator, the boiler and the water tank. Also, data related to the selected scroll expander is given. At the same time, information about all the temperature and pressure sensors positions is given, as well as about all manual the pneumatic valves in the system and the flow meter. This chapter also provides information about the ammonia and water system fluid circuits and how they interact for adsorption, desorption and condensation to be achieved. The existing design primary purpose was the machine to keep as simple and compact therefore some design limitation arise which are summarised below.

a) The main construction is steel based (easily available, cheap easily cut and joined) which means high sensible heat losses and since not the entire machine is insulated, heat losses are increased.
b) The electronic part of the V1 pneumatic valve (steam leaving the boiler) overheats and can become damaged because it is in contact with the boiler.
c) The water circuit (hot and cold water) is one single circuit in which the hot and cold stream are split using pneumatic valves. That means after the switch period, the hot water carrying from the reactor currently under cooling returns to the low temperature water tank and the cold water carrying from the reactor currently under heating returns to the high temperature boiler.
d) Figure 3-43 shows that the V1 pneumatic valve position (steam leaving the boiler) and the V3 (water leaving the water tank) do not interconnect but the piping actually interacts at the 3-way connections attached to the pneumatic valves. This mean that the cold and the hot water fluids meet at the 3-way connector (not direct contact, just heat transfer) and that affects mainly the cold water entering the reactor 1. More specifically, the cold water temperature enters reactor 1 at around 51^{O}C and 39^{O}C to reactor 2.

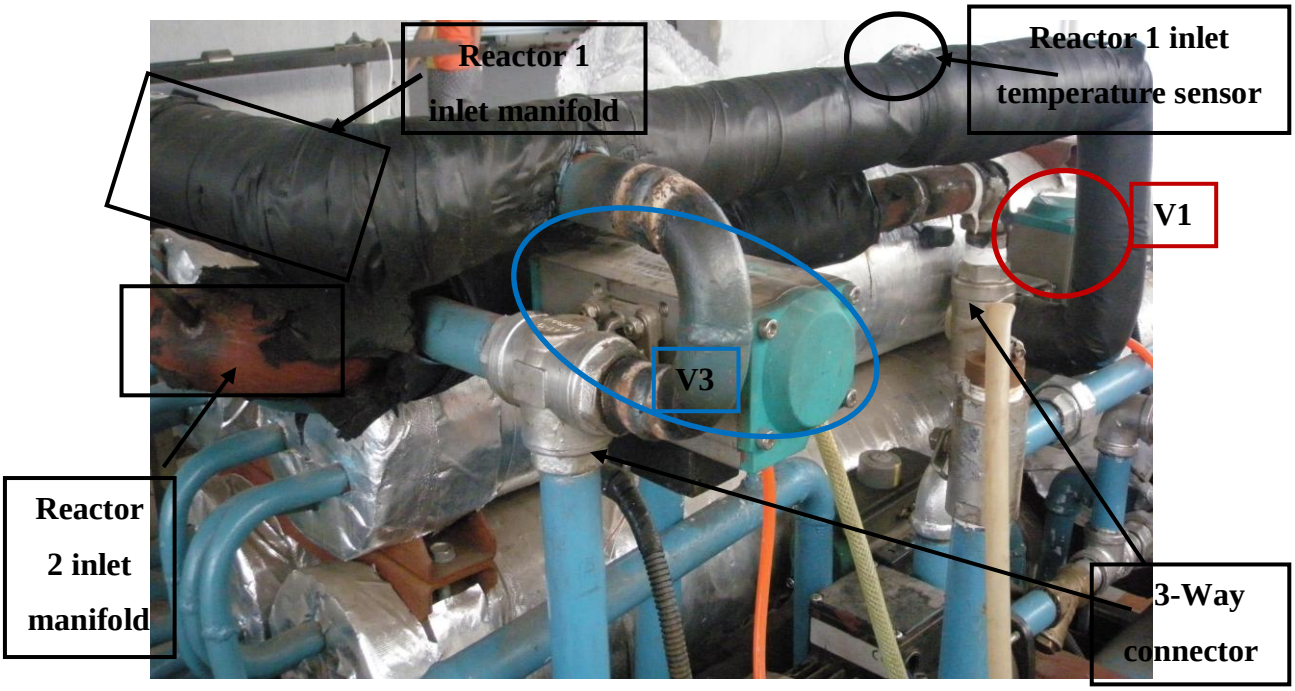

Figure 3-43: V1 and V3 pneumatic valve position and temperature sensor

e) The reactor 1 inlet temperature sensor is installed away from the reactor and close to the boiler. This position is not the ideal one (Figure 3-43) and should be on the inlet manifold since at the current position indicate higher water temperature than at the one at the entrance the reactor.

f) The copper pipes carrying the water to the reactors are not ammonia compatible. In order to ensure that no ammonia is in contact with the copper pipe it should be ensured that there is a perfect seal between the flanges and the pipes, as well between the flanges to the reactor cylinder. The efficiency of the welding process described above is critical.

g) The system cooling capacity is measured form the heater coil carried in each evaporator. The heater coil is placed in a heater cover which is warmed up initially before every time the heater is turned on and that means some heat losses.

h) The temperature and pressure sensors uncertainties are low and that strength the reliability and the accuracy of the experimental results measured.

During the expander power test the scroll expander's performance related to the gas inlet's pressure and temperature was found. There is a linear relationship between the inlet's pressure and temperature with the average power production. The pressure range the expander was tested at between 0.4 and 1.29MPa. The average inlet temperature

during the non-heating trials was 25.8^{O}C and 67.7^{O}C for the heating trials. The maximum power production during the non-heating trials was 531W and for the heating trials was 705W. At the same time, the lower expander's exit temperature was -23^{O}C and 3.7^{O}C respectively.

Chapter 4. Experimental results and discussion

In this chapter all the experimental results taken during this study will be presented and analysed. These include the only-cooling mode and cogeneration mode for the LH cogen system, as well as the scroll expander's power performance test using nitrogen. For the only-cooling mode operation of the machine, variable conditions were investigated, including the heating desorption temperatures, the evaporator temperatures (requiring cooling), basic cycle and mass recovery time and the overall ammonia the system carries. From the collected results, the refrigeration and the power performance of the machine will be calculated and the machine's optimum working conditions will be identified. The results and the experimental procedure will also provide valuable feedback for future work on how the system can be designed better as well as how to improve the experimental procedure. The cooling results were taken at two different periods, and the cogeneration and the expander tests were both taken during a third period of tests.

4.1 Cooling mode

Table 4-1 summarises all the working conditions for the only-cooling experimental results. These include the boiler set-up temperature which relates to the temperature of the vapour entering the reactor during desorption, the evaporator's set-up temperature (cycle cooling required), the cycle time (basic cycle and mass recovery) and the overall system's charged ammonia. The useful data the machine can provide are for the average cooling production (^{O}C) which is the average from a low-pressure evaporator during a cycle, the average cycle heating (Q_{high}) which is a measure of the power which the heaters provide at the boiler to establish the required system's high temperature, refrigeration power (kW) which is a measure of the time the heater at the evaporator stays ON when the temperature there drops below the set-up temperature. The average cycle's high pressure which is the average system's high pressure during desorption-condensation and the lower/ average low pressure recorded during the adsorption-evaporation process. The lower pressure is the lowest value recorded during the adsorption-evaporation process and the average low pressure is the average system pressure during that process. For all the results the heat sink temperature (cooling water temperature) has to keep constant either at $20^{O}C$ or $28^{O}C$ on average for the system to carry either 24kg or 28kg of ammonia. The ammonia quantity is the optimum for the

system and agree with the Li, et al. [74] study where a $CaCl_2$-NH_3 chemisorption system was under investigation. The cooling generation efficiency (COP_{ref}) is a measure of the system's cooling generation at the evaporator Q_{ref} (kW) during the cycle and the average heat input Q_{high} (kW) during desorption. Mathematically this is described by Equation 4.1 as it found in the literature [34, 105, 114].

$$\mathbf{COP_{ref} = \frac{Q_{ref}}{Q_{high}}} \qquad \textbf{4-1}$$

The experimental procedure during cooling only mode allows the machine to run for a long period of time at a specific amount of required cooling. When the results are repeatable, then the heating temperature increases for the same required cooling. This procedure is repeated for all the required cooling amounts. The presented results are a selection of continuous cycles of successful cooling production for similar operating conditions (high and low heat sources and set-up evaporator's set temperature). The cycle time (basic plus mass recovery) presented in Table 3-7 is for a half cycle so for one complete cycle this time is doubled. The ammonia quantity the system was charged with was initially around 4.5 moles (12kg) and later 5.2 moles (14kg) per side.

Boiler Set-Up Temperature (^OC)	**Evaporator Set-Up Temperature (^OC)**	**Cooling Water's Average Cooling Temperature (^OC)**	**Basic Cycle Time (min)**	**Mass Recovery Time**	**Ammonia Quantity (kg)**
135	0	20	10	1 min	28
			13	30 sec	28
				1 min	28
				2 min	28
			16	1 min	28
			18	1 min	28
		29	13	1 min	28
	-5	20	10	1 min	28
			13	30 sec	28
				1 min	28
				2 min	28
			16	1 min	28
			18	1 min	28
	-10	20	13	1 min	28
145	0	20	13	1 min	28
	-5				28
	-10				28
130	0	29	13 14	1 min 0	24
	5 0 -5	29	13	1 min	28
	0	29	13	0	28

	-5	29	25	1 min	28
110	0	20	13	1 min	28
	-5				28
100	0	20	13	1min	28

Table 4-1: Collected conditions for only-cooling experiments

4.1.1 Heating temperature

Figure 4-1 presents the refrigeration system's performance (COP_{ref}) with respect to the heating temperature when the system carries 28kg of ammonia for $0^{O}C$, $-5^{O}C$ and $-10^{O}C$ evaporating at the set-up temperature. Appendix 3 presents the overall results where Figure 4-1 shows the results taken and includes various heating temperatures for $0^{O}C$, $-5^{O}C$ and $-10^{O}C$ evaporating temperatures, assuming for a 14min (13+1min) overall cycle time (13min basic cycle and 1min mass recovery) when the average cooling water temperature is $20^{O}C$ when the system is charged with 28kg of refrigerant. Experimental data during only cooling mode shows the total error as it estimated on Table 3-8.

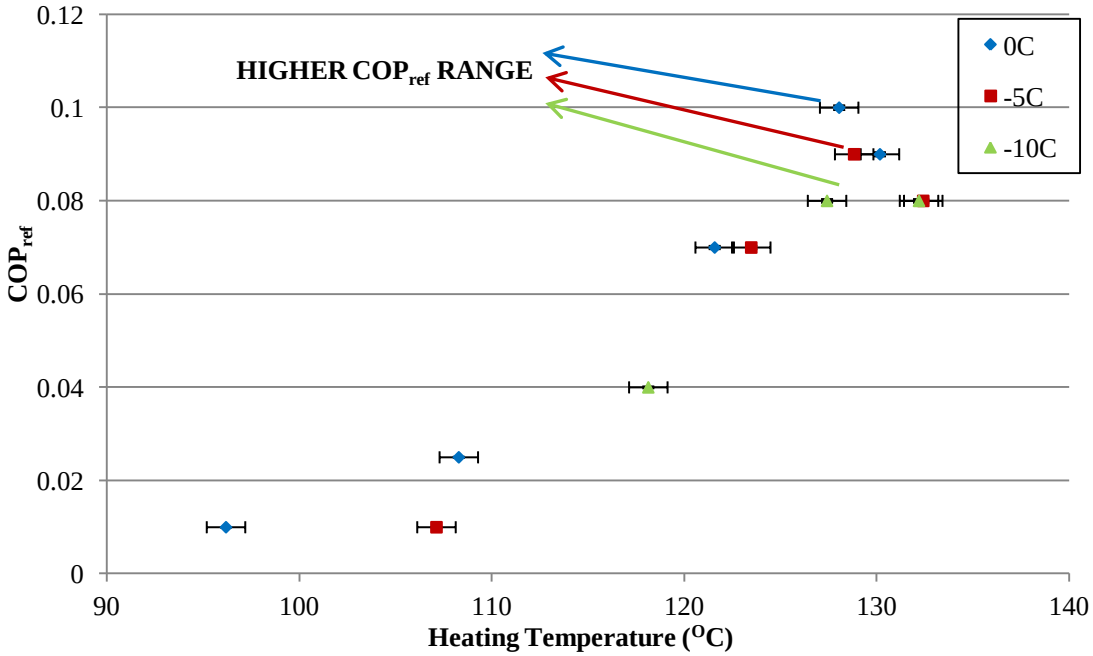

Figure 4-1: COP_{ref} for different heating and evaporating temperatures

From Figure 4-1 it can be observed that the refrigeration COP_{ref} increases as the heating temperature increases. This response is true up to the higher COP_{ref} range and later drops. This behaviour is the same for any evaporating temperature. As the vapour temperature increases, more energy is available for desorption (more heat in the reactor Q_{high}) resulting in a desorption rate increase. That results, later when the reactor will be

used for cooling, in an adsorption efficiency increase so the refrigeration effect. Any temperature above the higher COP_{ref} range point means no sufficient refrigerant can be desorbed sufficiently resulting in the COP_{ref}. That means more energy transfers to the high-pressure reactor without more ammonia to desorb, and at the same time the refrigeration power at the low-pressure side is not increased and that results in the COP_{ref} decrease.

Figure 4-1 also shows that the refrigeration COP_{ref} decreases as the evaporating temperature decreases for the same heating temperature. The system needs to consume more energy (the average cycle's heating power increases) as the evaporating temperature decreases to satisfy the increasing cooling demand. At the same time the refrigeration power is decreased because the required cooling at the evaporator is less. It is clear that there is an optimum desorption temperature range resulting in a maximum refrigeration performance when the machine operates only as an adsorption chiller. Beyond that point, any further heating will result in the refrigeration's COP_{ref} drop.

This response is similar to the compression air conditioning systems which, as the required cooling temperature decreases, more energy is required to be rejected from the cooling space before useful cooling can start, resulting in the overall cycle's COP decrease. For this machine useful cooling means the system's refrigeration production (during which the heaters at the evaporator are ON) is recorded when the evaporator's temperature reaches the set-up temperature and below. From Figure 4-1it can also be concluded that the more the COP_{ref} range is slightly shifted to the right as the evaporating temperature is decreased, i.e. the lower the evaporating temperature, a higher COP range is recorded for slightly higher vapour temperatures.

For these sets of results, the maximum cycle COP_{ref} is recorded for approximately $128^{O}C$ vapour temperature in the reactor which is the optimum vapour temperature for this machine, assuming 28kg of ammonia is for a 14min cycle time, one of which is the mass recovery.

Figure 4-2 shows the average refrigeration power production (kW) for $0^{O}C$, $-5^{O}C$ and $-10^{O}C$ evaporator set-up temperatures for various heating temperatures, with a 13+1

cycle time with a 20^{O}C cooling water average temperature for the overall system's 28kg of ammonia.

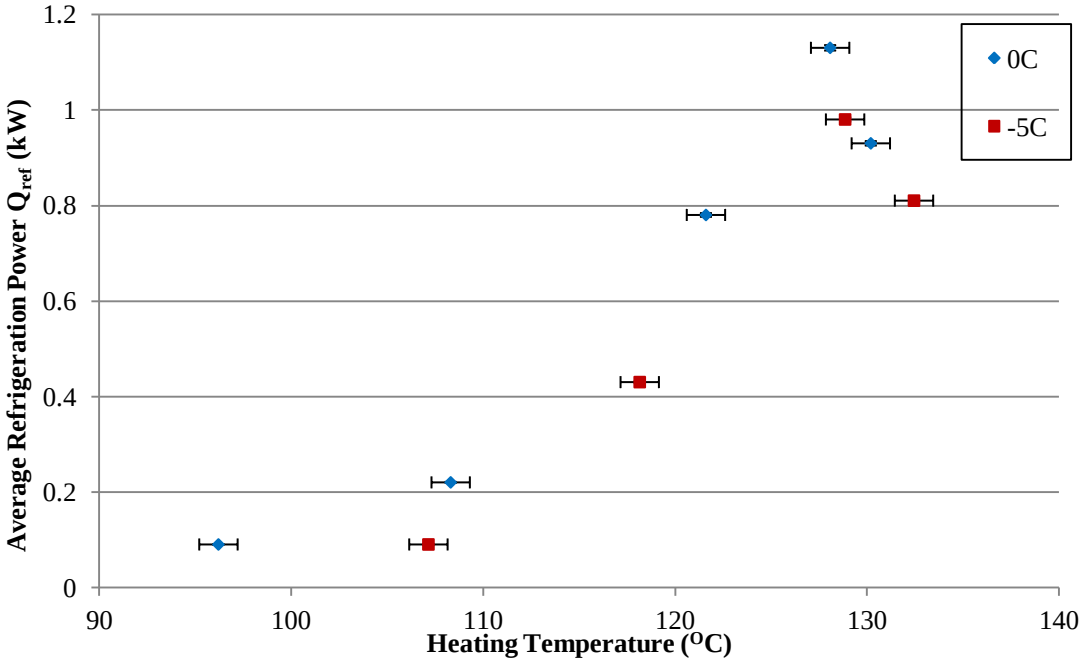

Figure 4-2: Average refrigeration power for different heating levels

Figure 4-2 has a similar response to Figure 4-1 which means that the average refrigeration power is linearly increased as the heating temperature increases. There is a maximum temperature resulting in the maximum refrigeration power and any further temperature increase afterwards results in a refrigeration power decrease. This response is true for any evaporator's set-up temperature. The higher the desorption temperature, the more ammonia is expected to be desorbed, resulting in the adsorption rate's increase since the reactor desorbs more refrigerant, therefore the average cooling power increases. The refrigeration power is less for the same heating temperature as the evaporator's set-up temperature is decreased since the machine produces less useful cooling.

The chiller does not increase its refrigeration effect infinitely with the vapour temperature's increase, and that does not agree with the theory which, for higher vapour temperatures, the desorption (so the adsorption rate) will be increased. The refrigerant desorbed is related to the system's ammonia quantity, the heating source, the cooling water temperature and the cycle time. For $CaCl_2$ composite with ammonia, the closer the composite is to the $CaCl_2$*$4NH_3$, the harder it is to desorb more refrigerant for the same conditions and for the same cycle time. Also, Figure 4-3 shows the average

cooling production at the evaporator (^{O}C) for 0^{O}C, -5^{O}C and -10^{O}C evaporator set-up temperatures for various heating temperatures, for a 13+1 cycle time, with a 20^{O}C average cooling temperature for the overall system's 28kg of ammonia.

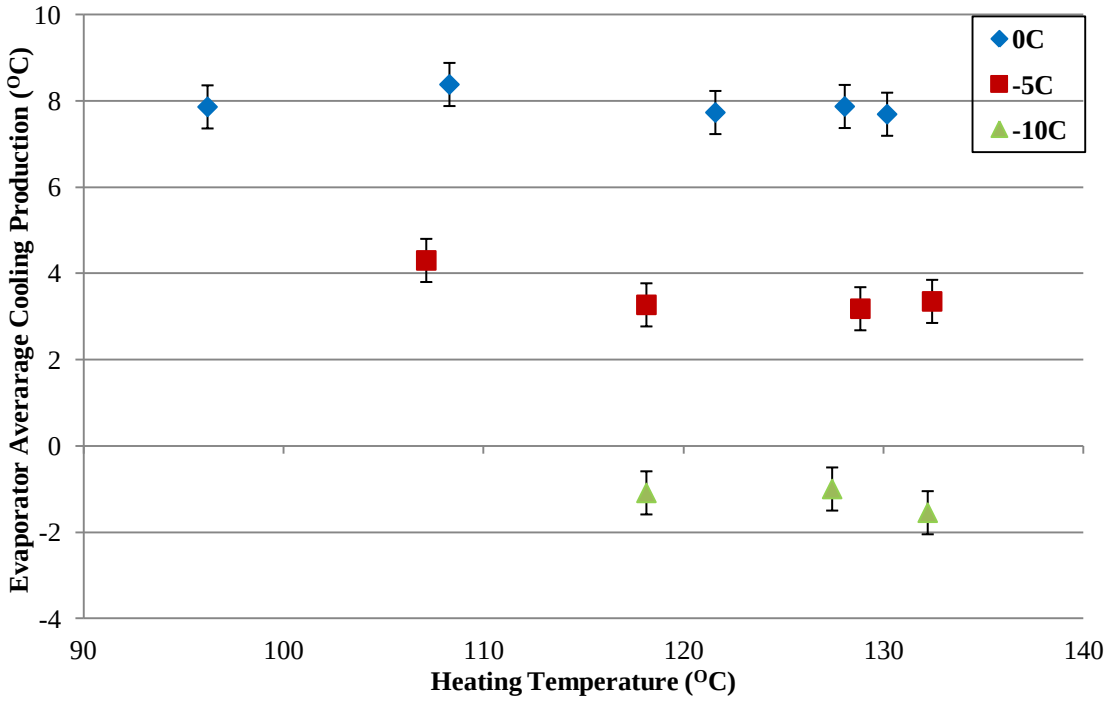

Figure 4-3: Average cooling production for different heating levels

From Figure 4-3 it can be said that for each evaporator's set-up temperature, the average cooling production at the evaporator is more or less the same for any heating temperature. At the same time, for the same vapour temperature, the average cooling production is decreased as the evaporator's set-up temperature decreases. From the above it is concluded that even the average cooling power is increased as the vapour temperature increases for each evaporator's set-up temperature, the average cycle's cooling production remains more or less the same. The reason is that as long as the heaters at the evaporators stay on, when turned off, the temperature at the evaporator steps up more than a cycle with less Q_{ref} production.

Figure 4-4 indicates the average high pressure (MPa) for 0^{O}C, -5^{O}C and -10^{O}C evaporator set-up temperatures for various heating temperatures in the 13+1 cycle time and 20^{O}C average cooling temperature for the overall system's 28kg of ammonia.

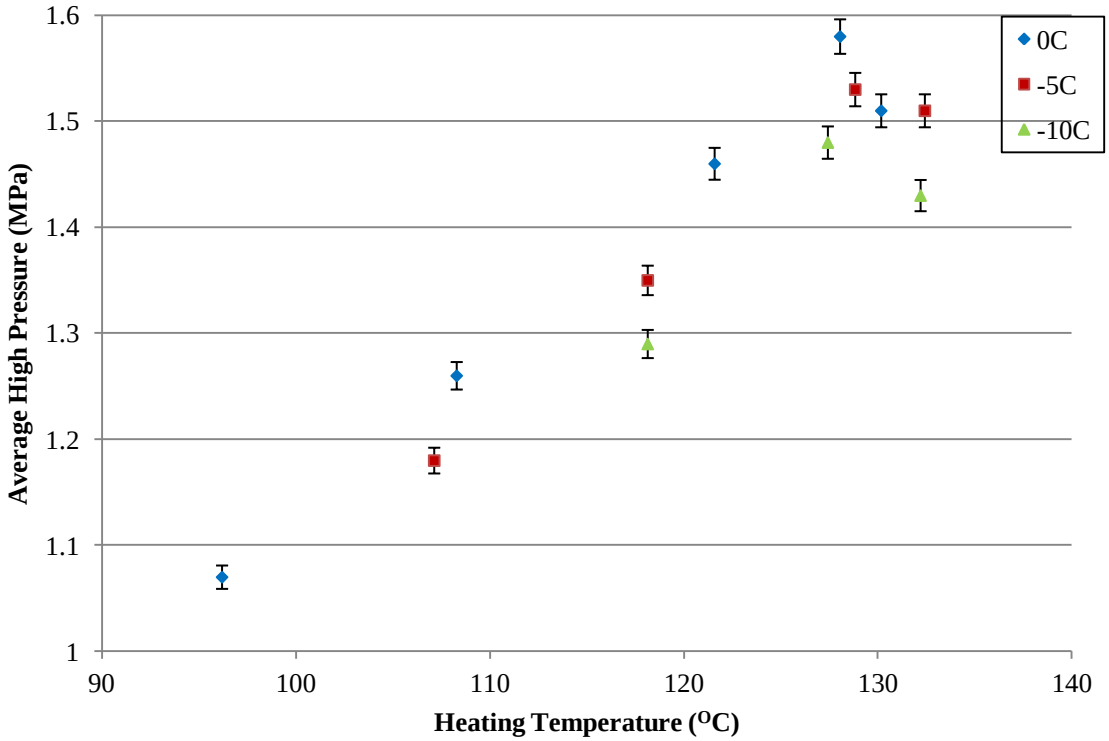

Figure 4-4: Average high pressure for different heating levels

From Figure 4-4 it can be concluded that the average system's high pressure is increased as the heating temperature increases. There is a peak value at around 128^{O}C and after that it drops down. This response is similar for all the evaporating temperatures. Figure 4-4 also shows that the average maximum high pressure for similar heating temperatures is slightly more as the evaporator's set-up temperature increases.

The more ammonia there is in the system, the more is the operating high pressure since the equilibrium pressure is higher assuming the same heating temperature. For 28kg of ammonia and approximately 128^{O}C vapour in the reactor's set of results, the maximum pressure recorded for the vapour temperature is 2MPa which is the machine's maximum pressure limits according to the manufacturer therefore no further results at a higher heating temperature could be considered.

It would be expected that Figure 4-4 would be a straight line with a positive slope but after approximately 128^{O}C heating the temperature in the reactor for each evaporator drops down. The reason could be related to the adsorbent material's properties, mass

and heat transfer limitations which reach the maximum performance under those conditions and further heat will result in heat losses.

Figure 4-5 shows the system's lower pressure data collected during the adsorption-evaporation process for 0^{O}C, -5^{O}C and -10^{O}C evaporator set-up temperatures for various heating temperatures, the 13+1 cycle time and 20^{O}C average cooling temperature for the overall system's 28kg of ammonia.

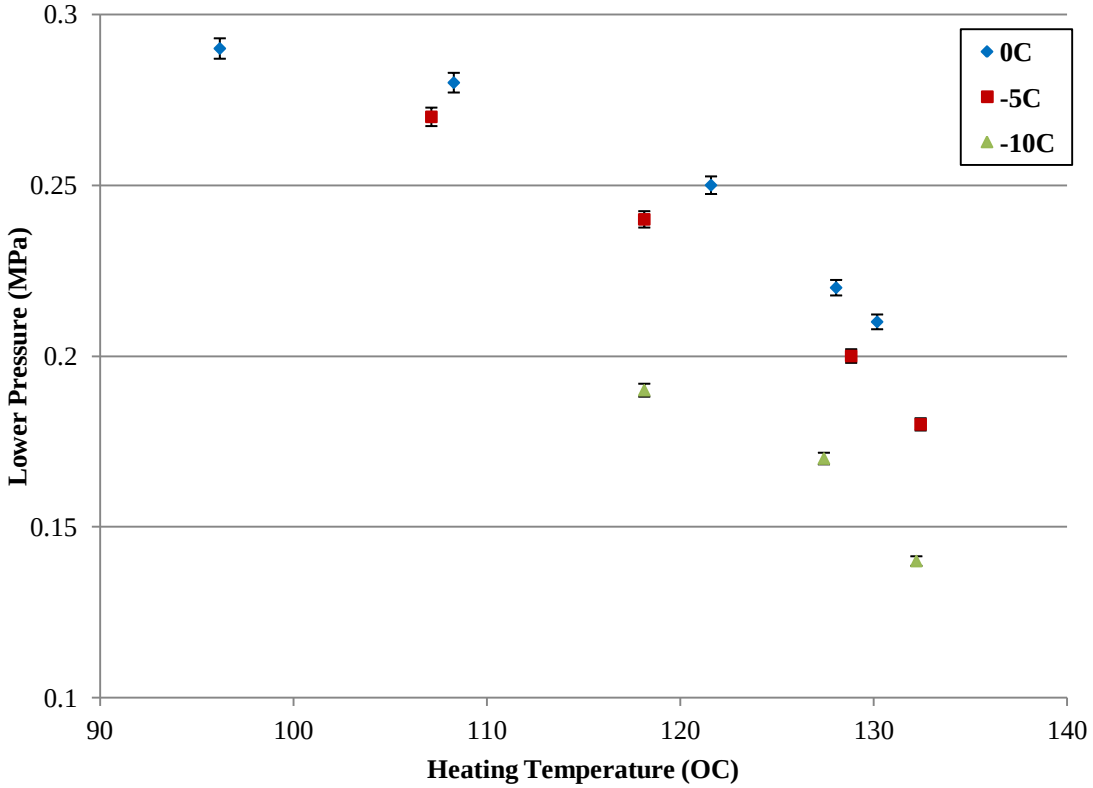

Figure 4-5: Lower pressure for different heating levels

Figure 4-5 shows that as the heating temperature increases, the pressure during the adsorption-evaporation process linearly decreases and this happens for all the evaporator's set-up temperatures. Also, as the evaporator temperature decreases, the system's pressure for the same heating temperature is decreased.

The lower the pressure recorded means the adsorption efficiency increases as a result of an increase in the adsorption capacity. That means the reactor is 'drier': i.e. it possesses less ammonia when the adsorption-evaporation process starts, as a result of the high desorption performance previously. The lower reactor's pressure is directly related to the cooling water used during the adsorption-evaporation process, which results in a lower system pressure.

If the lower pressure during the adsorption-evaporation process is higher, it can also mean a lot of ammonia appears at the evaporator before the system switches to the adsorption-evaporation process. That will increase the evaporator's sensible heat which is a drawback for the system's refrigeration performance. The result is the refrigerant at the evaporator is late in cooling down to the required cooling temperature, resulting in a reduction in refrigeration power. Similarly, if the lower pressure is higher, it can also mean that the reactors possess more ammonia during the process when the adsorption-evaporation process starts so resulting in a smaller adsorption capacity available in the adsorbent bed. The chiller's lower pressure is related to the lower temperature drop but not necessarily to the Q_{ref}. For these results, the lower the pressure is at the evaporator, the lower the temperature drop but in terms of Q_{ref} for the last heating point this is less.

The lower pressure decreases with the evaporator temperature decrease for the same heating temperature because for chemisorptions systems, temperature and pressure are directly related.

At the same time, the system's average low pressure during the adsorption-evaporation process is increased as the heating temperature increases for any evaporator's set-up temperature. This is happening even when the lower cycle pressure decreases with the heating temperature increase.

One reason for that is the pressure difference between the high and low pressure sides of the system before mass recovery takes place, which is more with the increase in the heating temperature. Therefore, after the mass recovery process, the system's pressure is higher as the heating temperature increases. This can be understood from Figure 4-6 which shows the evaporator's pressure for the $0^{O}C$ set-up evaporator's temperature, assuming a single cooling cycle for various heating temperatures ($96.2^{O}C$, $108.3^{O}C$, $121.6^{O}C$, $128.07^{O}C$, $130.19^{O}C$ on average).

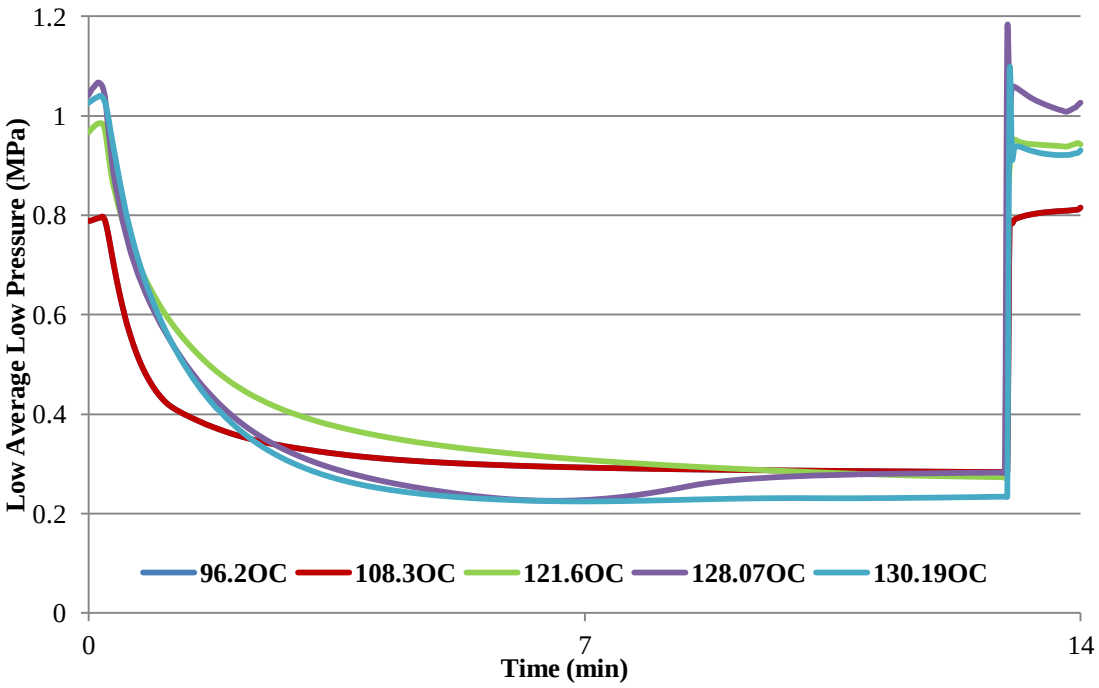

Figure 4-6: Low average pressure for different heating temperatures

Figure 4-6 shows that as the heating temperature increases, the evaporator can reach a lower pressure during the adsorption-evaporation process. Also the higher the heat source, the system possesses low pressure for a longer period of time and that is reflected in the cooling capacity increase.

Figure 4-7 shows the specific cooling power (SCP) per side for different heating temperatures. SCP is a measure of the refrigeration power (Q_{ref}) to the adsorbent mass per side as Equation 4.2 shows which is 17.5kg in that case [74, 115]. Therefore the response of Figure 4-7 is identical to Figure 4-2. The maximum SCP was 64.57W/kg per side for the 128.07^{O}C heating temperature and 0^{O}C the evaporator's set-up temperature. The maximum SCP for 0^{O}C and -5^{O}C evaporator set-up temperatures was 56 and 38.25W/kg per side for 128.85^{O}C and 127.44^{O}C heating temperatures respectively.

$$\mathbf{SCP} = \frac{\mathbf{Q_{ref}}}{\mathbf{kgAdsorbnet}} \qquad \mathbf{4\text{-}2}$$

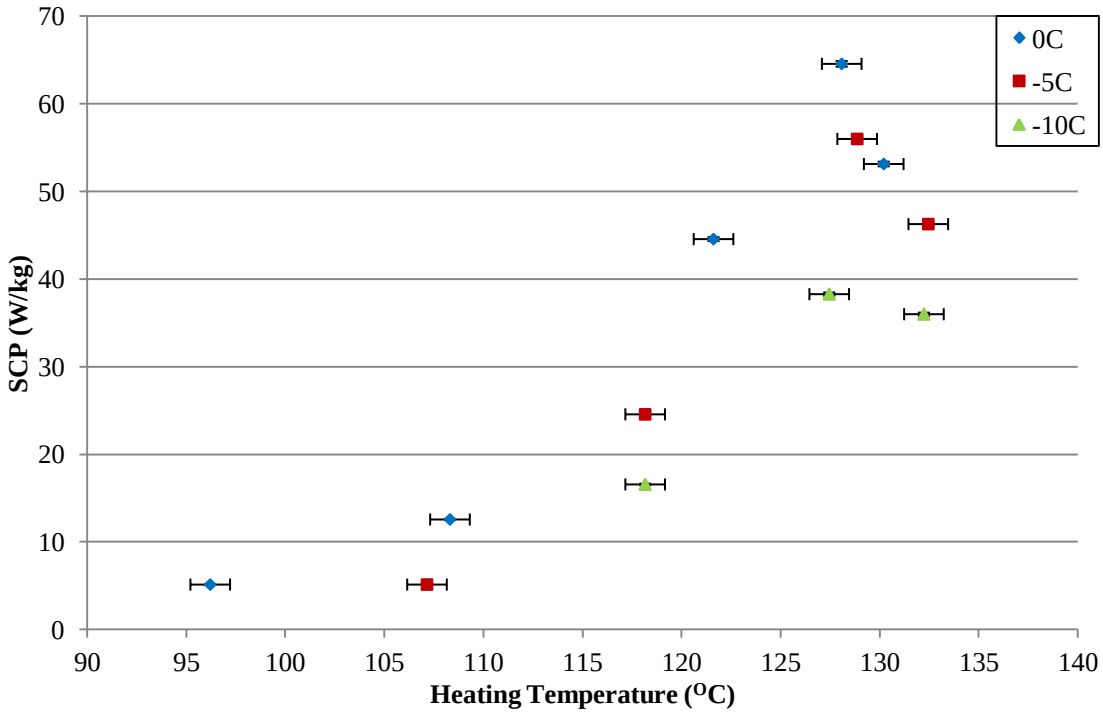

Figure 4-7: Specific Cooling Power for different heating temperatures

4.1.2 Mass recovery effect

Figure 4-8 shows the COP_{ref} results collected for the 13min basic cycle time with 30sec, 1min and 2min mass time. The overall results can be found in Appendix 4. The average heating temperature in the reactor and the average cooling water temperature are kept constant at 121^{O}C and 20^{O}C respectively and the results consider 0^{O}C and -5^{O}C evaporator set-up temperatures for the overall 28kg system ammonia.

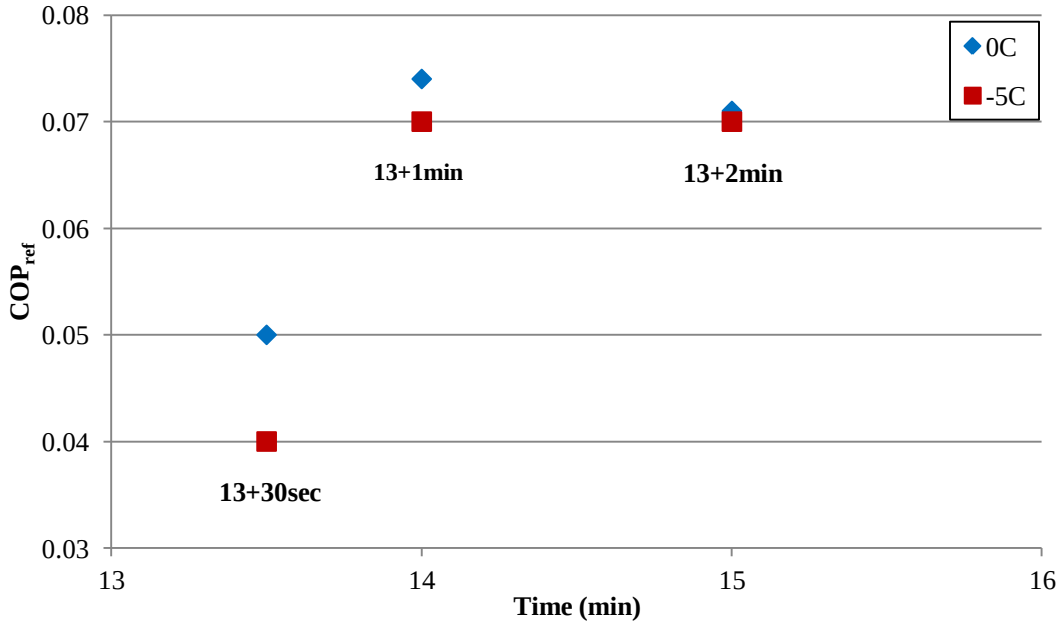

Figure 4-8: COP_{ref} for different mass recovery times

From Figure 4-8 it can be concluded that the mass recovery duration is directly connected to the system's refrigeration performance. There is an optimum mass recovery duration which is 1min for the LH cogen system that maximises COP_{ref}. The response for $0^{O}C$ and $-5^{O}C$ is similar to the $0^{O}C$ COP_{ref} to be higher. For 30sec mass recovery time (less than the optimum), the system's COP_{ref} is the minimum found. At the same time, after 1min mass recovery time, the COP_{ref} starts to decrease but will not be as low a value as the 30sec case. If the process lasts for less than the optimum, the system's cooling performance is poor because not all the potentially desorbed ammonia has been desorbed. In case the duration lasts more than the optimum, that results in the system's decreased performance since no further ammonia is efficiently desorbed even as the cycle time increases.

For the $0^{O}C$ evaporator's set-up temperature, there is an increase for the Q_{ref} of 32.05% from 30sec to 1min mass recovery and a 6.41% increase from 2min to 1min mass. For the $-5^{O}C$ evaporator's set-up temperature the increase is respectively 55.81% and 9.30%. In terms of the COP_{ref} for the $0^{O}C$ evaporator's set-up temperature, there is an increase of 32.43% from 30sec to 1min mass recovery and a 5.71% increase from 2min to 1min mass. For the $-5^{O}C$ evaporator's set-up temperature they are respectively 42.86% and 0%.

Figure 4-9 indicates the average cooling power for $0^{O}C$ and $-5^{O}C$ evaporating temperatures for an average $121^{O}C$ vapour temperature, for a 13min basic cycle with 30sec, 1min and 2min mass recovery times respectively. The average cooling temperature was $20^{O}C$ when the system carries a total of 28kg of ammonia.

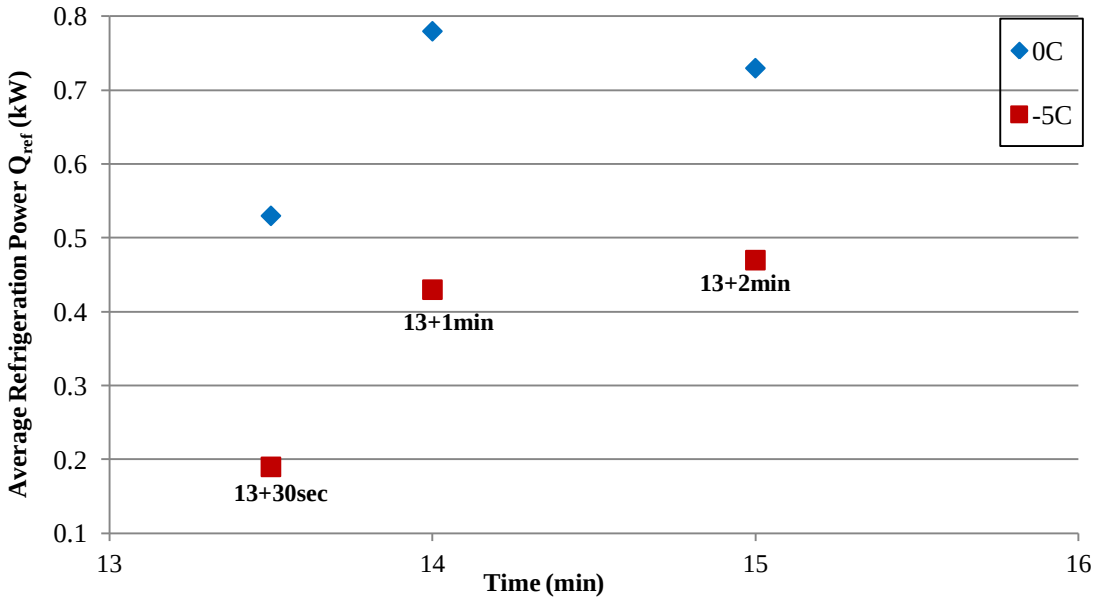

Figure 4-9: Average refrigeration power for different mass recovery times

Figure 4-9 indicates that the lower COP_{ref} is recorded when the mass recovery time is 30sec for both $0^{O}C$ and $-5^{O}C$ evaporator set-up temperatures. That means the reactor did not desorb the available refrigerant for desorption because the mass recovery process stops early. At the same time, when the mass recovery time is 1min, the system's average refrigeration power is the maximum recorded. In case the process lasts longer than 1min (13+2min, for example) the cycle's refrigeration performance starts to decrease.

Figure 4-9 shows that for the $-5^{O}C$ evaporator set-up temperature, the average refrigeration power for the 13+1 and 13+2 cycle times is almost the same compared to the $0^{O}C$ case where the 13+2min case is less frequent. The reason is that the average heating vapour temperature during the 13+1min trial is $116.96^{O}C$ compared to the rest of the trials that were around $121^{O}C$ on average (Appendix 4). In that case the heating temperature of that trial was $121^{O}C$, the response of the $-5^{O}C$ evaporator set-up temperature will be similar to $0^{O}C$.

To examine the mass recovery mechanism Figure 4-11, Figure 4-12and Figure 4-12 will be used where each one indicates the system's operating Pressure-Time (P-t) and Temperature-Time (T-t) graphs as recorded at the evaporator for one cycle each of 27min (13+30sec), 28min (13+1min) and 29min (13+2min). The graphs were plotted using data of two continuous cooling cycles, one per side, for a $0^{O}C$ evaporator set-up

temperature, 128^{O}C average temperature in the reactor, and 20^{O}C average cooling temperature for 28kg of ammonia. Figure 4-11, Figure 4-12 and Figure 4-12 are spotted with black perpendicular lines where the mass recovery process begins and finishes.

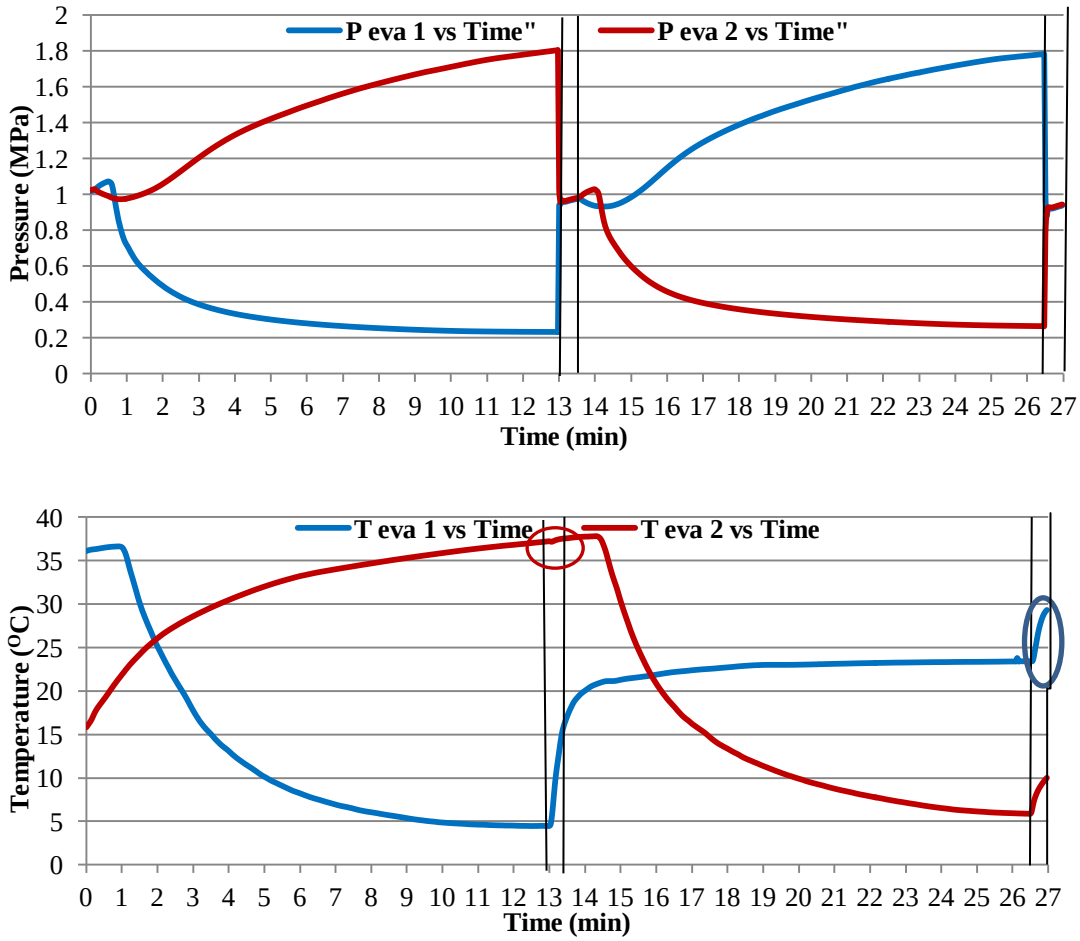

Figure 4-10: Pressure–Time and Temperature-Time graphs for 13+30sec cycle time

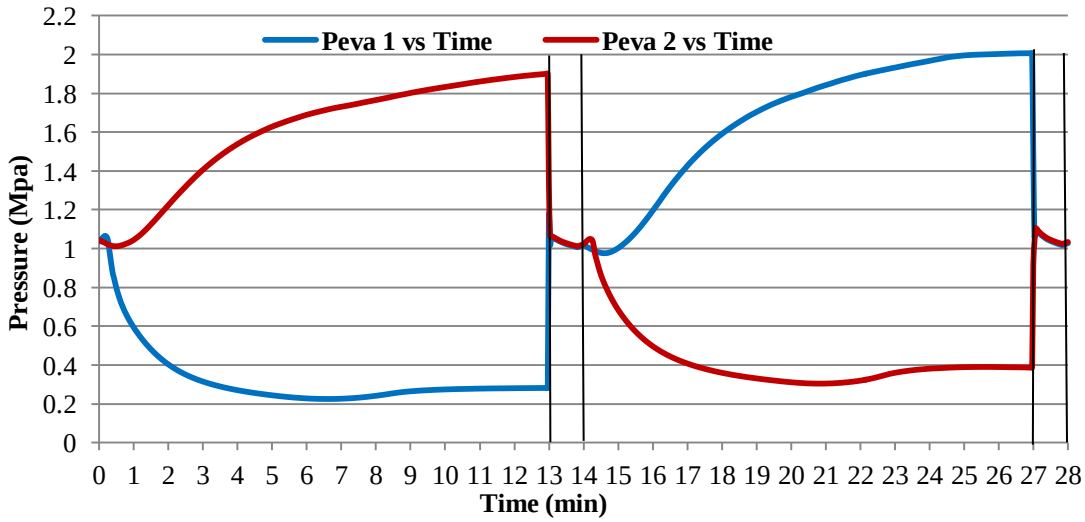

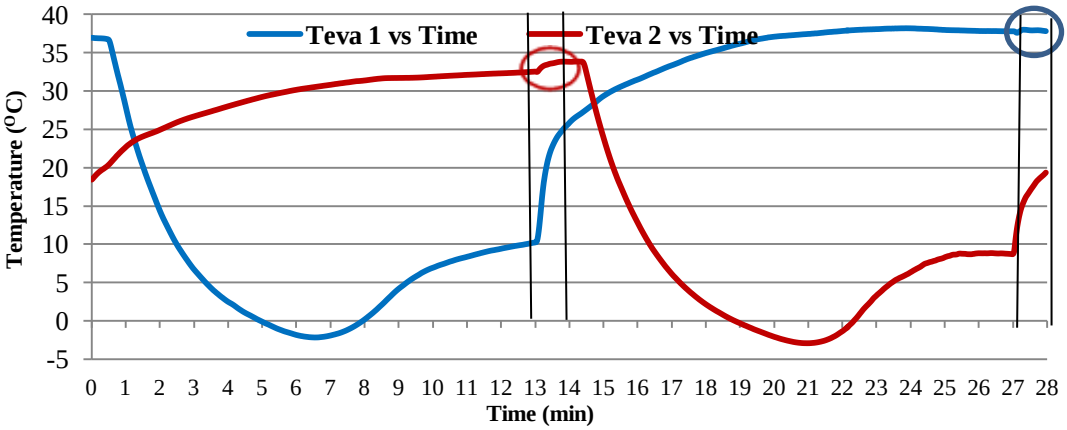

Figure 4-11: Pressure–Time and Temperature-Time graphs for 13+1min cycle time

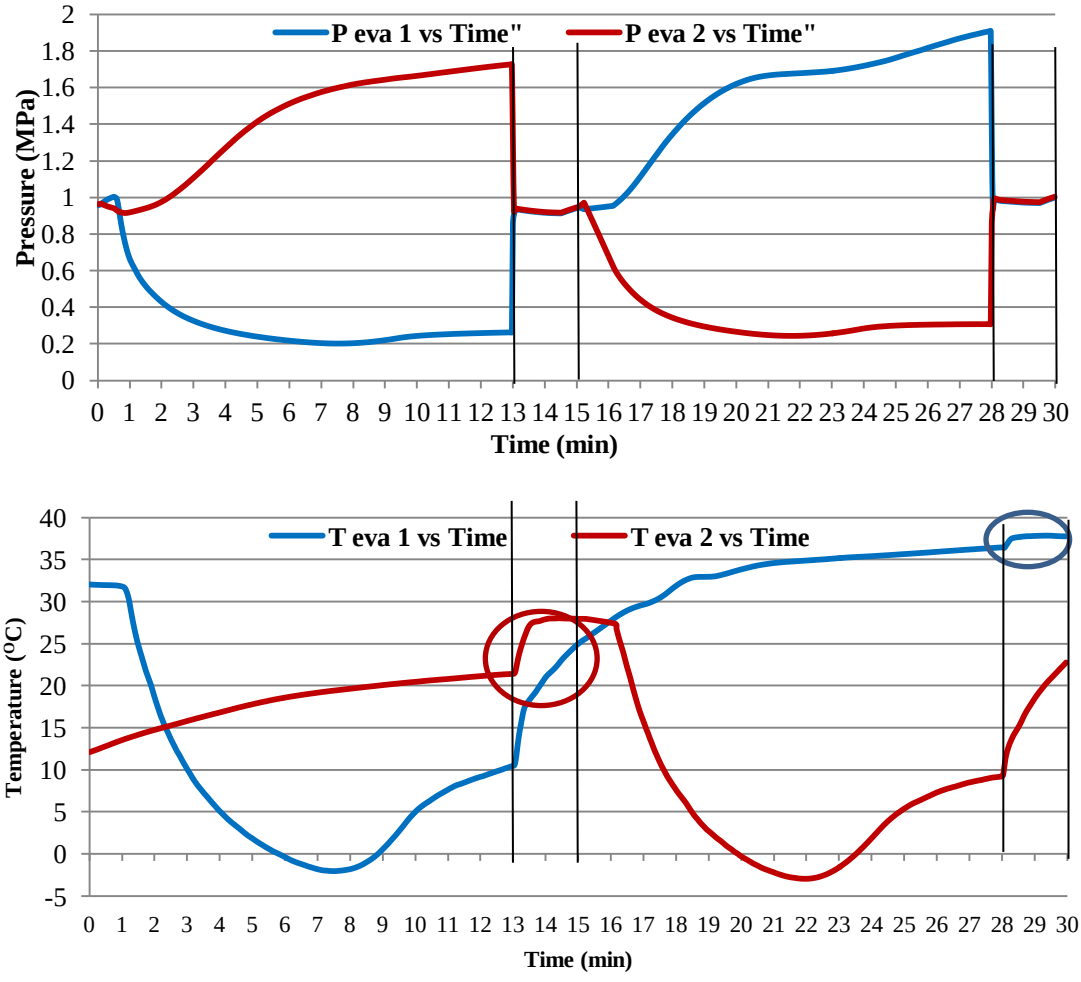

Figure 4-12: Pressure–Time and Temperature-Time graphs for 13+2min cycle time

From the above three Pressure-Time figures one can conclude that a few seconds after the mass recovery takes place, the system's pressure is equalised which means a pressure drop for the high-pressure side and a pressure increase for the low-pressure

side. This response is normal for any connected vessels of different pressure that link together with a valve soon after the valve opens.

The mass recovery process is used to increase the desorption rate when the two evaporators are connected, and that can be proved from the Temperature-Time graphs of Figure 4-11, Figure 4-12 and Figure 4-12. The mass recovery effect on the evaporator's temperature is spotted on red and blue circles on those graphs on the high-pressure side.

Using Figure 4-11 where side 2 is underheating (0-14min cycle time), just after the mass recovery valve V4 opens at 13min cycle time, the evaporator 2 temperature increases rapidly. Then it reaches a maximum value and remains high even for a minute after the mass recovery has finished. This rapid increase of the evaporator's temperature is a result of the spontaneous process at the reactor currently underheating that proves the desorption rate's increase.

To investigate further if the mass recovery process is beneficial for our system, Table 4-2 will be used which presents the chiller's refrigeration performance for 24 kg of ammonia under similar working conditions (125^{O}C average heating reactor temperature, 0^{O}C evaporator set-up temperature and 28^{O}C average cooling water temperature) for two cycles for the same 14min overall cycle time. The first cycle with 1min mass recovery time for a 13+1min cycle time and the other one, 14+0min, without mass recovery. The main cycle and mass recovery time (^{O}C), the average heating temperature (^{O}C), the evaporator's set-up temperature(^{O}C), the average cooling water temperature (^{O}C), average heating and cooling power (kW), cycle average COP and maximum cycle COP, average high pressure (MPa) and SCP are all listed in Table 4-2.

Cycle Time + Mass Recovery Time (min)	Average Heating Vapour Temperature (^{O}C)	Average Cooling Temperature (^{O}C)	Average Cooling Production (^{O}C)	Average Cycle Heating Power Q_{ref} (kW)	Average Cycle Cooling Power (kW)	Average Cycle COP_{ref}	Cycle Maximum COP_{ref}	Average High Pressure (MPa)	Lower / Average Lower Pressure (MPa)	SCP (W/kg)
13+1	125.5	27.84	-2.4	16	2.9	0.2	0.26	1.29	0.14/0.39	168.06
14+0	125.9	28.18	-0.02	15.7	1.7	0.14	0.2	1.14	0.21/0.37	97.14

Table 4-2: Comparison of results for 13+1min and 14+0min cycle times for 0^{O}C evaporator set-up temperature

Table 4-2 shows for the 13+1min cycle the average COP_{ref} is 0.2 compared to 0.14 of the 14+0min case. This is a significant 30% increase for COP_{ref} which proves the superiority of a cycle with a mass recovery process. In more detail, the maximum COP_{ref} recorded for the 13+1 cycle time is 0.26 with an average refrigeration power of 2.8kW compared to 0.2 for the 14+1 cycle which produces 1.7kW average refrigeration power. The SCP for the 13+1 cycle is 168.06W/kg, 42.2% more compared to the 14+1 cycle at 97.14W/kg. Comparing the Table 4-2 SCP where the system carries 24kg of ammonia overall with Appendix 3 where the system carries 28kg of ammonia, one can see that for 24kg, the SCP and the Q_{ref} is more even for the cycle without mass recovery.

From Table 4-2 it can also be observed that the average high pressure recorded for the 13+1min cycle is higher and the lower pressure is lower compared to the 14+0min cycle. If the reactor possesses more ammonia the adsorption-evaporation process starts sooner, as a result no sufficient desorption is established for the 14+0min cycle. That parameter affects the adsorption-evaporation process as well since the more refrigerant there is in the reactor during adsorption, the less is the reactor's adsorption capacity, therefore the less the refrigeration power.

The higher maximum pressure of the 13+1min case during desorption-condensation is because the reactor when the desorption-condensation process starts possesses more ammonia compared to the 14+0min cycle. Literature states that the more the refrigerant appears in the reactor, the more the operating system's high pressure and the lower the low pressure during cooling assuming similar heat sources. For the selected cycles, there is a difference of 0.15MPa for the mass recovery cycle.

In terms of the SCP, Figure 4-13 presents the system's response for different mass recovery times. For both evaporators' set-up temperatures, they start low when the mass recovery time is 30sec and then reach a maximum value for 1min mass recovery time, and after that it drops. It is the same reaction as in Figure 4-9 and the explanation why the 13+2min point of the $-5^{O}C$ evaporator set-up temperature is not lower than the 13+1min point is explained above. The SCP increase for the 13+1min cycle compared to the other two, is similar to the COP_{ref} increase as presented previously for $0^{O}C$ and $-5^{O}C$ evaporator set-up temperatures.

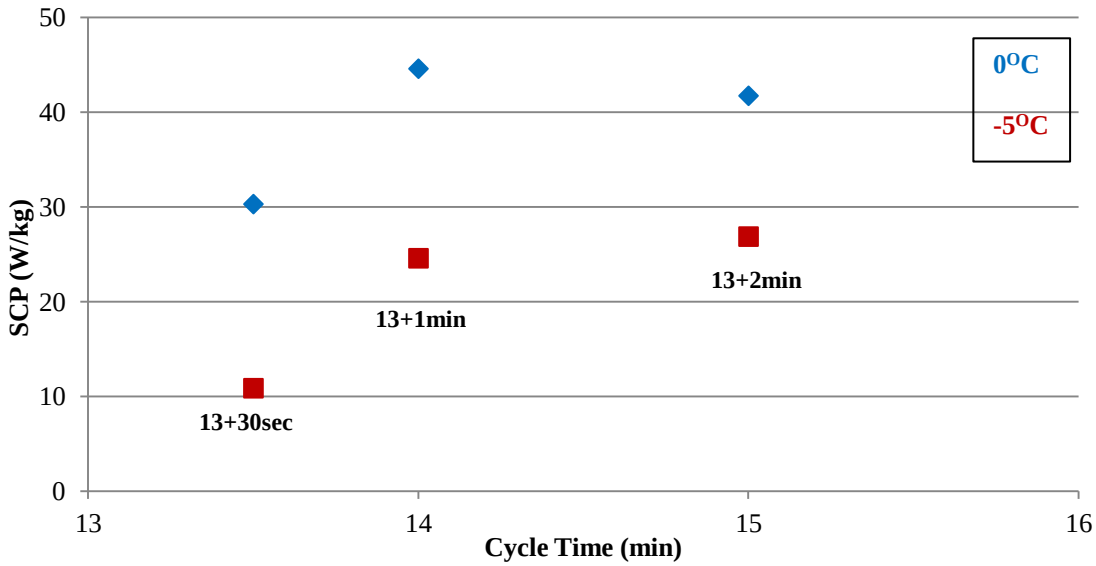

Figure 4-13: SCP for different mass recovery times

Figure 4-14 presents the useful cooling (evaporator temperature below the require temperature) for a complete cycle, side 1 and side 2 for -5^{O}C required cooling. Figure 4-14 tries to identify the overall time that the machine can produce a temperature at the evaporator below the required cooling for a 28min cycle time when the machine carries 24kg of ammonia. T1 is the period that evaporator 1 is below the require cooling and T2 for side 2.

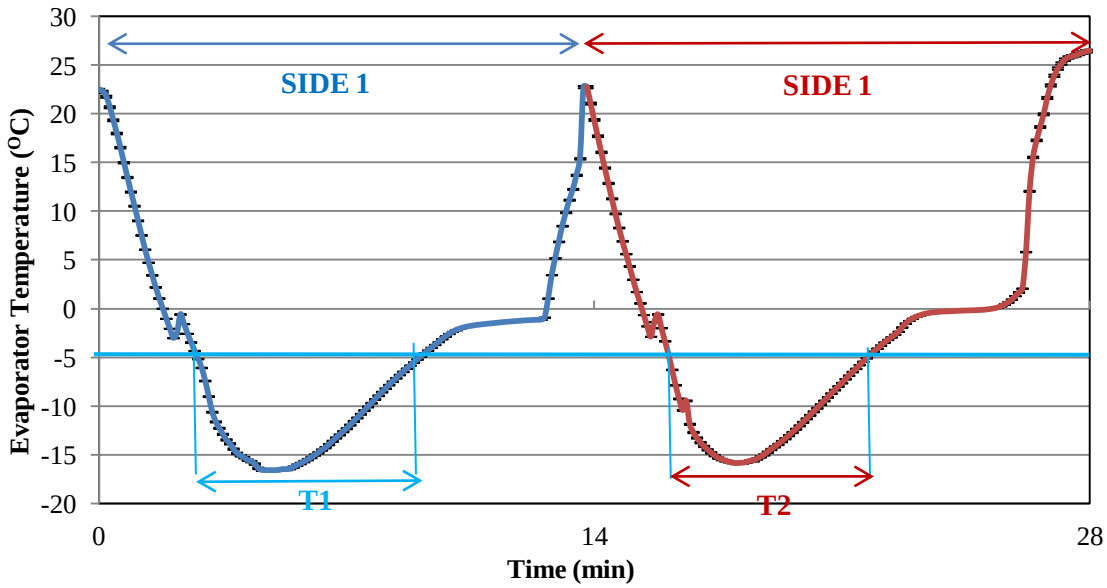

Figure 4-14: A complete cycle useful cooling for -5^{O}C require cooling

Results shows that the machine can operate below 0^{O}C when this is the required cooling for approximately 17.30min, for approximately 13.30min for -5^{O}C required cooling and

for approximately 9min for -10^{O}C require cooling. These numbers means that for 28min overall cycle time, for -0^{O}C required cooling, 62% of the overall cycle time the evaporator temperature is below the required cooling, 48% of the time for -5^{O}C and 32.1% for -10^{O}C required cooling.

Results indicate that as the required cooling decreases, the useful cooling also decreases. Figure 4-14 shows that even the useful cooling for -5^{O}C is 13.30min, the overall time that the evaporator temperature is below 0^{O}C is around 21min which means 75% of the cycle time. That means the machine can produce at low temperatures for sufficient period during the 28min cycle time.

4.1.3 Cycle time effect

Figure 4-15 presents graphically the results for COP_{ref} during the basic cycle time. The overall data for this parameter can be found in Appendix 5 and assume varying basic cycle times of 10min, 13min, 16min and 18min for 1min mass recovery time, 125^{O}C average reactor in temperature, and 20^{O}C average cooling water temperature for an overall system's 28kg of ammonia for 0^{O}C and -5^{O}C evaporator set-up temperatures.

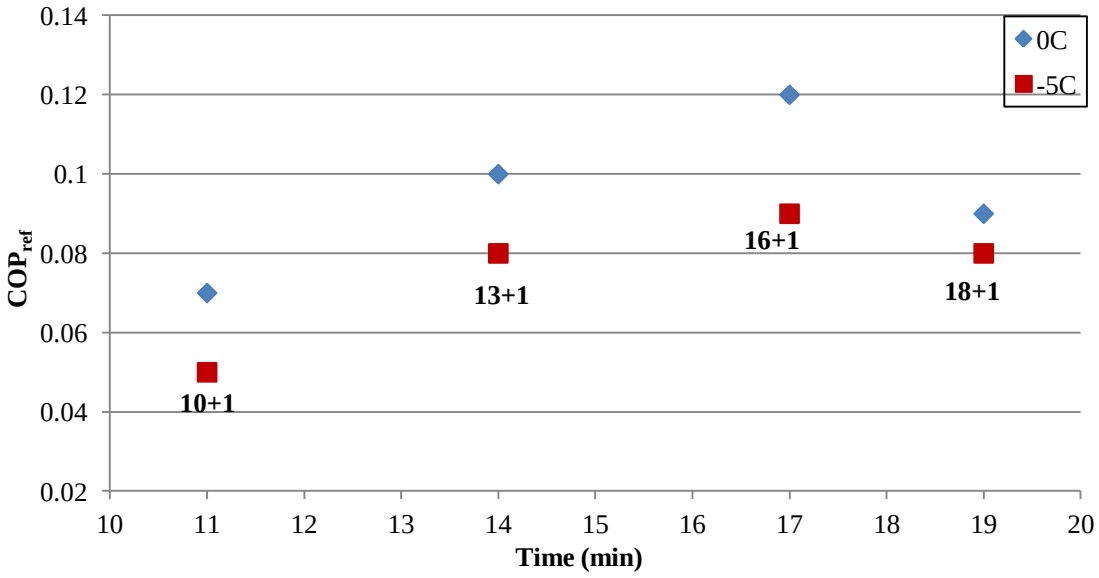

Figure 4-15: COP_{ref} for different basic cycle times

Figure 4-15 suggests that the cycle's refrigeration performance for 0^{O}C and -5^{O}C evaporating temperatures have similar responses but for the 0^{O}C the COP_{ref} is higher for the same evaporating temperature. The main outcome is that there is an optimum basic cycle time, which is between 13 and 16min and offers maximum system refrigeration

efficiency. Starting from 10+1min cycle time, the cycle COP_{ref} increases as the cycle time increases, reaches a peak at around 16+1min cycle time and then starts to decrease.

In terms of the Q_{ref}, from 10+1min to 13+1min cycle time, it is increased progressively and then up to a 16+1min cycle time when the machine offers its highest performance for both $0^{O}C$ and $-5^{O}C$ evaporator set-up temperatures and after that point is decreased. The machine after the 16+1min cycle cannot provide any further cooling and any increase of the cycle time results in the overall heating power per cycle's increasing (the average heating power decreases) which means the COP_{ref} decreases.

Figure 4-16 shows how the average heating power (kW) with varying basic cycle times (min) and 1min mass recovery for $0^{O}C$ and $-5^{O}C$ evaporating temperature for an average of $125^{O}C$ boiling temperature and $20^{O}C$ average cooling water temperature for a system of overall 28kg ammonia.

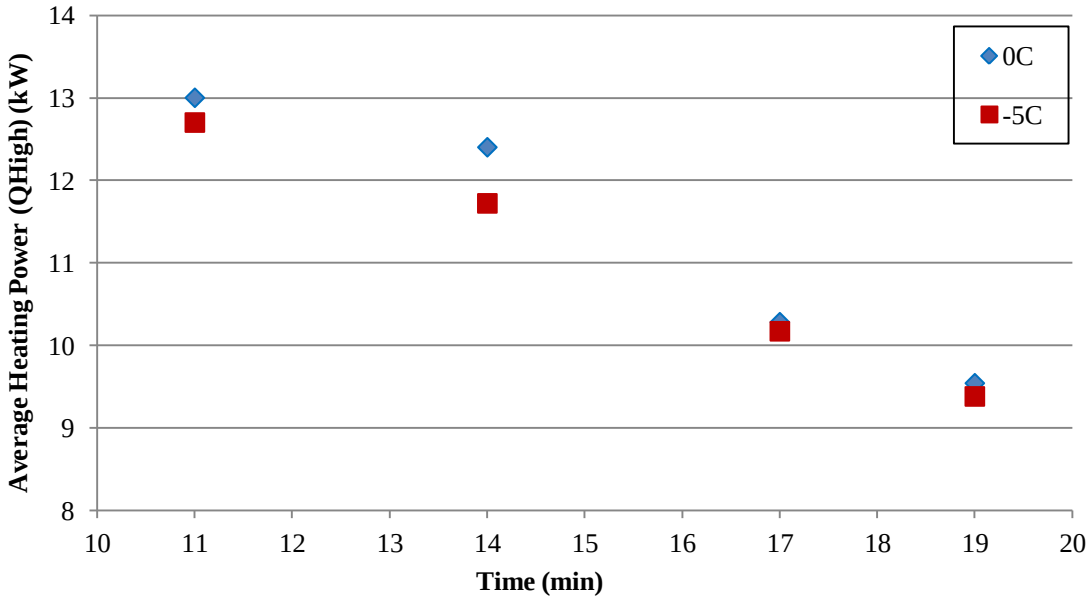

Figure 4-16: Average heating power for different basic cycle times

Figure 4-16 suggests that the average heating power for both $0^{O}C$ and $-5^{O}C$ evaporating temperatures starting from the 10+1min cycle is high and then drops proportionally. The average heating power is related to the duration that the heaters are ON and the cycle's duration. The overall heating energy increased as the time increased but the average heating power is decreased and at the same time the average cooling power is decreased. That means, for a shorter cycle time, the boiler possesses energy to provide

the reactor, but because the switch period takes place that energy is recorded for that cycle but utilised later from the other reactor. As the cycle time increases, heaters at the boiler operate more overall but less on average per cycle time and the heating energy recorded for the cycle is now utilised more efficiently from the side currently underheating.

Figure 4-17 shows the average cooling power production with a varying basic cycle time for 1min mass recovery for 0^{O}C and -5^{O}C evaporator set-up temperatures for an average of 125^{O}C boiling temperature and 20^{O}C average cooling temperature.

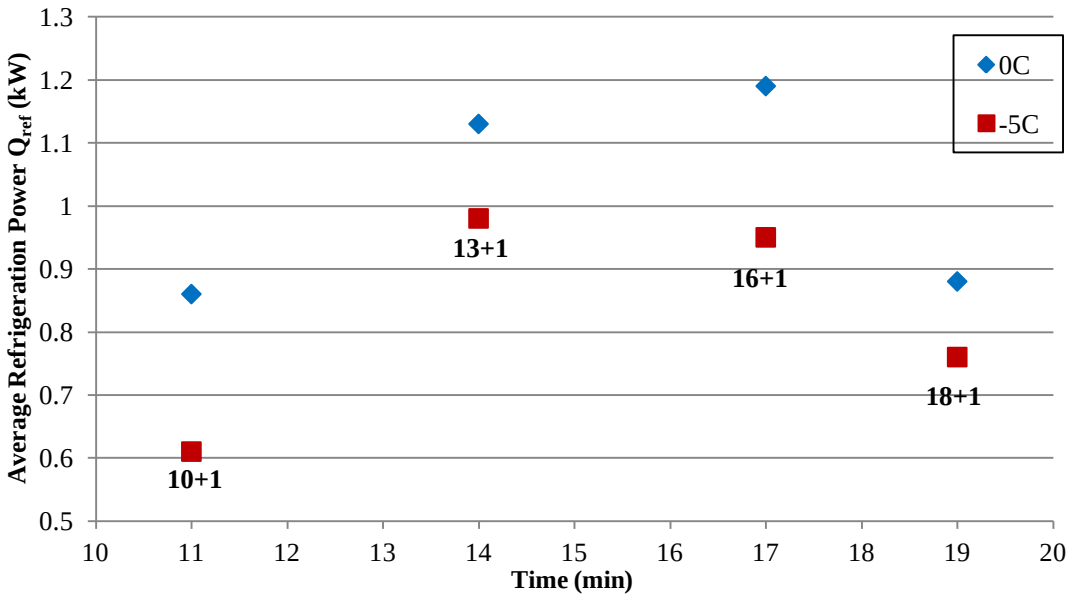

Figure 4-17: Average cooling power for different basic cycle times

In terms of the average refrigeration power that has a similar a response to the cycle COP_{ref} for both 0^{O}C and -5^{O}C evaporation. Initially for 10+1min cycle time up to 13+1min the Q_{ref} increases proportionally and from 13+1min to 16+1min the machine offers the maximum refrigeration performance and at 16+1min reaches a maximum value and after that point it starts to decrease. Figure 4-17 explains why in Figure 4-15 cycle COP_{ref} is decreased after 16+1min and even the 18+1 point has a lower average heating power than the 16+1min. From Figure 4-17, the maximum system Q_{ref} for 28kg of ammonia is slightly more than 1.2kW between 16 and 17min overall cycle time.

Figure 4-18 shows the SCP for different basic cycle times which has the same response as in Figure 4-17. As the cycle time increases, the SCP increases as well, reaches a peak

and afterwards starts to drop. From Figure 4-18 the cycle's maximum SCP is around 69W/kg at 16 to 17min cycle time.

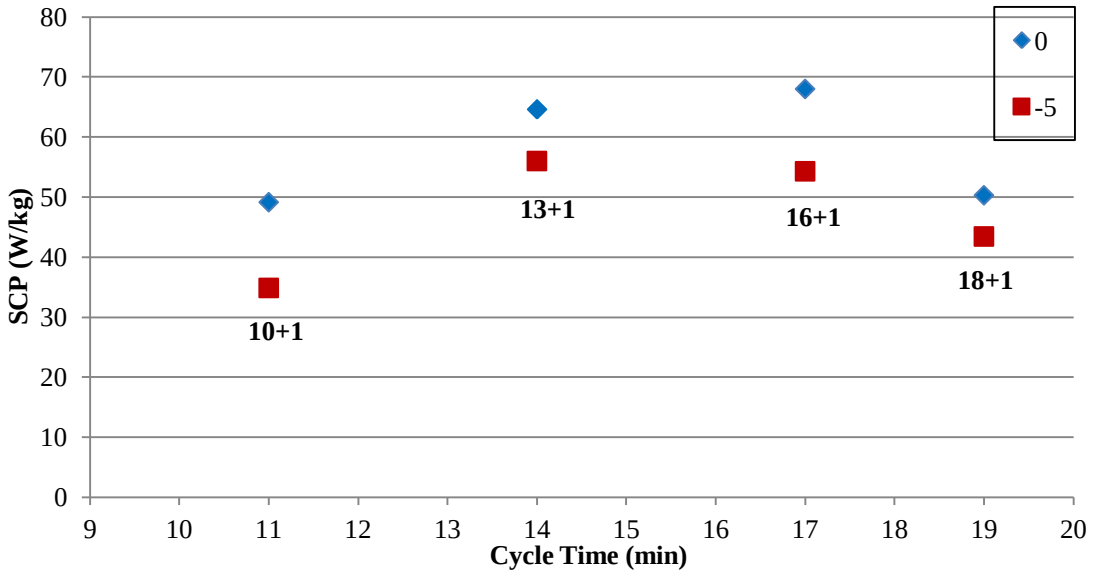

Figure 4-18: SCP per side for different basic cycle times

Figure 4-19 shows the system's cooling capacity (kJ/kg) for different basic cycle times. What can be said is that the cooling capacity increases as the cycle time increases reach a peak similar to the COP_{ref} and the SCP and then drop. For further investigation, even the cycle time increases, the cooling power will remain almost constant but since the cycle time will be increased, that will results to the cooling capacity increase.

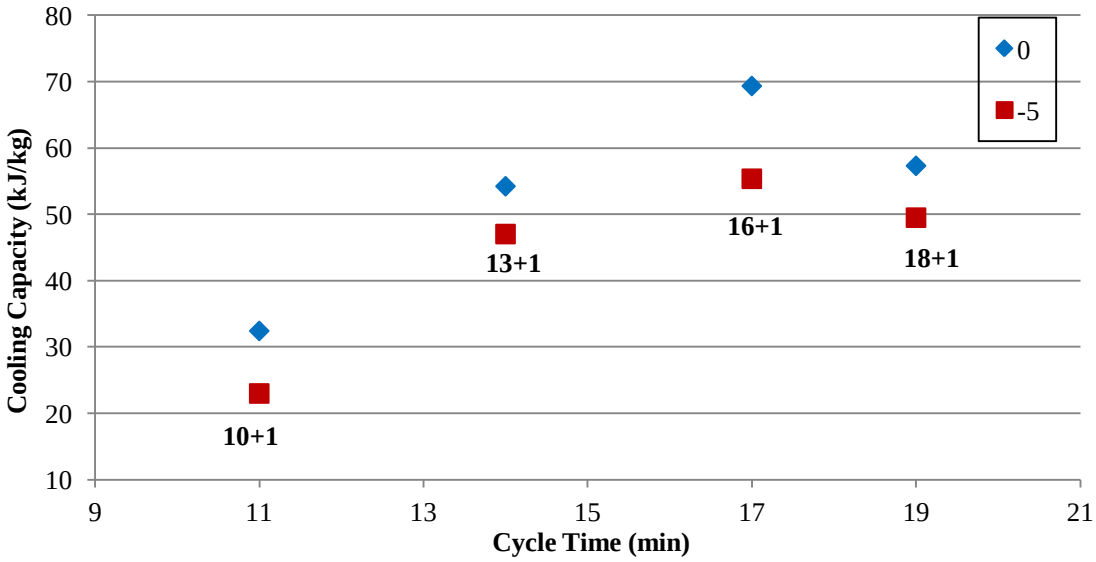

Figure 4-19: Cooling capacity per side for different basic cycle times

4.1.4 Ammonia mass effect

Another parameter under investigation for the adsorption chiller's performance is the amount of refrigerant the system is charged with. For the cooling test, initially overall 24kg of ammonia was used (1st period of trials) and later 28kg (2nd and 3rd periods of trials). The overall results for the system's ammonia quantity can be found in Appendix 6 and Appendix 7. Appendix 6 shows the overall results for a 13+1min cycle time, 0^{O}C evaporator set-up temperature, and 125^{O}C average heat reactor's temperature when the system is charged with 24 and 28kg of ammonia. Appendix 7 indicates the maximum values recorded during those two experiments.

For this analysis, Figure 4-21 and Figure 4-21 will be used to examine the ammonia system's quantity effect on the system's refrigeration performance. Figure 4-20 shows a Pressure-Time diagram for 24kg and 28kg for one complete cycle and Figure 4-21 shows a corresponding Temperature-Time diagram.

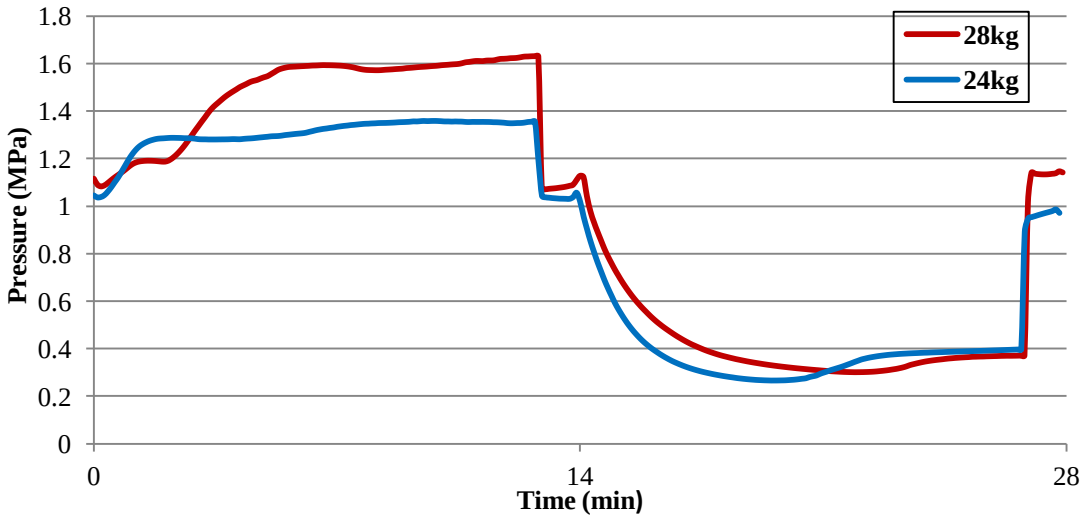

Figure 4-20: Pressure–Time diagram for overall system ammonia 24 and 28kg

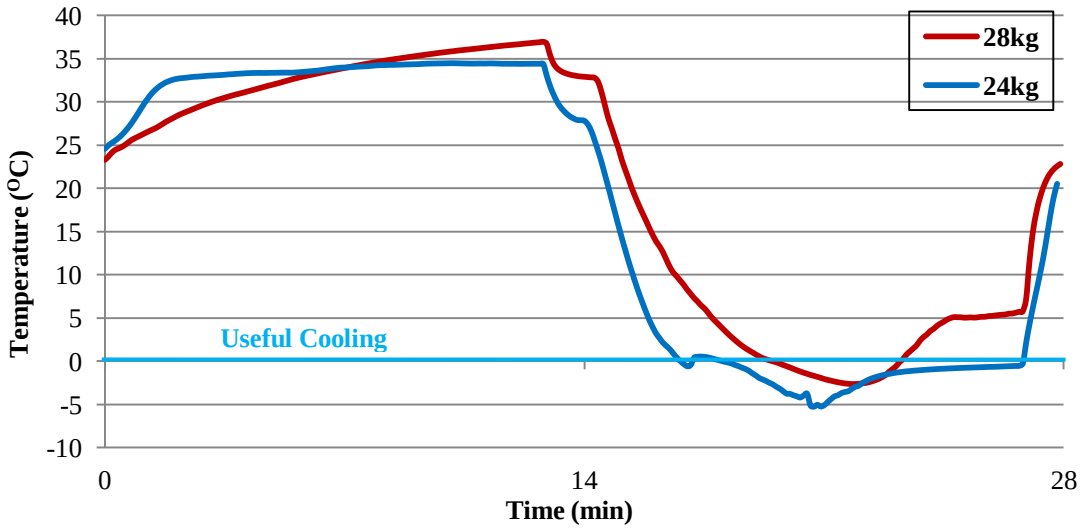

Figure 4-21: Temperature–Time diagram for overall system ammonia 24 and 28kg

For these sets of results, the average COP_{ref} and the maximum recorded COP_{ref} for the 24kg trials is much higher compared to the 28kg assuming similar working conditions. At the same time the average heating power is more as well as the COP_{ref}, and the result is the higher average cooling power production. The maximum performance recorded for this machine is when carrying 24kg of ammonia. More specifically, the maximum COP_{ref} is 0.26, it produces 3.52kW of Q_{ref}, which results in 201.14W/kg SCP and 168.96kJ/kg cooling capacity per side.

From the results, the average Q_{ref} and the COP_{ref} for the 24kg case is almost double compared to the 28kg case. That proves that the ammonia quantity directly affects the system's refrigeration performance and results in both reactor and evaporator operating at maximum performance.

The above can be supported from Figure 4-21 which shows the useful refrigeration, i.e. the evaporator's temperature below $0^{O}C$, starting around 3min earlier for the 24kg case and staying below for longer. The more ammonia in the system also means the reactor possesses more refrigerant when the adsorption-evaporation process starts and that decreases the system's adsorption capacity. The 24kg system's ammonia quantity is considered the optimum for this system based on the 24kg and 28kg experiments.

For an optimum ammonia quantity (24kg), the ammonia at the evaporator can reach the evaporator's set-up temperature faster, and at the same time the reactor is still dry

enough to continue adsorbing refrigerant at an efficient rate. That results in the Q_{ref} maximum.

In terms of the higher average heating power, for the 24kg it is more compared to 28kg which means the mass and heat transfer is higher compared to 28kg, therefore the desorption and adsorption rates are faster. It could also be related to a more efficient reactor material performance during the 24kg trials.

From Figure 4-20 it can be observed that the system's lower pressure is lower for the 24kg case. The pressure at the evaporators drops uniformly at the earlier stage of the cycle, reaches a minimum value then increases and remains stable until the end of the cycle. The cycle's minimum pressure is not only lower for the 24kg case but also drops faster for the same reasons that the temperature reacts like that. After the pressure at the evaporator for the 24kg case reaches its minimum value, it starts to increase and becomes slightly higher compared to the 28kg case before stabilising. The slower pressure drop for the 28kg case at the beginning of the adsorption-evaporation process is also related to the ammonia quantity at the evaporator and the reactor after the switch period.

The maximum and the average system high pressures for the 28kg case is higher. This agrees with the literature for which the more refrigerant the reactors have the higher the system's saturation pressure, therefore the higher the operational pressure for the same heating temperature. From Figure 4-20 one can observe that, for the 28kg case during the heating period, the pressure looks to have a tendency to increase in a case when the cycle time was more. For the 24kg case, half way during the heating period until the end of the cycle, the pressure is almost stable.

Figure 4-21 also indicates that just after the mass recovery process, for the 24kg case, the temperature drops more compared to the 28kg. That proves that for the 28kg there is an increase in the desorption rate during that mass recovery compared to the 24kg because of the spontaneous process and the more available ammonia for desorption. The mass recovery looks more useful for the 28kg case, but the fact that the system's pressure is equalised within the few seconds does not allow further ammonia to desorb from the high-pressure reactor.

The performance difference can also be identified from the SCP difference which for the case of 24kg overall ammonia, the maximum SCP is 201.14W/kg and for 28kg of ammonia is 81.14W/kg which means a 147.8% SCP increase for the 24kg case.

4.2 Cogeneration mode

In this section, the cogeneration performance of the machine will be investigated. Mainly the analysis will refer to the system's power performance and how the parameters affect the cogeneration system's performance. The collected data include in-and-out expander pressure (MPa) and temperature (^{O}C), reactor pressure (MPa), the condensation temperature (^{O}C), and the evaporator's temperature (^{O}C). The operating conditions for the cogeneration experiments are a 0^{O}C evaporator set-up temperature for the 28min cycle time (14min per side), 125^{O}C average vapour temperature in the reactor, and 42^{O}C average cooling temperature for the system's 28kg ammonia.

4.2.1 Power-related graphs

Appendix 8 presents the whole results collected during the cogeneration experiments. These include the average and maximum power (kW), the desorption heat input Q_{high} (W), the expander's inlet average pressure (MPa), the refrigerant expander's inlet average temperature (^{O}C), the average pressure difference across the expander (MPa), the power duration reported (sec) from the cogeneration data logger, for a 0^{O}C evaporator set-up temperature, 28min cycle time (14min per side), 125^{O}C average boiling temperature, 34^{O}C average cooling temperature when the machine carries 28kg of ammonia and 600W load at the bank load. Also the power generation efficiency COP_W is reported. The data are for a single cycle where side 1 was initially used for during power generation and side 2 for refrigeration during the 0-14min cycle time. Later during the 14-28min cycle time, side 2 is used for power production and side 1 for refrigeration production. The power trail number from No. 1 to No. 8 was from side 1 and No. 9 to No. 11 is from side 2. The power production duration denotes the period that the power meter collects data. The power generation efficiency (COP_W) is a measure of the system's power generation from the expander (W) over the average heat input Q_{high} (W) during desorption following a similar approach to L.W.Wang., et al. [34] and is expressed in Equation 4.3 similar to the COP_{ref} estimation (Equation 4.1). Appendix 8 shows the collected results recorded during the experimental cogeneration trials.

$$COP_W = \frac{Power}{Q_{high}} \qquad 4\text{-}3$$

Previously was explained the procedure followed for the power generation using the v8 valve to store the refrigerant before releasing it between the reactor and the expander in the direction of increasing its pressure and flow rate. The reason for that is because when the v8 valve was always open, a very small power production was achieved (307W maximum and 128W average) and then no more power could be produced from the desorbed flow rate. After that, the ΔP_{exp} was almost zero with the high pressure side's having a uniform pressure. Therefore, when no sufficient pressure difference across the expander could be established and presuming a very small flow rate during the desorption which decreased after reaching its peak, the expander could not rotate further.

Figure 4-22 presents the expander's inlet pressure (MPa) variations just after v8 opens and the power production for each of the eleven power trials.

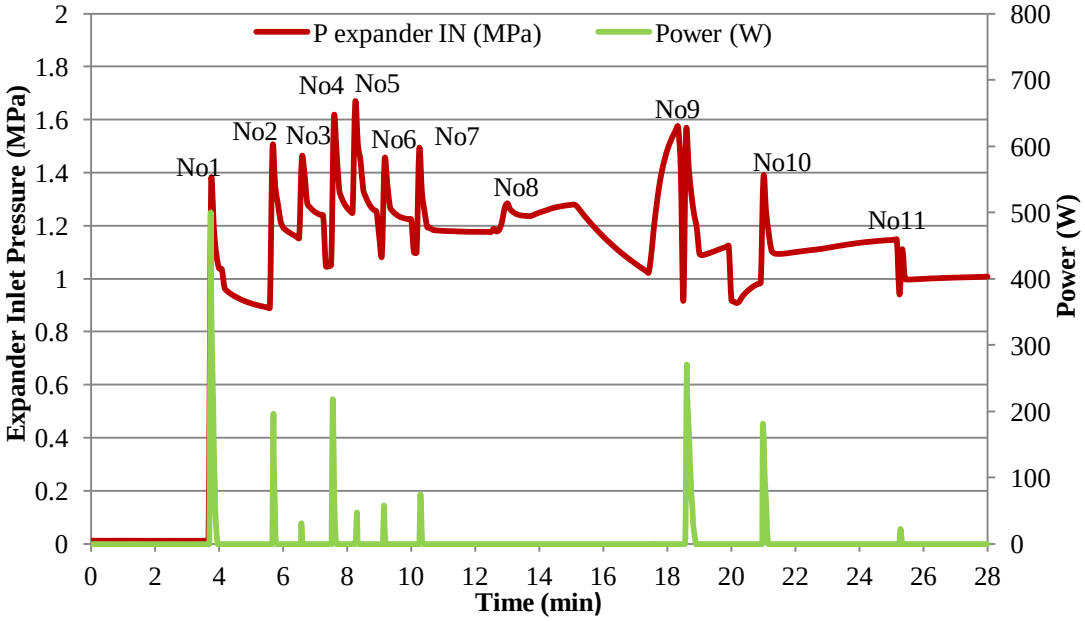

Figure 4-22: Average power for different expander Inlet pressures

Figure 4-22 indicated a pulse response of the power production and not a stable constant output as a result of storing refrigerant before releasing it to the expander. Every peak value of the expander's inlet pressure denotes the maximum refrigerant pressure in the expander as well as a peak value in power production. The highest cycle power

generation is achieved during the first power trial (No. 1), when side 1 is at high pressure. The maximum power generated was 486W and 206W was the average power production from power trial No. 1 which lasts for 15sec. The maximum expander pressure recorded during this trial was 1.360MPa.

When side 2 was used for power production, the maximum power was recorded during the power trial No. 9 which is side 2 of the first power trial. The maximum power for this trial was 265W and 105W the average power production, and the process lasts 20sec. This is almost half the power that was generated from trial No. 1 – even the power production's duration was longer. The overall power production for the 28min cogeneration cycle time was 1573W for 89sec. The overall power production of side 1 was 1106W for 53sec and 467W of side 2 for 36sec. For side 1, the power trial No. 8 produces nothing.

The highest power production was recorded at the first trial for each side, trial No. 1 for side 1 and trial No. 9 for side 2. That proves the desorption rate (therefore the ammonia quantity) drives the expander at the early stages of the heating process just after the switch period is the cycle maximum.

For the next power trials, as soon as the reactor cannot desorb ammonia as efficiently and since high pressure cannot establish at the expander's inlet, the overall power production and the process duration are decreased.

The reason that trial No. 9 (first trial of side 2) lasts longer than trial No. 1 (first trial of side 1) is possibly because the v8 valve for that trial possibly did not fully open or was not open as long as the No. 1 trial or progress as fast as possible; it was open initially and after a while was fully open. The above explanation has been extracted from the No. 9 trial expander's inlet pressure (Figure 4-22) which half way during the process the pressure decreases and then increases again. In case that response is not a power meter delay, then it is related to the v8 valve's behaviour. Generally, the procedure following with v8 was to try to open it manually in full when the pressure was high enough as quickly as possible. The v8 manual valve is a hand wheel lever kind which takes some time to open fully and for some trials, that happens after the end of the power production.

The highest cycle's pressure inlet to the expander was 1.66MPa and recorded for power trial No. 5. Even though that pressure was higher than the maximum power production in trial No. 1, the maximum power production was around 48W and 21W the average over the 7sec trial time. The above proves that the power production not only depends on the inlet expander's pressure since the maximum pressure trial results in very poor power production.

When side 2 was used for power production, it could attain only three power trials. Looking at the reactor much earlier, it was unable to desorb sufficient refrigerant. Figure 4-23 shows the combination of the reactors' high and evaporators' low pressure for side 1 and side 2 and will be used for the analysis of the side 2 response.

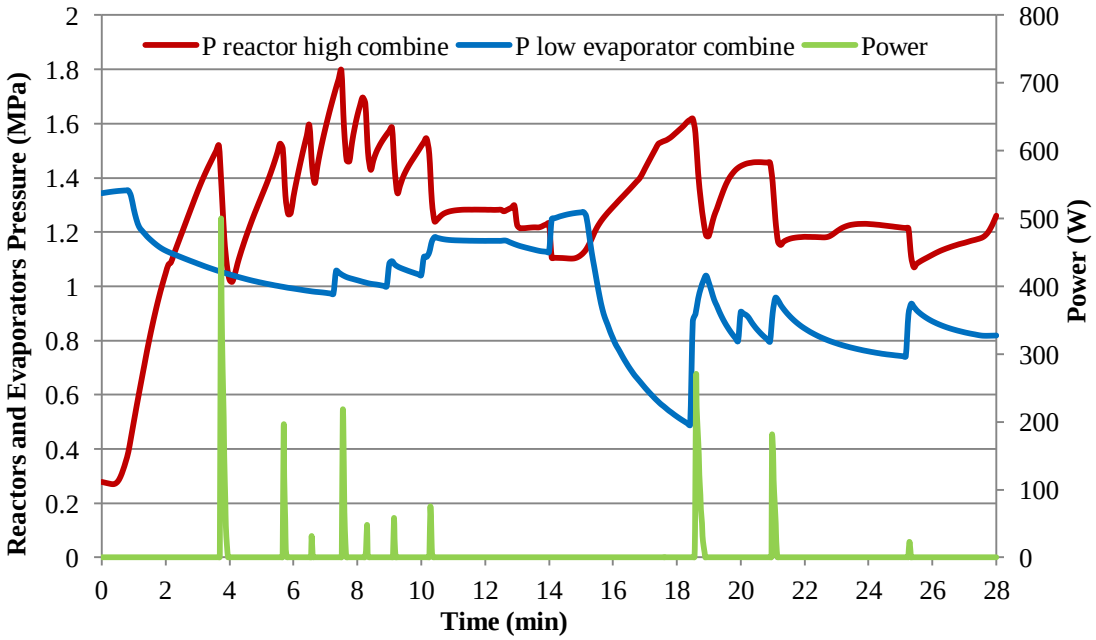

Figure 4-23: Average power for reactors and evaporators combining high and low pressures

From Figure 4-23 after the No. 7 power generation around 11min cycle time and after trial No. 11 at around 22min cycle time, the reactor's pressure remains almost constant and even if v8 is closed cannot be established at high pressure. Both reactors look as though they would run out of sufficient available ammonia for desorption, therefore they cannot set up high pressure beyond these points. For reactor 2, that behaviour is noticed earlier and only after two power trials compared to reactor 1 where it happens at the late stage of the cycle. Both reactors were constructed identically, and this huge

performance difference is not explicable. At the same time, when side 1 is used for refrigeration, the pressure development is lower than side 2. More specifically, the pressure drop of evaporator 1 is faster and also after each power trial can maintain a lower pressure.

There is a significant gap for the higher and lower pressure developments between side 1 and side 2 even for similar heating and cooling sources as Figure 4-24 proves. The explanation is related to some adsorbent material escaping reactor 2, decreasing like that of reactor 2's adsorption capacity. In case a reactor cannot adsorb efficiently, that will affect its adsorption performance, as well as the desorption performance, so also the power generation production.

Figure 4-24 presents the cooling water temperature source combined with the low-pressure reactor and the heating vapour combined with the high-pressure reactors.

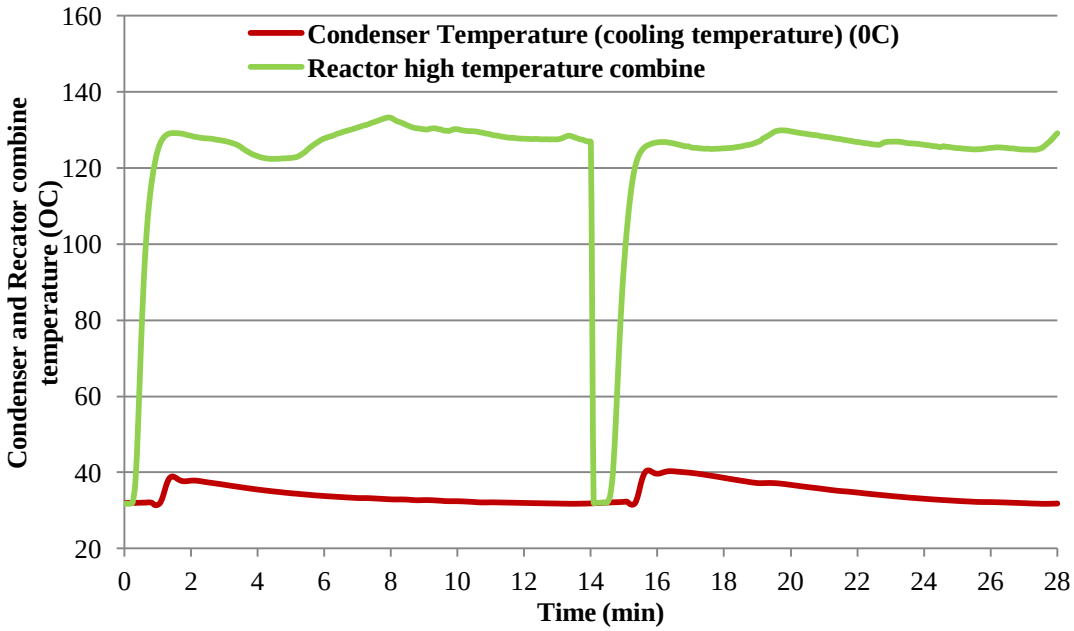

Figure 4-24: Combining condenser and reactor high Temperatures for side 1 and side 2

Another important parameter for the power generation production is the pressure difference across the expander (ΔP_{exp}). The pressure outlet of the expander is simply the currently connected condenser-evaporator to the high-pressure reactor. Figure 4-25 presents the combined expander's ΔP_{exp} for side 1 and side 2 with the average power

production. It indicates the system's ΔP_{exp} before every power production trial (before v8 opens).

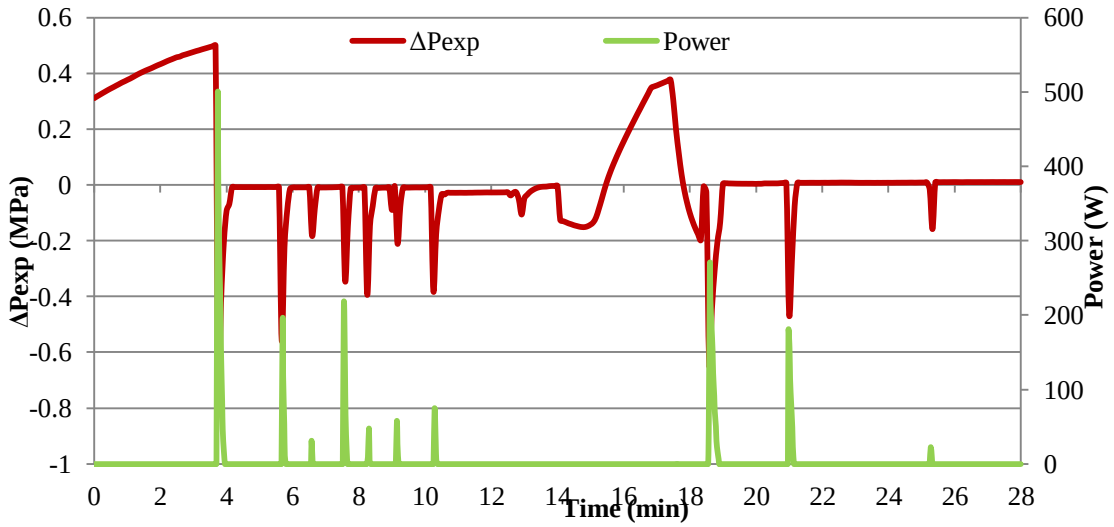

Figure 4-25: Average power for different expander ΔP_{exp}

As in any other ORC cycle, the pressure difference across the rotary machine is an important parameter affecting the rotary machine's performance. A larger ΔP_{exp} means an increase of the rotary machine's speed during power generation maximising the power production. For these experiments, to ensure the expander's low pressure, the mass recovery valve is used by utilising the low-pressure side of the reactor under cooling. The use of a mass recovery valve is necessary because the expander cannot rotate otherwise since the ΔP_{exp} is almost zero as mentioned previously. The condenser cannot establish low pressure at the evaporator since the cooling water temperature used during cogeneration was high, resulting in the saturation pressure at the expander's exit to be close to the expander's inlet pressure. The inefficient desorption rate was also another reason to use the mass recovery valve as well as the inconstant desorption rate during the process.

From Figure 4-25 the highest power production is achieved for trial No. 1 where the ΔP_{exp} is the maximum reported. The next maximum power production was recorded for trial No. 9 where the ΔP_{exp} difference is high but not as much as in trial No. 1. Trials No. 2 and No. 10 (second trial from side 1 and side 2) have large ΔP_{exp} as well and also high power is produced. Trial No. 4's ΔP_{exp} is lower than trial No. 7 even though the power production is higher (109W compared to 37W on average). In general, the power

production in Figure 4-25 is almost always proportional to the ΔP_{exp}. That makes pressure across the exapnder another important parameter for the system's power production which becomes less significant at the later stages of the cycle when the reactors run out of ammonia available for desorption.

Figure 4-26 presents the refrigerant temperature leaving the reactor and into the expander (^{O}C) with the average power production (W). The average ammonia temperature entering the expander for 28min cycle time is around 40^{O}C and the average temperature leaving the reactor was 80^{O}C (95^{O}C was the maximum recorded). The desorbed refrigerant is much higher than the expander's refrigerant temperature. That means for this set of results the power generation was a matter of the expander's high pressure, the expander's ΔP_{exp} and the mass recovery process rather than the temperature inlet since the inlet temperature was too low.

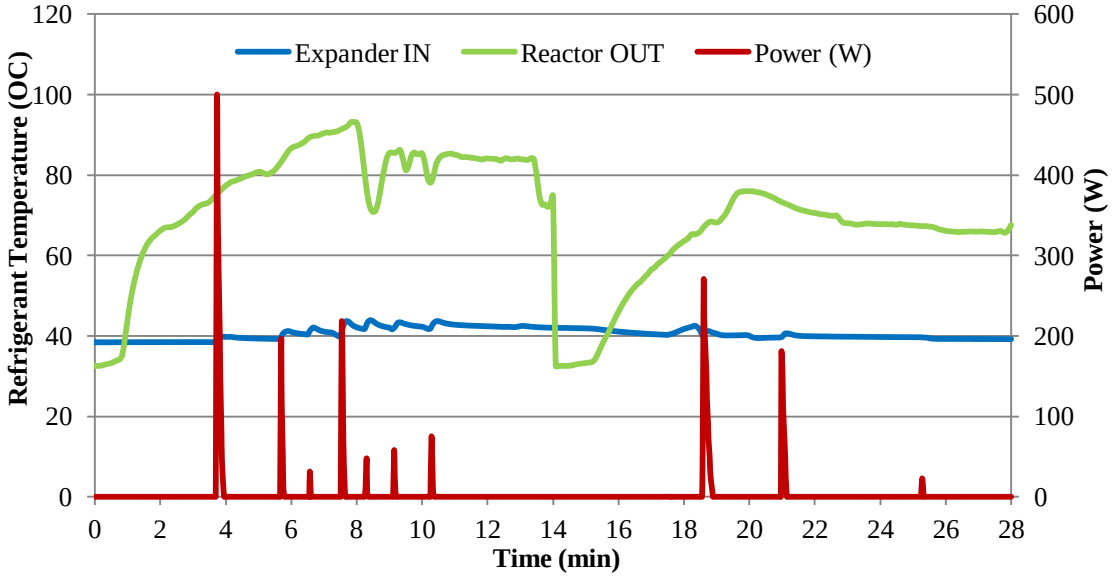

Figure 4-26: Average power for different ammonia temperatures out of the reactor and into the expander

The reason for this temperature difference is related to the heat transfer temperature difference between the reactor and the expander; the ammonia's temperature at the exit of the reactor cannot reach 125^{O}C. The temperature in the expander cannot be similar to the desorption temperature for the same reasons and because of non-insulated pipes to the expander that result in losses to the environment and because of heat transfer losses.

Figure 4-26 also indicated that the desorbed gas when side 1 was underheating was more than side 2.

Figure 4-27 shows the average power and the power efficiency (COP_W) for each of eleven power trials. It can be said that the COP_W is directly related to the average power produced. The maximum COP_W is recorded for power trial No. 1 at which the power production was the maximum for the cycle and the lowest is for power trial No. 11 where the average power recorded was the minimum. Every time the average power increases or decreases, the COP_W follows the same response.

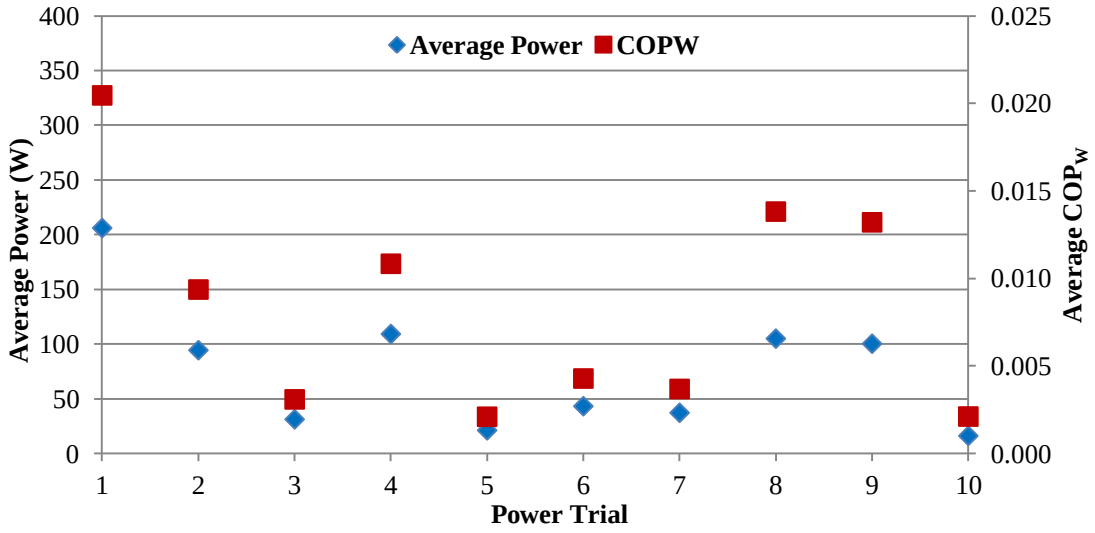

Figure 4-27: COP_W for different average power levels

The maximum COP_W for these experiments is 0.02 for power trial No. 1 and the lowest exclusive power trial No. 8 is 0.002 of power trial No. 11. The maximum theoretical COP_W assuming 1000W of power production and 10070W average heat is 0.1. The COP_W found for the eleven trials is far away from the ideal 0.1 value but if we assume the maximum power production per trial instead the average, the maximum COP_W could be 0.048 (power trial No. 1 for 486W) and the lowest is 0.002 (power trial No. 11 for 23W). The 0.048 shows a potential to increase the COP_W around 50% in case the power production increases further or the heat input decreases.

4.2.2 Flow-rate-related graphs

In this section, the flow rate recorded data from the flow meter during cogeneration production at the expander's inlet will be analysed. Figure 4-28 shows the average power production for different flow rates as recorded for all the power generation trials.

Appendix 9 presents the overall power trial results including the average expander's inlet pressure (MPa) and inlet temperature (^{O}C), the flow rate (kg/s) and the average power production (W) for a 600W power load at the load bank.

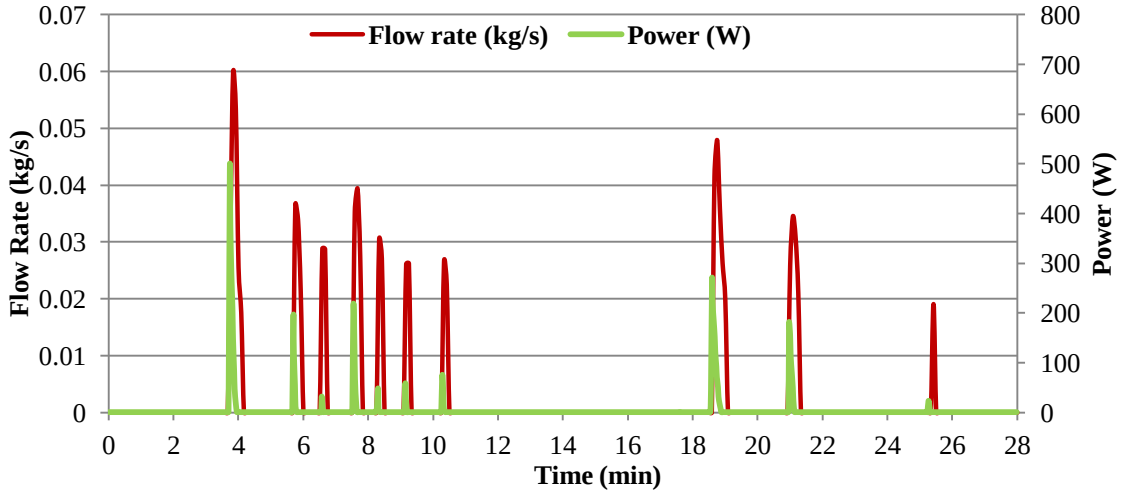

Figure 4-28: Power production for different flow rates

From Figure 4-28 it can be concluded that there is a connection between the power production and flow rate since the cycle's maximum power production is reported in trials No. 1, No. 2, No. 4, No. 9 and No. 10 where the maximum average flow rate recorded was the maximum ranged between 0.028kg/s and 0.034kg/s. The average power production for those five trials is 94-206W and the power generation process lasts 20-32sec.

For trials No. 2 and No. 10 (the second trial for each side), the average inlet pressure and temperature, the power production and the flow rate duration were similar. The average flow rate for trial No. 2 (0.031kg/s) is more compared to trial No. 10 (0.028kg/s), but the average power production for trial No. 10 is 100W compared to 94W in trial No. 2. The reason is the ΔP_{exp} for trial No. 10 (-0.202MPa) which is more compared to trial No. 2 (-0.109MPa).

The maximum average flow rate during the experiments was 0.038kg/s and 0.034kg/s recorded for trials No. 1 and No. 9. These two trials are the first power production of each side which confirm that the desorption rate at the earlier stage of the desorption process is the higher and has maximised the power output. The process duration in both cases is around 30 and 32sec which is the maximum for these sets of results.

For trials No. 3, No. 6, No. 7 and No. 11, the average flow rate does not exceed 0.029kg/s (0.019-0.029kg/s) and the average maximum power production is 31W, 43W, 37W and 16W respectively. The trial No. 5 has an average flow rate of 0.031kg/s but the average power production is 37W. The flow rate is similar to the No. 2 trial but less power was produced compared to 94W in trial No. 2. The trial No. 2 has a lower average expander's inlet pressure than trial No. 5 but both have a similar expander's ΔP_{exp}, so the reason is the overall ammonia quantity entering the expander since the No. 2 trial lasts 25sec compared to 15sec in trial No. 5.

4.2.3 Cooling-effect-related graphs during cogeneration

In this part, will be explored the system's refrigeration performance during cogeneration. Figure 4-29 presents the combined cooling production from side 2 and side 1 with the cooling water temperature for one complete cogeneration cycle for $0^{O}C$ requiring cooling.

The combined average refrigeration effect of both sides is $23^{O}C$. The average cooling effect at evaporator 1 (14-28min cycle time) is around $18^{O}C$ and for evaporator 2 (0-14min cycle time) is $27^{O}C$. The lowest temperature collected was $5^{O}C$ from evaporator 1. For approximately three minutes (17-20min cycle time), the evaporator 1 temperature was below $15^{O}C$ which is ideal for space cooling but not for refrigeration. The gap in the refrigeration's production between the two evaporators is another verification of the inefficiency of reactor 2.

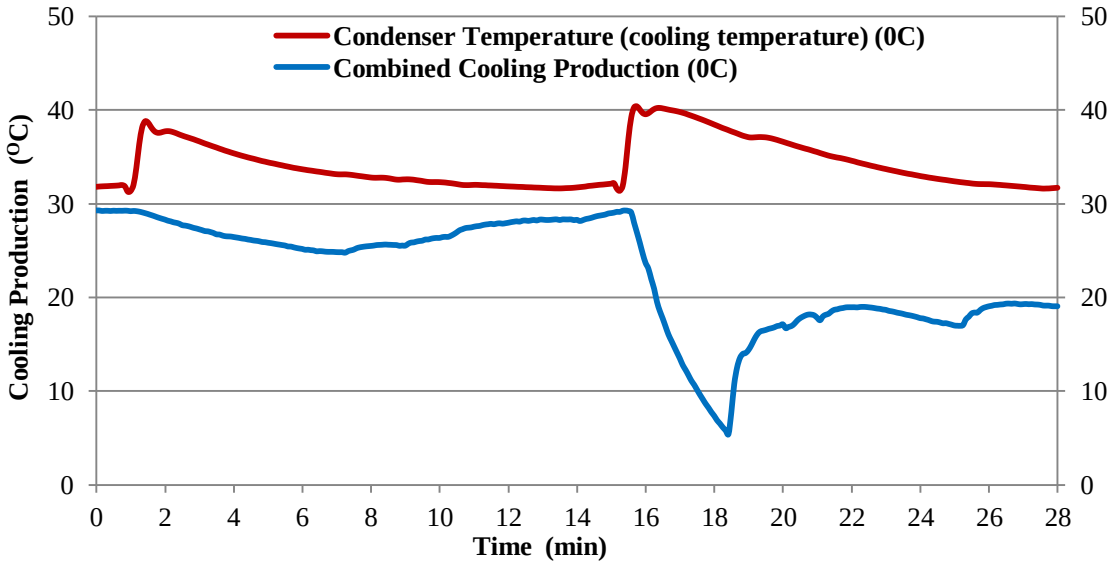

Figure 4-29: Combined cooling production and condenser temperatures for a cycle

Figure 4-29's main outcome is that neither evaporator was able to reach $0^{O}C$ which could easily be achieved during the only-cooling operation. The ability of both the reactors (reactor 2 mainly) not to adsorb efficiently do not allow the evaporator's temperature to drop further. The reason is the mass recovery valve use which eventually reduces the machine's refrigeration ability. The mass recovery process results in a significant amount of ammonia transferred to the low-pressure reactor resulting in its dramatic adsorption capacity dropping by just using it once.

On examining side 1 it starts to behave as a normal cooling cycle (rapid temperature drop for the first 4min) but after the first mass recovery that ability never recovers. A significant amount of ammonia transfers to side 1 (reactor and evaporator), also resulting in a temperature increase ($5^{O}C$ to $17^{O}C$ after the mass recovery was used for the first time at around 18min). The first mass recovery when side 1 produces power destroys any possibilities for cooling production.

Another parameter that affects the system's cooling performance is the cooling water temperature which was $34^{O}C$ on average during the cogeneration test. This is higher than the $20^{O}C$ and $29^{O}C$ on average used during the only-cooling chiller's performance investigation. The higher the cooling water temperature during the adsorption-evaporation process, the lower is the adsorption capacity, and the higher the adsorption-evaporator pressure which both mean a smaller refrigeration effect.

4.3 LH cogen system Flow diagram

The LH cogen as a system has one heat input and four output energy flows. The heat input is the heat during desorption process (Q_{high}) and the heat outputs are the cooling power (Q_{ref}), the power production (Q_w), the heat of adsorption (Q_{ads}) at the low pressure reactor and the rejected heat of condensation (Q_{cond}) during heating. The experimental data can provide the system high heat, the cooling power and the power production. For the estimation of the condensation and adsorption heat an equation similar to the one used to chapter 2 will be applied ($Q=\dot{m}cp\Delta T$).

The mass flow rate ($\dot{m}$) is defined by the cooling water circuit pump (1.305kg/s), the cp is the water specific heat (4.186kJ/kgK) and ΔT is the temperature difference at the exit and inlet of the high pressure side condenser and the low pressure side reactor. The

temperature difference across the condenser was found to be 4^{O}C and across the reactor 10.6^{O}C.

Figure 4-30 provides the system flow diagram using the maximum Q_{high} and Q_{ref} recorder, Q_w is the overall maximum power generation for a complete cycle produced from the machine (side1). Also, the energy lost by the system (Q_{loss}) is presented which is the difference between the heat input to the sum of the heat output. The results are for a 14min cycle time.

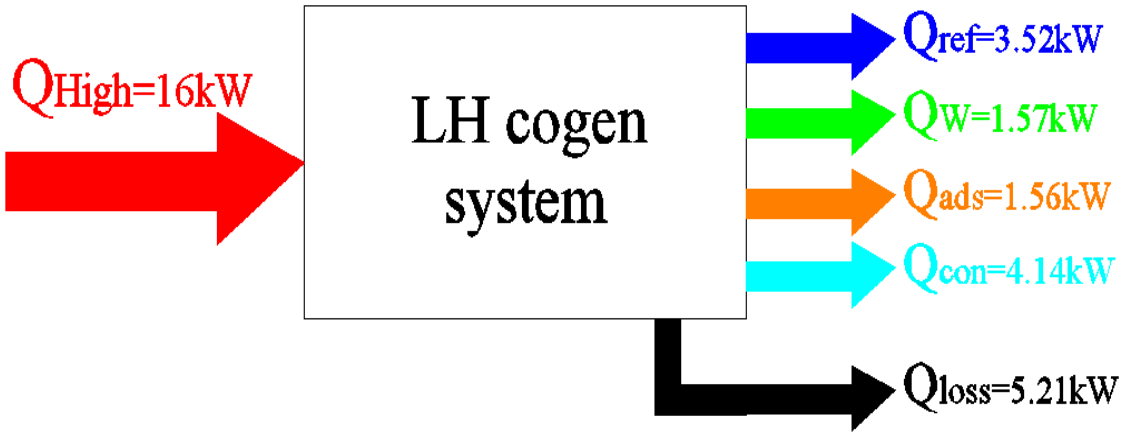

Figure 4-30: LH cogen energy flow diagram.

Using Figure 4-30 data, the system COP_{ref} is 0.22, the COP_W is 0.1 and the overall system COP, which summarises all the $Q_{outputs}$ is 0.67. For a 16kW energy input, 22% is used for cooling (3.52kW), 9.8% for the power production (1.57kW), 25.8% is heat rejection from the condenser (4.14kW) and 9.7% heat rejection during adsorption (1.56kW). The remaining 33% (5.21kW) of the overall energy input are the system overall losses.

These losses are mainly sensible heat in each component at the piping system and to the surrounding. In the reactor part of the energy is consumed by the adsorbent, the fin type heat exchangers and the water copper pipes. Also, heat losses to the surroundings appear from the steel construction. Similar losses appear to the condenser and the evaporator as well as to the surroundings during the ammonia transfer within the system. The losses at the reactor and the condenser cannot be eliminated but can be minimised.

The flow diagram is useful to identify the energy consumed by each component in order to take actions to reduce the heat input, the heat of adsorption and condensation and at the same time maximise the refrigeration power and the overall system power production. Hence the losses are decreased and the overall system efficiency improves.

4.4 Conclusions and Discussion

This chapter discusses the experimental studies of the LH cogen system running in only-cooling mode, in cogeneration mode and for the scroll expander's power generation. The test results have proved that the machine can produce cooling and power under certain conditions when it is driven by a low-grade heat source. Also, it presents all the parameters affecting the adsorption chiller's performance. Some conclusions were drawn from the above results and are summarised below.

a) When the adsorption chiller was investigated for its refrigeration performance, assuming a trial period of 28kg of ammonia, we found that the maximum COP_{ref} was 0.1 for $128^{O}C$ and $19^{O}C$ average maximum vapour and water-cooling heat-sink temperatures, for $0^{O}C$ it requires refrigeration at the evaporator. The maximum SCP and cooling capacity per side under those conditions were 64.57W/kg and 54.24kJ/kg.

b) For the investigation of the heating temperature, a range from $96^{O}C$ to $132^{O}C$ was recorded at the high-pressure reactor's inlet. The COP_{ref} starts to increase as the heating temperature increases, reaches a peak at around $128^{O}C$ and then drops since after that the desorption rate is very slow so resulting in the loss of refrigeration power. This is true for any evaporator's set-up temperature. At the same time, the average refrigeration effect at the evaporators was $7.71^{O}C$ for the $0^{O}C$ evaporator's set-up temperature, $4.53^{O}C$ for the $-5^{O}C$ evaporator's set-up temperature and $-1^{O}C$ for the $-10^{O}C$ evaporator's set-up temperature. The COP_{ref} for the same heating temperature decreases as the evaporator's temperature decreases but at the same time the overall refrigeration effect at the evaporator is lower as well. The system's higher pressure recorded during the desorption-condensation process was 2MPa and 1.6MPa was the average high pressure. At the same time, the lower pressure recorded during the adsorption-evaporation process was 0.13MPa and 0.35MPa was the cycle average.

c) During the investigation of the overall cycle time (basic cycle and mass recovery time) we found that an optimum basic cycle time of 13-16min with 1min extra

mass recovery time maximised the adsorption chiller's refrigeration performance. For the basic cycle time, when investigating from 10 to 18min with 1min mass recovery time, the COP_{ref} increases with the increase of cycle time, reaches a peak at 17min cycle time and then drops. A similar response follows the Q_{ref} and SCP. The system's cooling capacity increases and the Q_{high} decreases linearly with time. The reason there is a peak in the system's performance is that it cannot desorb ammonia efficiently after that point so the cooling effect actually decreases resulting in a decrease in the COP_{ref}. In terms of the mass recovery time, three cases were investigated, for 30sec, 1min and 2min for similar basic cycle times. The results show that there is an optimum of 1min mass recovery time which maximises the COP_{ref}. The system's performance initially is low (30sec), then reaches a peak for 1min mass recovery time and then drops (1-2min). The same response follows the Q_{ref} and SCP. The increase in the COP_{ref} can be up to 55.81% and for the Q_{ref} up to 42.86% from 30sec to 1min mass recovery time.

d) Another important parameter which affects the adsorption chiller's refrigeration performance is the overall ammonia the system is carrying. Experiments were taken for 24kg and 28kg of ammonia for the same trial period. Results for the maximum performance for each case under similar conditions show a significant increase for 24kg at the magnitude of 136.36% in terms of COP_{ref} (0.26 for 24kg and 0.11 for 28kg) and 147.89% increase for Q_{ref} (3.52kW for 24kg and 1.42kW for 28kg) and SCP (201.14W/kg for 24kg and 81.14W/kg for 28kg). The reason for this gap is the sensible heat losses at the evaporator which increase when the system carries excess refrigerant. As a result, the evaporator is late in decreasing its temperature and pressure since more refrigerant is available for cooling and the cooling process is shorter.

e) When the system runs in cogeneration mode, the desorption temperature was $125^{O}C$ and 1.276MPa the average high pressure in the expander. The actual desorbed ammonia's temperature at the reactor's exit was $80^{O}C$ on average and could reach up to a maximum of $95^{O}C$. At the same time, the average expander's inlet temperature is $41^{O}C$. The difference between the desorption temperature to the desorbed gas temperature and the one into the expander is related to heat transfer losses to the pipelines (friction and heat losses) at the various

components similar to ORC cycles. Also, the absence of insulation at the connection pipes from the reactor to the expander increases the losses.

f) The maximum COP_w recorded was 0.048 and 0.029 was the cycle average for 486W maximum power output and for 206W the cycle average. The use of the v8 valve to store the desorbed ammonia before being released to the expander, in order to increase the expander's inlet pressure and flow rate, results in a pulsed non-steady power production.

g) The parameters affecting the system's power production during cogeneration are the expander's inlet pressure, the flow rate and the ΔP_{exp} which are related to how low the pressure at the expander's exit is. To satisfy low pressure at the expander's exit and maximise ΔP_{exp} so increasing the power production, the mass recovery valve was used so utilising the low pressure at the system's low-pressure side. That was necessary because the expander was unable to drive with the v8 valve open since a single and poor power production was produced, and after that the high-pressure side (reactor, expander inlet and evaporator) had a similar pressure since no sufficiently low pressure at the expander's exit could be established. Also, a mass recovery valve was necessary because the desorption rate decreased with the time and later on in the process the flow rate was even lower to drive the expander. On top of these, the system's adsorption capacity was decreased because the adsorbent escapes the reactors and that the cooling water temperature was high enough to produce a low pressure at the expander's exit.

h) The mass recovery and the v8 valve utilities during cogeneration are positive and essential to produce power even if the procedure followed was not the ideal one. The mass recovery as well as the v8 valve used indicate the mismatch of the expander's specification with the operating conditions during desorption – mainly the flow rate.

i) The use of a mass recovery valve during cogeneration has a negative effect on the system's refrigeration performance. The average refrigeration temperature was $5.4^{O}C$ and the evaporator's temperature never reaches the required cooling temperature of $0^{O}C$. The reason is the mass recovery valve usage which transfers a significant amount of refrigerant to the low-pressure reactor. The result is that the reactor's adsorption capacity decreases and no further adsorption can be efficiently carried out further by just using it once. The low-pressure side reacts

as with a normal cooling cycle before the mass recovery valve is used, but it never recovers after that. The system for three minutes has a temperature below $15^{O}C$ which is good for space cooling.

j) The overall period that useful cooling can be produced from the chiller for a 28min overall cycle time is approximately 17.30min for $0^{O}C$ required cooling, approximately 13.30min for $-5^{O}C$ required cooling and for approximately 9min for $-10^{O}C$ required cooling.

k) The system energy flow shows 33% energy is lost mainly during the refrigerant transfer and as sensible losses at the reactor, the condenser and the evaporator. The losses to the reactor and the condenser cannot be eliminated completely, but by increasing the adsorbent mass and heat transfer, selecting higher thermal conductivity material for the heat exchanger and the water circuit, and replacing the steel construction, can be reduced.

l) This chapter also provides an error bar for each of the instrument used (temperature and pressure sensor, power meter and flow rate) which shows a tight response from the collected indicating their accuracy.

Chapter 5. Modelling and simulation

5.1 Introduction

The development of computer science helps the growth of a very useful tool for analysis and optimisation purposes, modelling and simulation. That was proven to be an easier, more effective and cheaper approach to collecting data analysing the system's behaviour without physically building them.

This chapter describes how the LH cogen system using ECLIPSE was used for modelling and simulation purposes mainly to validate the cooling model using the experimental results and to create a model exclusive for the LH cogen system which can predict the system cooling performance for fixed evaporator temperatures, varying the system low pressure. Later, before any power results are extracted, the conditions from the cooling results will be used to predict the system power generation. After the power data is collected experimentally, those power experimental results will be used to validated the model and to further investigate the system power generation and to effect system optimisation. The system was tested under different conditions which, combined with the experiments, will identify the system's optimised conditions. The experimental cogeneration and cooling results as well as data from the power expander's nitrogen test were used as input to the simulation. It was developed within the Energy Research Centre (UU) in 1992, originally for the analysis of coal liquefaction technology and was developed by the European Community Third Non-Nuclear Energy R&D and JOULES Programmes. Through the years, ECLIPSE has been used to simulate many different chemical and engineering processes for industrial plants but not a chemical adsorption chiller until now.

5.2 The basic principle and the software

The reaction of adsorbate and adsorbent is shown in Equation 5.1. That is, $CaCl_2$ reacts with NH_3 which is to take place in three stages. As ammonia starts to react with $CaCl_2$, the compound $CaCl_2*2NH_3$ is formed, later the $CaCl_2*4NH_3$ and the complete reaction with 8 moles of ammonia $CaCl_2*8NH_3$. MX from Equation 5.1 is the reactive solid salt (usually a metal chloride), G is the reactive gas, usually ammonia. ΔH is the heat of the chemical reaction (reaction enthalpy difference) of the refrigerant at the end and at the

start of each process [53]. The simulation assumes that 4 moles of ammonia are used to react with the $CaCl_2$.

$$\mathbf{MX.nG + pG\ 2\leftrightarrow 1\ \ MX.\ (n+p)G + p\Delta H} \qquad \mathbf{5\text{-}1}$$

ECLIPSE assumes that adsorption and desorption processes are constant under a certain pressure or temperature. The analysis made by ECLIPSE is based on energy and the mass balance point of view.

A technical evaluation begins by gathering sufficient data to enable ECLIPSE to calculate the equilibrium mass and energy balance and utilise usages of the process. All the compounds' properties involved in the process must be defined in the compound database, i.e. the $CaCl_2$, NH_3 and $CaCl_2NH_3$ and all the utilities must be defined in the utilities database. The stages involved in the simulation of the process are as below:

- The preparation of the process flow diagram using the flow diagram file;
- The addition of technical data to the process like compounds' specifications using the compound data file;
- The calculation of the mass and energy balance by using the mass and energy balance file (here we can add all the compounds' specifications);
- The calculation of the utilities' usages by using the utilities usages file;
- The economic analysis.

The simulation of the LH cogen system on ECLPISE describes the reaction process during adsorption by considering the reaction rates of $CaCl_2$ with NH_3 as flow streams to form a $CaCl_2NH_3$ stream. During desorption, the $CaCl_2NH_3$ flow is broken into $CaCl_2$ and NH_3. The reaction process on ECLIPSE is not similar to the real process where the only flow is mainly the NH_3 and a very small percentage of $CaCl_2NH_3$.

5.3 The preparation of the process flow diagram

A chemical process is defined in terms of chemical engineering unit operations, or modules connected together by process flows or streams. The streams within a process are composed of a number of chemical components or compounds, the standard state and critical properties of which are defined in the compound database. A process flow diagram gives each module and stream a unique identity.

Figure 5-1 below shows a flow diagram for the LH cogen power production process during desorption.

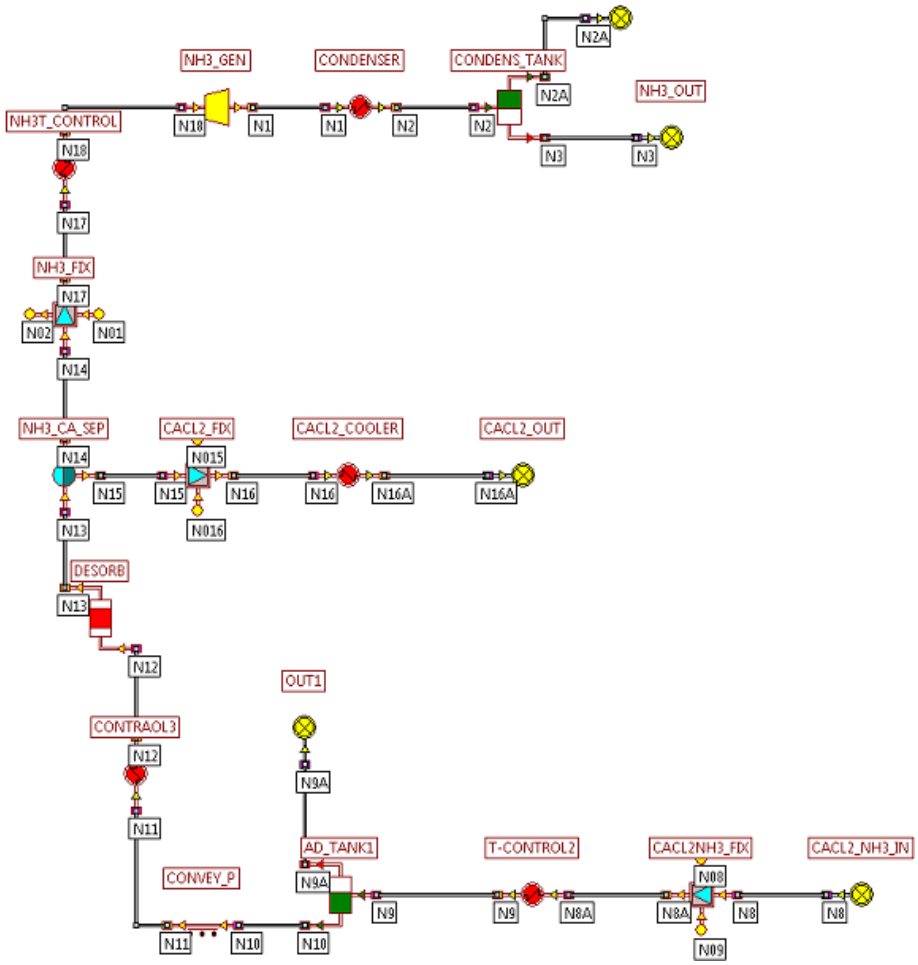

Figure 5-1: Flow diagram for power production

A compound database looks like Figure 5-2 below which presents the three databases for the $CaCl_2$, NH_3 and the $CaCl_2NH_3$. The properties listed below are taken from the literature and were those used as inputs to the simulation.

Compound Name	CACL2	NH3	CACL2NH3
Standard State	Solid	Gas	Solid
Molecular Weight	110.990	17.030	186.770
Critical Temperature (Deg C)	----	132.4	----
Critical Pressure (Bar abs)	----	112.770	----
Acentric Factor	----	0.250	----
Specific Heat Consts (kJ/kg mole K)			
Const.A	70.75002	27.31600	73.49997
Const.B (x10-2)	1.15074	2.38301	0.00000
Const.C (x10-5 Sol+5)	0.00000	1.70801	0.00000
Const.D (x10-9)	0.00000	-11.84900	0.00000
Min Valid Temp. (Deg C)	-100.0	-150.0	-150.0
Max Valid Temp. (Deg C)	1600.0	2000.0	2000.0
Heat of Form (MJ/kgmole)	-798.004	-45.720	-0.040
Heat of Comb (MJ/kg)	----	----	----
Gibbs F.E. (MJ/kgmole)	-0.750	-16.161	-0.001
Normal B Pt (Deg C)	----	----	----
Specific Gravity (kg/l)	2.152	----	44.000
Watson Char. Factor	----	----	----
Element Analysis (%)			
	CA 36.11	N 82.25	CA 22.38
	CL 63.89	H 17.75	CL 39.59
			N 31.28
			H 6.75

Figure 5-2: Compound data for $CaCl_2$, NH_3 and $CaCl_2NH_3$

5.4 LH cogen system's simulation procedure

The LH cogen system was initially simulated as a single continuous procedure before splitting into two. For reasons related to the function of the simulation and its ability to provide accurate results. Assuming the cycle starts producing power, a compound of $CaCl_2NH_3$ entering the high pressure and temperature is desorbed, and is then fully separated at the separator into $CaCl_2$ and an ammonia gas flow. The ammonia gas is then expanded in the expander and produces power. All the gas is liquefied at the condenser and ends at the condenser tank. From that point the cooling cycle starts when the liquid ammonia decreases its pressure and temperature and produces a refrigeration effect to the evaporator. At the same time, refrigerant from the evaporator meets the $CaCl_2$ left from the power simulation for adsorption to take place and create the $CaCl_2NH_3$ compound. One cogeneration cycle is completed at that point and the compound is now ready for desorption for a new cycle to start again. The above is a single procedure presented in Figure 5-3 which brings together the two simulations: power on the left and the cooling on the right.

Since the two are linked together, the flow of NH_3 and $CaCl_2$ from the power simulation should be the same as used for the cooling. Similarly, the flow of the $CaCl_2NH_3$ from the cooling should be the same as for the power.

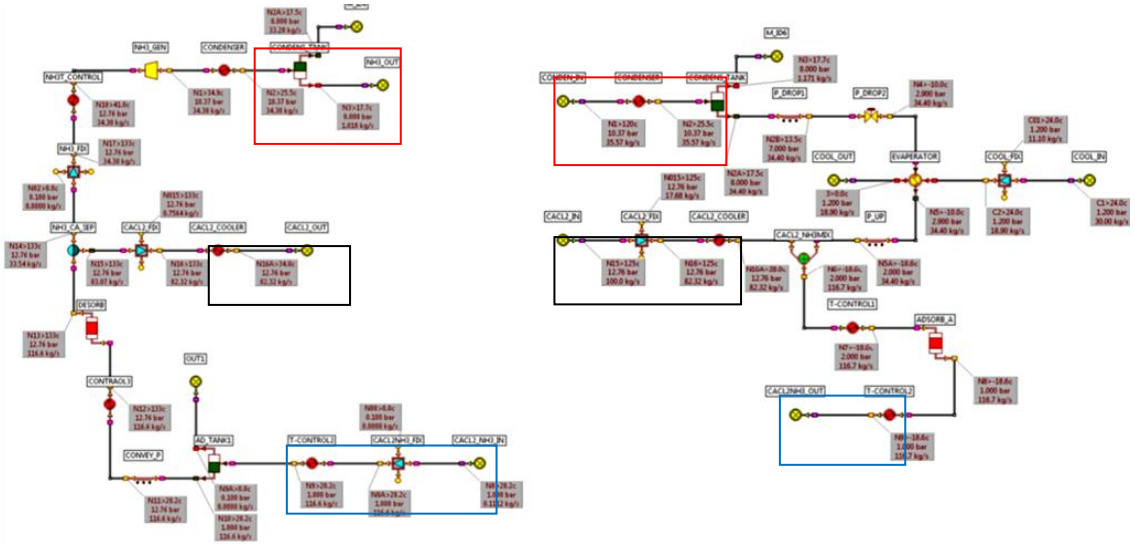

Figure 5-3: The two separate simulations: power (to the left) and cooling (to the right)

Figure 5-3 shows the three points where the flows are linked together. The NH_3 refrigerant leaves the expander from the power simulation to condensate and is collected at the condenser tank. The same arrangement appears at the cooling simulation where a condenser is followed by a condenser tank before reducing its pressure for the cooling cycle to start. These two points are indicated with red squares on Figure 5-3. For the $CaCl_2$ flow it leaves the power simulation and continues to the cooling simulation as the black squares indicate. The $CaCl_2NH_3$ is presented in blue squares where the compound from the cooling simulation enters the power simulation.

The above procedure would be followed in case the cogeneration simulation was in a single flow diagram. Since it is split in two, that means the state properties and condition of the NH_3 and $CaCl_2$ leaving the power simulation should be manually identified at the cooling simulation.

A simplified diagram of the model is shown in

Figure 5-4 which depicts the cogeneration procedure as a single stage. The cooling simulation is called phase 1 and is indicated with a blue dotted line and the power simulation shown by a red dotted line and is called phase 2. With black are the flow rate directions (NH_3, $CaCl_2$ and $CaCl_2NH_3$) and the black arrows towards the components are indicate the values of the experimental results used at that component to validated the model or for the further system examination. The blue and the red arrows outwards,

are indicate the collected data from the cooling and the power simulation respectively. Similarly, the green arrows outwards are the parameters which vary to further investigated further the system power performance.

The $CaCl_2NH_3$ flow rate at high pressure and temperature desorbed at the desorber, and the NH_3 and $CaCl_2$ are split completely. The NH_3 enter the expander to produce power and the expanded mixture is condensed and cools down at the condenser temperature. Afterwards, ammonia at low pressure and temperature provide the cycle cooling power at the evaporator and later still, the NH_3 flow rate from the evaporator and the $CaCl_2$ flow rate from the desorber, are mixed again in the adsorber to form a $CaCl_2NH_3$ mixture at condensation temperature and low pressure. The mixture then enters the boiler increasing the system pressure and temperature before it enters the desorber to start a new cycle.

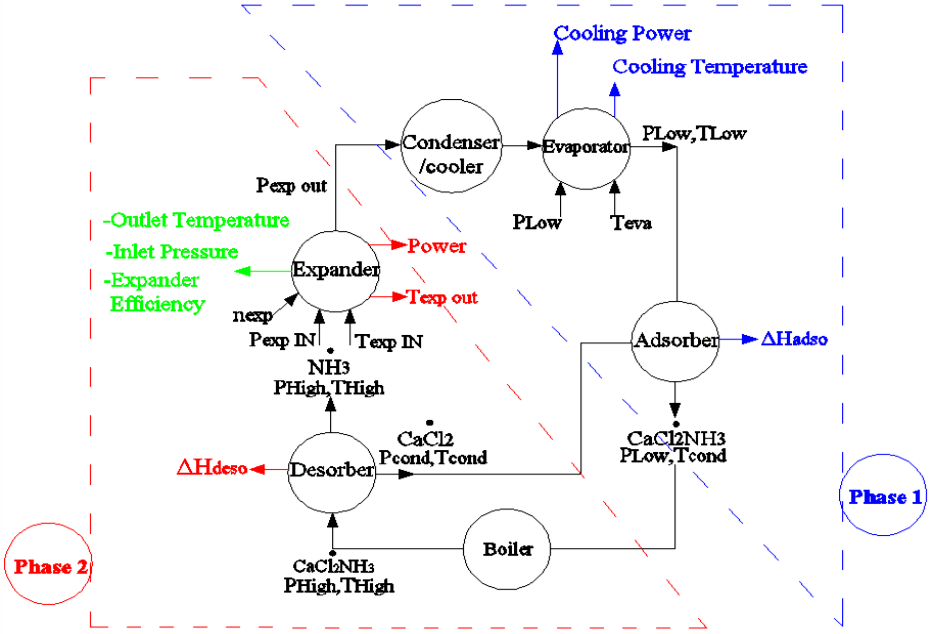

Figure 5-4: Schematic of the LH cogen based on ECLIPSE modelling

Phase 1 in

Figure 5-4 is actually a validation of the model using data from the only cooling operation of the machine for evaporator temperature of $0^{O}C$, $-5^{O}C$ and $-10^{O}C$. The purpose of the cooling simulation is to be used after validation to accurately predict the system cooling performance for different system low pressure for $0^{O}C$, $-5^{O}C$ and $-10^{O}C$

evaporator temperatures. This model is valid and can be used only for the LH cogen system.

For phase 2, cooling results are used (maximum pressure and temperature, pressure at the expander exit and flow rate) to predict the system power performance before any power results are reported experimentally. Later, after the power experiments trials, the simulation will be validated using experimental results and later still this model will be used to further investigate the system power generation (green lettering).

5.5 Cooling simulation

For the cooling simulation of the LH cogen system the maximum experimental refrigeration performance used to validate the model from the only cooling experimental data and to build a reliable model to identify the system's refrigeration performance. Figure 5-5 shows the flow diagram of the cooling simulation.

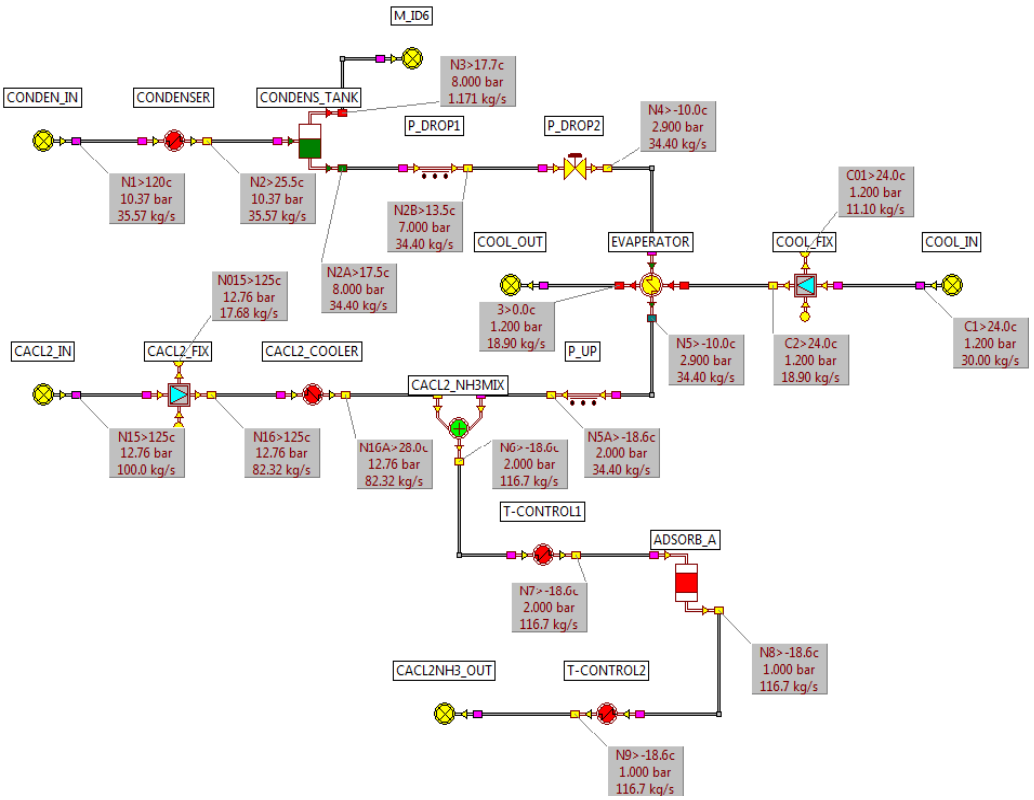

Figure 5-5: Cooling simulation diagram (phase 1)

The adsorption chiller's refrigeration performance is attained by simulating the evaporation process of the adsorption process. The refrigeration effect is based on the principle of ammonia evaporation absorbing heat during the process from the

evaporator and its surroundings. The ammonia flow rate represents the average evaporation rate.

The cooling simulation results can be found at ECLPISE from the balance table similar to Figure 5-6 from which can be identified the evaporator's temperature (Hot Side Out) and the refrigeration power Q_{ref} (Heat Transfer). Also there can be identified the cooling circuit entering the evaporator's temperature (Hot Side In) and data about the condensers.

Tank/Vessel ID	Pressure (Bar ABS)	Temperature (C)	Flash (%)
CONDENS_TANK	8.000	17.67	3.29

Heater or Cooler ID	Inlet Temperature(C)	Outlet Temperature(C)	Heat Transfer (MJ/s)
CACL2_COOLER	125.00	28.00	0.000
CONDENSER	120.00	25.54	0.000
T-CONTROL1	-18.63	-18.63	0.000
T-CONTROL2	-18.63	-18.63	0.000

Heat Exchanger	Hot Side Inlet	Hot Side Outlet	Cold Side Inlet	Cold Side Outlet	Heat Transfer
ID	TEMP (Deg C)	TEMP (Deg C)	TEMP (Deg C)	TEMP (Deg C)	(MJ/s)
EVAPERATOR	24.00	0.04	-9.96	-9.96	2.940

Reactor (ID)	Enthalpy Change	Elemental Balance Error
ADSORB_A	2114.022	H -0.0084

Figure 5-6: Balance table of cooling simulation

5.5.1 Experimental cooling results validation

Appendix 10 presents the experimental results which provide the maximum refrigeration power. These were when the machine was carrying overall 24kg of NH_3 running for 13+1 cycle time, when the desorption temperature was $125^{O}C$. Appendix 10 includes the experimental average cooling and heating power (W), the maximum COP_{ref} recorded, the average evaporator temperature and the lower pressure used in the simulation (MPa) for 0, -5 and $-10^{O}C$ evaporator set-up temperatures. Appendix 11 presents the validated simulation results from the experimental cooling results and includes the average cooling and heating power (W), the maximum COP_{ref}, the average evaporator temperature, the SCP and the evaporator's cooling water circuit flow rate for 0, -5 and $-10^{O}C$ evaporator set-up temperatures.

Appendix 12 presents the deviation of the average cooling power, the average heating power, the cooling refrigeration's performance, the SCP and the average cooling temperature at the evaporator between the experimental and simulation data. Table 5-1 presents the cooling experimental data used to validate the cooling model.

Quantity	Value
System Low pressure for $0^{O}C$	0.29MPa
System Low pressure for $-5^{O}C$	0.246MPa
System Low pressure for $-10^{O}C$	0.23MPa
NH_3 Flow Rate	0.034 kg/s
$CaCl_2NH_3$ Flow Rate	0.113 kg/s
$CaCl_2$ Flow Rate	0.082 kg/s

Table 5-1: Collected cooling results input for simulation validation

Figure 5-7 shows a comparison of the average refrigeration power between the experimental and simulation results for $0^{O}C$, $-5^{O}C$ and $-10^{O}C$ evaporator set-up temperatures.

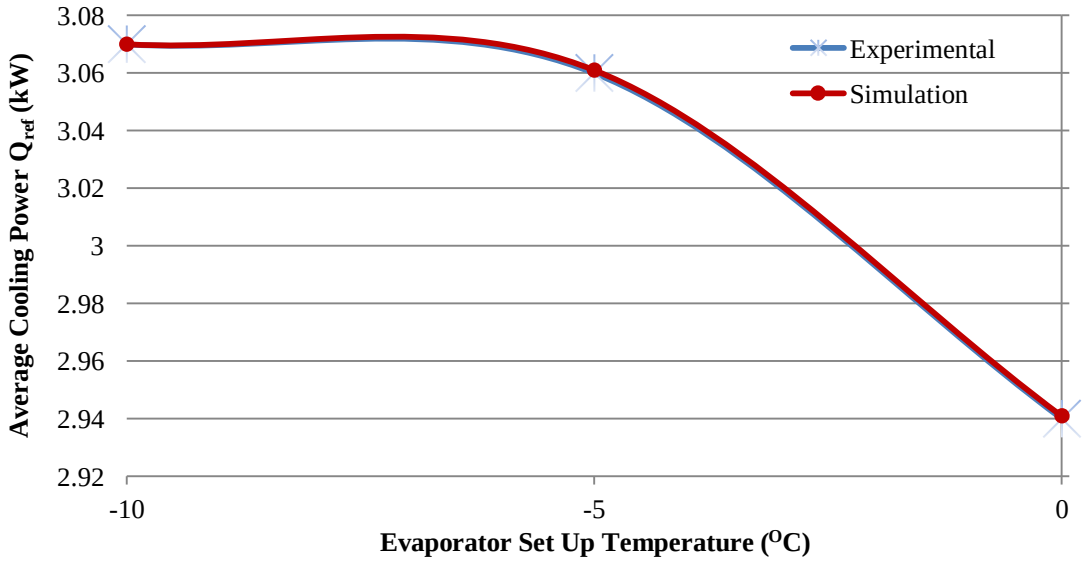

Figure 5-7: Average cooling power for 0, -5 and $-10^{O}C$ evaporator set-up temperatures

Figure 5-7 shows that the average refrigeration power for $0^{O}C$, $-5^{O}C$ and $-10^{O}C$ evaporator set-up temperatures between the experimental and simulation results is almost identical. The deviation for this parameter is actually zero for any evaporator set-up temperature (0.03% the maximum). The maximum average Q_{ref} is 2.94kW, 3.05kW and 3.07kW for $0^{O}C$, $-5^{O}C$ and $-10^{O}C$ the respective evaporator set-up temperatures. These values are close to each other which mean for the 24kg of ammonia, the system can produce almost the same Q_{ref} for any evaporator temperature.

Figure 5-8 shows a comparison of the average evaporator temperatures between the experimental and simulation results for 0^{O}C, -5^{O}C and -10^{O}C evaporator set-up temperatures.

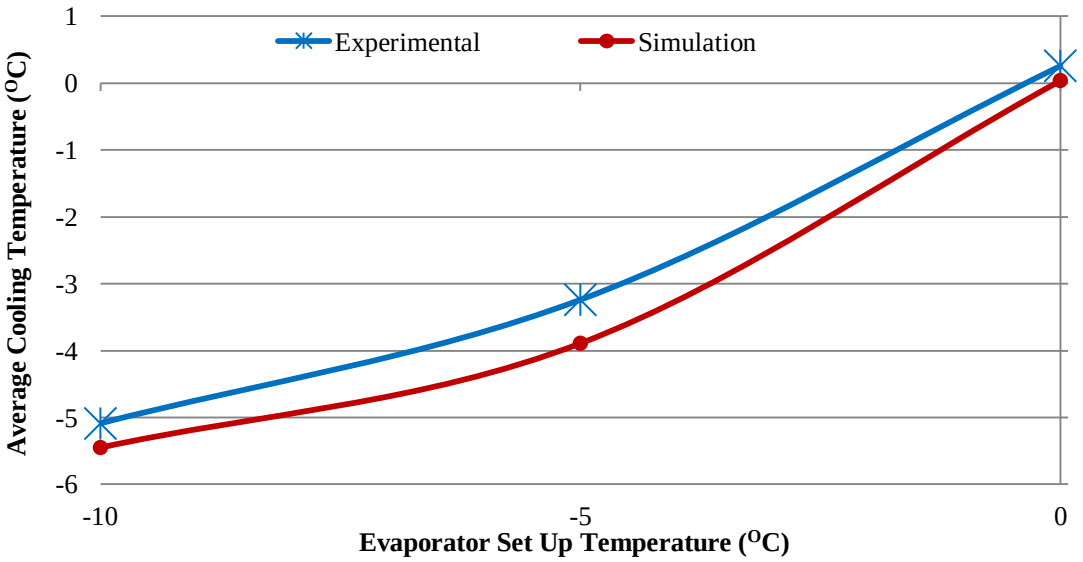

Figure 5-8: Average evaporator temperature for 0, -5 and -10^{O}C evaporator set-up temperatures

Figure 5-8 shows that the temperature difference between the experimental and simulation results is 0.22^{O}C for 0^{O}C, 0.65^{O}C for -5^{O}C and 0.36^{O}C for -10^{O}C evaporator set-up temperatures. These numbers are translated into 0.08% for 0^{O}C, 0.24% for -5^{O}C and 0.13% for -10^{O}C evaporator set-up temperatures. The temperature differences between the experimental and simulation results are small so it can be said that the simulation can be validate the average evaporator temperature very accurately.

Figure 5-9 shows a comparison of the average heating power between the experimental and simulation results for 0^{O}C, -5^{O}C and -10^{O}C evaporator set-up temperatures.

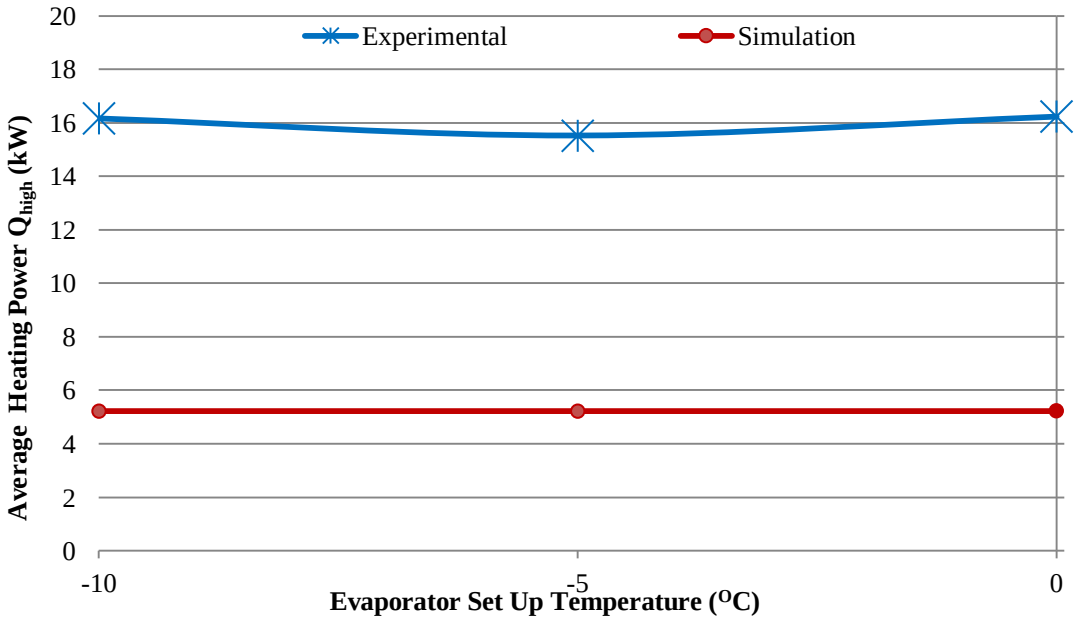

Figure 5-9: Average heating power for 0, -5 and -10^{O}C evaporator set-up temperatures

Figure 5-9 shows that in terms of the average heating power, the simulation provides a constant value of 5.2kW, but at the same time the experiments also provide an almost constant value of 15.9kW. The gap between the experimental and simulation Q_{high} is huge, which is 10.7kW, otherwise a 67.3% deviation on average. This difference is even bigger than the 30% if we assume sensible losses as discussed previously. There are several reasons why the simulation's desorption heat is almost triple compared to the experimental one.

The main reason has to do with the 30% sensible losses referred to previously so the system runs with 28kg of ammonia compared to 24kg which the analysis is based on. The literature states that the more ammonia there is in the system the easier it is for desorption to take place, i.e. the adsorbent to release ammonia. The $CaCl_2$ reaction with NH_3 takes place in 3 stages (2, 4 and 8 moles of NH_3), the 24kg system is closer to the 4 moles rather than the 28kg, therefore for the latter, the bond needs more energy to consume for desorption to brake. For the cooling trials, for 28kg NH_3, the average heating power was around 12kW which is closer to the cogeneration's Q_{high}.

The second reason is related to the period for each trial. The maximum refrigeration results (24kg) were collected when the machine was first operated. Later the machine is

proven to lose some adsorbent from the reactors which means the adsorption capacity decreases, so the Q_{high} because the heat should heat a smaller volume of adsorbent.

Figure 5-10 shows a comparison of the refrigeration's efficiency between the experimental and simulation results for $0^{O}C$, $-5^{O}C$ and $-10^{O}C$ evaporator set-up temperatures.

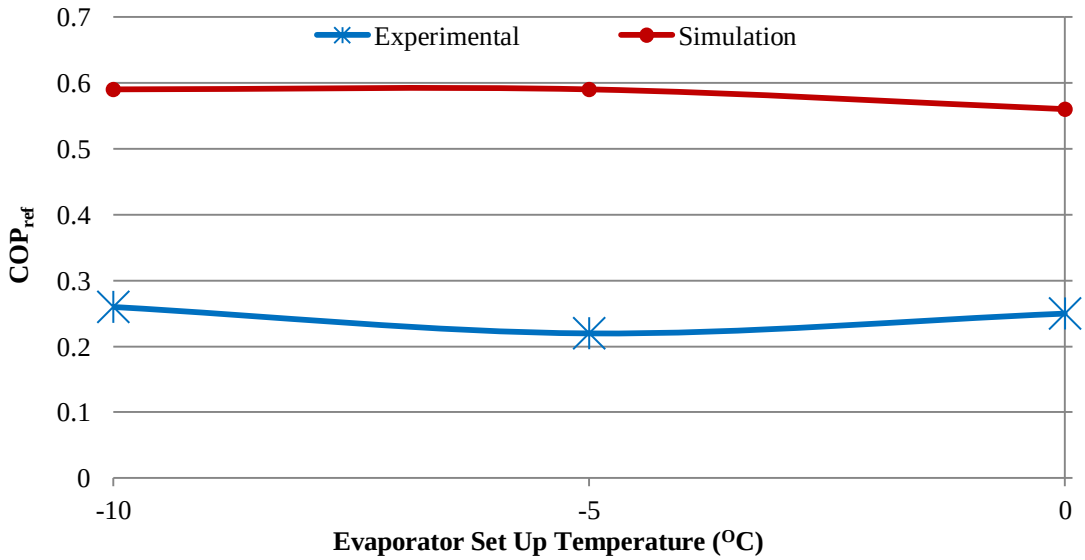

Figure 5-10: COP_{ref} for 0, -5 and $-10^{O}C$ evaporator set-up temperatures

Figure 5-10 suggests that for both the experimental and simulation results, the COP_{ref} is almost constant for any evaporator's set-up temperature but there is a gap between the experimental and simulation COP_{ref} values. That difference was expected since, even though the refrigeration power was identical, the heating power was not. The experimental COP_{ref} is in between 0.18 and 0.19 compared to 0.57-0.59 that the simulation provides.

Since the simulation can be validated almost at 100% accuracy the Q_{ref}, therefore the SCP and the cooling capacity will have the same response as will the deviation be almost zero, similar to Q_{ref}. Figure 5-11 and Figure 5-12 show the SCP and the cooling capacity comparison between the experimental and simulation results. The SCP range is between 168 and 175W/kg and the cooling capacity is 141-147kJ/kg per side. Both the SCP and cooling capacity are almost constant for $0^{O}C$ to $-10^{O}C$ so require a cooling range between them.

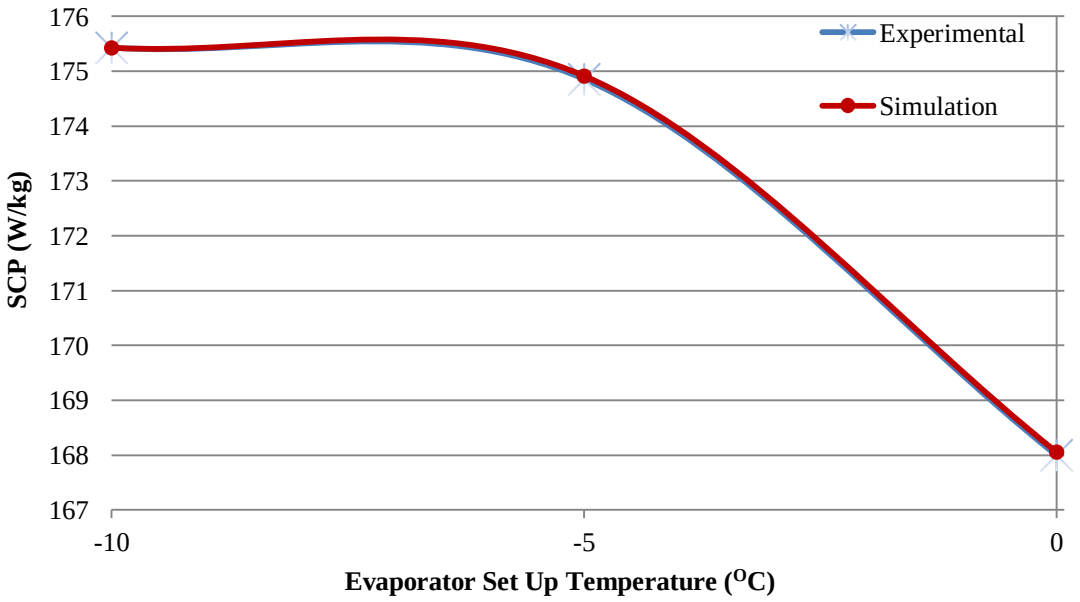

Figure 5-11: SCP for 0, -5 and -10^{O}C evaporator set-up temperatures

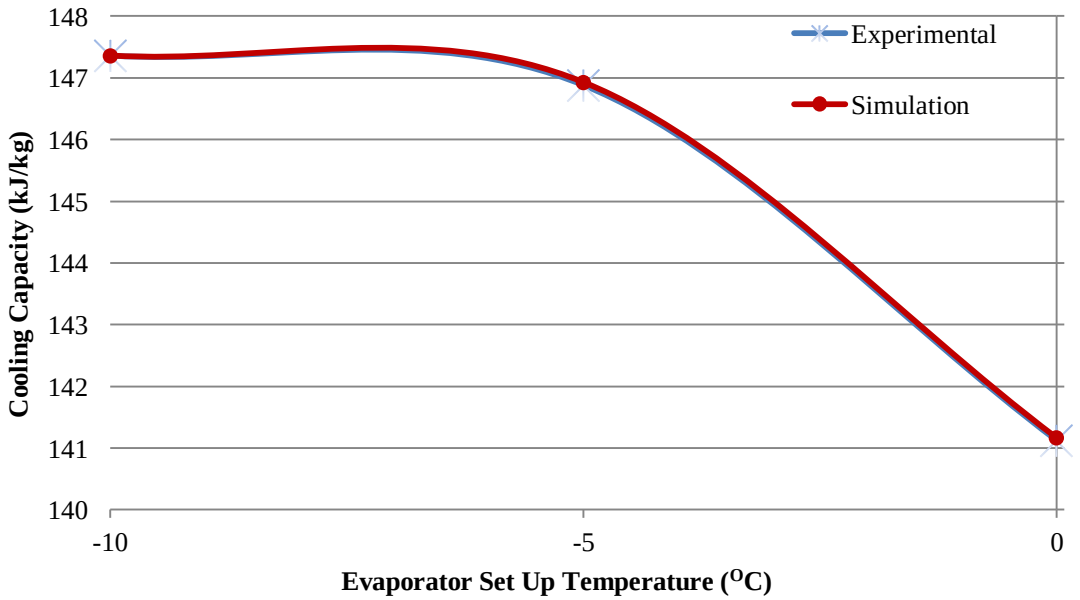

Figure 5-12: Cooling capacity for 0, -5 and -10^{O}C evaporator set-up temperatures

5.6 Power simulation

The simulation analysis will start with the power by assuming a continuous process during desorption. The compound of $CaCl_2NH_3$ is heated up, increasing its pressure on the chemical reactor and then $CaCl_2$ and NH_3 are 100% split at the separator. Then the high-pressure refrigerant expands in the expander resulting in the power production. Figure 5-13 shows the power-generation diagram as presented by ECLIPSE on the mass and energy balance.

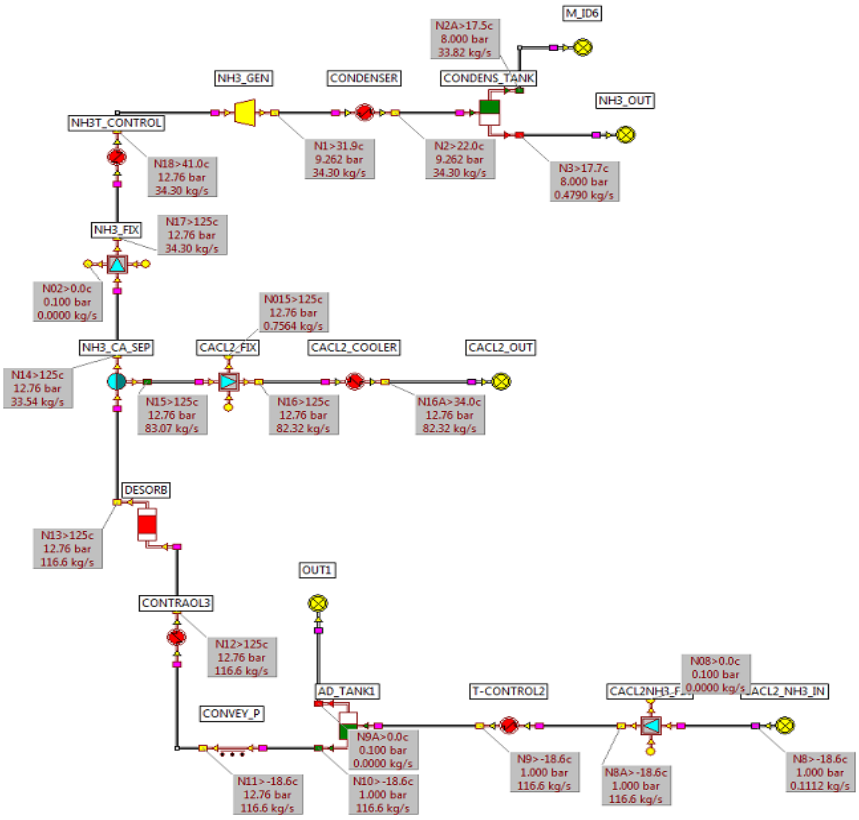

Figure 5-13: Power simulation diagram (phase 2)

Before running the power simulation, one should identify the expander's efficiency by using data from the expander's nitrogen test. For that reason, a simulation for the nitrogen expander test when using ammonia is designed (Figure 5-14) to validate the simulation using the experimental results. The same inlet pressure and temperature as well as the outlet pressure, when the expander was tested with varying inlet temperatures, are used as inputs to the simulation. Appendix 13 shows the experimental results used as inputs to the simulation and Appendix 14 shows the simulation results for the expander's nitrogen test and compares also the experimental and simulation results for the same inlet and outlet pressures and similar inlet temperatures. Appendix 14 shows the average outlet temperature (^{O}C), the power (W), expander flow rate (kg/s), as well as the expander's efficiency. Figure 5-15 presents graphically the comparison in average power production between the experimental and simulation results.

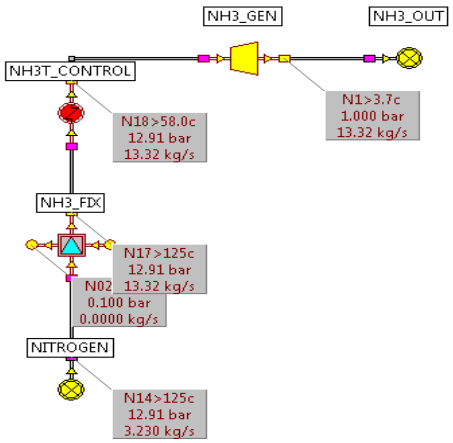

Figure 5-14: Nitrogen test simulation

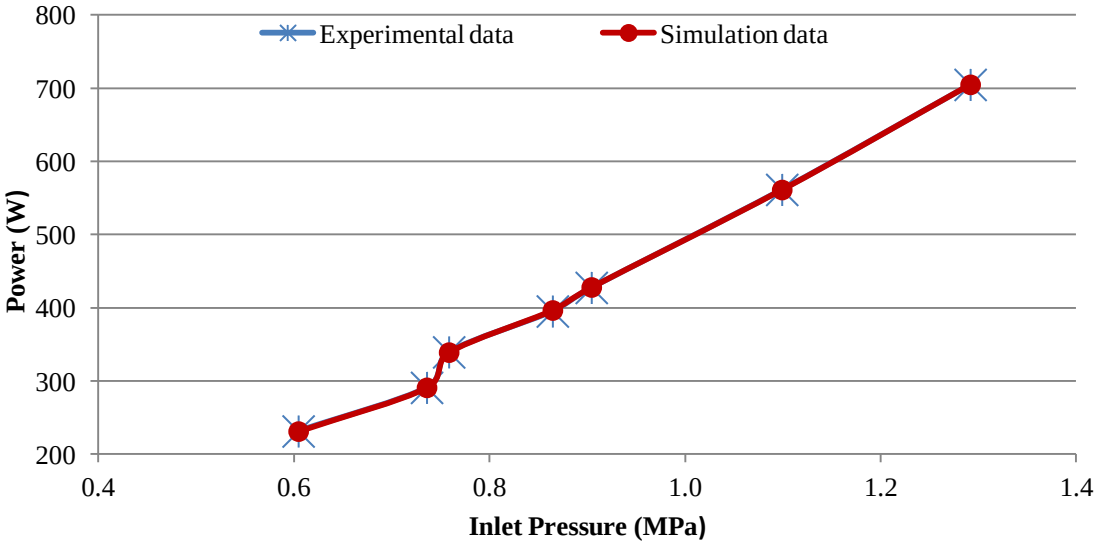

Figure 5-15: Comparison of experimental and simulation scroll expander power when using nitrogen

Figure 5-15 suggests that the average power production given from the simulation is almost identical to the experiments. This founding is important since it proves the simulation can describe the system's response and this is the result considered most reliable. The average expander efficiency for the nitrogen test according to the simulation is 29.7 and the average flow rate found is 0.085kg/s.

Since the LH cogen system uses ammonia as a refrigerant, one should repeat the trials to identify the expander's efficiency when it runs with ammonia. Figure 5-16 shows a comparison of the simulated power production when using nitrogen and ammonia for the same inlet pressure when the flow rate was varied to match the nitrogen test's power production.

The results show that the average power production deviation is very similar, a sign that the simulation can describe the power production of the selected scroll expander when running with ammonia. Appendix 15 shows the overall results when using ammonia as a refrigerant. It indicates the power production (W), the ammonia's average outlet temperature (^{O}C) and the average flow rate (kg/s). The simulation suggests that for the selected scroll expander when running with ammonia, the average efficiency is 17.3%.

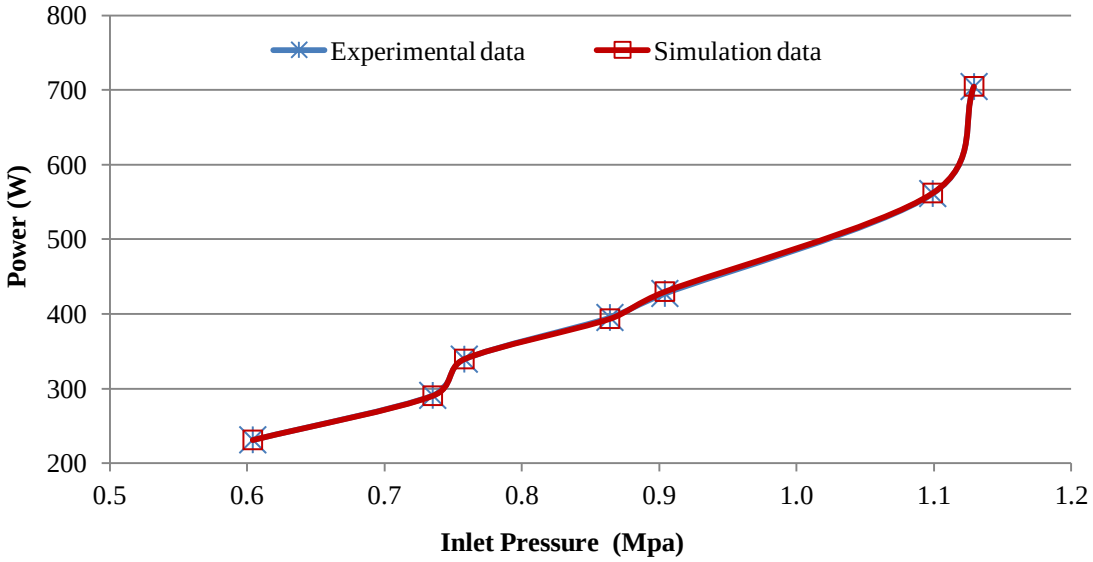

Figure 5-16: Comparison of simulation scroll expander's power when using nitrogen and ammonia

Now all the data require to predict the system power performance using experimental data from the cooling experiments are known. This data applies for 24kg of ammonia which provide the maximum cooling performance the system maximum pressure (1.55MPa), the system lower pressure during mass recovery process (0.9MPa) and the maximum desorption temperature (133^{O}C). The selected data chosen to be the maximum value are assumed to be continuous and repeatable. Under these conditions, the power generation is 473.65W and the exit expander ammonia temperature is 121^{O}C. The COP_W is 0.08.

Now is time to validate the power simulation using the experimental results provided in chapter 4. The procedure followed for the power simulation was for ECLIPSE to be validated using the experimental power results above 100W which are given in Appendix 8. These are trials No. 1, No. 2 and No. 4 from side 1 and trials No. 9 and No. 10 from side 2. From the cogeneration results, the average flow rate for trials No. 1, No.

2 and No. 4 is 0.0343kg/s and 0.0310kg/s for trials No. 9 and No. 10. The procedure followed to identify the $CaCl_2NH_3$ and $CaCl_2$ flow rate is to keep constant the NH_3 flow rate and by varying the $CaCl_2$ flow rate to estimate the $CaCl_2NH_3$ flow rate which is the sum of the two for side 1 and side 2 that matches the experimental power. The cogeneration results are taken when the machine was carry 28kg of ammonia overall.

The experimental data imported into the simulation were the expander's efficiency where a value of 14.7 is used and not 17.3 assuming 85% generator efficiency as well. The maximum desorption pressure was 1.6MPa, the expander's inlet pressure used was 1.276MPa and the expander's inlet temperature was $41^{O}C$. The expander's inlet pressure and temperature are the average values from the five selected experimental trials. The expander's discharge pressure for each trial found from the experimental results was the pressure of the evaporator currently connected to the expander before power generation starts, i.e. before v8 opens. The maximum vapour for side 1 was found to be $133^{O}C$ and for side 2 $130^{O}C$. The high-pressure reactor's temperature just before desorption starts is $-8.16^{O}C$ for side 1 and $28^{O}C$ for side 2. The flow rates of NH_3, $CaCl_2$ and $CaCl_2NH_3$ for side 1 and side 2 are different based on the ammonia flow meter recorder.

Table 5-2 presents the data input into ECLIPSE used to validate the model and Table 5-3 shows the generated from ECLPISE power results for the 5 trials under study. Table 5-3 presents the average power output (W), the average expander's inlet pressure (MPa), the average expander inlet and outlet temperatures (^{O}C), the average heat input (Q_{high}) and the power generation coefficient of the performance (COP_W).

Quantity	Value
Desorption Maximum Pressure during Cogeneration	1.6MPa
Desorption Higher Temperature (side 1)	$133C^{O}$
Desorption Higher Temperature (side 2)	$130C^{O}$
Reactor Temperature When Desorption Starts (side 1)	$-8.16C^{O}$
Reactor Temperature When Desorption Starts (side 2)	$28C^{O}$
Scroll Expander's Average Inlet Pressure	1.276MPa
Scroll Expander's Average Inlet Temperature	$41C^{O}$
Scroll Expander Efficiency	14.7
Expander Discharge Pressure (Trial 1)	0.929MPa
Expander Discharge Pressure (Trial 2)	1.01MPa

Expander Discharge Pressure (Trial 4)	1.082MPa
Expander Discharge Pressure (Trial 9)	1.069MPa
Expander Discharge Pressure (Trial 10)	1.075MPa
NH_3 Flow Rate (side 1)	0.034 kg/s
$CaCl_2NH_3$ Flow Rate (side 1)	0.113 kg/s
$CaCl_2$ Flow Rate (side 1)	0.082 kg/s
NH_3 Flow Rate (side 2)	0.031kg/s
$CaCl_2NH_3$ Flow Rate (side 2)	0.105kg/s
$CaCl_2$ Flow Rate (side 2)	0.074kg/s

Table 5-2: Collected power results input for simulation validation

Power Trial No.	Average Power Output (W)	Average Expander Inlet Pressure (MPa)	Expander Outlet Pressure (MPa)	Average Expander Inlet Temperature (^OC)	Expander Outlet Temperature (^OC)	Average Heat Input/side Q_{high} (W)	COP_W
1	208.7	1.276	0.929	41.0	31.9	7596	0.03
2	96.0	1.276	1.01	41.0	36.7	7596	0.01
4	108.6	1.276	1.082	41.0	36.1	7596	0.01
9	105.5	1.276	1.069	41.0	35.8	4956	0.02
10	102.2	1.276	1.075	41.0	35.9	4956	0.02

Table 5-3: Power simulation inputs and results

Figure 5-17, Figure 5-18, Figure 5-19, Figure 5-20, Figure 5-21and Figure 5-22 show the comparison for power (W), average inlet pressure (MPa), average inlet temperature (^OC), average outlet temperature (^OC), reactor heat input (Q_{high}) (W) and COP_W for the five trials under investigation between experimental and simulation results. Appendix 16shows the deviation between the experimental and the simulation results for all the above as presented in Figure 5-17 to Figure 5-22.

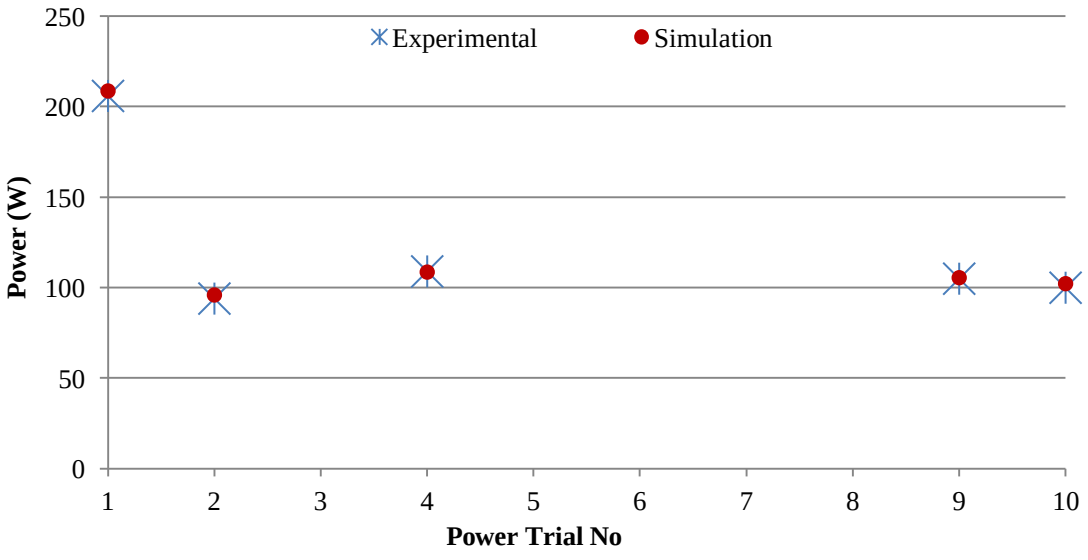

Figure 5-17: Comparison of power: experimental and simulation results

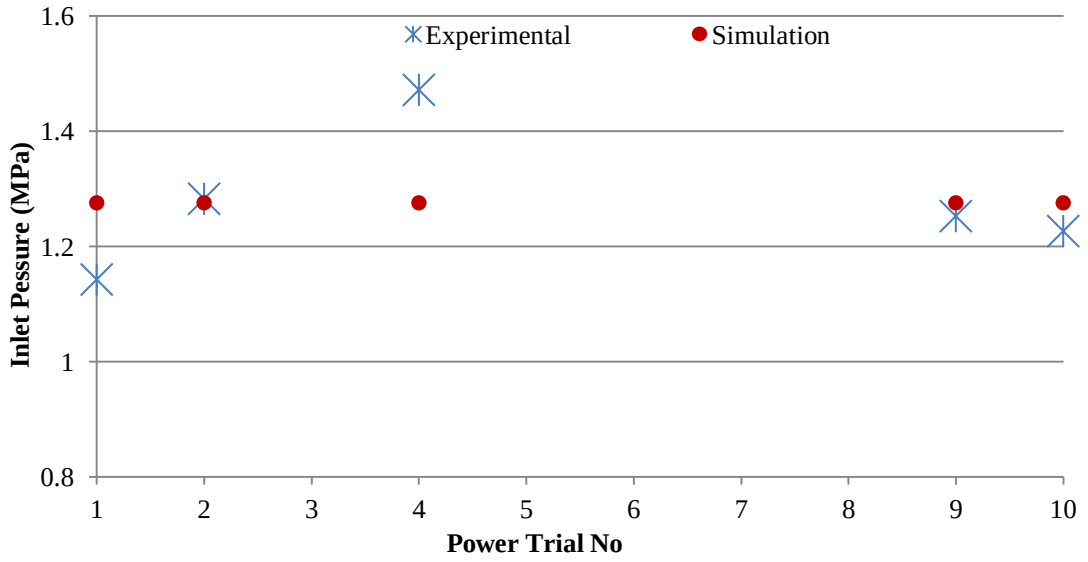

Figure 5-18: Deviation of average expander's inlet pressure: experimental and simulation results

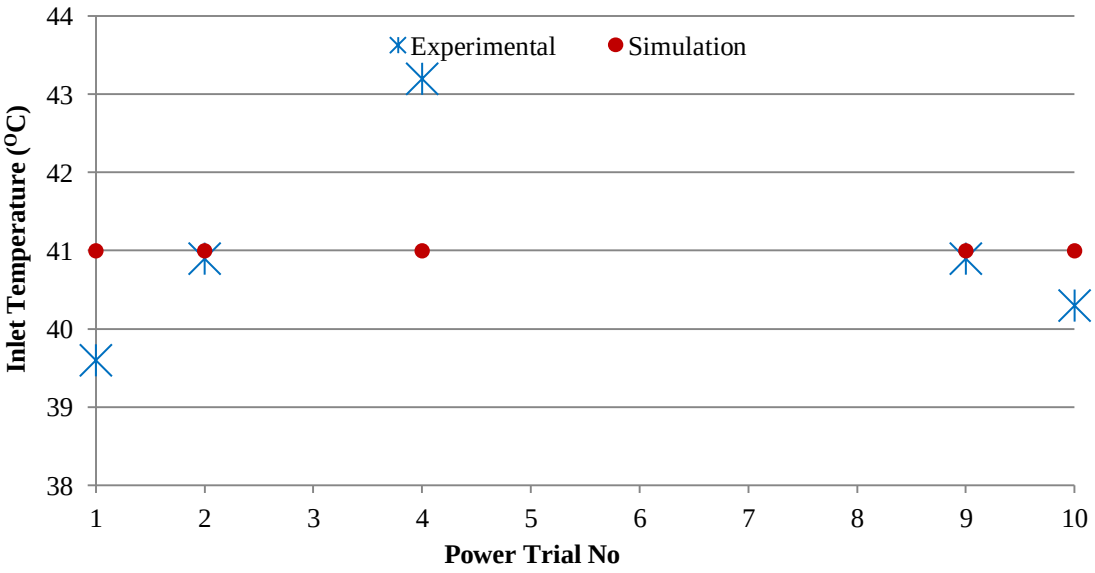

Figure 5-19: Deviation of average expander's inlet temperature: experimental and simulation results

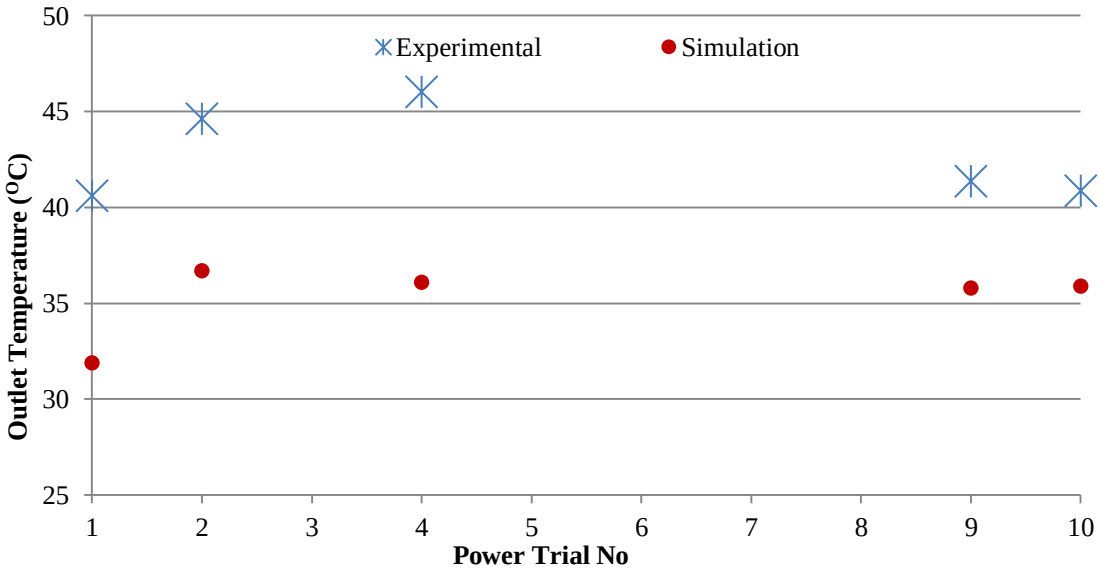

Figure 5-20: Deviation of average outlet temperature: experimental and simulation results

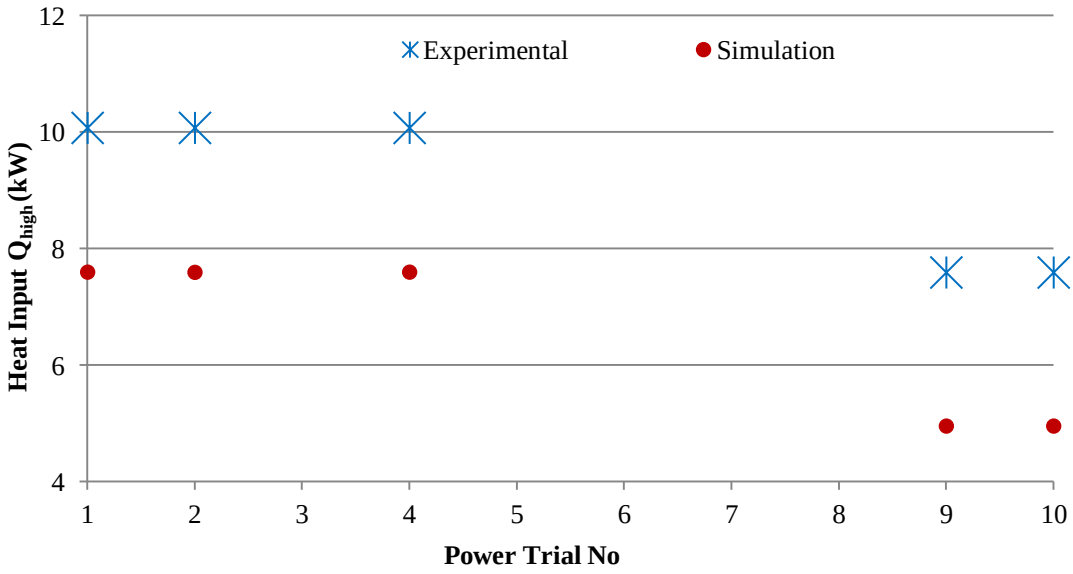

Figure 5-21: Deviation of average heat input (Q_{high}): experimental and simulation results

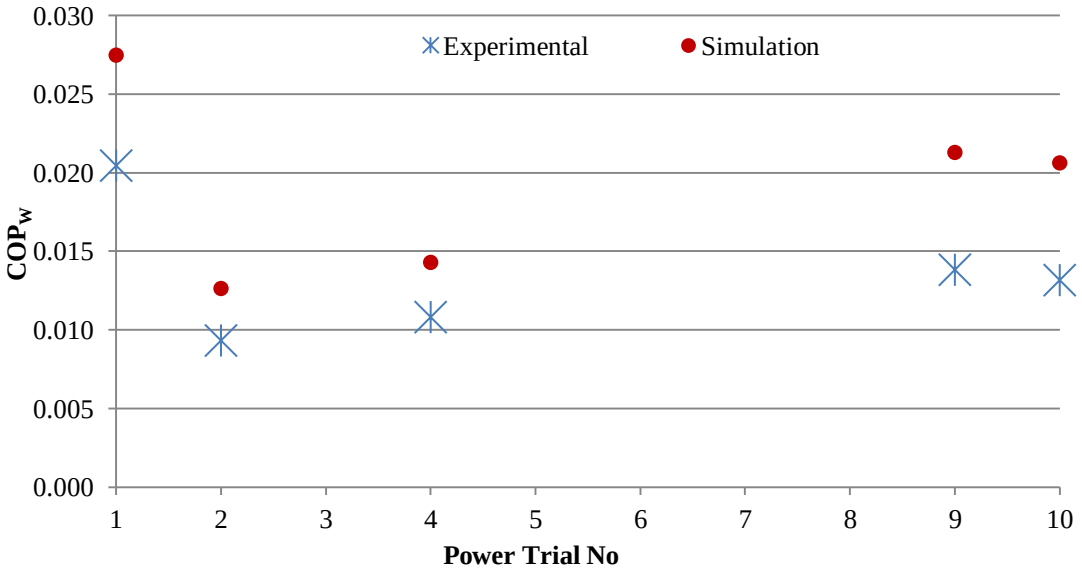

Figure 5-22: Deviation of power generation efficiency (COP_W): experimental and simulation results

By examining the average power production from Figure 5-17 it can be observed that the simulation can match exactly the experimental results. That is confirmed by the deviation of which the biggest one is 2.24% for power trial No. 10 which is a minor difference.

In terms of the expander's inlet pressure from Figure 5-18 and inlet temperature from Figure 5-19, they suggest that the experimental and simulation results are in between the acceptable deviation limits. The maximum deviation for the inlet pressure is 13.34% for power trial No. 4 and 5.09% for the inlet temperature again for power trial No. 4. For some trials the deviation was expected since the input into the simulation for the inlet pressure and temperature was their average from the experiments.

In terms of the average expander's outlet temperature from Figure 5-20 there is a difference between 9.9 and 5^{O}C. The maximum deviation between the experimental and simulation results is 21.56% for power trial No. 4 and 12.16% for power trial No. 10 which is the minimum. Power trial No. 1 (21.45% deviation) and No. 2 (17.75 deviation) offer the biggest deviations compared to the experimental data. The reason for this gap is the sensible heat losses at the pipeline from the expander's exit to the condensers as explained previously. Therefore, in terms of the expander's outlet temperature, the simulation results are considered more reliable and realistic to provide the ideal expansion temperature outlet to the expander.

In terms of the average heat input from Figure 5-21 there is a big gap between the simulation and experimental results. More specifically, Q_{high} for side 1 is 10070W from experiments and 7596W from the simulation which is a 2474W difference, and a 24.7% deviation. Q_{high} for side 2 is 7590W from experiments and 4956W from the simulation which is a 2634W difference, and a 34.7% deviation.

Literature states that for similar chemisorption cycles (adsorption and resorption), there are significant sensible heat losses related to the adsorbent material and mainly with respect to the reactor material [70, 71]. That effect is more significant for the resorption system. The simulation actually provides the heat input for desorption (reaction enthalpy, ΔH) considering only the energy required for the chemical reaction to take place without taking into account any sensible losses. Based on the theoretical analysis of Charalambous [116], for a resorption system the sensible losses during desorption at the high-temperature salt can be up to 44%. Assuming heat losses of 30% when heating the new Q_{high} for side 1 it becomes 9847.8W and for side 2 6442.5W which means a deviation of 1.94% for side 1 and 15.11% for side 2. This limit is acceptable in case we ignore side 2's heat input during cogeneration experiments which were far away from the average recorded compared to side 1.

The reaction enthalpy provided from side 1 (7596W), is very similar to the one provided by Ph. Touzain [53] which is 39.6kJ/mol. For a 14min cycle time and for 17.5kg $CaCl_2$, this value is 7455.5W.

The heat input obviously affects the power generation efficiency as well (Figure 5-22) since it is a measure of the power production over the heat input. The deviation for the power generation efficiency is between 32.13% and 56.58%. In case the simulation heat input used is the one with 30% more, then the COP_w deviation for side 1 is no more than 4%.

5.6.1 Influence of expander's outlet pressure

In order to identify the potential of the system one should investigate the influence of the discharge pressure which affects the expander's ΔP_{exp}, the expander's inlet pressure, the expander's inlet temperature and the expander's efficiency to power generation. Before that, the ideal power generation scenario which maximises power production according to the recorded results and the modelling results will be introduced. The data

input on ECLIPSE for the ideal scenario for every power generation trial will produce the same power since they assume all the parameters remain the same for all power trials. The parameters which are changed now from the validation procedure (Table 5-2) are the desorption's high temperature which for both sides is now 133^{O}C and the reactor's temperature when desorption starts is 28^{O}C. The scroll expander's inlet pressure is fixed to 1.38MPa which is the maximum that the selected scroll expander can undertake, the expander's discharge pressure which is fixed to 0.9MP as the minimum system found from the cooling results after the mass recovery process and the flow rates used for $CaCl_2$, NH_3 and $CaCl_2NH_3$ which used the one of side 1.

The first parameter under study is the expander's outlet pressure. A comparison between the power levels produced during the experiments, the ideal case and the ideal case again but this time the expander's exit pressure of each trial is the same as found from the following experiments (Table 5-2). Figure 5-23 compares the power generation of each trial for the above three cases under study. Appendix 17 collects the results for the three cases under study including the power generation (W), the heat input (W), the COP_W and the power increase between them.

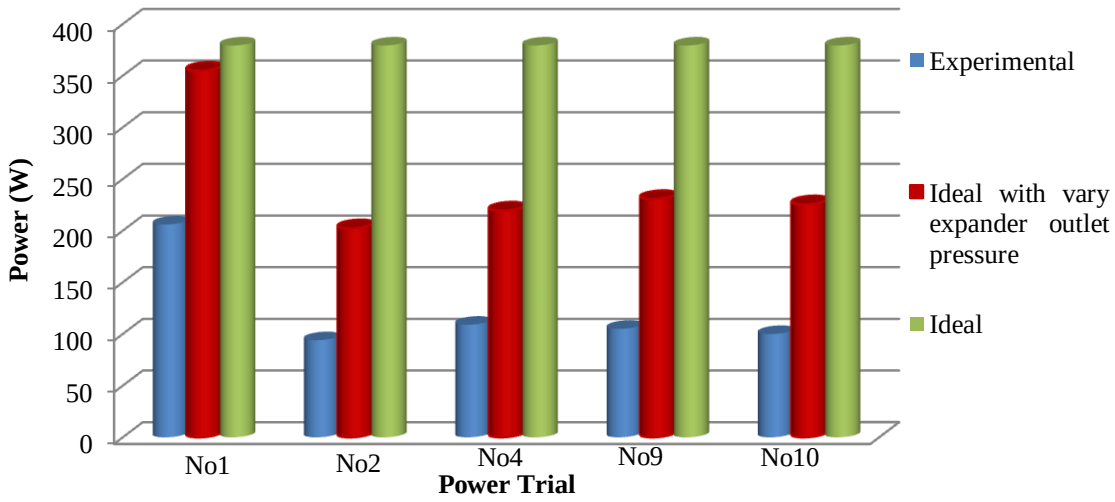

Figure 5-23: Average Power comparison to examine the expander's ΔP_{exp}

Figure 5-23 shows that the average power generation for the ideal scenario is the same for each trial at 379.3W since it assumes similar and repeatable conditions compared to the other two cases. The experiment offers the minimum power production between 206 and 94W and for the ideal case with a varying expander's outlet pressure which is in between 354 and 202W.

Comparing the experimental power output with the varying expander's outlet pressure, the power production's increase can be up to 125% for power trial No. 10. This is a significant increase, assuming that the expander's outlet pressure are kept the same as the experiments, but the rest of the parameters assume the ideal scenario. Comparing the experimental power output to the ideal scenario, the power production increase can be up to 303% for power trial No. 2. That shows a tremendous potential for a power production increase. Comparing the ideal scenario to the one with a varying expander's outlet pressure, the power production increase can be up to 87% for power trial No. 2. The range of the power increase is between 6.9% for power trial No. 1 and the rest of the trials have an increase of 65% and more. Those two cases under study prove the significance of the expander's outlet pressure to the power generation production.

In terms of the power generation's efficiency, for the heat of desorption it requires a Q_{high} simulation (note the same values for the two ideal scenarios). Therefore, the COP_W is a measure of the power production. For the ideal case reported the COP_w is 0.07, and for the varying expander's outlet pressure scenario is in between 0.04 and 0.06. The experimental COP_W is much lower: between 0.01 and 0.02. In the case when the power production was 1000W the power generation efficiency will be 0.18 based on the ideal scenario.

Table 5-4 compares the average expander's outlet pressure (MPa) and the average power production (W) for the ideal scenario and the ideal with a varying expander's outlet pressure added.

	Power Trial No	Average Expander Outlet Pressure (MPa)	Average Expander Outlet Pressure Decrease %	Average Power Difference (W)	Power Increase %
	1	0.026	-2.8	24.3	6.9
	2	0.204	-18.5	176.9	87.4
	4	0.182	-16.9	159.8	72.8
	9	0.169	-15.8	148.6	64.4
	10	0.175	-16.3	153.7	68.2
AVERAGE		**0.151**	**-14.1**	**132.7**	**59.9**

Table 5-4: Average expander's outlet pressure and average power production comparison for the two ideal scenarios

The average percentage power increase of the ideal scenario for the five power trials is 132.7W which means a 59.9% power production increase on average. These numbers consider a 0.151MPa (14.1%) decrease on average for the 5 power trials for the expander's outlet pressure. For power trial No. 1, the expander's outlet pressure difference was the minimum when comparing the two ideal scenarios (0.026MPa, 2.8% difference), therefore the power increase was only 24.3W (6.9%). For the power trial No. 2, the expander's outlet pressure was the maximum compared to the ideal case (182.7kPa, 16.9% difference) and the power increase was 176.9W (87.4%).

Table 5-4 shows a significant power increase with a small decrease in the expander's outlet pressure assuming the rest of the parameters are constant. For cogeneration, it is important the expander's outlet pressure at the high pressure evaporator-condenser remains as low as possible since it is proven to produce more power.

The salt selection is important for the system's power performance since it can define the low pressure on the low-pressure side assuming similar heat sources. The most preferable is to avoid the use of the mass recovery valve and ensure low pressure at the expander's outlet when using the condenser. From the above analysis, there is a significant potential to extract more power generation in case we keep the expander's outlet pressure as low as possible.

5.6.2 Influence of expander's efficiency

In order to identify the influence of the expander's efficiency on the power production, the ideal scenario will be used by assuming a different expander efficiency. The expander efficiency used was 14.713 but for this analysis, four more will be used: 7.356; 29.427; 36.786; and 44.140. The selected scroll efficiency increases respectively by 7.356, which is half of the 14.713.

Figure 5-24 presents the power generation for varying the expander's efficiency. Appendix 18 presents the overall results for the ideal scenario when varying the expander's efficiency. It includes the average expander's inlet and outlet temperatures (^{O}C), the expander's efficiency and the average power production (W).

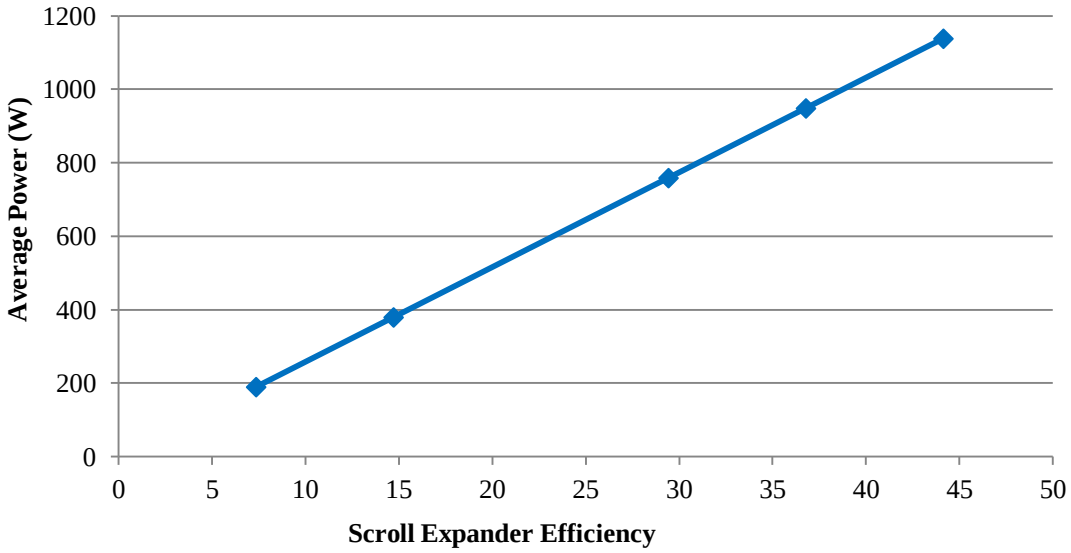

Figure 5-24: Power generation of the ideal case with varying expander efficiencies

From Figure 5-24 it can be observed that the power generation is increased proportionally to the expander's efficiency increase. The power output for a 7.356 expander efficiency is 189.6W and for 14.713 it is double (379.3). Every time the expander's efficiency increases by 7.356, the power production is increased by 189.6W.

The power production for a 44.14 expander efficiency is 1137.7W. Founding shows that the expander's efficiency is a very important parameter to increase the power production, and the selection of the appropriate expander device becomes crucial. In reality the scroll expander's efficiency is not just a number but related to its design and the specifications of the device and to losses. In any case, selecting better performing equipment that matches the operating conditions and the refrigerant's properties will result in a power generation increase.

In terms of the expander's outlet temperature, it can be concluded that there is a small decrease as the expander's efficiency increases, which is not proportional to the enormous power increase. That can be translated as the selected expander running with ammonia under these conditions, the inlet pressure is more critical rather the inlet temperature for a fixed expander's outlet pressure. Obviously, that response can be related to the ammonia's quantity flow to the expander which could be much lower than the expander's optimum points.

In terms of the power generation efficiency for varying the scroll expander's efficiency, Figure 5-25 will be used which indicates how the power generation's efficiency changes with the scroll expander's efficiency.

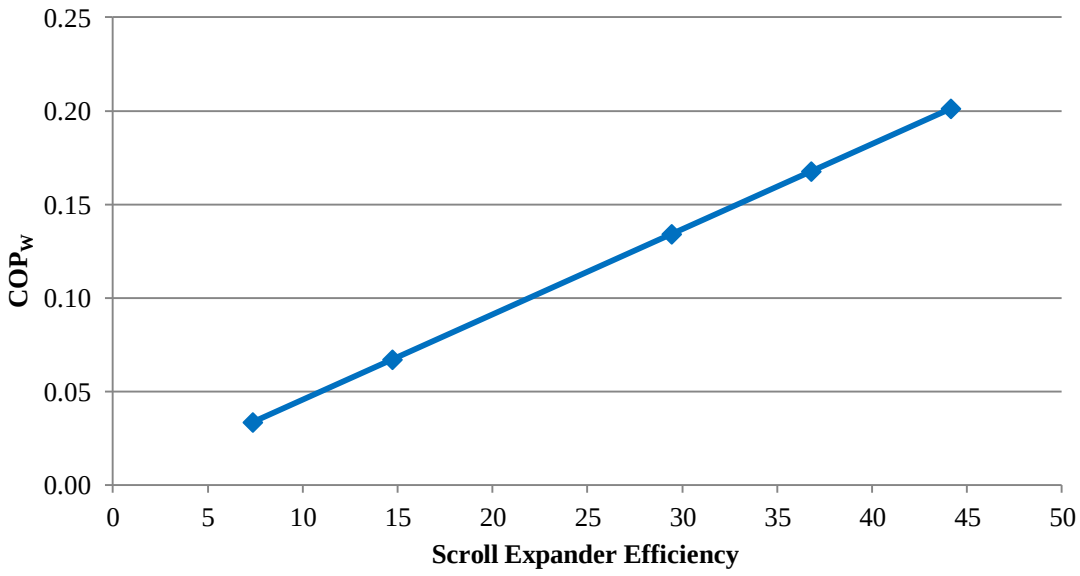

Figure 5-25: Power generation efficiency (COP_W) for varying expander efficiencies

Figure 5-25 shows that the power generation's efficiency increases proportionally with the scroll expander's efficiency increase having an actual response in Figure 5-24. That was expected since the desorption energy (Q_{high}) remains the same for each trial and the power increases proportionally. The COP_W for a 7.356 expander efficiency is 0.03 and for 44.14 is 0.2 which is an increase of 666.7%.

5.6.3 Influence of expander's inlet pressure

The procedure to examine the expander's inlet pressure influence to the power production considers six cases by using the ideal and varying the expander's inlet pressure by 0.2MPa at each trial, from 1MPa to 2MPa.

The reason the maximum of 2MPa was chosen as the maximum pressure is because when the machine is running in cooling mode and carrying 28kg of ammonia, the maximum pressure can reach approximately $135^{O}C$ in the vapour reactor's temperature. Another reason is that the 2MPa is the operational pressure limit for our test rig. From cooling results, when a new cycle starts after mass recovery, the pressure at the reactor is approximately 0.9MPa. From that point the reactor increases its pressure and it seems

that desorption starts at round 1.2MPa. Therefore, the pressure range selected for this analysis is realistic.

Figure 5-26 presents the power production for the ideal scenario by assuming variations in the expander's inlet pressure. The 1.4MPa point is the closest to the ideal case where the inlet pressure was 1.38MPa. Appendix 19 shows the overall results of the ideal scenario when assuming a varying average expander's inlet pressure. The results include the expander's inlet and outlet temperatures (^{O}C), the heat input (W) and the power generation's efficiency (COP_w).

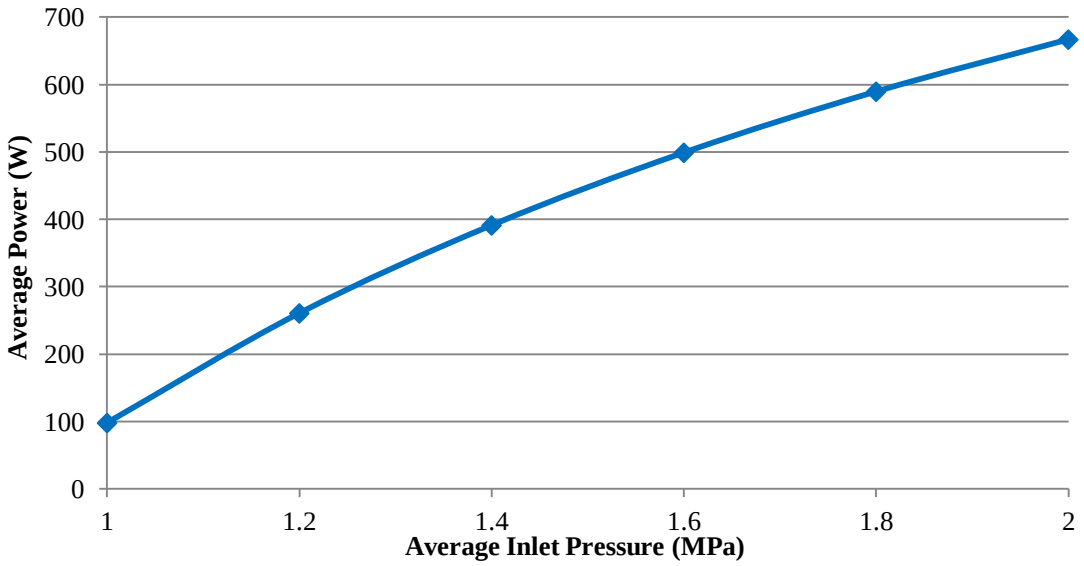

Figure 5-26: Average power generation for varying average expander's inlet pressures

Figure 5-26 suggests that any increase in the expander's inlet pressure results in an almost linear power increase. That means in the real system, it is important to provide the expander with a refrigerant with as high a pressure as possible and make sure the reactor contains enough ammonia during the power generation. Also, it is important the selected expansion device can deal with this much high pressure.

The 1MPa case results in 98W average power production and the 1.2MPa 260.6W. The ideal case assumes 1.38MPa inlet pressure which provides similar results to 1.4MPa (391.1W). For the 1.6MPa inlet pressure which is the average for the system when carrying 24kg of ammonia, the power production is 498.9W which means a 27% power increase compared to the 1.4MPa case. For the 2MPa trial, the average power is 666.8W, which means approximately a 70% increase from the ideal case. That indicated

a potential for more power generation in the case of a 2MPa refrigerant pressure when driven in the expander. These conditions cannot be repeated for the real system in use continuously since the desorption process starts at low pressure and develops high pressure later in the cycle. In terms of the flow rate in the early stages of desorption it reaches a peak and is then decreased. It should be an experimental investigation when varying the system's ammonia quantities to find the optimum between the inlet pressure and the flow rate.

The simulation shows 98W average power even when the inlet pressure is 1MPa for 0.9MPa expander's outlet pressure. That finding is important since even when the inlet pressure is very close to the expander's outlet pressure (0.9MPa), power can be produced. This is not the case for the real system because at that low-desorption pressure, the desorption rate is very low since it is away from the optimum pressure's desorption window. The simulation shows that a combination of high inlet pressure with as constant as possible an outlet pressure is necessary for high power production. For the real system the optimum average inlet pressure is between 1.5 and 2MPa when the system carries 24-28kg of ammonia.

In terms of the power generation's efficiency for varying inlet pressures, Figure 5-27 will be used which indicates how the power generation efficiency changes with the scroll expander's efficiency.

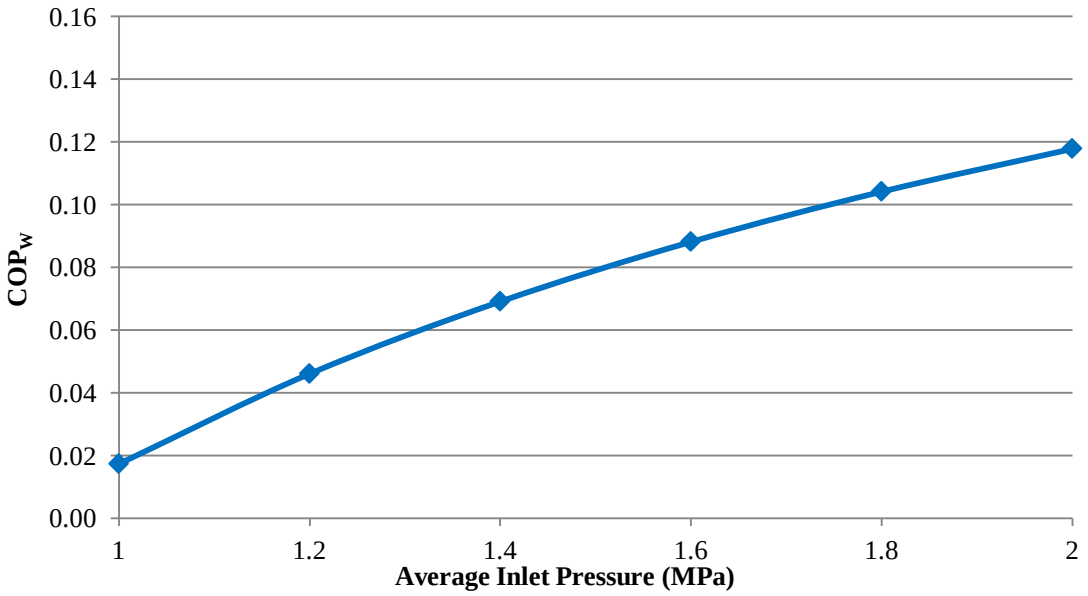

Figure 5-27: Power generation efficiency (COP_W) for varying expander's inlet pressures

Figure 5-27 shows that the COP_W increases as the expander's inlet pressure increases, and there is a similar response in Figure 5-26. That was expected since desorption heat requires Q_{high} which is the same for all the trials and the power production increases with the inlet pressure's increase. The power generation's efficiency increases by 1.6MPa and 2MPa compared to the 1.4MPa case which is 28% and 71% respectively.

In terms of the expander's outlet temperature for the same inlet temperature, as the expander's inlet pressure increases that is decreased. It was the expected response since as the pressure increases the expansion efficiency also increases and that also has an effect on the outlet's temperature. The decrease might not be significant from trial to trial but there is a decrease. Again the simulation's results show that for this selected expander for the running flow rate, the power production mainly depends on the inlet pressure rather the inlet temperature.

5.6.4 Influence of expander's inlet temperature

The procedure to examine the expander's inlet temperature influence is to consider eight cases of the ideal scenario by using as the inlet temperature ranges from 41 to 145^{O}C. The reason that the range of these temperatures is selected is because 41^{O}C is the maximum refrigerant temperature into the expander during cogeneration experiments and 145^{O}C is the maximum temperature the boiler temperature is set up at during only-cooling experiments. Figure 5-28 shows the power production for varying the expander's inlet temperature. Appendix 20 provides the overall results of the ideal scenario when assuming varying the average expander's inlet temperature for which results include the expander's inlet and outlet temperatures (^{O}C), the heat input Q_{high} (W) and the power generation's efficiency (COP_W).

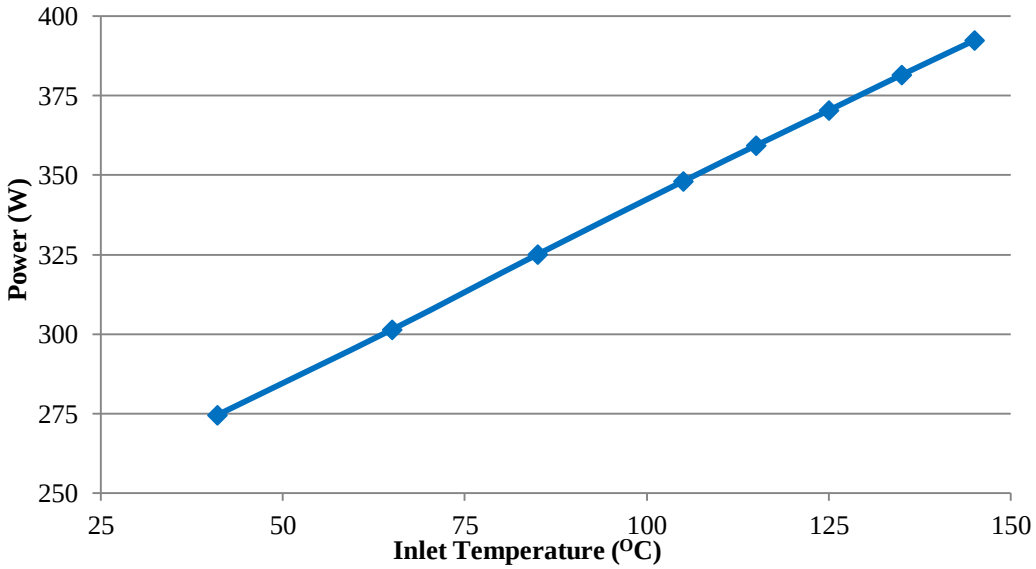

Figure 5-28: Power generation of the ideal case for varying expander's inlet temperatures

From Figure 5-28 it could be noticed that the increase in the refrigerant's temperature results in the linear increase of the power production. That tendency remains the same since simulation results up to 205^{O}C show the same response.

The 145^{O}C compares to the 41^{O}C and results in a 43% average power production increase which shows a potential in terms of the refrigerant's expander inlet temperature. That means it should make it possible to feed the expander with as high as possible a temperature refrigerant. For the LH cogen system, a theoretical ammonia temperature in the expander between 125 and 135^{O}C is possible based on the cooling experiments but a more likely range is 80-95^{O}C as the desorbed gas temperature is more realistic.

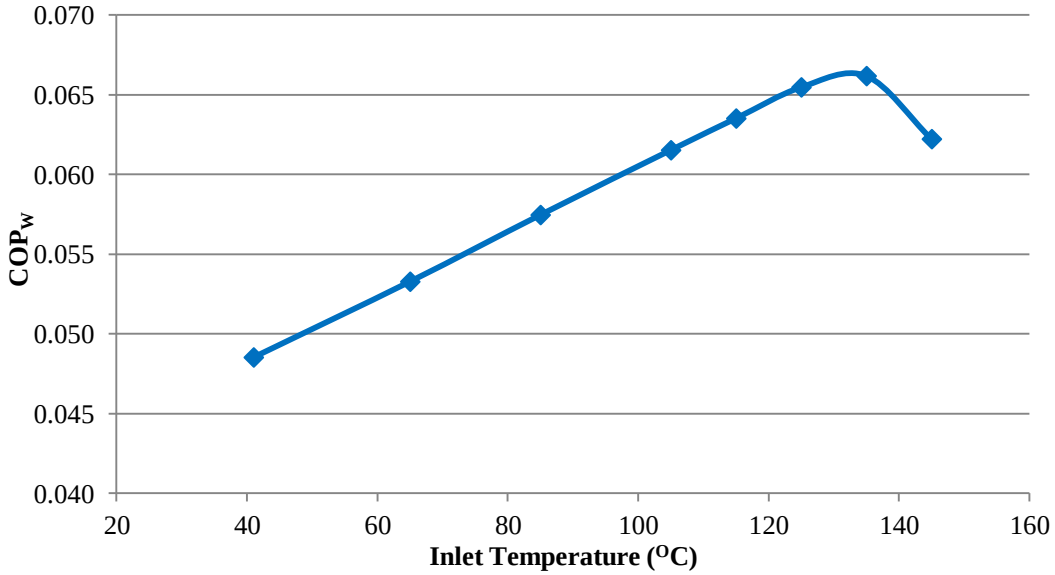

Figure 5-29: Power generation efficiency (COP_W) for varying expander's inlet temperatures

In terms of the power generation efficiency for varying the inlet pressure, Figure 5-29 indicates how the power generation efficiency changes for varying the expander's inlet temperature. Figure 5-29 shows that the power generation's efficiency increases proportionally to the expander's inlet temperature until the temperature of 135^{O}C and then drops even as the power production increases for every increase of the inlet temperature above 145^{O}C. That has to do with the desorption heat (Q_{high}) that is provided by the simulation which for all trials between 41^{O}C and 125^{O}C is the same, but for the 135^{O}C and 145^{O}C trials is more. The reason is that for the 41^{O}C and 125^{O}C trials, the reactor's set-up temperature which defines the desorption heat as fixed at 133^{O}C, similar to the ideal case. For the 135^{O}C and 145^{O}C trials, the reactor's set-up temperature was 135^{O}C and 145^{O}C respectively. The reason that that approach was followed is because desorption cannot appear efficiently at low temperatures (41^{O}C and 105^{O}C), therefore it was decided that the 133^{O}C heating temperature was to stay constant until the 125^{O}C trial. The reason for the decrease is that the rate of power production increase for any temperature increase above 145^{O}C is lower compared to the reactor's heat requirements.

In terms of the expander's inlet temperature, the 135^{O}C level maximises the power generation. Figure 5-29 agrees with the cooling results found where, for higher desorption temperatures than 128^{O}C, the system's cooling performance decreases.

5.7 Power results comparison for experimental and simulation data

The experimental power generation results prove that the parameters that affect the LH cogen power generation are the expander's inlet pressure and temperature, refrigerant flow rate, the scroll expander's ΔP_{exp} as well as the expander's efficiency. Since not many experimental results were collected, the simulation results were validated using the experimental data in order later the system to examine further for its power performance. Simulation was used to identify how the power production was affected by the expander's output pressure as well as the ΔP_{exp}, the expander's efficiency, the inlet pressure and the inlet temperature.

In terms of ΔP_{exp}, the expander's efficiency and expander's inlet pressure were proved to have significant effects and should be kept at maximum and be repeatable to maximise power. The expander's inlet temperature shows a smaller influence compared to the other parameters and that could mean that the selected expander's efficiency is mainly related to the pressure rather than temperature based on the running conditions. Also it means the selected expander for the operating flow rates is out of range (oversized) and that could be explained from the small temperature decrease at the expander's exit compared to the inlet temperature even as the power increases.

The experimental results confirm the theory regarding the ΔP_{exp}, flow rate and inlet pressure on how they affect the system's power performance. Simulation proves the importance of the scroll expander's efficiency or any other selected expansion device and the temperature input also. In terms of the flow rate, not many data were collected during cogeneration experiments but when using the simulation and assuming the side 2 flow rate is similar to side 1 and keeping all the other parameters the same, there is a power increase around 11% as proven from Table 5-5. Table 5-5 shows the percentage power increase on side 2 when the side 1 flow rate is used in assuming the ideal scenario with a maximum inlet pressure of 1.276MPa and varying the expander's outlet pressure.

Power Trial No.	**Power For varying Flow Rate (W)**	**NH_3 Flow Rate (kg/s)**	**Power For Maximum Flow Rate (W)**	**NH_3 flow rate (kg/s)**	**% Power Increase**
1	288.5	0.0343	288.5	0.0343	0
2	132.8	0.0343	132.8	0.0343	0

4	150.4	0.0343	150.4	0.0343	0
9	146.2	0.0310	161.7	0.0343	10.6
10	141.3	0.0310	156.8	0.0343	11.0

Table 5-5: Power comparison for different flow rates

The importance of the flow rate and the expander's outlet temperature is proven from the simulation's expander test by using nitrogen where we could achieve very low temperatures for the same expander's outlet pressure. The flow rate was increased when the inlet pressure increased, so resulting in a lower expander's outlet temperature for a similar expander's outlet pressure. For the LH cogen system, by using the experimental and the simulation results it seems that the flow rate of the power generation process is lower than the scroll expander's optimum point resulting in a high refrigerant expander's temperature. The desorption flow rate is less than the recorded one. With a power trial when v8 was always open and the desorption flow rate was used to rotate the expander, the power recorded was poor and used only once. Later no power was recorded.

From the experimental results it can be said that the lack of a sufficient quantity of ammonia and the low refrigerant expander's inlet temperature are the main reasons for the non-uniform power production. The simulation provides an ideal power production scenario in the case when all the parameters stay constant. In reality, this is not realistic since the high pressure and temperature and the flow vary during the cycle. The average values for the selected power trials were used in the simulation flow rate but we have in mind that more power was needed with a lower than 100W average power. Maybe the power trial should be limited to four per cycle and decrease also the cycle time.

During the experiments, the use of the mass recovery valve (which is not taken into consideration from the simulation) leads to dry out the high-pressure reactor a few times after it is used. The use of an expansion device that could produce power from the desorption flow rate by eliminating the v8 valve is necessary. Like that, it is possible to extract more uniform power for a longer period. At the same time, the mass recovery valve could be used only if required. Even like that, the refrigerant's desorption flow rate will decline during the process, therefore the adsorbent's adsorption capacity should be increased in order for more ammonia to be available. Also, the significant system heat losses identified during the experiments should be considered.

The ideal simulation scenario is a good tool to show the direction in which a new system should be designed in order to maximise power production for repeatable cycles. At the moment there is an effort to increase the adsorbent's adsorption capacity but in terms of the expander's specification, we could do much better by selecting a more suitable one.

5.8 Cogeneration results comparison

Now we are ready to bring the cooling and power results together in order to identify the system's cogeneration performance COP_{cogen}. The COP_{cogen} is the sum of the COP_{ref} and COP_W similar to Equation 5.2.

$$\mathbf{COP_{cogen}=COP_{ref}+COP_W} \qquad \mathbf{5\text{-}2}$$

The analysis will initially compare the experimental and validated results and, later, the cogeneration system's performance will be compared, assuming the ideal power scenario as well as for every scenario examined the power generation parameter under study together with the best refrigeration simulation result. Figure 5-30 presents the system's COP_{ref} for two experimental scenarios of 24kg and 28kg of ammonia and the simulations.

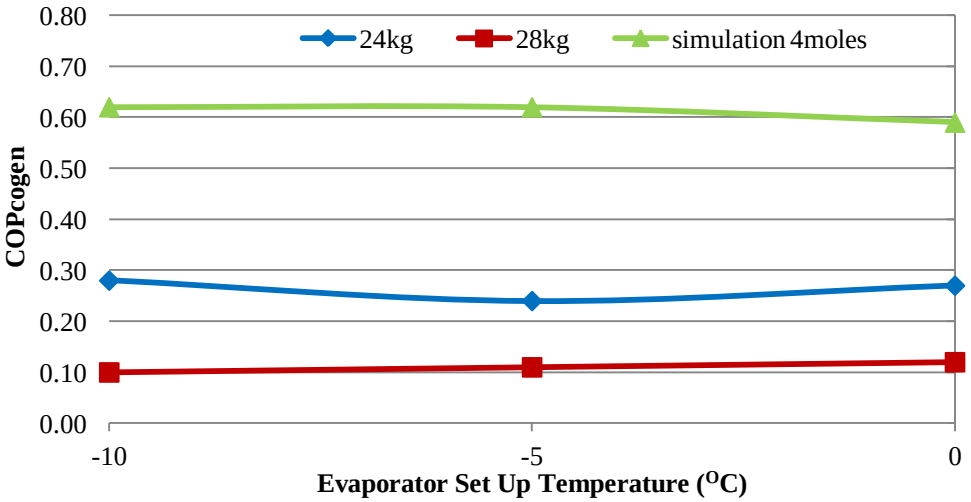

Figure 5-30: Combined cogeneration results from experiment and simulation

Appendix 21 shows the collected cogeneration system's performance based on the experimental results. In terms of cooling, the max COP_{ref} for 24 and 28kg ammonia for 0, -5 and -10^{O}C set-up evaporator temperatures using the maximum COP_{ref} for each case and the maximum COP_W, the one from power trial No. 1. Appendix 22 shows the

collected cogeneration results taken from the simulation. It was used with the maximum COP_{ref} found for 0, -5 and -10^{O}C set-up evaporator temperatures and the maximum plus the maximum value for the COP_W which is the one for power trial No. 1.

Figure 5-30 indicates that the COP_{cogen} is almost constant for any evaporator set-up temperature. The results show that the COP_{cogen} mainly depends on the COP_{ref} which is higher compared to the COP_w for both experimental and simulation results.

For the comparison between the two experimental results, the COP_{cogen} for 24kg is higher. More specifically, the COP_{cogen} for 24kg of NH_3 is between 0.24 and 0.28 and where the COP_{ref} varies from 0.22 to 0.25 for a constant 0.2 COP_W. For 28kg of ammonia, the COP_{cogen} varies in between 0.08 and 0.1 where the COP_{ref} varies from 0.22 to 0.25 for a constant 0.2 COP_W. Assuming average values, when the COP_{cogen} switches the system from 28kg to 24kg of ammonia, the COP_{cogen} increases 139.4%. The reason for this response is explained in the previous section and related to the COP_{ref} of the 24kg trials that was more assuming a similar COP_W.

In more detail the COP_{ref} for 24kg is the 92.4% of the COP_{cogen} and the COP_W the rest of 7.6%. At the same time, the COP_{ref} for 24kg is the 81.8% of the COP_{cogen} and the COP_W the rest of 18.2%. These numbers mean the COP_{cogen} is mainly related to the refrigeration system's performance rather the power. For 1000W power production and Q_{high} 10070W, the maximum COP_W for the machine is 0.1.

Comparing the ECLIPSE validated results with the experimental results, it is clear that the simulation provides higher COP_{cogen} efficiency than the experiments. The range of the COP_{cogen} for the simulation is between 0.59 and 0.62. More specifically, compared to the 28kg case an increase of 454.5% is noticed and 131.6% compared to the 24kg case. The experimental and simulation maximum COP_W values were similar (0.02 for the experimental process and 0.03 for the simulation) therefore the COP_{ref} is the difference which is related to desorption Q_{high} given from ECLIPSE which is less compared to the experimental process.

The simulation will be used to investigate the cogeneration system's performance for varying the expander's efficiency, inlet pressure and temperature and how these

parameters affect the cogeneration system's performance. For this analysis, the COP_{ref} from the simulation will have a fixed value of 0.58 which is the average for the $0^{O}C$, $-5^{O}C$ and $-10^{O}C$ evaporator set-up temperatures from the validated cooling results. Then the COP_{cogen} will be found by adding the COP_{W} as found for any parameter under study.

Table 5-6 shows the COP_{cogen} for the ideal power case. Appendix 23 presents the COP_{cogen} for varying the expander's efficiency, Appendix 24 for varying the expander's inlet pressure and Appendix 25 for varying the inlet temperature. The COP_{cogen} for the ideal scenario is 0.65. This number is the baseline for investigating the system's cogeneration reaction when varying further the parameters under study.

Average COP_{ref}	COP_{W} Ideal scenario	COP_{cogen}
0.58	0.07	0.65

Table 5-6: Ideal case COP_{cogen} from simulation

Figure 5-31 presents the COP_{ref}, COP_{W} and COP_{cogen} for different expander efficiencies, Figure 5-32 presents the COP_{ref}, COP_{W} and COP_{cogen} for different expander inlet pressures and Figure 5-33 presents the COP_{ref}, COP_{W} and COP_{cogen} for different expander inlet temperatures. Figure 5-32 Figure 5-33 and Figure 5-33 prove graphically that the COP_{cogen} performance is mainly dependent on the COP_{ref} value which is constant and higher compared to COP_{W}.

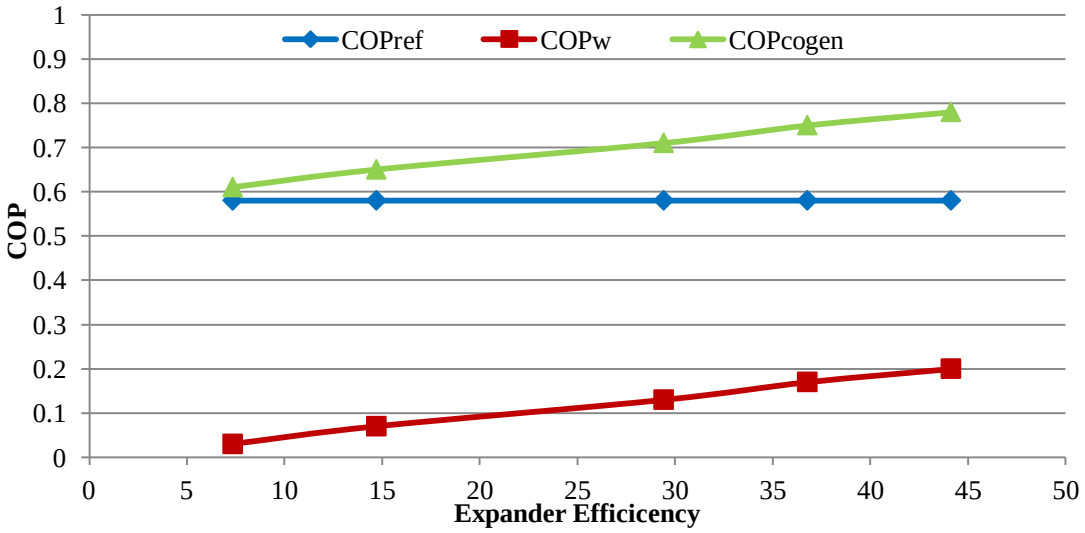

Figure 5-31: COP_{ref}, COP_{W} and COP_{cogen} for different expander efficiencies

By examining the cogeneration performance for varying scroll expander efficiencies from Figure 5-31 we can see that for the ideal case of 14.713 the cogeneration performance is 0.65 compared to 0.78 when the scroll expander's efficiency is the maximum for this set of results at 44.14 it can translate into a 20% COP_{cogen} increase. At the same time the COP_W shows an increase of 185.7% (from 0.2 to 0.07) and it is the COP_w increase which makes the difference in the COP_{cogen} since the COP_{ref} has a fixed value of 0.56.

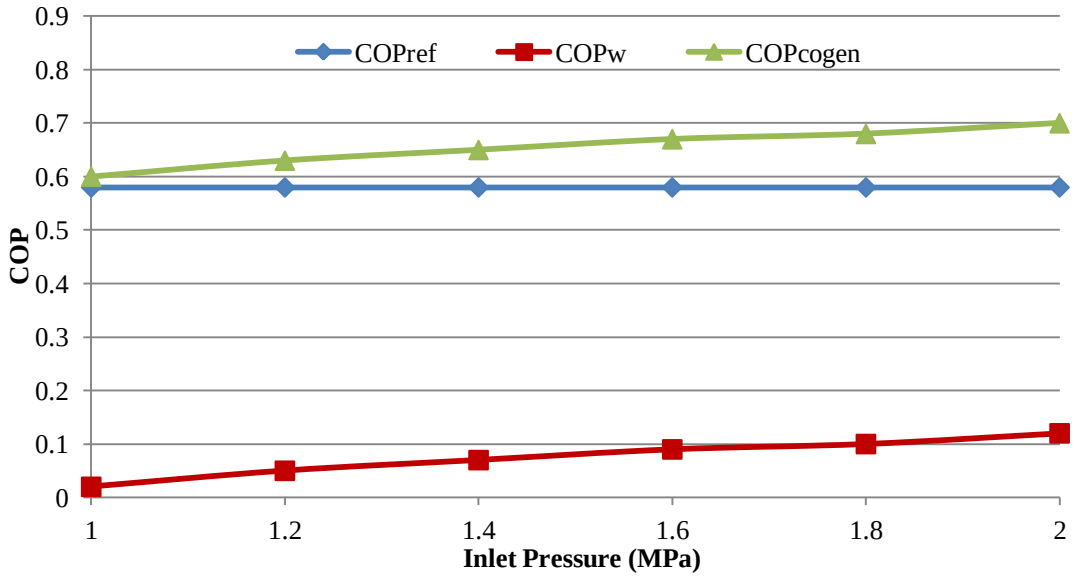

Figure 5-32: COP_{ref}, COP_W and COP_{cogen} for different inlet pressures

In terms of the inlet pressure investigation from Figure 5-32, the ideal case is at 1.4MPa which provides the same COP_{cogen} as the 1.38MPa expander inlet pressure's ideal scenario. Increasing the pressure to 2MPa, which is the maximum the system reaches during desorption, the COP_{cogen} is increased to 0.7, i.e. a 7.7% increase. The COP_{ref} increases only 0.1 (0.6-0.7) from 1MPa to 2MPa.

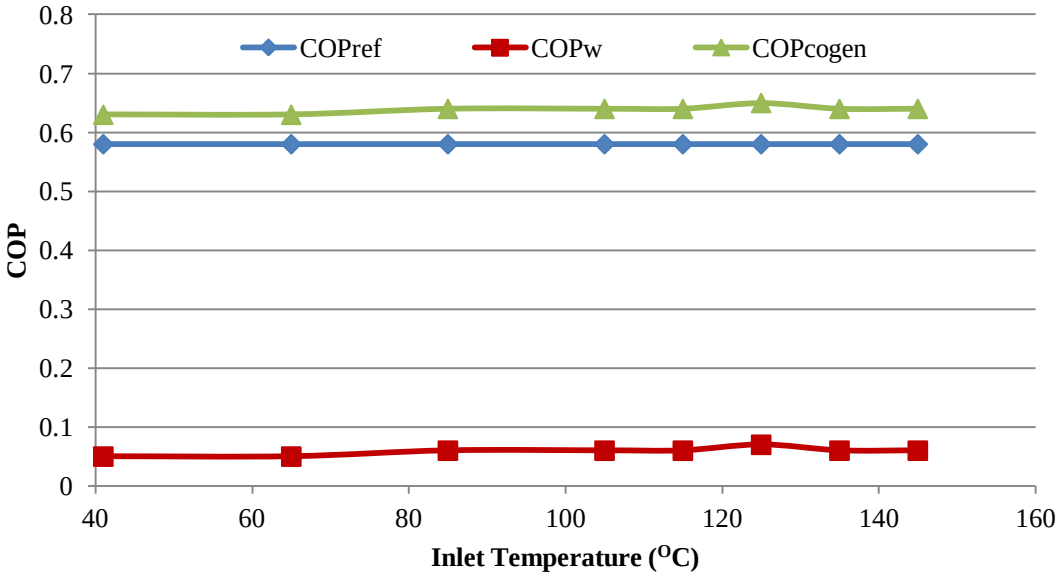

Figure 5-33: COP_{ref}, COP_{W} and COP_{cogen} for different inlet temperatures

In terms of the inlet temperature investigation from Figure 5-33 the ideal case is the one closest to 135^{O}C which results in 0.64 COP_{cogen} compared to 0.65 of the ideal case. Between the ideal and the 41^{O}C case (0.63 COP_{cogen}) which is the average of the expander inlet during the experiments, the COP_{cogen} increases by only 1.59%.

The results show that after the 133^{O}C temperature, the COP_{cogen} starts to decrease because the simulation shows an increase of the Q_{high} for the same Q_{ref}. In a real system the heat's inlet temperature also affects the lower pressure so the cooling effect, but this cannot be identified from the simulation. Desorption starts at around 115^{O}C and goes up to 145^{O}C for the inlet temperature's COP_{cogen} which is stable and does not actually vary. From Figure 5-33 it can be said that for this selected scroll expander, the COP_{cogen} is mainly related to the inlet pressure rather than the inlet temperature under those conditions.

From Figure 5-32 Figure 5-33 and Figure 5-33 it can be concluded that the system's COP_{cogen} mainly depends on the inlet pressure and the expander's efficiency rather than the inlet temperature based on the selected scroll expander. The expander's efficiency is related to the flow rate and how that matches the expander's specification. Also, it depends on losses and the working refrigerant. The inlet temperature looks to have the smaller effect but still needs to carry as much energy in the expander (temperature and pressure) to ensure maximum power production.

5.9 LH cogen system's optimisation

Since the analysis for the LH cogen system performance is finished, it is time to find the optimum conditions that the system's performance needs to maximise its cogeneration performance. The answer to that will come from the experimental and the simulation results. The optimisation includes mainly the optimum scroll expander's working conditions which will help to select the correct expander size. That will result in extracting as much power to maximise the system's power, so the cogeneration performance. The idea is to run the LH cogen system in cogeneration mode without the use of v8 and the mass recovery valve which means the refrigeration performance will be similar to the only-cooling mode.

The procedure followed for cogeneration with the use of the mass recovery valve results in the refrigeration effect decreasing dramatically compared to the only-cooling mode. In the case when no use of the mass recovery valve is required for the power production, then the refrigeration performance of the system during cogeneration will be similar to the only-cooling mode.

For 24kg ammonia, the machine's cooling performance is the highest recorded but the cogeneration test under 28kg is based on the fact more refrigerant will be available for desorption and that will increase the power production. Since no power trial will take place for 24kg, we cannot be sure which ammonia quantity will maximise the cogeneration system's performance. What it is known for sure is that, at the early stages of desorption, the desorption rate is high, reaches a maximum and afterwards decreases. The power trial No. 4 is the last power trial with a high power production from side 1, at around 8min cycle time. Similarly, when the reactor is undercooling, the cycle stops producing any useful cooling at around 12min cycle time. For $-5^{O}C$ evaporator set-up temperature and 24kg of ammonia, this time is around 9min. Therefore the 14min cycle time for cogeneration maybe is a lot. A cycle around 10min sounds more promising in case the system runs with 24kg of ammonia or more. An experimental investigation can justify the optimum cogeneration cycle time.

The cooling approach of the machine during cogeneration is limited from the mass recovery valve's use. In case there can be avoided the use of the mass recovery valve,

then the system refrigeration's performance during cogeneration will be similar to the only-cooling experiments according to the overall system ammonia.

For the power system generation, the optimum high pressure is related to the overall ammonia quantity in the system. In case the system carries 24kg of ammonia, the average high pressure is around 1.3MPa and the maximum 1.6MPa and for 28kg is 1.6MPa average and 2MPa maximum. The more the ammonia, the higher the inlet pressure, and higher is the power production in theory but at the same time the cooling production is less.

For 28kg of ammonia, the higher pressure is more, but for the 24kg the maximum value could be reached faster but, for the 28kg case, sometimes the pressure increases until the end of the cycle. That might lead to an optimum ammonia system quantity to between 24 and 26kg. Like that, the cooling production will still be high (not as much the 24kg) and the reactor will contain sufficient refrigerant for power production.

The high expander inlet vapour temperature should be around 125-133^{O}C according to the results. In the case of the power production, the recorded expander's inlet temperature during the experiments is much lower than the reactor's inlet vapour temperature and the desorbed gas temperature. That is mainly related to heat losses and temperature differences within the system, also the non-insulated piping ammonia system and the high ammonia specific heat. In case the piping system is well insulated, the refrigerant's temperature into the expander will increase and will be closer to the desorbed gas temperature. The water circuit should also be insulated entirely to reduce heat losses and be as low as possible for the heat sink temperature to be recirculated to the system.

In terms of the power production the expander's outlet pressure is also critical. In case the expander's outlet pressure stays constant and as low as possible without the use of the mass recovery valve, the power generation will be maximised. The expander outlet pressure for this system is defined by the condensation's cooling water temperature and mainly from the low-pressure side when the mass recovery valve is used. Elimination of the mass recovery valve means there should alternatively be found a way to maintain low pressure at the expander's exit. One idea is use a lower condensation temperature.

Figure 5-34 is a typical T-v diagram for ammonia which indicates the condensation pressure for three different temperatures (22^{O}C, 28^{O}C and 34^{O}C) and will be used to explain the importance of the cooling water temperature.

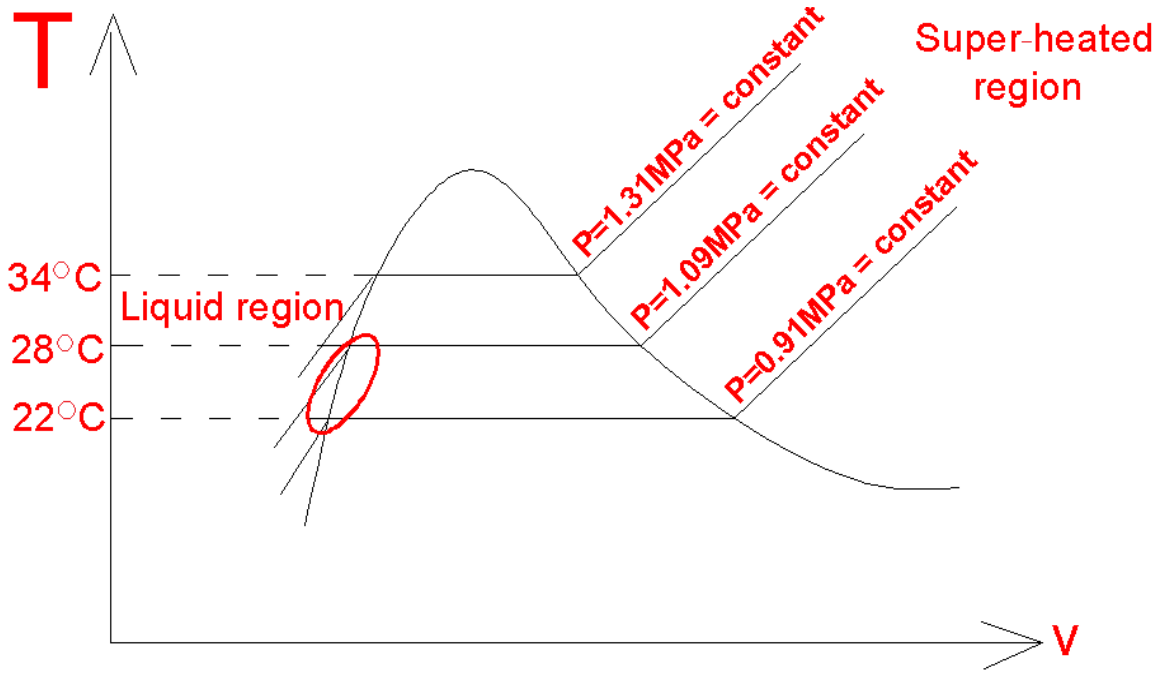

Figure 5-34: Typical T-v diagram for ammonia

Figure 5-34 indicates the pressure at the expander's exit in case the cooling water circuit at the condenser has the indicated values. The condenser is used to condensate (liquefy) the super-heated vapour so leaving the expander as much as possible for the refrigerant after the condenser to be in the liquid form in the liquid region or as much. The red circle at the limit of the liquid region indicates an area which to the left of the line (liquid region) is pure liquid or just to the right is almost all liquid and a small fraction is vapour. The lower the condensation temperature, the lower is the condenser's pressure (so the expander's outlet pressure) and that will help for the refrigerant to be liquefied.

In the report it was mentioned that the condensation temperature during the cogeneration experiments was 34^{O}C and that means the condensate's expanded refrigerant at the condenser would be around 1.31MPa. Having in mind that the average inlet pressure at the expander for the maximum power trials was 1.276MPa, this is a small positive pressure difference across the expander. The smaller the pressure

difference, the lower the power production assuming similar flow rates. The idea is to reduce the condensation temperature to decrease the expander's outlet pressure. The 28^{O}C condensation temperature provides 1.09MPa condenser pressure and for 22^{O}C 0.91MPa. The 28^{O}C water temperature is a realistic temperature in hot humid areas so that a cooling tower provides the cooling water. The 22^{O}C can actually give an expander outlet pressure of around 0.91MPa which is the condition used for the ideal power scenario. Using a cooling tower in a hot humid climate, the 22^{O}C is not realistic but it is using geothermal heat sources.

The average flow rate recorded during cogeneration from the side 1 trials was 0.0343kg/s. This number is recorded when the v8 valve is used because the desorption flow rate was less and unable to rotate the expander. The idea is to eliminate the use of the v8 valve and, in order to do that, the desorption flow rate should be able to drive the expander and produce power. Uzakov A. Kh, et al. [117] found the desorption rate of $CaCl_2$*$8NH_3$ to be about 0.00074-0.0033x10^{-5}kg/s, far less than the power production flow rate recorded. This number proves that the selected scroll expander was oversized but it was the only one available at the time of selection.

The LH cogen system looks more ideal to store the power production in batteries or by using supercapacitors. That is preferable since even the desorbed gas produces power so, without the use of the v8 valve, the power production will not be constant but at least will not have a pulse response.

5.10 Conclusions

In this chapter two models that link together were set up (power and refrigeration) to investigate the performance of the LH cogen system. Experimental data were used as inputs for the models which proved accurate in terms of the average expander's power production (W), refrigeration power (Q_{ref}) and the evaporator's refrigeration temperature (^{O}C). The simulation indicates less Qhigh compared to the experiments because they do not consider any sensible heat losses at the reactor and only consider the temperature before desorption starts as well as the desorption's pressure and temperature. A number of conclusions from the power and refrigeration simulation are summarised below.

a) The cooling part of ECLIPSE has been validated from the experimental results accurately and is now ready for further investigation of the refrigeration cooling performance of this specific test rig.

b) Using data which maximise the power generation from the cooling experiments for 24kg of ammonia to the ECLIPSE, the theoretical power output is 473.65W and the COP_w is 0.08. The ammonia expander outlet temperature is 121^{O}C. This value is lower than the collected power results because the real conditions in and out the expander are not similar.

c) The parameters affecting the system power generation are the pressure at the expander's exit, the expander's efficiency, the inlet pressure, the inlet temperature and the flow rate. The maximum COP_W of the machine is a combination of these parameters.

d) Decreasing the expander's outlet pressure results in a ΔP_{exp} increase so in the expander's power generation. Even for a small increase of 0.2MPa for the ΔP_{exp}, the power can increase around 177W. The ΔP_{exp} should be kept as low as possible by keeping the pressure at the expander's exit as low as possible by assuming that the inlet continues to be more or less the same.

e) The simulation indicates that the power production as well as the COP_W increases proportionally with the expander's efficiency increase. The expander's efficiency was 14.7% which gives 379.3W average power production and 0.07 COP_W. The maximum expander efficiency used was 44.1 which results in 1137.7W average power production and 0.2 COP_W.

f) The power generation of the COP_W increases almost proportionally with the expander's inlet pressure. The power generation, assuming the maximum pressure the selected expander can undertake at 13.8MPa is 391.1W, results in 0.07 COP_W. For the maximum pressure recorded during desorption at 2MPa, the power generation increases to 666.8W and the COP_W to 0.2 which means a 70% increase.

g) The simulation indicates that the inlet pressure has a smaller effect on power production as it increases. The power production increases proportionally with the temperature as it increases up to 135^{O}C. For a 41^{O}C inlet temperature which is the average recorded during the experiments, the power production is 274.5W and the COP_W 0.049. For a 135^{O}C inlet temperature which is the maximum vapour temperature recorded at the reactor's inlet, the power production is

381.5W and the COP_W 0.061. That means for a 229.3% temperature increase the COP_W increases 38.9%.

h) The simulation even accurately calculates the power production (W) and the Q_{ref} did not match the COP_W and the COP_{ref} because ECLIPSE's Q_{high} is less than the experiments.

i) The LH cogen COP_{cogen} performance from ECLIPSE considers the maximum COP_W (0.03) from the simulation results and the average COP_{ref} for 0^OC, -5^OC and -10^OC requiring cooling when the machine carries 24kg of ammonia (0.58) to be 0.61.

j) Assuming the average COP_{ref} of 0.58 for 0^OC, -5^OC and -10^OC require cooling, the COP_{cogen} for 44.14 expander efficiency is 0.78, for 2MPa inlet pressure is 0.7 and for 135^OC inlet temperature is 0.64.

k) From the results it is clear that the LH cogen COP_{cogen} mainly depends on the machine's cooling performance. The maximum COP_W from the simulation assumes 1kW of power is 0.18 for 5665W Q_{high}

Chapter 6. Conclusion and recommendations

The purpose of this study was to investigate the LH cogen system for power and cooling by using low-grade heat. The results from experimental tests and computational simulations showed that the LH Cogen system generated electricity and cooling simultaneously when driven by low-grade heat. Conclusions and recommendations for future work are drawn and presented as follows.

6.1 Conclusions

Chapter 2 presented a literature study covering these aspects: a) cogeneration systems for power and cooling using low-grade heat; b) principles of adsorption; c) chemical and composite adsorbents; d) chemical adsorption cycles and their current application; and e) the scroll expander as media generation media. It was found that the main problem for Kalina and Goswami cogeneration systems which based their working principle on the absorption cycle is the limited cooling effect at the turbine's exit which extracted from the sensible heat. The condensation process for those cycles eventually leads to a lack of the system's refrigeration performance. In order to overcome this issue, based on the background study a chemical adsorption cogeneration system which based its operation on two offset adsorption cycles was designed and constructed. At the same time, compared to the resorption cogeneration cycle the LH cogen system possessed no superheater because the LH cogen system attempts to investigate a lower temperature range. Compared to cogeneration systems that carry an ejector, the proposed cycle is simpler and suggests that it can operate with lower heat sources. The adsorption refrigerator compared to the absorption alone is superior in terms of reliability since it is less complex, has a greater variety of applications and also the cooling and power cycles are separated into different half cycles. The system keeps the basics of the well-known adsorption chiller and improves the condensation process by using the already-installed condensers of the adsorption or the condensation-adsorption process when the two cycles are connected. The result is an improvement in the power generation. This chapter also provide the theoretical background for the adsorption chiller. The experimental apparatus, instrumentation, test plan and procedures are presented in Chapter 3.

Chapter 4 discusses the experimental study when the system was running in only-cooling mode and in cogeneration mode. Also, the scroll expander itself was tested for its power generation performance. Test results have proved that the LH cogen system can produce power and cooling. It might conclude that:

a) During the only-cooling operation of the chiller it was found that the heating temperature, the cycle time and mass recovery time as well as the overall ammonia carried by the system affects the system's performance. For all these there is an optimum point that maximises the refrigeration performance. Also the use of the mass recovery valve was found to have a positive effect on the system's refrigeration performance.

b) The parameters affecting the system's power performance are the inlet pressure and temperature, the pressure at the expander's exit and the flow rate. The power production is based on the mass recovery valve to ensure a sufficiently low pressure at the expander's exit and to the v8 valve to ensure a sufficient ammonia quantity (flow rate) and high pressure at the expander's inlet so releasing the refrigerant when the working conditions allow it.

c) During the cogeneration operation the power production pulses and is not continuous because of the v8 valve used. At the same time, the cooling effect is compromised for the power production and never reaches a performance similar to the only-cooling mode as a result of the mass recovery valve used during the cycle. The cooling performance during cogeneration decreases because a significant amount is transferred to the low-pressure reactor early in the cycle and results in a decrease in adsorption capacity.

d) The refrigerant in the expander had a very low temperature (lower than the desorbed gas temperature and much lower than the vapour entering the reactor) as a result of the sensible losses as a result of the temperature difference in various components from the reactor to the expander's outlet.

e) The selected expander cannot produce power without the use of the v8 valve and this is because it is oversized. That means the desorption flow rate cannot rotate the selected expander. For the selected expander's performance under those experimental conditions and the use of the v8 valve, its performance mainly depends on the inlet pressure, the flow rate and the expander's exit pressure (ΔP_{exp}) rather than the inlet temperature. The selected expander was the one most convenient to buy at the time to run the experiments.

f) The condensation process during cogeneration was considered poor to produce and maintain low pressure at the expander's exit. This is mainly due to the high condensation temperature which results in high pressure at the expander's exit. That results in the pressure difference at the inlet and exit of the expander to be

low. Also, the condensation process performance can be poor because the condensers are designed for the chiller and not for ORC purposes. At the same time, the adsorption-condensation process through the mass recovery valve has a very positive effect on power production.

j) The machine's adsorption cycle 1 and adsorption cycle 2 (side 1 and side 2) do not perform similarly because evidence shows that adsorbent material escapes from the reactors. That results in the adsorption capacity's decrease mainly on side 2.

k) The heat losses for the system can be up to 33% of the overall heat input.

l) When the expander was tested using nitrogen, it was proven that more power could be produced for any increase of inlet pressure and temperature assuming the same outlet pressure. The flow rate is also important for the power production.

In Chapter 5, a model was set up using ECLIPSE software to simulate and predict the system's performance. The cooling model was validated by the cooling experimental results and later was used to predict the system power performance. Later after the power trials, the power simulation was validated from the power experimental results. The simulation can provide the refrigeration capacity (Q_{ref}), average evaporator temperature (^{O}C) and power production (W) very accurately. The simulation also provides the desorption heat (Q_{high}) which is lower than the experiments because it does not take into account any sensible losses. This is the reason why the COP_{ref} and COP_{W} so the COP_{cogen} of the simulation are higher than the experimental data. The ideal power generation using data from the cooling results is lower than in reality because the conditions in the expander are not the same as the reactor.

Because of the experimental lack of power results the modelling was used to explore further the system's power generation. The parameters under study were the expander's efficiency, the expander's inlet pressure and temperature and the expander's pressure at the exit. Also the importance of the flow rate was reported. The power production was increased proportionally to the expander's efficiency. When investigating the inlet pressure, we found that as it increased linearly the power increased linearly as well. There was a similar response in the system when the inlet temperature was investigated. A significant parameter for the system's power production is the pressure at the

expander's exit (ΔP_{exp}). Also, the flow rate is critical which improves the system's power performance as it increases.

6.2 Recommendations for future work

So far, intensive research has been carried out on the LH cogen system. Experimental and simulation results have proven the feasibility of the system running under different working conditions, either in only-cooling or in cogeneration mode. Based on the experience we have gained so far, further investigation should be done without limits in the following aspects.

6.2.1 Expander power test

The test rig to investigate the power generation of the expander using nitrogen was simple when having the expander's output pressure the same. Looking to the future, further improvements are suggested in order to extract more valuable results.

a) *New test rig for desorption flow rate investigation.* Since the working fluid of the LH cogen system is ammonia, there could be designed a small experimental adsorption cycle set up to use $CaCl_2$ or any other reactive salt. The system will consist of a reactor and one more vessel operates as a condenser or as an evaporator. A suitable flow meter will be installed at the reactor exit that will be able to measure the non-uniform flow rate during desorption. Using this test rig, the flow rate during desorption could be identified and that will be beneficial to identify the correct expander's specification. Also, any rotary machine can be attached to the set-up later to investigate the process's power potential. Also we should investigate the effect on the system's pressure drop when an expander is attached between the reactor and the condenser during desorption. The condensation temperature effect could also be investigated.

6.2.2 General LH cogen system design

The prototype of the LH Cogen system was used to investigate the feasibility of the concept. Therefore some designs and some parts of the system were selected by theoretical calculations. The performance of the chiller and the whole system was affected or compromised. Below suggestions are given to improve the efficiency and workability of the existing design.

a) *Adsorbent material.* The selected adsorbent is a composite mixture of $CaCl_2$ and activated carbon. The activated carbon is used as an inner material to improve the $CaCl_2$ mass and heat transfer for the system's adsorption capacity. A further improvement to the adsorption capacity should be done in order to improve the

system's cogeneration performance. The new material will eventually decrease the system's required Q_{high}, and that will increase the system's COP.

b) *Adsorbent preparation.* Re-examine the absorbent preparation and drying process to avoid adsorbent leakage.

c) *Cooling water circuit*. The cooling water circuit is one circuit which after it cools using an external source through the heat exchanger, is passses through both condensers for condensation and then continues to the reactor currently under cooling. The cold water leaving the heat exchanger could be split into two circuits, one used to go around the condensers and the other to cool the reactor directly. In such a way, the heat sink temperature at the entrance to the reactor will be as low as possible resulting in the adsorption capacity improvement. This however will add complexity and cost to the existing design.

d) *Reactor water circuit design*. Since the reactor consisted of two parts, the cold or hot water stream could split into two from the inlet manifold and each stream enter the reactor. Therefore, cold and hot stream will enter the lower reactor at the same heat sink temperature similar to the upper reactor part. Hence that the adsorption and desorption process efficiency will be improved. It should be noted however that any of the above will add complexity and cost.

e) *Pneumatic valve position*: The V1 pneumatic valve (steam leaving the boiler) should not be installed next to the boiler since it overheats and its electronic part becomes damaged.

f) *Temperature sensor position:* The water temperature sensor at the reactor inlet should be installed just before the inlet manifold or somewhere in the inlet manifold.

g) *System's sensible heat losses.* The main material for the machine used is steel. That results in huge sensible heat losses either during heating which results in a higher Q_{high}, or during cooling which results in a lower Q_{ref}. A new material should be used of as low as possible thermal conductivity for the development of the machine which minimises sensible heat. That material should be easily available, flexible to cut and join, ammonia-compatible and should also be cheap. Also, the aluminium fins heat exchanger at the reactor can be replaced with a higher thermal conductivity ammonia compatible material to improve the heat transfer between the water entering the reactor and the adsorbent. Similar, the copper pipe carrying the water to the reactor can also be replaced.

h) *Heat pipe technique.* After the switch period, the hot and the cold stream are mixed in the reactor and also cold water from the reactor enter the cold water tank. Therefore the hot and the cold streams in the reactor can be carried by different pipes eliminating the above losses. This will results in the reactor to being warmed up and cooled down faster which will eventually decrease the cycle time and improve the efficiency of the system

i) *Insulation.* Any exposed pipe to the atmosphere for water or refrigerant circuit should be well insulated. That will minimise the waste energy and maximise the system's energy utilisation.

j) *Manual valves on ammonia circuit.* The manual valve could be replaced with a hand-wheel type. This type is easier and faster to open and close and it is also easier to adjust the flow for cogeneration especially in case v8 was one of those.

6.2.3 System's power generation during cogeneration

The system power generation during cogeneration depends on the amount of refrigerant and the inlet pressure and temperature before entering the expander. In that direction for the selected expander the v8 valve is used to concentrate the refrigerant before being released. The suggestions below will be in the direction of avoiding the use of the mass recovery valve and the v8 valve in the direction of maximising the overall power, extending the power production's duration and to achieve a more uniform path rather than pulsing. The above will improve the refrigeration performance as well.

a) *Suitable expander selection.* In case the desorption flow rate is identified, that means the correct expander selection will be able to produce variable power for a longer period of time. The power production will vary since the desorption flow rate is not constant but since the selected expander will be based on the desorption flow rate, that will increase the overall cycle's power production. That will eliminate the v8 valve's use especially in the case of new adsorption material use which improved the mass and heat transfer.

b) *Power generation procedure.* When running power trials, the v8 valve was trying to open fully as quickly as possible. The effect on power production has to be adjusted for but when it is not fully open it should be investigated.

c) *Refrigerant expander inlet re-heating.* Since the expander's inlet temperature is too low around 41^{O}C, and the hot water leaving the reactor is around 80^{O}C on average, therefore a heat exchanger before the expander inlet can be used to re-heat the refrigerant before it enters the expander. The design of the heat

exchanger is critical to reduce the pressure drop at the heat exchanger. On the other hand, the flow rate entering the expander should be steadier.

d) *Decrease the expander's outlet pressure.* The use of the mass recovery valve was necessary during power production to ensure the expander's low pressure (increasing ΔP_{exp}) so the power production but that reduces the system refrigeration production. We should make sure that sufficient low pressure at the expander exit is established during cogeneration. One solution is to provide the condenser with a heat source of $22^{O}C$ or lower (using a geothermal heat source if available) to ensure an expander's exit pressure around 0.9MPa, similar to the ideal scenario. To achieve that the condenser might need to be designed to suit an ORC rather than an adsorption chiller.

Also there should be examined the potential to use another reactor which will alternatively be connected to the evaporators. That reactor can carry any chloride which will provide the required low pressure when cooling down from the heat sink's temperature. The higher the ΔP_{exp}, the more the power production and this will also improve the desorption's efficiency. Increasing the ΔP_{exp} might lead to a high expander's rotational speed and cause reliability issues in the expander. That reactor ideally will eliminate the use of the mass recovery valve leading to improving dramatically the system's refrigeration performance during cogeneration.

The extra reactor will need to dry quickly before the next cooling cycle. That is possible through the mass recovery process at the end of the cycle. To improve that, a few minutes after the end of the cycle, no cooling will be provided to that reactor but heating instead in case the reactor is designed according to heat pipe technology, therefore the hot and cold streams enter from different pipes [55]. When the pressure is high enough, the mass recovery process will then take place and ammonia from the high-pressure side including from the extra reactor as well will transfer to the low-pressure side. It will actually be double the mass recovery process from the high-pressure reactor and the extra reactor to the current low-pressure reactor. Like that, the extra reactor will be dry of ammonia and ready to establish one more power cycle. That idea is actually a resorption power, adsorption and resorption cooling cogeneration cycle. An extra cooling

cycle will be added in case at the expander's exit the pressure will be low enough. The correct selection of the adsorbent at the extra reactor and the ammonia quantity is critical since the resorption system suffers from low mass transfer during adsorption.

This idea can use two extra reactors of similar reactive salt that will alternatively be undercooling and heating. When it is underheating it will enhance power production since it will provide extra refrigerant to the expander.

e) To make sure that the condenser can cool down the expanded refrigerant efficiently, a secondary condenser can be used after the primary one and that one can utilise part of the cooling that the P_{low} side produces. That will provide the required low pressure at the expander's exit to increase power generation but at the same time it will reduce the cycle's cooling production.

f) *Vacuum pump.* Another suggestion is to use a vacuum pump at the condenser's exit in order to ensure low pressure there. Similar pumps are common in power stations to improve the power output by lowering the pressure at the turbine exit and, at the same time, increasing the turbine speed so also the power production.

g) *Pressure drop between the connection of the chiller and the expander.* By integrating the adsorption chiller and scroll expander together, the connection pipe connects them which results in a pressure drop from the reactor's exit to the expander's inlet. This issue cannot be avoided and the only thing that can be done is to reduce the pipeline length as much as possible, without affecting any extra instruments attached there.

6.2.4 ECLIPSE software

ECLIPSE can predict the cooling the refrigeration capacity (Q_{ref}), average evaporator temperature (^{O}C) and power production (W) accurately. This can be done for a single point under a certain conditions using mass and energy balance. Having in mind that the adsorption and desorption processed take place under no constant rates, therefore different software should be used to evaluate the system performance. A software that use kinetics and a heat transfer model can be used to simulate adsorption and desorption process and a dynamic model to evaluate the expander performance. The design

parameters of the scroll expander such us number of chambers, the basic circle radius, the scroll pitch, wrap thickness and the wrap height should be considered by the software. What ECLIPSE can do is to predict accurate the system cooling performance by varying the system low pressure for a fix evaporator temperature. Is very simple to use and can generate results very fast providing an accurate approximation for the system performance.

References

[1] W. H. Organization. (2013, 14/12/2013). *Climate change and human health* Available: http://www.who.int/en/

[2] U. o. C. Scientists. (2011, 14/12/2013). *Global Warming Effects Around the World*. Available: http://www.climatehotmap.org/

[3] A. Jenkins. (14/12/2013). *The current and future consequences of global change-Effects*. Available: http://climate.nasa.gov/

[4] N. G. Society. (14/12/2013). *Effects of Global Warming* Available: http://environment.nationalgeographic.co.uk/

[5] P. Stevens. (2012, 14/12/2013). *Oil Prices:Energy Investment, Political Stability in the Exporting Counties and POEC's Dilemma*. Available: http://www.chathamhouse.org/

[6] S. N. HD. (2013, 14/12/2013). *Oil Forecast: Instability To Keep Prices High*. Available: http://news.sky.com/

[7] eia. (2013). *International Energy Outlook 2013*. Available: http://www.eia.gov/

[8] thequardian.com. (2010, 14/12/2013). *BP oil spill: Clean-up efforts along the Gulf coast*. Available: http://www.theguardian.com/

[9] thequardian.com. (2013). *BP cheers investors with $10bn asset sale and dividend hike*. Available: http://www.theguardian.com/

[10] U. N. F. C. o. C. Change. (14/12/2013). *Kyoto Protocol*. Available: http://unfccc.int/2860.php

[11] H. D. Madhawa Hettiarachchi, M. Golubovic, W. M. Worek, and Y. Ikegami, "Optimum design criteria for an Organic Rankine cycle using low-temperature geothermal heat sources," *Energy*, vol. 32, pp. 1698-1706, 2007.

[12] Yunus A.Cengel and M. A. Boles., *Thermodynamics an Engineering Approach*: McGraw-Hill, Inc, 1998.

[13] X. Zhang, M. He, and Y. Zhang, "A review of research on the Kalina cycle," *Renewable and Sustainable Energy Reviews*, vol. 16, pp. 5309-5318, 2012.

[14] H. Chen, D. Y. Goswami, and E. K. Stefanakos, "A review of thermodynamic cycles and working fluids for the conversion of low-grade heat," *Renewable and Sustainable Energy Reviews*, vol. 14, pp. 3059-3067, 2010.

[15] K. H. Kim, "Thermodynamic Performance of Regenerative Organic Rankine Cycle," *International Science Index*, vol. 5, 2011/11/21 2011.

[16] T. Yamamoto, T. Furuhata, N. Arai, and K. Mori, "Design and testing of the Organic Rankine Cycle," *Energy*, vol. 26, pp. 239-251, 3// 2001.

[17] F. Xu., D. Y. Goswami., and S. S. Bhaqwat., "A combined power cooling cycle," *Energy*, vol. 25, pp. 233-246, 2000.

[18] P. K. Nag and A. V. S. S. K. S. Gupta, "Exergy analysis of the Kalina cycle," *Applied Thermal Engineering*, vol. 18, pp. 427-439, 1998.

[19] G. Wall., C.-C. Chuang., and M. Ishida., "Exergy study of the kalina cycle," *Analysis and Design of Energy Systems: Analysis of Industrial Processes*, vol. 10-3, pp. 73-77, 1998.

[20] P. Bombarda, C. M. Invernizzi, and C. Pietra, "Heat recovery from Diesel engines: A thermodynamic comparison between Kalina and ORC cycles," *Applied Thermal Engineering*, vol. 30, pp. 212-219, 2// 2010.

[21] R. U. Nasruddin, Maulana Rifaldi, Agus Noor, "Energy and exergy analysis of kalina cycle system (KCS) 34 with mass fraction ammonia-water mixture variation," *Journal of Mechanical Science and Technology*, vol. 23, pp. 1871-1876, 2009.

[22] P. A. Lolos and E. D. Rogdakis, "A Kalina power cycle driven by renewable energy sources," *Energy*, vol. 34, pp. 457-464, 2009.

[23] E. D. R. Periklis A. Lolos, "THERMODYNAMIC ANALYSIS OF A KALINA POWER UNIT DRIVEN BY LOW TEMPERATURE HEAT SOURCES," *Thermal Science*, vol. 13, pp. 21-31, 2009.

[24] S. Lu and D. Y. Goswami, "Theoretical analysis of ammonia-based combined power refrigeration cycle," presented at the Sunrise on the Reliable Energe economy, 2002.
[25] S. Lu and D. Y. Goswami, "Optimization of a Novel Combined Power/Refrigeration Thermodynamic Cycle," *Journal of Solar Energy Engineering*, vol. Vol. 125 / 217, p. 212, May 2003 2003.
[26] C. Martin and D. Y. Goswami, "Effectiveness of cooling production with a combined power and cooling thermodynamic cycle," *Applied Thermal Engineering*, vol. 26, pp. 576-582, 2006.
[27] R. V. Padilla, G. Demirkaya, D. Y. Goswami, E. Stefanakos, and M. M. Rahman, "Analysis of power and cooling cogeneration using ammonia-water mixture," *Energy*, vol. 35, pp. 4649-4657, 2010.
[28] H. J. Chen. (2012, 28/03/2014). *Converting Low-Grade Heat into Electrical Power*. Available: http://www.eng.usf.edu/
[29] A. Vidal, R. Best, R. Rivero, and J. Cervantes, "Analysis of a combined power and refrigeration cycle by the exergy method," *Energy*, vol. 31, pp. 3401-3414, 12// 2006.
[30] G. Tamm, D. Y. Goswami, S. Lu, and A. A. Hasan, "Theoretical and experimental investigation of an ammonia–water power and refrigeration thermodynamic cycle," *Solar Energy*, vol. 76, pp. 217-228, 1// 2004.
[31] A. A. Hasan, D. Y. Goswami, and S. Vijayaraghavan, "First and second law analysis of a new power and refrigeration thermodynamic cycle using a solar heat source," *Solar Energy*, vol. 73, pp. 385-393, 11// 2002.
[32] J. Wang, Y. Dai, T. Zhang, and S. Ma, "Parametric analysis for a new combined power and ejector–absorption refrigeration cycle," *Energy*, vol. 34, pp. 1587-1593, 2009.
[33] B. Zheng and Y. W. Weng, "A combined power and ejector refrigeration cycle for low temperature heat sources," *Solar Energy*, vol. 84, pp. 784-791, 2010.
[34] L.W.Wang., D.Li., A.P.Roskilly., Y.D.Wang., and R.Z.Wang., "A novel type resorption cycle for electrical generation and refrigeration," presented at the Sustainable Energy Managemnet in the Process Indusstries International Conference (SsuTEM2011), Newcastle upon Tyne, UK, 2011.
[35] B.Agnew., M.Talbi., and M.Mostavi., "Combined power and cooling an analysis of the combined diesel absorption cycle," *Applied Thermal Engineering*, vol. 19, pp. 1097-1105, 1999.
[36] G.Paloso., JR., and B.Mohanty, "Cascading vapour absorption cycle with organic rankine cycle for enhancing geothermal power generation," *Renewable Energy*, vol. 3, pp. 669-681, 1993.
[37] S. Takezawa, K. Wakahara, T. Araki, K. Onda, and S. Nagata, "Cycle analysis using exhaust heat of SOFC and turbine combined cycle by absorption chiller," *Electrical Engineering in Japan*, vol. 167, pp. 49-55, 2009.
[38] X.-Q. Kong, R.-Z. Wang, Y. Li, and J.-Y. Wu, "Performance research of a micro-CCHP system with adsorption chiller," *Journal of Shanghai Jiaotong University (Science)*, vol. 15, pp. 671-675, 2010.
[39] L. Vasiliev, O. Filatova, and A. Tsitovich, "Application of sorption heat pumps for increasing of new power sources efficiency," *Archives of Thermodynamics*, vol. 31, 2010.
[40] H. Zhai, Y. J. Dai, J. Y. Wu, and R. Z. Wang, "Energy and exergy analyses on a novel hybrid solar heating, cooling and power generation system for remote areas," *Applied Energy*, vol. 86, pp. 1395-1404, 2009.
[41] J. Porteiro, J. L. Míguez, S. Murillo, and L. M. López, "Feasibility of a new domestic CHP trigeneration with heat pump: II. Availability analysis," *Applied Thermal Engineering*, vol. 24, pp. 1421-1429, 2004.
[42] T. Li, R. Wang, and L. Wang, "High-efficient thermochemical sorption refrigeration driven by low-grade thermal energy," *Chinese Science Bulletin*, vol. 54, pp. 885-905, 2009.
[43] F.Rouquerol., J.Rouquerol., and K.Sing., *Adsorption by powders and porous solids*, 1999.

[44] www.thedictionary.com. (2005, 22/11/2011). *Adsorption*. Available: www.thedictionary.com
[45] IAS. (02/01/2014). *What is adsorption.* Available: http://ias.vub.ac.be/
[46] Z. Tamainot-Telto, S. J. Metcalf, R. E. Critoph, Y. Zhong, and R. Thorpe, "Carbon–ammonia pairs for adsorption refrigeration applications: ice making, air conditioning and heat pumping," *International Journal of Refrigeration*, vol. 32, pp. 1212-1229, 2009.
[47] GBU, "Adsorption chiller NAK," in *Technicsl description*, ed. Germany: GBU mbH, 1999, pp. 1-19.
[48] M. Pons. (15/10/2010). *Principle of adsorption cycles for refrigeration or heat pumping*. Available: http://perso.limsi.fr/Individu/mpons/pricyc.htm
[49] T. X. Li, R. Z. Wang, J. K. Kiplagat, H. Chen, and L. W. Wang, "A new target-oriented methodology of decreasing the regeneration temperature of solid–gas thermochemical sorption refrigeration system driven by low-grade thermal energy," *International Journal of Heat and Mass Transfer*, vol. 54, pp. 4719-4729, 2011.
[50] T. X. Li, R. Z. Wang, R. G. Oliveira, and L. W. Wang, "Performance analysis of an innovative multimode, multisalt and multieffect chemisorption refrigeration system," *AIChE Journal*, vol. 53, pp. 3222-3230, 2007.
[51] L. W. Wang, R. Z. Wang, and R. G. Oliveira, "A review on adsorption working pairs for refrigeration," *Renewable and Sustainable Energy Reviews*, vol. 13, pp. 518-534, 2009.
[52] H.-B. Lu., N. Mazet., and B. Spinner., "Modelling of gas solid reaction coupling of heat and mass transfer," *Chemical Engineering Science*, vol. 51, pp. 3829-3845, 1996.
[53] P. Touzain., "Thermodynamic values of ammonia-salt reactions for chemical sorption heat pumps.," presented at the Proceedings of the Interantional Sorptio Heat Pump Conference, Munich, Germany, 1999.
[54] F.Meunier., "Solid sorption heat powered cycles for cooling and heat pumping applications," *Applied Thermal Engineering*, vol. 18, pp. 715-729, 1998.
[55] T. X. Li, R. Z. Wang, L. W. Wang, and Z. S. Lu, "Experimental study on an innovative multifunction heat pipe type heat recovery two-stage sorption refrigeration system," *Energy Conversion and Management*, vol. 49, pp. 2505-2512, 2008.
[56] R. Z. Wang and R. G. Oliveira, "Adsorption refrigeration—An efficient way to make good use of waste heat and solar energy," *Progress in Energy and Combustion Science*, vol. 32, pp. 424-458, // 2006.
[57] Y. Fan, L. Luo, and B. Souyri, "Review of solar sorption refrigeration technologies: Development and applications," *Renewable and Sustainable Energy Reviews*, vol. 11, pp. 1758-1775, 10// 2007.
[58] K. Wang, "New opporduntities for Solar, Adsorption Refrigeration," *ASHRAE Journal*, 2011.
[59] T. X. Li, R. Z. Wang, R. G. Oliveira, J. K. Kiplagat, and L. W. Wang, "A combined double-way chemisorption refrigeration cycle based on adsorption and resorption processes," *International Journal of Refrigeration*, vol. 32, pp. 47-57, 2009.
[60] J. Cot-Gores, A. Castell, and L. F. Cabeza, "Thermochemical energy storage and conversion: A-state-of-the-art review of the experimental research under practical conditions," *Renewable and Sustainable Energy Reviews*, vol. 16, pp. 5207-5224, 2012.
[61] W. Wongsuwan., S. Kumar., P. Neveu., and F. Meunier., "A review of chemical heat pump technology and applications," *Applied Thermal Engineering*, vol. 21, pp. 1489-1519, 2001.
[62] L. L. Vasiliev, D. A. Mishkinis, A. A. Antukh, and A. G. Kulakov, "Resorption heat pump," *Applied Thermal Engineering*, vol. 24, pp. 1893-1903, 2004.
[63] Y. Zhong and R. E. Critoph, "Review of trends in solid sorption refrigeration and heat pumping technology," *Proceedings of the Institution of Mechanical Engineers, Part E: Journal of Process Mechanical Engineering*, vol. 219, pp. 285-300, 2005.
[64] T. X. Li, R. Z. Wang, J. K. Kiplagat, and L. W. Wang, "Performance study of a consolidated manganese chloride–expanded graphite compound for sorption deep-freezing processes," *Applied Energy*, vol. 86, pp. 1201-1209, 2009.

[65] L. W. Wang, Z. Tamainot-Telto, R. Thorpe, R. E. Critoph, S. J. Metcalf, and R. Z. Wang, "Study of thermal conductivity, permeability, and adsorption performance of consolidated composite activated carbon adsorbent for refrigeration," *Renewable Energy*, vol. 36, pp. 2062-2066, 2011.
[66] H. S. Bao, R. G. Oliveira, R. Z. Wang, L. W. Wang, and Z. W. Ma, "Working pairs for resorption refrigerator," *Applied Thermal Engineering*, vol. 31, pp. 3015-3021, 2011.
[67] H.S.Bao., R.G.Oliveira., R.Z.Wang., and L.W.Wang., "Choice of low temperature salt for a resorption refrigeration," *Industrial & Engineering Chemistry Research*, vol. 49, pp. 4897-4903, 2010.
[68] V.Goetz., B.Spinner, and E.Lipinasse, "A solid gas thermochemical cooling systemj using BaCl2 and NiCl2," *Energy*, vol. 22, pp. 49-58, 1997.
[69] E.Lipinasse., M.Marion., and V.Goetz., "Cooling storage with a resorption process.Application to abox temperature control," *Applied Thermal Engineering*, vol. 21, pp. 1251-1263, 2001.
[70] L. W. Wang, H. S. Bao, and R. Z. Wang, "A comparison of the performances of adsorption and resorption refrigeration systems powered by the low grade heat," *Renewable Energy*, vol. 34, pp. 2373-2379, 2009.
[71] T. X. Li, R. Z. Wang, J. K. Kiplagat, and H. Chen, "Experimental study and comparison of thermochemical resorption refrigeration cycle and adsorption refrigeration cycle," *Chemical Engineering Science*, vol. 65, pp. 4222-4230, 2010.
[72] P. Neveu and J. Castaing, "Solid-gas chemical heat pumps: Field of application and performance of the internal heat of reaction recovery process," *Heat Recovery Systems and CHP*, vol. 13, pp. 233-251, 1993.
[73] L. Xu, R. Z. Wang, T. X. Li, and L. W. Wang, "Experimental study on the performance of double-effect and double-way thermochemical sorption refrigeration cycle," *Applied Thermal Engineering*, vol. 31, pp. 3658-3663, 2011.
[74] S. L. Li, Z. Z. Xia, J. Y. Wu, J. Li, R. Z. Wang, and L. W. Wang, "Experimental study of a novel CaCl2/expanded graphite-NH3 adsorption refrigerator," *International Journal of Refrigeration*, vol. 33, pp. 61-69, 2010.
[75] G. Qiu, H. Liu, and S. Riffat, "Expanders for micro-CHP systems with organic Rankine cycle," *Applied Thermal Engineering*, vol. 31, pp. 3301-3307, 11// 2011.
[76] C. Invernizzi, P. Iora, and P. Silva, "Bottoming micro-Rankine cycles for micro-gas turbines," *Applied Thermal Engineering*, vol. 27, pp. 100-110, 1// 2007.
[77] L. Y. Pei Gang, Li Jing, Ji Jie. (2010). *An experimental study of a micro high-speed turbine that applied on Organic Rankine Cycle* Available: http://ieeexplore.ieee.org/stamp/stamp.jsp?arnumber=5449529
[78] I. Turbines. (12/11/2011). *Introducing the radial Outflow Turbine Generator*
[79] I. K. S. H Leiboweitz, N Stotic, "COST EFFECTIVE SCALE ORC SYSTEMS FOR POWER RECOVERY FROM LOW HEAT SOURCES," in *2006 ASME International Mechanical Engineering Congress and Exposition*, Chicago, Illinois, USA, 2006.
[80] W. Wang, Y.-t. Wu, C.-f. Ma, L.-d. Liu, and J. Yu, "Preliminary experimental study of single screw expander prototype," *Applied Thermal Engineering*, vol. 31, pp. 3684-3688, 12// 2011.
[81] O. S. o. P. a. E. B R Singh, "Analytical investigations on different air injection angles to optimize power output of a vaned-type air turbine," *Journal of Power and Energy*, pp. 224-305, 2009.
[82] B. Yang, X. Peng, Z. He, B. Guo, and Z. Xing, "Experimental investigation on the internal working process of a CO2 rotary vane expander," *Applied Thermal Engineering*, vol. 29, pp. 2289-2296, 8// 2009.
[83] C. Corporation. (2004, 02/05). *Scroll Compressor*. Available: www.carrier.com
[84] K. J. Harada, "Development of a Small Scale Scroll Expander," MSc, Mechanical Engineering, Oregon State University, 2010.
[85] H. A. Ingley, R. Reed, and D. Y. Goswami, "Optimization of a scroll expander applied to an ammonia/water combined cycle system for hydrogen production," presented at the Proceeding of the Solar World Congress, Orlando, Florida, 2005.

[86] H. W. R B Peterson, T Herron, "Performance of a small-scale regenerative Rankine power cycle employing a scroll expander," *Proceedings of the Institution of Mechanical Engineers, Part A: Journal of Power and Energy,* vol. 222, pp. 222-271, 2008.
[87] V. Lemort, S. Quoilin, C. Cuevas, and J. Lebrun, "Testing and modeling a scroll expander integrated into an Organic Rankine Cycle," *Applied Thermal Engineering,* vol. 29, pp. 3094-3102, 2009.
[88] Sylvain Quoilin, "Experimental Study and Modeling of a Low Temperature Rankine Cycle for Small Scale Cogeneration," ElectroMechanical Engineer, (Energetic engineering), Faculty of applied sciences, Aerospace and Mechanical Engineering Department, Thermodynamic Laboratory, University of Liege, 2007.
[89] R. B. P. H Wang, T Herron, "Experimental performance of a compliant scroll expander for an organic Rankine cycle," *Proceedings of the Institution of Mechanical Engineers Part A Journal of Power and Energy* vol. 01, pp. 863-872, 2009.
[90] T. C. B. Smith, "Low organic rankine cycles for grid connected power generation," Hopkinson Laboratory,, Cambridge, England.
[91] H. Wang, R. Peterson, K. Harada, E. Miller, R. Ingram-Goble, L. Fisher, *et al.*, "Performance of a combined organic Rankine cycle and vapor compression cycle for heat activated cooling," *Energy,* vol. 36, pp. 447-458, 2011.
[92] S. Quoilin, V. Lemort, and J. Lebrun, "Experimental study and modeling of an Organic Rankine Cycle using scroll expander," *Applied Energy,* vol. 87, pp. 1260-1268, 2010.
[93] N. Yamada, T. Minami, and M. N. Anuar Mohamad, "Fundamental experiment of pumpless Rankine-type cycle for low-temperature heat recovery," *Energy,* vol. 36, pp. 1010-1017, 2011.
[94] S. Q. Vincent Lemort, Christophe Pire, "Experimental invetsigation on a hermetic scroll expander," Thermodynamic laboratory, University of Liege, Campus du Sart Tilman B49, B-4000 Liege, Belgium2009.
[95] D. F. R. Zanelli, "Experimental Investigation of a Hermetic Scroll Expander-Generator," presented at the International Compressor Engineering Conference 1994.
[96] AirSquared. Available: http://airsquared.com/
[97] L. W. RZhu Wang, JinGyi Wu, *Adsorption Refrigeration Technology: Theory and Application*. Singapore: John Wiley and Sons, 2014.
[98] F. Vélez, J. J. Segovia, M. C. Martín, G. Antolín, F. Chejne, and A. Quijano, "A technical, economical and market review of organic Rankine cycles for the conversion of low-grade heat for power generation," *Renewable and Sustainable Energy Reviews,* vol. 16, pp. 4175-4189, 8// 2012.
[99] A. C. O. Jorge Facao, "ANALYSIS OF ENERGETIC, DESIGN AND OPERATIONAL CRITERIA WHEN CHOOSING AN ADEQUATE WORKING FLUID FOR SMALL ORC SYSTEMS," presented at the Asme 2009 International Mechanical Engineering Congress & Exposition, Lake Buena Vista, Florida, USA, 2009.
[100] R. Chacartegui, D. Sánchez, J. M. Muñoz, and T. Sánchez, "Alternative ORC bottoming cycles FOR combined cycle power plants," *Applied Energy,* vol. 86, pp. 2162-2170, 10// 2009.
[101] L. J. Pei Gang, Ji Jie, "Working Fluid Selection for Low Temperature Solar Thermal Power Generation with Two-stage Collectors and Heat Storage Units " Department of Thermal Science and Energy Engineering, University of Science and Technology of China, China 978-953-307-142-8, 2010.
[102] K. H. Kim, "Thermodynamic Performance of Regenerative Organic Rankine Cycles " *International Science Index,* vol. 5, pp. 932-936, 21/11/2011 2011.
[103] M. Lebrun and B. Spinner, "Simulation for the development of solid—gas chemical heat pump pilot plants Part I. simulation and dimensioning," *Chemical Engineering and Processing: Process Intensification,* vol. 28, pp. 55-66, 10// 1990.
[104] M. Schicktanz and T. Núñez, "Modelling of an adsorption chiller for dynamic system simulation," *International Journal of Refrigeration,* vol. 32, pp. 588-595, 6// 2009.
[105] H. Bao, Y. Wang, and A. P. Roskilly, "Modelling of a chemisorption refrigeration and power cogeneration system," *Applied Energy,* vol. 119, pp. 351-362, 4/15/ 2014.

[106] J. Castaing-Lasvignottes and P. Neveu, "Development of a numerical sizing tool applied to a solid-gas thermochemical transformer—II. Influence of external couplings on the dynamic behaviour of a solid-gas thermochemical transformer," *Applied Thermal Engineering*, vol. 17, pp. 519-536, 6// 1997.
[107] D. F. C. Bernard Aoun, "Theoretical and experimental study of an oil free scroll expander," presented at the INTERNATIONAL COMPRESSOR ENGINEERING CONFERENCE, Purdue, 2008.
[108] Z. S. Lu, R. Z. Wang, L. W. Wang, and C. J. Chen, "Performance analysis of an adsorption refrigerator using activated carbon in a compound adsorbent," *Carbon*, vol. 44, pp. 747-752, 2006.
[109] A. Fakheri, "Heat Exchanger Efficiency," *Journal of Heat Transfer*, vol. 129, pp. 1268-1276, 2006.
[110] H. Elements. (2012, 22/02/2015). *Energy Efficient Electric Heating*. Available: http://www.heatrod.com/
[111] S. Exchanger. (2015, 22/02/2015). *What type of electric heating system is the most energy efficient?* Available: http://diy.stackexchange.com/
[112] C. J. Chen, R. Z. Wang, L. W. Wang, and Z. S. Lu, "Studies on cycle characteristics and application of split heat pipe adsorption ice maker," *Energy Conversion and Management*, vol. 48, pp. 1106-1112, 2007.
[113] T. X. Li, R. Z. Wang, L. W. Wang, Z. S. Lu, and J. Y. Wu, "Influence of mass recovery on the performance of a heat pipe type ammonia sorption refrigeration system using CaCl2/activated carbon as compound adsorbent," *Applied Thermal Engineering*, vol. 28, pp. 1638-1646, 2008.
[114] B. B. Saha, S. Koyama, T. Kashiwagi, A. Akisawa, K. C. Ng, and H. T. Chua, "Waste heat driven dual-mode, multi-stage, multi-bed regenerative adsorption system," *International Journal of Refrigeration*, vol. 26, pp. 749-757, 11// 2003.
[115] S. J. Metcalf, Z. Tamainot-Telto, and R. E. Critoph, "Application of a compact sorption generator to solar refrigeration: Case study of Dakar (Senegal)," *Applied Thermal Engineering*, vol. 31, pp. 2197-2204, 10// 2011.
[116] C. Charalambous, "An Investigation of a new Cogeneration system for Electricity and Cooling using low grade heat sources " SWAN institute, Newcastle Upon Tyne UK2012.
[117] Uzakov A. Kh, Mirzaef Sh. M, Modiev O. Kh, and Yakubov Yu. N, "Use of strontium chloride octaammoniate in solar-powered refrigerators," *Electrochemical, Radiational, and Thermal Energy Technology*, pp. 7-9, 1990.

Appendices

Appendix 1: Overall power scroll expander results for varying inlet pressure using nitrogen

Average Inlet Pressure (MPa)	Average Power (W)	Average Inlet Temperature (^{O}C)	Average Outlet Temperature (^{O}C)
0.404	52.73	27.5	10.9
0.560	126.1	27.2	3.61
0.606	198.8	26.9	0.11
0.746	297.9	26.5	-7.82
0.922	434.4	28.6	-9.9
1.115	531.4	18.5	-23.1

Appendix 2: Overall power scroll expander results for varying the inlet pressure and temperature using nitrogen

Average Inlet Pressure (MPa)	Average Power (W)	Average Inlet Temperature (^{O}C)	Average Outlet Temperature (^{O}C)
0.604	231.4	67.2	28.0
0.735	290.9	76.8	28.9
0.758	339.4	65.8	18.4
0.864	395.2	69.3	22.1
0.904	427.4	74.6	20.0
1.099	561.3	62.0	7.1
1.291	704.7	58.0	3.7

Appendix 3: Overall cooling results for 28kg ammonia system

Cycle time + Mass Recovery (min)	Evaporator Set-up Temperature (^{O}C)	Average Heating Vapour Temperature (^{O}C)	Cooling Water Average Cooling Temperature (^{O}C)	Average Cooling Production At Evaporator (^{O}C)	Average Cycle Heating power Q_{high} (KW)	Average Cycle Refriger-ation Power Q_{ref} (KW)	Maximum Average Cycle COP_{ref}	Average High Pressure (MPa)	Lowest/ Average Low Pressure (MPa)	SCP (W/kg)
13+1	0	96.2	18.47	7.86	7.54	0.09	0.01	1.07	0.28/0.38	5.14
13+1	0	108.3	18.65	9.38	9.09	0.22	0.03	1.26	0.24/0.39	12.57
13+1	0	121.6	19.85	7.73	10.86	0.78	0.07	1.46	0.25/0.41	44.57
13+1	0	128.07	18.79	7.87	12.69	1.13	0.10	1.58	0.21/0.43	64.57
13+1	0	130.19	20.34	5.69	11.11	0.93	0.09	1.51	0.21/0.42	53.14
13+1	-5	107.14	19.17	8.3	8.85	0.09	0.01	1.24	0.27/0.38	5.14
13+1	-5	116.96	18.85	3.27	10.08	0.43	0.07	1.29	0.24/0.36	24.57
13+1	-5	128.85	18.39	3.18	11.72	0.98	0.09	1.53	0.2/0.38	56.00
13+1	-5	132.44	19.64	3.35	11.83	0.81	0.10	1.54	0.18/0.39	46.29
13+1	-10	118.15	17.43	-1.95	10.31	0.29	0.04	1.29	0.19/0.32	16.57
13+1	-10	127.44	17.19	-1	11.88	0.67	0.08	1.48	0.17/0.34	38.29
13+1	-10	132.22	17.8	-0.09	12.3	0.63	0.07	1.43	0.13/0.34	36.00

Appendix 4: Overall cooling results for varying the mass recovery time for $0^{O}C$ and $5^{O}C$ evaporating temperature for 28kg ammonia system

Cycle time + Mass Recovery (min)	Evaporator Set-up Temperature (^{O}C)	Average Heating Vapour Temperature (^{O}C)	Cooling Water Average Cooling Temperature (^{O}C)	Average Cooling Production At Evaporator (^{O}C)	Average Cycle Heating power Qhigh (KW)	Average Cycle Refrigeration Power Qref (KW)	Maximum Average Cycle COPref	Average High Pressure (MPa)	Lowest/ Average Low Pressure (MPa)	SCP (W/kg)
13+30sec	0	121.82	19.48	10.65	11.02	0.53	0.05	1.45	0.22/0.39	30.29
13+1	0	121.6	19.85	7.73	10.86	0.78	0.074	1.46	0.25/0.41	44.57
13+2	0	122.38	19.67	10.75	10.46	0.73	0.07	1.45	0.210.43	41.71
13+30sec	-5	120.42	22.11	5.97	10.76	0.19	0.04	1.39	0.19/0.43	10.86
13+1	-5	116.96	18.85	3.27	10.08	0.43	0.07	1.29	0.24/0.36	24.57
13+2	-5	122.43	19.76	6.12	10.58	0.47	0.07	1.45	0.18/0.41	26.86

Appendix 5: Overall cooling results for varying the basic cycle time for $0^{O}C$ and $-5^{O}C$ evaporator set-up temperatures

Cycle time + Mass Recovery (min)	Evaporator Set-up temperature (^{O}C)	Average Heating Vapour Temperature (^{O}C)	Cooling Water Average Cooling Temperature (^{O}C)	Average Cooling Production At Evaporator (^{O}C)	Average Cycle Heating power Q_{high} (KW)	Average Cycle Refriger-ation Power Q_{ref} (KW)	Maximum Average Cycle COP_{ref}	SCP (W/kg)	Cooling Capacity (kJ/kg)
10+1	0	125.46	20.21	8.91	12.8	0.86	0.07	49.14	32.43
13+1	0	128.07	18.79	7.87	12.69	1.13	0.1	64.57	54.24
16+1	0	125.54	18.64	8.83	10.28	1.19	0.12	68.00	69.36
18+1	0	124.09	21.37	8.94	9.54	0.88	0.09	50.29	57.33
10+1	-5	123.33	19.39	3.77	12.7	0.61	0.05	34.86	23.01
13+1	-5	128.85	18.39	3.18	11.72	0.98	0.08	56.00	47.04
16+1	-5	124.82	18.45	3.32	10.17	0.95	0.09	54.29	55.37
18+1	-5	125.02	19.2	4.25	9.38	0.76	0.08	43.43	49.51

Appendix 6: Overall results for 13+1 cycle time for overall system ammonia under investigation

Cycle Time + Mass Recovery (min)	Evaporator Set-up Temperature (^{O}C)	Average Heating Vapour Temperature (^{O}C)	Cooling Water Average Cooling Temperature (^{O}C)	Average Cooling Production At Evaporator (^{O}C)	Average Cycle Heating power Q_{high} (KW)	Average Cycle Refrigeration power Q_{ref} (KW)	Maximum Average Cycle COP_{ref}	Average High Pressure (MPa)	Lowest/ Average Lowest Pressure (MPa)	SCP (W/kg)
13+1 (24kg)	0	125.5	27.80	-2.40	16.04	2.83	0.2	1.30	0.14/0.41	160
13+1 (28kg)	0	128.1	18.79	7.60	12.69	1.13	0.10	1.58	0.21/0.43	97.14

Appendix 7: Maximum results for 13+1 cycle time for overall system ammonia under investigation

Cycle Time + Mass Recovery (min)	Evaporator Set-up Temperature (^{O}C)	Average Heating Vapour Temperature (^{O}C)	Maximum Average Refrigeration Power Q_{ref} (KW)	Cycle Maximum COP_{ref}	Maximum Pressure (MPa)	Lowest Temperature Recorded (^{O}C)	SCP (W/kg)
13+1	0	125.5	3.52	0.26	1.66	-18	201.14
13+1	0	128.1	1.42	0.11	2	-3	81.14

Appendix 8: Collected results recorded during the cogeneration experimental trial, power-related

Power Trial Number	Side Under Heating	Average Power (W)	Maximum Power on Trial (W)	Average Expander Inlet Pressure (MPa)	Average Expander Inlet Temperature (^{O}C)	ΔP_{exp} (kPa)	Average Heat Input/Side Qhigh (W)	COP_W	Power Duration (sec)
1	1	206	486	1.143	39.6	-311.1	10070	0.02	15
2	1	94	193	1.283	40.9	-109.8	10070	0.009	8

3	1	31	31	1.425	41.7	-134.1	10070	0.003	3
4	1	109	215	1.472	43.2	-169.0	10070	0.011	8
5	1	21	48	1.474	42.5	-111.4	10070	0.002	7
6	1	43	58	1.403	42.7	-144.4	10070	0.004	5
7	1	37	75	1.288	43.3	-133.7	10070	0.004	7
8	1	0	0	0	42.9	0	10070	0	0
9	2	105	265	1.253	40.9	-217.9	7590	0.014	20
10	2	100	179	1.227	40.3	-202.3	7590	0.013	11
11	2	16	23	1.000	39.5	-158.7	7590	0.002	5

Appendix 9: Overall results recorded during the cogeneration experimental trial, flow-rate related

Power Trial number	Side under heating	Average Expander Inlet Pressure (MPa)	Average Expander Inlet Temperature (^{O}C)	Average Flow Rate (kg/s)	Average Power (W)	Average ΔP_{exp} (MPa)	Flow Rate Duration (sec)
1	1	1.143	39.6	0.038	206	-0.311	30
2	1	1.283	40.9	0.031	94	-0.109	25
3	1	1.425	41.7	0.029	31	-0.134	15
4	1	1.472	43.2	0.034	109	-0.169	20
5	1	1.448	42.5	0.031	21	-0.111	15
6	1	1.403	42.7	0.026	43	-0.144	15
7	1	1.288	43.3	0.025	37	-0.133	15
8	1	1.298	42.9	0	0	0	0
9	2	1.253	40.9	0.034	105	-0.219	32
10	2	1.227	40.3	0.028	100	-0.202	25
11	2	1.000	39.5	0.019	16	-0.158	20

Appendix 10: Experimental cooling results that give the maximum cooling performance

Evaporator Set-Up Temperature (^{O}C)	Average Cooling Power (W)	Average Heating Power (kW)	Max COP_{ref} Recorded	Average Cooling Temperature at Evaporator (^{O}C)	Lower Pressure Recorded (MPa)	SCP (W/kg)
0	2940	16.2	0.25	0.26	0.23	168.08
-5	3060	15.5	0.22	-3.24	0.19	174.86
-10	3070	16.1	0.26	-5.09	0.19	175.43

Appendix 11: Validated experimental cooling results

Evaporator Set-Up Temperature (^{O}C)	Average Cooling Power (W)	Average Heating Power Q_{high} (kW)	COP_{ref}	Average Cooling Temperature At Evaporator (^{O}C)	Cooling Water Circuit Flow Rate To The Evaporator (kg/s)	SCP (W/kg)
0	2941	5.22	0.56	0.04	0.0189	168.08
-5	3061	5.22	0.59	-3.89	0.0215	174.91
-10	3070	5.22	0.59	-5.45	0.0202	175.43

Appendix 12: Collected cooling results comparison for experimental and simulation data

	Evaporator Set-Up Temperature (^{O}C)	Average Cooling Power Q_{high} (kW)	Average Heating Power Q_{ref} (kW)	COP_{ref}	Average Cooling Temperature at Evaporator (^{O}K)	SCP (w/kg)
Simulation	0	2.94	5.22	0.56	0.04	168
Experimental	0	2.94	16.2	0.18	0.26	168.06
Deviation % for 0^{O}C		**0.03**	**67.8**	**212.7**	**0.08**	**-0.03**
Simulation	-5	3.06	5.22	0.59	-3.89	174.86
Experimental	-5	3.06	15.5	0.19	-3.2	174.91
Deviation % for -5^{O}C		**0.03**	**66.3**	**208.4**	**0.24**	**-0.03**
Simulation	-10	3.07	5.22	0.59	-5.45	175.43
Experimental	-10	3.07	16.1	0.19	-5.09	175.43
Deviation % for -10^{O}C		**0**	**67.7**	**209.3**	**0.13**	**0**

Appendix 13: Experimental data used for simulation during the expander test using nitrogen

Average Expander Inlet Pressure (MPa)	Outlet Expander Pressure (MPa)	Average Inlet Temperature (^{O}C)
0.604	0.1	67.2
0.735	0.1	76.8
0.758	0.1	65.8
0.864	0.1	69.3
0.904	0.1	74.6
1.1099	0.1	62.0
1.291	0.1	58.0

Appendix 14: Overall simulation results for nitrogen test

Power (W)	Average Outlet Temperature (C^{O})	Flow Rate (kg/s)	Scroll Expander Efficiency
231.2	27.8	0.06	28.5
291	28.9	0.06	25.8
339.1	18.4	0.07	31.4
396.6	22.1	0.09	29.5
428.1	20.1	0.08	29.6
561.1	7.1	0.10	32.4
704.8	3.7	0.13	30.8

Appendix 15: Overall simulation expander results using ammonia as refrigerant

Inlet Pressure (MPa)	Power (W)	Average Outlet Temperature (^{O}C)	Flow Rate (kg/s)	Scroll Expander Efficiency
0.604	231.2	40.9	0.06	17
0.735	290.4	37.1	0.06	15
0.758	339.6	33.1	0.07	18.6
0.864	393.6	35.6	0.09	17.26
0.904	429.9	31.1	0.08	17.26
1.099	562.0	19.6	0.10	18.85
1.291	704.9	12.0	0.13	17.2

Appendix 16: Deviation between experimental and simulation results for power generation

Power Trial No.	Expander Power Output (kW)	Expander Inlet Pressure (kPa)	Average Expander Inlet Temperature (^{O}C)	Average Expander Outlet Temperature (^{O}C)	Average Heat Input for sides 1 and 2 (kW)	COP_W
1	-1.33	-11.64	-3.5	21.45	24.57	-34.34
2	-2.12	0.58	-0.24	17.75	24.60	-35.43
4	0.33	13.34	5.09	21.56	24.57	-32.13
9	-0.51	-1.82	-0.24	13.46	34.70	-53.93
10	-2.24	-3.93	-1.74	12.16	34.70	-56.58

Appendix 17: Overall results for the ideal and ideal with varying expander outlet pressure cases

Power Trial No.	Experimental Power (1) (W)	Ideal With Varying Expander Outlet Pressure Power (2) (W)	Ideal case Power (3) (W)	Heat Input Q_{high} (2 and 3) (W)	COP_W (1)	COP_W (2)	COP_W (3)	Power (1) vs (2) Increase %	Power (1) vs (3) Increase %	Power (2) vs (3) Increase %
1	206	354.9	379.3	5656	0.02	0.06	0.07	72.3	84.1	6.9
2	94	202.3	379.3	5656	0.01	0.04	0.07	115.3	303.5	87.4
4	109	219.5	379.3	5656	0.01	0.04	0.07	101.4	248.0	72.8
9	105	230.7	379.3	5656	0.01	0.04	0.07	119.7	261.2	64.4
10	100	225.5	379.3	5656	0.01	0.04	0.07	125.5	279.3	68.2

Appendix 18: Overall results for the ideal case assuming varying scroll expander efficiency

Average Expander Inlet Temperature (^{O}C)	Average Expander Outlet Temperature (^{O}C)	Expander Efficiency	Average Power (W)	Simulation Heat Input Q_{high} (W)	COP_W
133	126	7.356	189.6	5656	0.03
133	124	14.713	379.3	5656	0.07
133	119	29.427	758.4	5656	0.13
133	117	36.783	948.1	5656	0.17
133	114	44.14	1137.7	5656	0.20

Appendix 19: Overall results for the ideal case for varying the expander's inlet pressure

Inlet Pressure (MPa)	Average Expander Inlet Temperature (^{O}C)	Average Expander Outlet Temperature (^{O}C)	Average Power (W)	Simulation Heat Input Q_{high} (W)	COP_W
1	133	131	98	5656	0.02
1.2	133	127	260.6	5656	0.05
1.4	133	123	391.1	5656	0.07
1.6	133	120	498.9	5656	0.09
1.8	133	117	589.5	5656	0.10
2	133	114	666.8	5656	0.12

Appendix 20: Overall results of the ideal case for varying the expander's inlet temperature

Average Expander Inlet Temperature (^{O}C)	Average Expander Outlet Temperature (^{O}C)	Average Power (W)	Simulation Heat Input Q_{high} (W)	COP_W
41	28.6	274.5	5656	0.05
65	53.8	301.4	5656	0.05
85	74.6	325.0	5656	0.06
105	95.1	348.0	5656	0.06
115	105	359.3	5656	0.06
125	116	370.3	5656	0.07
135	126	381.5	5764	0.06
145	136	392.4	6305	0.06

Appendix 21: Experimental cogeneration performance

Evaporator Set-Up Temperature (^{O}C)	Ammonia Quantity	COP_{ref} max	COP_W max	COP_{cogen}
0	24	0.25	0.02	0.27
-5	24	0.22	0.02	0.24
-10	24	0.26	0.02	0.28
0	28	0.11	0.02	0.13
-5	28	0.09	0.02	0.11
-10	28	0.08	0.02	0.1

Appendix 22: Simulation cogeneration performance for the model

Evaporator Set-Up Temperature (^{O}C)	COP_{ref}	COP_W max	COP_{cogen}
0	0.56	0.03	0.59
-5	0.59	0.03	0.62
-10	0.59	0.03	0.62

Appendix 23: COP_{cogen} for expander efficiency investigation

Expander Efficiency	Average COP_{ref}	COP_W	COP_{cogen}
7.356	0.58	0.03	0.61
14.713	0.58	0.07	0.65
29.427	0.58	0.13	0.71
36.783	0.58	0.17	0.75
44.14	0.58	0.2	0.78

Appendix 24: COP_{cogen} for inlet pressure investigation

Inlet Pressure (MPa)	Average COP_{ref}	COP_W	COP_{cogen}
1	0.58	0.02	0.6
1.2	0.58	0.05	0.63
1.4	0.58	0.07	0.65
1.6	0.58	0.09	0.67
1.8	0.58	0.1	0.68

2	0.58	0.12	0.7

Appendix 25: COP_{cogen} for inlet temperature investigation

Inlet Temperature (^{O}C)	Average COP_{ref}	COP_{W}	COP_{cogen}
41	0.58	0.05	0.63
65	0.58	0.05	0.63
85	0.58	0.06	0.64
105	0.58	0.06	0.64
115	0.58	0.06	0.64
125	0.58	0.07	0.65
135	0.58	0.06	0.64
145	0.58	0.06	0.64